Effect of Surface Topography upon the Quality of Autobody Panels

A thesis submitted for the Degree of Doctor of Philosophy

Fabrizio Benati

Department of Systems Engineering,

Brunel University

June 2003

Abstract

Improvements in the quality of the autobody panels can lead the automotive industry to large savings, where metal scrap levels always exceed 50%, and global losses are running into millions of pounds per annum. The production of new tooling also runs into the order of millions of pounds, often taking many weeks of trials to achieve the correct profiles and clearances.

*It is therefore important to identify the correct material to use in term of substrate mechanical properties and surface (**topography** and coating type) in order to achieve better quality and minimise manufacturing costs.*

The most useful approach to surface topography characterisation in engineering is to describe a surface by a set of parameters, which can be measured objectively, correlated to functional behaviour and used for process control.

The research work presented in this thesis consisted in the study of the different stages of the autobody manufacturing process through an extensive experimental activity. The phenomenon of oil retention of a surface and friction were studied and novel 3D surface topography parameters were deployed. Then, the experimental results were correlated with the surface topography parameters in order to understand how surface topography is influencing these phenomena. Finally, a similar approach was attempted with semi-industrial experimentation to probe for correlation between surface topography parameters and ability of a material to be deep drawn.

Acknowledgements

I would like to thank Brian for his patience, Clive for his wisdom, Franco and Stefano for their friendship, my family for their support and the Autosurf team for the good work presented in this thesis (Haizhuang, Alessandro, Marco, Jan Mark, Hans, Michel, Hendrik, Jan, Louisa, Paul, DJ, Kaj, BG, Elisabetta, Enzo, Gaetano and many others).

Table of Contents

Table of Figures

Index of Tables and Equations

1. Background and overview of this thesis

1.1 Introduction

Automobiles are one of the largest consumer products influencing human life. Henry Ford was one of the early 20th century pioneers who bought the automobile into mass ownership as a result of an emphasis on quality, mass-production and reducing costs. Even at the end of the 20th century, the emphasis had not changed because as Nagagawa [1993] points out, the goals of low cost, high quality and high productivity are the common targets of all automotive manufacturing companies. Indeed, the emphasis is essentially the same in this 21st century as much money is employed to research higher quality products and cost reduction in an increasingly competitive market.

An automobile consists of many thousands of components and one of the most important families of car-components is the body element called "autobody panels". They are the "skin" of the car, hence the customer immediately perceives their quality and this has a direct influence on sales. These panels are usually manufactured from steel sheet, albeit aluminium and plastics are increasingly used. The steel body panels are manufactured by a family of processes generally named "forming". Thus, there is a significant need to ensure the forming and related processes are of the highest quality and as efficient as possible. It was for this reason that the research in this thesis was undertaken sponsored by a consortium of European automobile companies.

In the late 1990's the European Union (EU) decided the automotive industry needed to be as efficient as possible to compete with the Far East and North American car manufacturers. Hence, Brussels announced an automotive efficiency research programme. Recognising the need for a holistic approach, thirteen organisations involved in automotive work assembled as a consortium and made a bid for research funding for the study of body panel forming. The bid was approved and the research programme started in 1997. The participants christened the programme "Autosurf". The thirteen organisations consisted of car manufacturers, steel manufacturers and Universities. It was given the programme number "BE-97-4140". The stated **objective** of this

research programme was to *"increase the knowledge of the manufacturing process of autobody panels in order to further improve quality and reduce their manufacturing costs through the correct design of sheet material surface finish (topography)".*

The work undertaken during the Autosurf research programme relating to the forming of autobody panels to 3D surface roughness parameters is described in this thesis. The main outcome of the work was the definition of a new set of 3D surface descriptors, called "surface finish parameters" related to autobody manufacture. These parameters have been accepted by the international community and are now approved by the International Standard Organisation (ISO) and embodied in new draft standards approved in 2001. The author is proud of the fact that the research community has accepted these new 3D parameters.

However, before the detailed Autosurf work can be presented, background aspects like processes and techniques needs to be understood. Therefore, the basic family of forming processes and the nature of surfaces needs to be explained and this is the subject of the remainder of this opening chapter.

1.2 The forming processes and deep drawing

The most frequently used process in autobody manufacturing is known as "deep drawing". Deep drawing can be any process employed to produce a three-dimensional (3D) product from a flat sheet (called a blank).

One of the basic operations as far as autobody manufacture is concerned consists of forming a circular blank formed into a cup-shape. This can be achieved by moving a punch toward a die with the blank held in position by a plain blankholder. One of the classic examples of this is shown in Figure 1.1 where a flat sheet is made into a domed shape by a semi-circular punch being pushed in this case upwards.

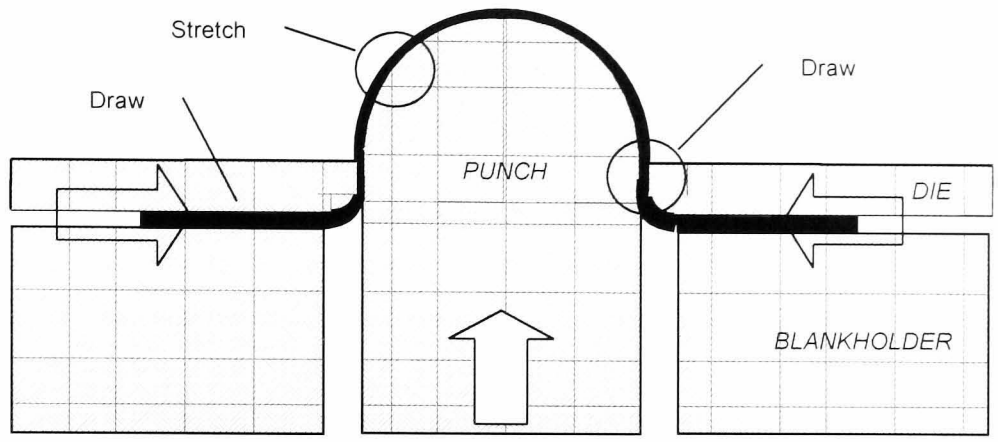

Figure 1.1– Schematic description of a simple cup-forming process

Simplistically, three regions of deformation can be identified. Firstly, there is the pulling and stretching of the work material over the shape of the punch. This is essentially a 3D deformation and it results in a thinning of the work material as it follows the shape of the punch. In some extreme cases, this can result in thinning of up to 50% [Elliot et al 2000(b)]. Secondly, there is stretching along the vertical sides of the punch as the work material is pulled upward. This results in a unidirectional stretching of the material. Thirdly, there is the horizontal pulling of the work-material through the blankholder. This results in thickening of the work-material because it is drawn radially inwards and compressed. Wherever there is plastic deformation, there is the possibility of work-hardening which further complicates the process. This combination of processes makes the study of deep drawing a very complex matter.

As a means of understanding and predicting things like the forces, various modelling has been done using rules and design laws. A useful overview of techniques is the "Handbook of Metal Forming" by Lange [Lange 1985]. Good progress has been made in recent years in modelling plastic deformation processes by the use and development of Finite Element Modelling (FEM) techniques. However, although they are very good for the modelling of bulk deformation, the complex interfacial conditions make accurate prediction difficult. Thus, unfortunately, the prediction of friction forces in still a limiting factor. This is because in deep drawing, the interfacial friction conditions are complex and several factors complicate the situation. For example, firstly, the sheet has topography that results in intermittent contact between the sheet and the die. Secondly, a lubricant is used but here is no guarantee that it reaches all the contact points. Thirdly, the sheet surface can be plated so that

there are two materials involved in the deformation process. These are now considered in more detail.

1.3 Complexities in the deep drawing process

Focusing on the contact generated between the sheet steel material and the tool during the deep drawing process, it can be noted that:

At the micro level, a surface can never be perfectly flat. This is illustrated in Figure 1.2, which is a plan view of a surface having a micro topography in the form of ring shaped craters.

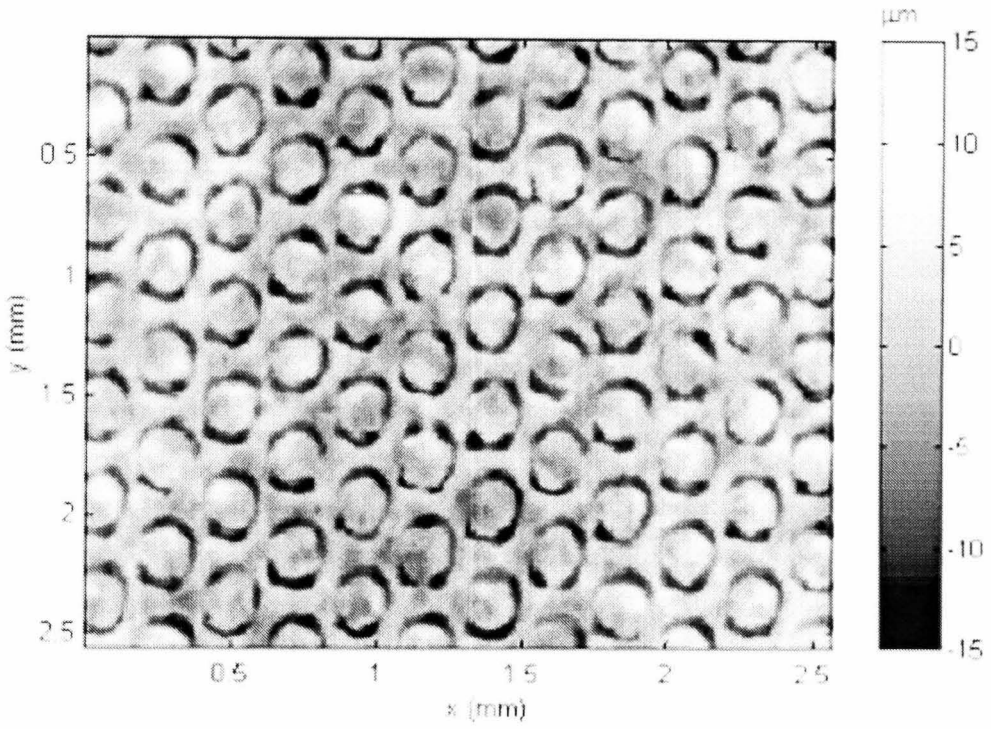

Figure 1.2 - 3D representation of an EBT texture of a steel sheet used in deep drawing

This is a surface produced especially for deep drawing by the Electron Beam Texturing (EBT) process in order to minimise friction and galling. When such a surface comes into contact with a flat forming tool, the peaks are the first part of the profile to contact the tool. Because of the circular craters, the individual contacts are in the form of a series of rings that trap the oil in the enclosed valleys. Such surfaces designed for deep drawing are called "textured" surfaces in that they are produced with specially designed 3D micro-shapes (texture or surface topography). This means that peaks are the first to contact the tool and can be deformed by it. Such valleys have two advantages as far as deep drawing is concerned. Firstly, they can contain oil, which

minimises friction. Secondly, they can retain any debris created and thus prevent it lying on the surface. There are a variety of different processes like EBT, which create textures to minimise friction and provide oil retention. The most commonly used processes are described in Chapter 2. Because these various textures have different geometries, the surfaces will behave differently in terms of friction, when employed in deep drawing processes.

The steel manufacturing process and the techniques to measure surface topography are described in Chapters 2 and 3.

The second complication is that surfaces are not dry (see Figure 1.3): in fact various types of liquids are applied at several stages of the autobody manufacturing processes to do things like prevent oxidation and to provide lubrication. The situation is further complicated by transportation factors. The sheets are transported between factories, plants and processes. Oil can be applied between the stages. The sheets can be transported in the form of stacked flat sheets or rolls. Oil migrates across the sheet surfaces over time and the time between stages can be days. This all means that migration across a sheet surface leaves dry spots, no lubrication. Thus, during pressing, the friction can vary significantly. This means that the classic friction laws (i.e. Coulomb) cannot always be employed. Furthermore, the ability of a surface to retain oils can depend on several factors (i.e. chemistry or surface micro-geometry).

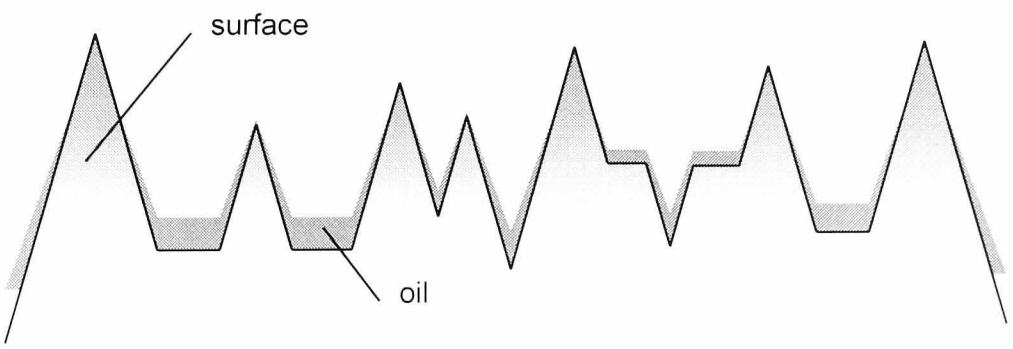

Figure 1.3 - Schematic representation of a lubricated steel surface

During this research work, oil retention (the ability of a metal sheet surface to retain oils within the surface valleys) was perceived as an important factor and it seems to have been largely ignored by the researchers of deep drawing processes. In this research programme, this ability of a surface to retain oil

was considered to be important. A new experimental procedure to measure oil retention was therefore deployed and the experimental work performed (design, analysis and results) which is presented in Chapter 4.

The third complication is that the autobody sheets can be coated with zinc to prevent corrosion. This means that, during plastic deformation, we are not dealing with one single material but layers of different materials, each of which will have different properties as far as plastic deformation is concerned. This is complicated by the fact that the coating generally follows the surface topography. However, the coating is not necessarily of constant thickness, which means that the topography is modified locally and the mechanical and chemical properties will not be constant over the surface. The zinc coating can be applied using different techniques and these can influence the process. Since this coating is important in the deformation process, the various techniques will be described in Chapter 2 which is concerned with the steel manufacturing processes.

1.4 The overall picture

Each of the above-mentioned processes and phenomenon interact with each other and all together will affect the final panel quality. Therefore, considering the technical elements inherent at the manufacturing process of an autobody panel, it is possible to isolate the phenomenon relevant to this investigation.

These elements are shown schematically in Figure 1.4. They can be summarised by the following statements:

- The forming (deep drawing) processes are affected by the material's mechanical properties and friction.
- Surface (topography and coating) is a major element that influences lubrication and oil retention, hence friction. These influences are still partially unknown hence requiring further investigation.
- Hence, forming cannot be studied without considering lubrication and friction and the sheet material's surface topography.

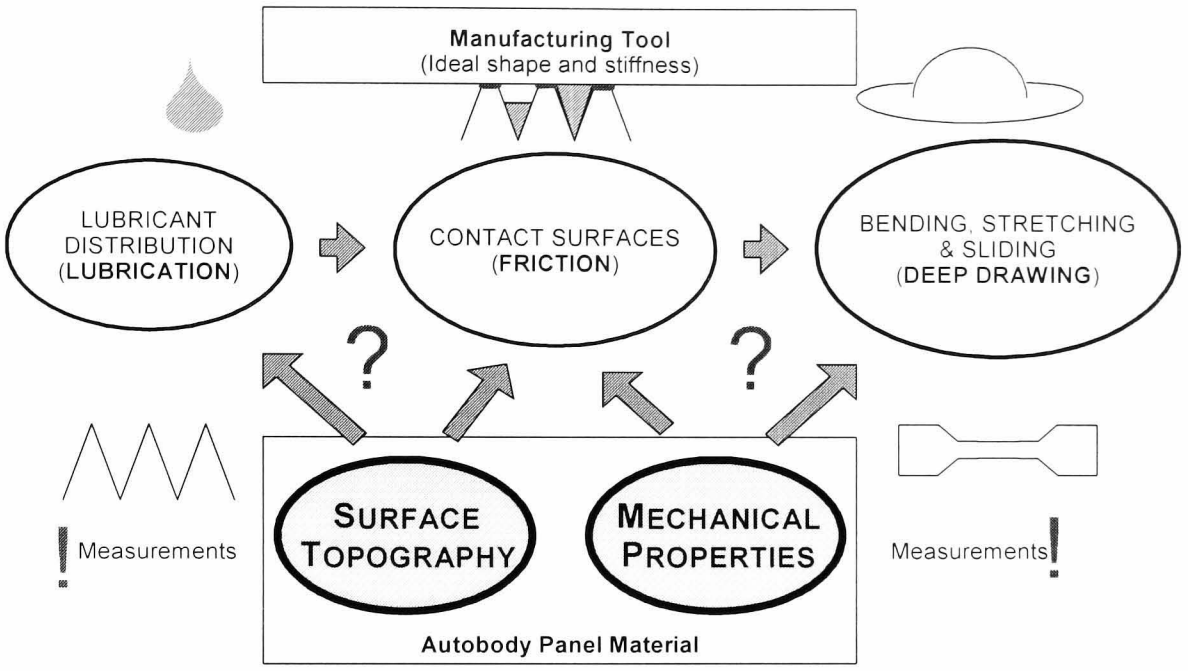

Figure 1.4 - Interactions between material characteristics and processes

This thesis is constructed in such a manner as to reflect the order of the autobody sheet manufacturing processes and the experimental work undertaken to model the deep drawing process. The thesis chapters's are as follows:

- **Chapter 2** will give an introduction of the manufacturing process of steel metal sheets and texturing techniques.
- **Chapter 3** will describe the state of the art in surface topography (what to measure and how to measure it).
- **Chapter 4** will detail the experimental work on oil retention.
- **Chapter 5** will detail the experimental work on friction.
- **Chapter 6** will compare the results of the latter with a laboratory forming experiment.
- **Chapter 7** will draw the conclusions.

1.5 Summary

- ✓ Autobody panels are one of the most important car components since the customers immediately perceive their quality.

- ✓ Deep drawing is a family of forming processes used to manufacture autobody panels.

- ✓ The steel sheet, during a deep drawing operation, is bent and stretched.

- ✓ The material flow is controlled through friction, which, in these processes, is still a complex phenomenon.

- ✓ The main reasons why friction is difficult to predict are related to the surface topography, the oil on the surface and the coating.

- ✓ The aim of this work is to improve the understanding of deep drawing through the extensive study of friction, lubrication and the correct design of panel's surface topography.

2. The steel sheets for the automotive industry

2.1 Introduction

Depending on their applications, autobody panels need to meet a number of requirements. Typically these are strength, appearance and corrosion resistance [*Wilson 1997*]. Strength is needed not only for normal operation but also for crash resistance. These are linked to improved safety, which is one of the driving forces the industry is imposing on itself. The cosmetic appearance is critical since the customer uses this as a measure of his or her confidence in the quality, particularly when the car is in the showroom. This is also linked to the car design and the ergonomic appeal. Corrosion resistance is perceived by the customer to be part of the ongoing quality. It is assumed to be a built in part of the car "performance". There are of course many other things that contribute to the success of a car as far as the customer is concerned but these three are the ones that are determined by the autobody panels. These three things are related to both the base material and the plating of a autobody panel. Thus, in order to meet these three requirements, the steel employed needs to be processed in a way that provides the highest strength, the best appearance and high corrosion resistance at minimum cost. This means that careful attention should be paid to the body panel base material (substrate) and the plating (surface) since both will influence these three things.

Material characteristics can be therefore divided into the two mentioned categories (see Figure 2.1):

- **Substrate** properties – mechanical properties represent the ability of the material to oppose external forces without breaking.
- **Surface** properties – the term "surface" represents the combination of micro-geometrical (topologic) and micro-mechanic/chemical characteristics. The surface topography is perceived to be of prime importance for material behaviour during the panel manufacturing process [*Siekirk 1986, Staeves et al 2001*]. The surface topography is the characteristic on which this work will focus.

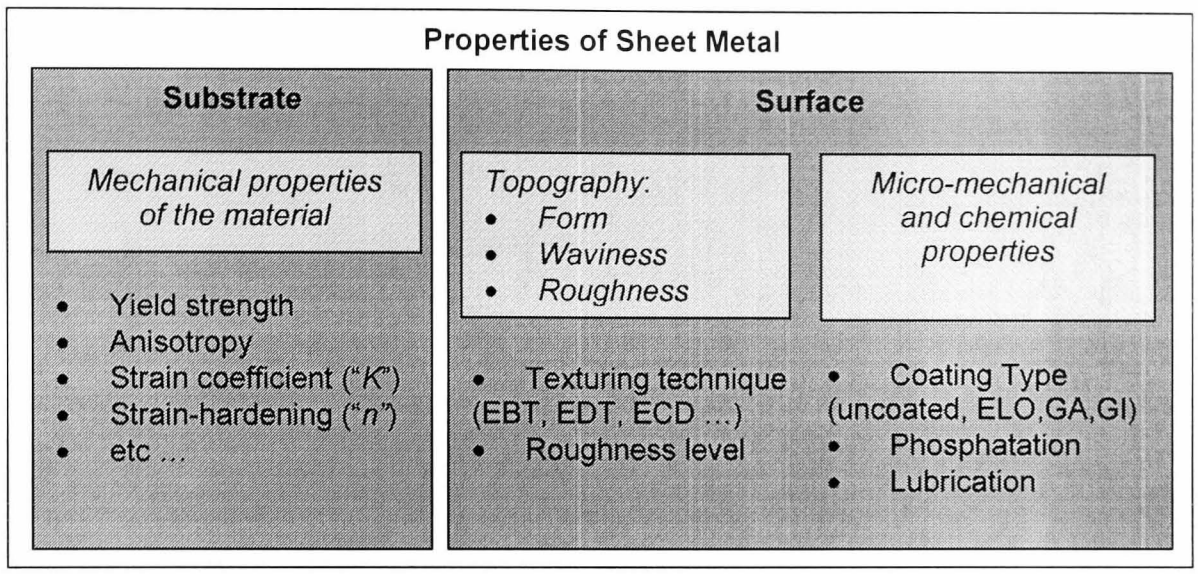

Figure 2.1 - Properties of Sheet Metal

The steel sheet manufacturing process is the same one for all the steel shapes up to the hot rolling stage (see Figure 2.2). The sheet mechanical properties are mainly imparted to the material during the final cold rolling stages but they will be also influenced by conditions of the hot rolling processes like the cooling processes and of course, the base composition of the steel itself.

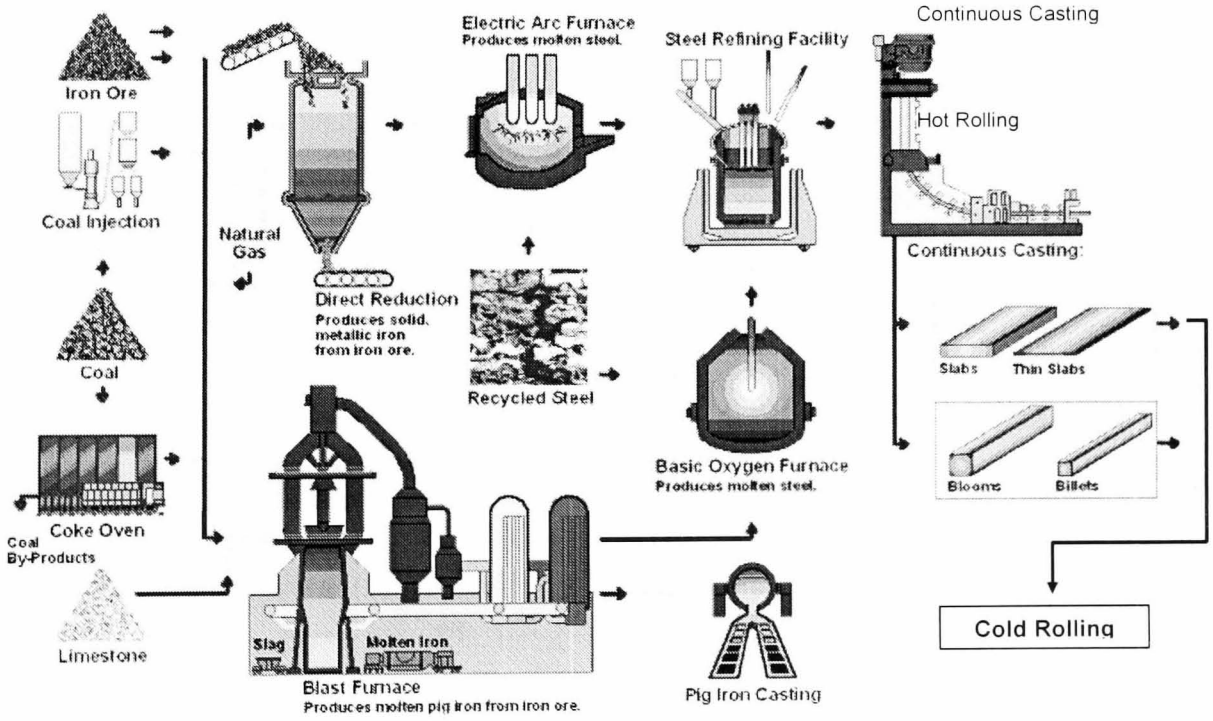

Figure 2.2 - Steel manufacturing process from iron ore and coal to cold rolling

Furthermore, surface properties are almost exclusively determined by the cold rolling conditions. Because of the importance of this cold rolling stage of the sheet metal deformation processes, cold rolling is detailed below.

2.2 The cold rolling process

The cold rolling process employs cooled thin slabs, one of the products of continuous casting (see Figure 2.2). Thin slabs are usually in the form of a coil (sometimes obtained from the welding of a number of slabs) and are named "cold strips".

The cold rolling process consists of a series of stages imparting different forming conditions to the steel strip, those being (see Figure 2.3):

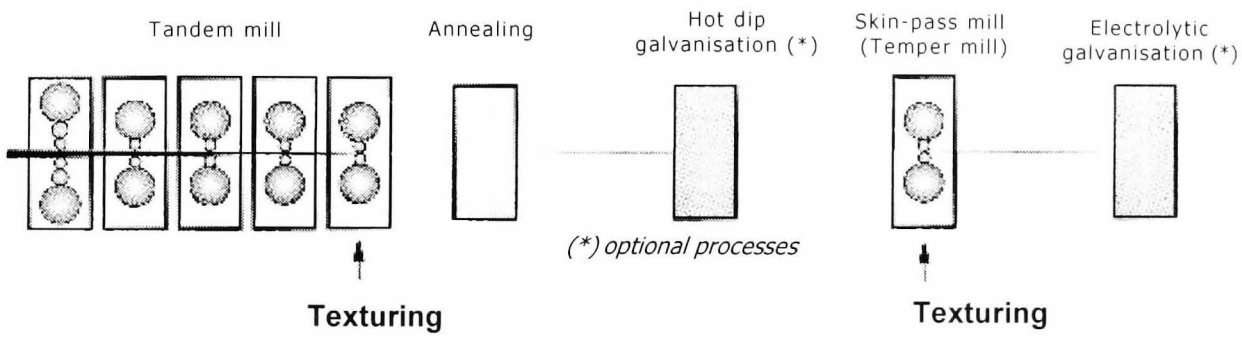

Figure 2.3 – Cold Rolling Process [*Amici et al 2001*]

- **Tandem mill** – this is the "first" process in the cold rolling set of processes. It is employed to *reduce the material thickness* to "almost" the target one. The Tandem mill is usually fed with hot-rolled steel of the appropriate grade, cleaned of scale and surface oxidation and appropriately lubricated. The heavy thickness reduction causes the material to workharden. Hence, to avoid the material cracking in subsequent operations, it undergoes an annealing stage.
- **Annealing** – this is a thermo-chemical treatment employed to *reduce workhardening* and achieve the desired grain dimensions. It can be performed in coil-batches or while the sheet is rolling (in which case it is named "continuous annealing").
- **Hot dip galvanisation (GI) and hot dip galvanisation with annealing (GA) –** are the zinc coating process. The difference between GI and GA is explained below. The zinc coating is applied to protect the

steel sheet from corrosion. In the diagram of figure 2.3, it is called "hot dip" because the sheet is literally dipped in the galvanising solution. This term is used to distinguish it from other galvanising processes like electrolytic galvanisation. In the work described here, all three galvanisation processes were used. They are described in the next section.

- **Skin-pass mill –** during this last rolling operation the final *surface topography* is applied to the material. There is virtually no thickness reduction. The roll imparts texture to the steel in a negative-positive manner. Several roll-texturing techniques are currently available, and they are discussed in detail in the following sections. It is important to notice that, sometimes the surface topography application starts earlier, at the tandem mill stage (by employing one or more textured rolls). This is performed to impress more complex patterns to the sheet metal surface.
- **Electrolytic Galvanization (ELO) –** if the coating required is not to be hot dip process (i.e. either GA or GI) but rather an electrolytic coating, it is applied after the final skin-pass process. This is because ELO coating exhibit good optical properties and any further texturing might deteriorate them. Due to the good optical quality, the ELO coated materials are frequently employed to manufacture both autobody external panels and white goods.

Therefore, from the general description of the above stages, the whole cold rolling process provides:

- The required final thickness.
- The correct mechanical properties.
- The final surface topography.
- The required flatness.

To further understand material behaviour it is now necessary to give a more detailed description of the zinc coating and texturing techniques.

2.3 Zinc coating techniques

During the manufacture of the sheet, a 5-10μm thick zinc-layer is applied to the steel surface using one of three different techniques. Scanning Electron Microscope (SEM) pictures of the zinc coatings (before deep drawing) produced by these processes are shown in figure 2.4.

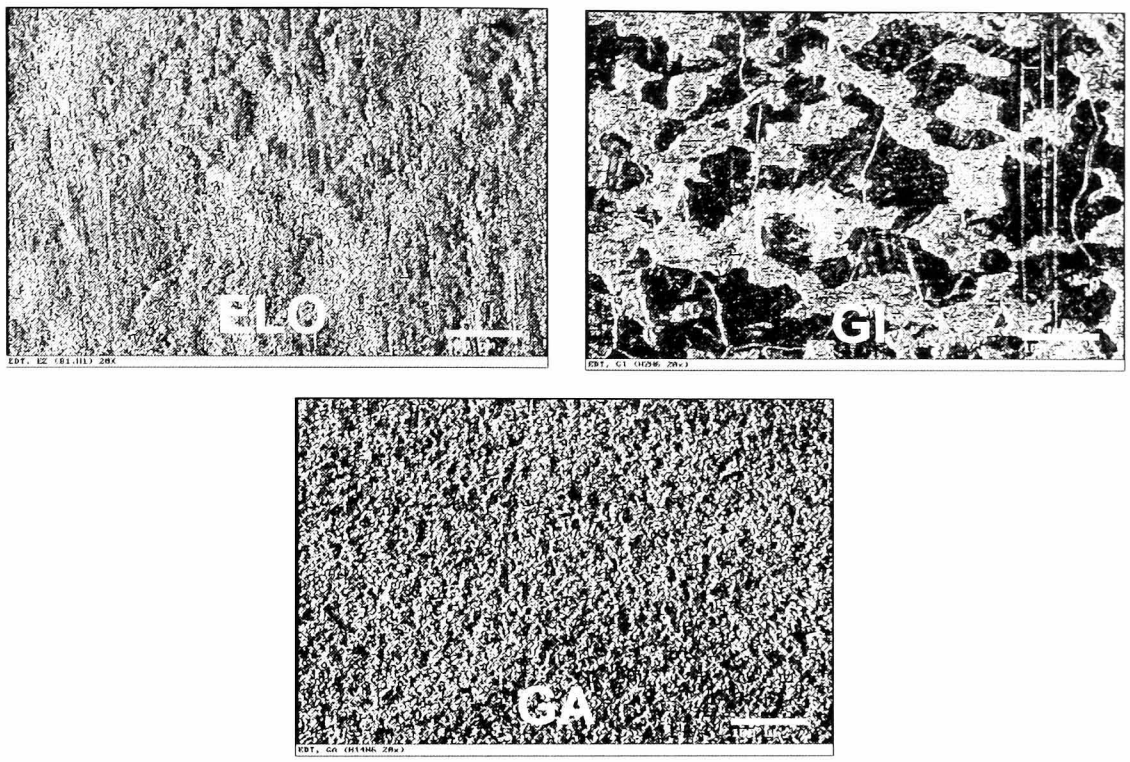

Figure 2.4 – Optical microscope images of different zinc coating techniques over similar substrates and texture materials at the same magnification

The three zinc coating processes are:

- Electrolytic deposition (**ELO**) – electrolytic deposition after temper rolling.
- Hot dip galvanisation (**GI**) – hot zinc bath usually before temper rolling.
- Galvannealing (**GA**) – similar to GI, but followed by an annealing process.

The surface characteristics of these coatings are markedly different from each other.

The ELO coating has the coating "grown" on it by electro-deposition and, since the bond between coating and substrate is chemically based, there is very high adhesion. The surface resembles a plane with "blobs" on it at the deposition initiation sites. The longer the deposition time, the more blobs there are. In this case, the deposition time is such that the blobs build up in multiple layers to a thickness of tens of microns. Hemispheres sticking up from the surface can simplistically represent the "blobs" one can see. However, it must be remembered that the substrate base surface will not be flat but textured by the previous skin-pass process so the blobs will follow the undulations of the texturing.

The GI and GA coatings are more complex than ELO coatings because the coating is applied by dipping the sheet in a bath of molten zinc. The zinc will adhere to the steel due to simple casting and minimal diffusion. In the GI coating process, this is all that the coating process consists of, i.e. a cast zinc coat on the steel substrate. The adhesion between coating and substrate is just that of conventional casting, i.e. mechanical locking and some diffusion. If the GI zinc cast sheet is then heated, or annealed, the process is called "galvannealing" or "GA". The galvannealing temperature is high enough for crystalline growth of the coating to occur as well as significant diffusion between the coating and substrate. This means that the bond between the coating and substrate is higher with GA than with GI. The exposure of the coating and substrate to high temperatures means that the coating is complex, consisting of up to four Fe-Zn phases, each of which will have different hardness's and therefore strengths [*Carless 2001*]. Due to the manufacturing process, GI coatings are effectively zinc castings on sheet steel, whereas the GA coatings are made of a number of Fe-Zn alloy layers of increasing adhesion. The GA surface structure is thus more crystalline than the GI structure. It resembles a cavern-like structure with numerous microscopic cracks, overhangs, undercuts and porosities. Indeed, a useful analogy is sea coral. The GI structure is less crystalline and cavern-like, resembling more of a normal dendritic cast structure.

The above descriptions of GA and GI structures would seem to indicate that they are clearly two separate classes as far as surface structure is concerned. This is not the case because there is some overlap, for example, if the zinc bath temperature is high and the annealing temperature is low, the GA structure may be little different to the GI structure.

2.4 Texturing techniques

Texturing is applied to the steel by the temper rolls (sometimes also by the tandem roll) in a positive-negative manner. The result is that the imprint of the rolls remains on the sheet surface. Whatever the pattern is on the rolls it is transferred to the sheet and therefore, the different texturing techniques will lead to very different surface topographies, as shown in Figure 2.5. These are SEM photomicrographs of three different topographies produced by the

three processes: Electro-Discharge Texturing (EDT), Electron-Beam Texturing (EBT) and Electro-Chromium Deposition (ECD) texturing. The main difference between the first two texturing techniques (EDT and EBT) is that the former applies random valleys to the surface, while the latter applies a truly deterministic pattern. The last technique (ECD) applies randomly distributed deterministic-shaped valleys (hence a pseudo-deterministic pattern). The idea underlying a consideration of deterministic vs. random textures is related to the controllability of the texturing process. Better controlled processes (i.e. EBT) should allow one to "engineer" the surfaces and hence to lead to a more predictable surface-to-surface contact behaviour. Unfortunately, the deterministic patterns are easier to perceive with human eyes (i.e. orange peel look) and this might be a cause of rejection by the automobile customer. These texturing processes will now be described.

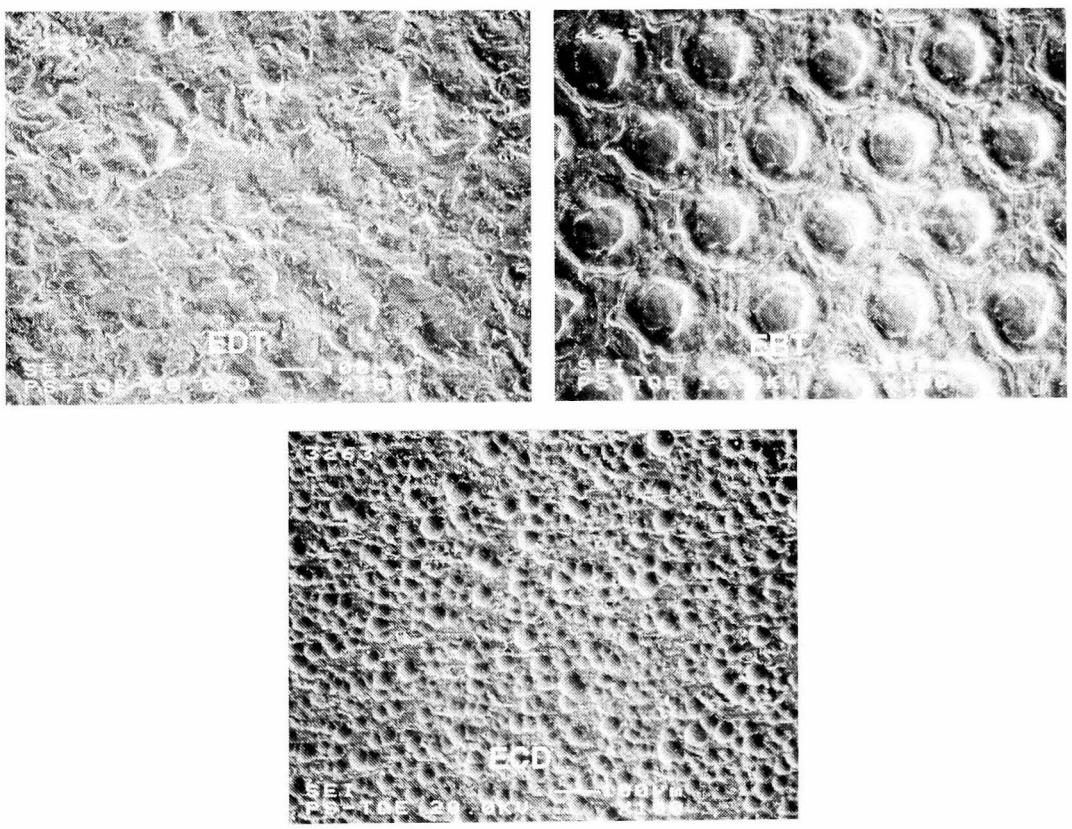

Figure 2.5 – Metal surface topographies obtained with the different texturing techniques

Until a while ago, the so-called shot-blast texturing (SBT) technique was the only texturing process used. It had shortcomings due to particles which embedded in the surface and the random nature of the topography that did not lend itself to providing good lubrication. Hence, to overcome the disadvantages of the SBT process, new processes were developed which did

not have these disadvantages and which provided structured topographies, which are able to enable the lubricant to be retained. Nowadays, the three most popular processes are Electro-Discharge Texturing (EDT), Electron-Beam texturing (EBT) and Electro-Chromium Deposition (ECD) texturing. These produce what are described as "engineered" surface topographies. They will now be described.

- ***Electrical Discharge Texturing*** (**EDT**) employs a number of electrodes subject to an cyclic electric impulse which are moved radially and axially toward a rotating roll [*Aspinwall et al 1992*] as shown in Figure 2.6.

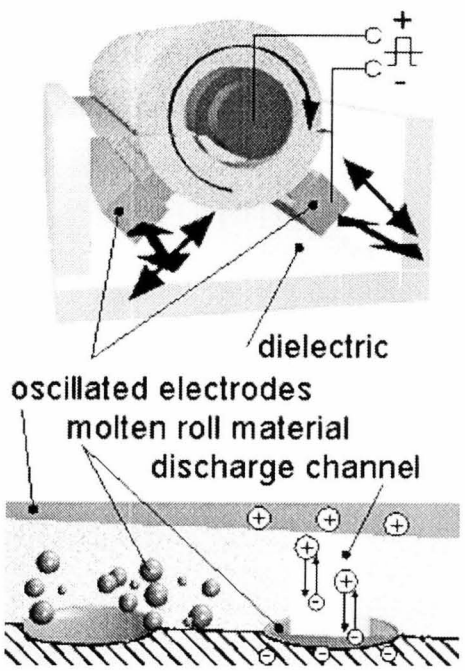

Figure 2.6 - Electrical Discharge Texturing technique [Staeves et al 2001]

Craters on the roll surface are created by numerous "sparks" which jump between the electrodes and the roll. This is the same thing that happens in the conventional electro-discharge machining process. The surface thus consists of numerous small craters caused by the spark discharge, as can be seen in the SEM photomicrograph of figure 2.5. The craters are randomly distributed across the surface. The main advantage of this technique is that the texture can be created regardless of the roll hardness. For this reason EDT is now the most common texturing technique.

Several process parameters can be controlled to change texture characteristics (typically average crater dimensions). Because of the reasons mentioned above, EDT can be considered to create a *random surface topography*.

- ***Electron Beam Texturing*** (**EBT,** which is often referred to as "Sibetex") uses an electron beam to melt the surface of the roll material and create small craters, much like EDT (see Figure 2.7). The difference is that with EDT the craters are randomly distributed whereas with EBT the craters are arranged in a structured pattern. This regular pattern can be seen in the SEM photomicrograph of the EBT surface shown in figure 2.5. Technically, the electron beam is extremely fast and the energy pulse easy to control. This allows a good surface reproducibility. During EBT the roll is rotated and moved axially in a vacuum chamber, to control the crater position and it can create very complex patterns.

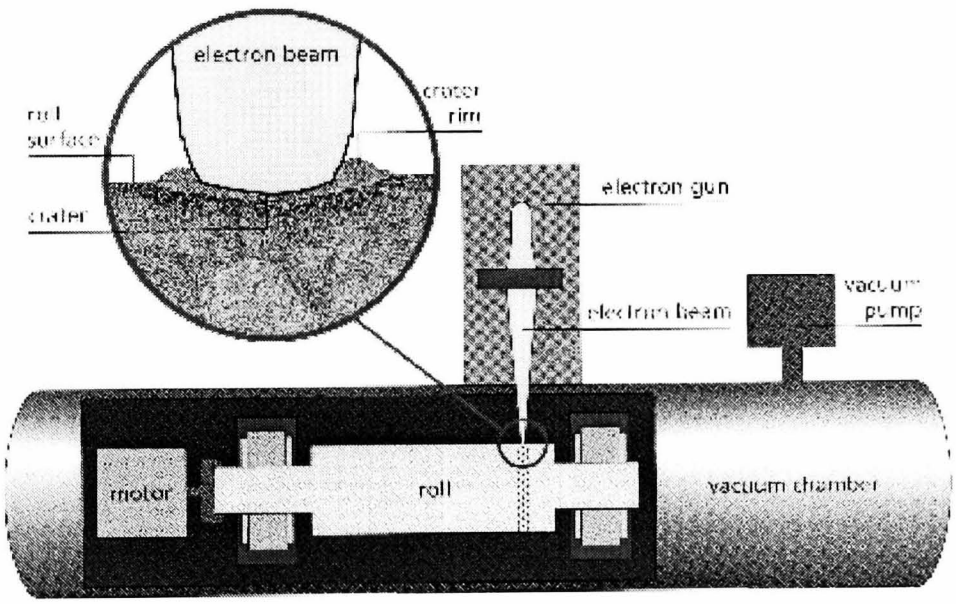

Figure 2.7 - Electron Beam texturing technique

Although the final texture can be extremely complex, the resulting *surface topography is always deterministic* and the pattern identifiable with statistical algorithms [*Porrino et al 2000*].

- The latest and least-known texturing technique is the ***Electro-Chromium Deposition*** (**ECD,** which is referred to as "Pretex"). This texture is created by the electro-deposition of chrome spheres onto the roll surface.

This is achieved by immersing the roll into a reactor filled with chrome electrolyte with a number of electrodes forming a cage [*Behrens 2000*]. Controlling the electrical potential between the anode cage and the roll (cathode) causes spheres to form on the surface of the rolls, as shown in Figure 2.8. The result of this deposition is a hard-chromium "coating" consisting of a large number of spheres distributed across the roll surface in a random manner. When a sheet is rolled, these spheres create small crater depressions on the sheet surface as shown in the SEM photomicrographs of figure 2.5.

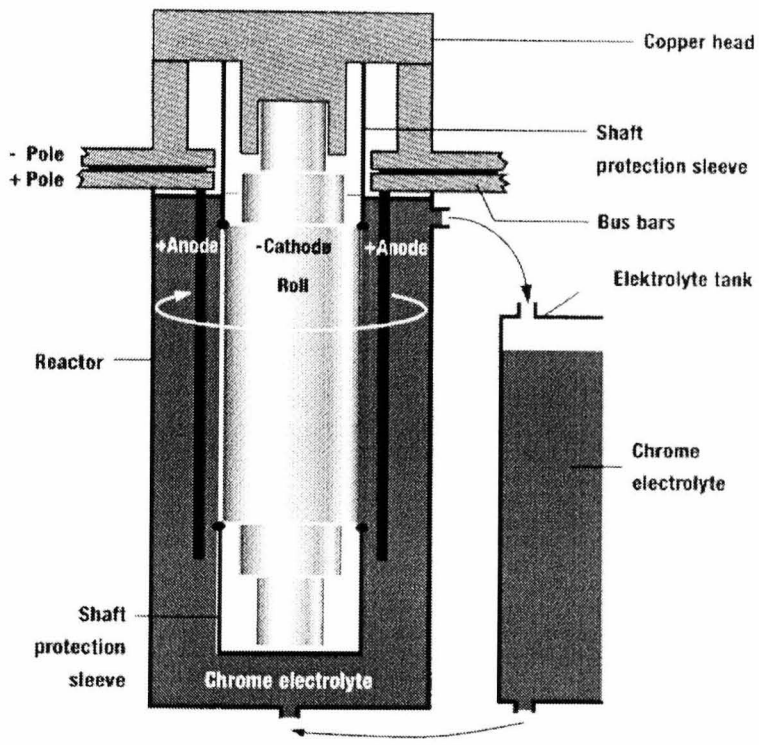

Figure 2.8 – Electro-Chromium Deposition texturing technique

Although the generated chrome "drops" are spherical, this texturing technique is considered to generate *random surface topographies*.

2.5 Measurements of steel sheet properties

In order to study the effect of the various surface topographies explained above on the efficiency of the forming processes, an assessment of the steel sheets characteristics is required. The main characteristics are the following:

- **Mechanical properties** – this group of metal properties is extremely important to quantify the "formability" (ability to undergo a forming process) of the steel sheet. These characteristics had been long studied by many researchers in order to model the forming processes (strain and stress analysis) and are not the objective of this thesis. Therefore in the following chapters, when the substrate or mechanical properties are referred to it will be the yield strength value.
- **Zinc coating** – the zinc coating is extremely important with respect to the formability. As stated by Vermeulen et al [*2001(a)*], during friction processes the coating can powder or flank (loss of small particles) hence leading to scratches on the final product. Although for a complete quantification of the ability of a coating to powder (i.e. grade of adhesion), a chemical analysis would be required (and this is not within the objective of this thesis). Therefore, the coating will be simply referred to as "type of coating".
- **Surface topography** – the topological characterisation of autobody sheet metal and its effect on forming is the main objective of this work. For this reason all the following chapter (chapter 3) will be dedicated to the techniques employed to measure surfaces and their mathematical modelling.

2.6 Summary

- ✓ The properties of the steel sheet are important for the correct design of the autobody panel's manufacturing processes.

- ✓ The manufacturing process of a steel sheet for the automotive industry differs from the process of any other steel from the cold rolling stage onward.

- ✓ During cold rolling a zinc coating is frequently applied to protect the steel from corrosion.

- ✓ The main zinc coating techniques are ELO, GI and GA. These produce very different surface characteristics.

- ✓ During cold rolling the final surface topography is also applied (during temper mill and sometimes also tandem mill).

- ✓ The texturing techniques used in industry today are EDT, EBT and ECD.

- ✓ The effect of the surface topography on forming of steel sheets for the automotive industry requires scientific investigation.

3. Characterisation of surface topography

3.1 Introduction

Steel sheet surfaces need to have good oil retention capabilities, and good consistent frictional behaviour in order to achieve good performances in deep drawing operations. To achieve this, the current practice is to texture the rolls employed in the steel sheet manufacturing process. In turn, the rolls impress in a positive-negative manner its texture to the steel sheet surface. The final texture (surface topography) is expected to improve sheet's oil retention and reduce friction. In order to assess the topography, we need a means of measuring, assessing and characterising it. Simplistically, this involves three steps.

Firstly, the surface is measured using an instrument that traverses a stylus (similar to a record stylus), in a line across the surface. The detailed instruments and techniques used to do this are described below. The vertical movements of the stylus correspond to the surface deviations and hence the surface topography because a 2D data set (of X-Y information) of heights and corresponding horizontal positions is obtained. Such a 2D data set will define the topography along the line traced. If the stylus is raster scanned over the surface, a 3D data set (of X-Y-Z information) is obtained which provides a map of the surface or as it is often called, an areal scan. Historically, a 2D profile was considered enough to describe a surface, although with just a simple line profile, directionality information is lost. Nowadays, many surface topography instruments have the capability to perform 3D measurements by simply measuring multiple parallel 2D profiles, forming a grid of data points i.e. a raster scan to represent the surface topography. Because it is only 3D information that gives directionality and texture information, during the work described in this thesis, only 3D surface representation will be performed.

Secondly, the data set is analysed statistically (or otherwise) to produce parameters, which characterise the surface. This begs the question as to what parameter should be used to describe the surface. This is the big question because we want parameters that are robust, easy to use and which relate to some physical aspect (i.e. oil retention). Many parameters have been suggested, some of which are defined in ISO standards. These are mostly 2D

parameters but they cannot describe directionality so one must turn to 3D parameters if we are going to apply parameters to sheet metal forming. Little has been published on 3D characterisation. However, some work has been done in an attempt to define 3D parameters that are not simply extensions of 2D parameters. These will be described later in this chapter.

Thirdly, such measured parameters can be compared with the ideal values to ascertain if the surface is acceptable or not. The values of ideal parameters are determined through careful research in the laboratory and these can then be used for quality control on the shop floor.

These steps will be explained in more detail in the following sections in the following order. Firstly, the most commonly used instruments are described then the measurement techniques and finally a description of published and proposed 3D parameters.

3.2 Instruments used to measure surface topography

Technically, contact instruments are still the most used. Although on soft zinc coatings (i.e. GI coatings) the surface might be damaged and non-contact (optical) instruments might be preferred. Several optical methods have been developed so far. Laser scanners or faster CCD cameras as well as interferometers are examples of these principles.

- **Stylus** based instruments [Whitehouse 1994] are the most commonly employed devices to measure surface topography on steel sheet surfaces. The measuring method is based on the direct contact between the sensor (see Figure 3.1 [Scheers 1999(b)]) and the surface.

  The main advantage of stylus instruments is that the technique is well known and applicable to most kinds of surfaces. Some disadvantages are that it can deform surface asperities elastically or even plastically which can influence the measured result and due to the slow traversing speed the measuring times will be long, especially for 3D measurements.

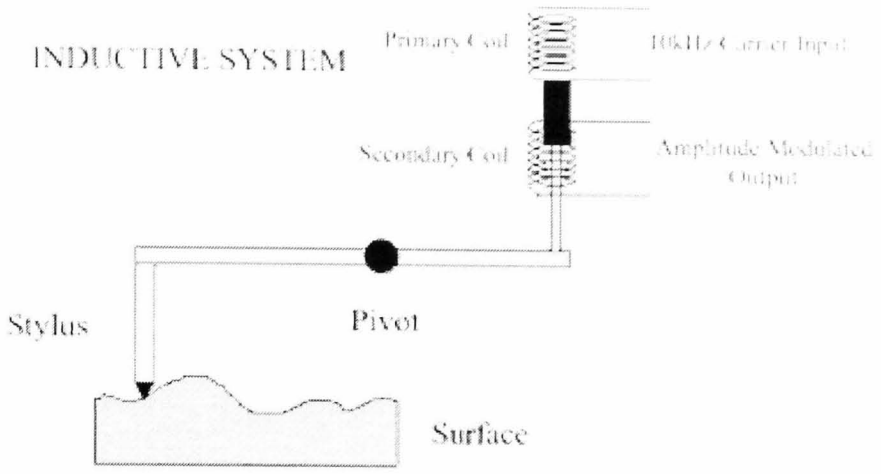

Figure 3.1 – Stylus working principle

- **Optical** instruments, compared to stylus instruments, have the advantage of measuring in non-contact mode and hence, do not affect the surface at all. Optical instruments are based upon two measuring principles:

    - The **focus detection** instruments work in a similar manner to stylus instruments (see Figure 3.2 [Scheers 1999(b)]) except that instead of a stylus the measurement is performed by a light beam, which is focused onto the measurement surface as a spot of about 1µm in diameter. The measuring speed is often considerably greater than that of stylus instruments and is dependent on the control system, which keeps the light beam in focus at the surface. Since this method completely relies on how accurate the focus can be detected on top of the surface it is sensitive to high slopes in the surface topography. The critical angle of surface inclination is often between 10-15 degrees [Scheers 1999(b)]. For steel sheet surfaces the maximum slope is between 5-10 degrees hence [Scheers 1999(b)], steel sheet surfaces are suitable for measurement with focus detection systems.

      The working principle: *a small lens directs a laser beam to the surface, and the reflected beam is fed to a photodiode focus detector. The movement of the focusing lens is recorded as the height variation of the surface.*

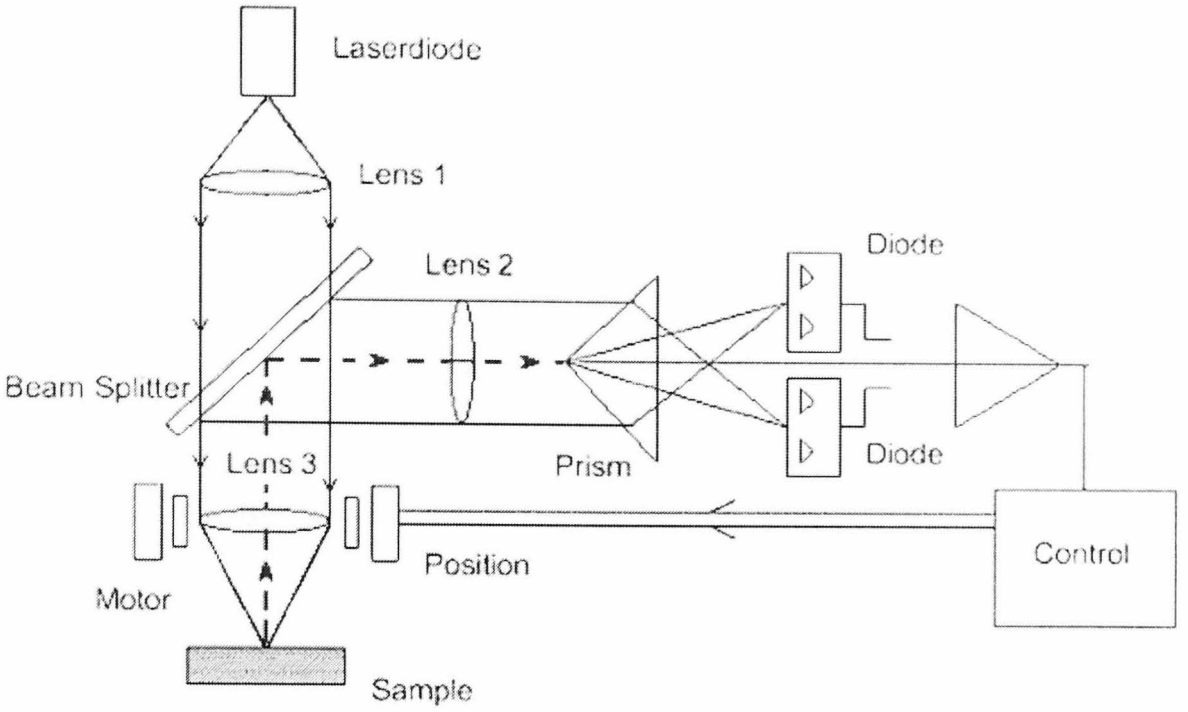

Figure 3.2 Focus detection principle

- Within the instruments based on the **interferometry** principle, the Vertical Scanning Interferometers (VSI) are the most common ones. VSI instruments are fast, only a few minutes are needed to perform a measurement. Depending on the optical set up, it is possible to measure areas from a few square-microns up to 50mm^2. The main advantage of a VSI instrument is the short measurement time. The main disadvantage is the limited vertical range (circa 0.5mm). Nevertheless, for flat surfaces such as steel sheets, the vertical range is more than required even for large measurements. Another disadvantage, which is common to all optical instruments, is the sensitivity to contaminants such as oil and dust, which may yield inaccurate results.

3.3 Surface topography representation

The surface measurement obtained from the surface can be described as a signal. Signals can be represented with a spectrum of wavelengths, ranging from the shortest (lower bound is the sampling interval between two consecutive measured points) up to the highest wavelengths (of the size of the measurement length). The different wavelengths in the surface profile signal can be divided into intervals, which represents:

- **Form** is long wave errors, caused by i.e. thermal distortion, misalignments in slideways, and errors in rotating machine components.
- **Waviness** is often a result of improper manufacturing. An example of this is the uneven wear of the roll causing scarce material flatness.
- **Roughness** is often a direct result of the manufacturing process. For example, marks made by textured rolls when rolling steel sheets.

Since the sheet metal employed in deep drawing is bent and stretched, form and waviness are not of interest. Therefore, for the purposes of this work, only roughness will be considered.

In order to evaluate the surface roughness, the longer wavelengths (represented by the "form" and the "waviness") must be removed from the surface profile measured by the instrument.

Form is typically removed by subtracting a regression line (or polynomial curve), while waviness is removed applying a high-pass filter. There exists no absolute definition stating what constitutes roughness, waviness, and form. For this reason, during the measurement taken for the purposes of this work, the cut-off is chosen according to recommendations given by standards, such as the [ISO 4288].

3.4 Surface roughness parameter categories

When the roughness is isolated from the acquired signal, it is possible to calculate a surface parameter. Every surface parameter relates either to "peak heights" (Amplitude) or "peak distances" (Spatial) or a combination of the two (Hybrid). Due to the necessity to describe material behaviour, a category of surface parameters was created and it is known as "Functional" and it can include parameters from any of the previous three as shown in Figure 3.3.

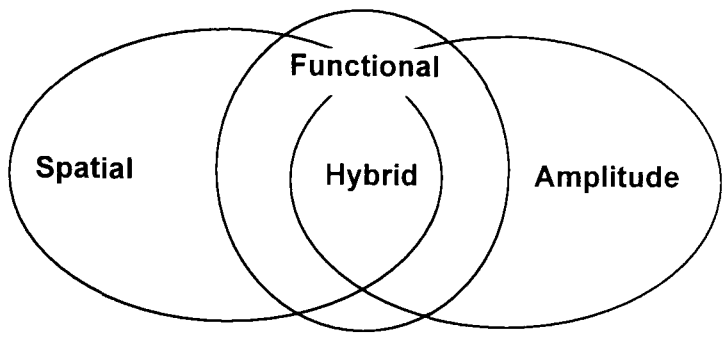

Figure 3.3 – Characterisation Approaches

The search for better surface characterisation parameters has led to a parameter rash, in which many users invented their own parameters in order to describe a specific texture or function [Whitehouse 1994].

A large volume of literature has been published on the various relationships between deep drawing performance and 2D topography. It is not within the scope of this research work to review the 2D literature because 2D parameters cannot provide directionality or texture information. Readers interested in pursuing the subject of the influence of functional performance in general will see from [Griffiths 1998] that the same surface characterisation affects different functions of the products.

Since most surfaces interact with a 3D environment, it has become increasingly obvious that an actual understanding of the connections between surface topography and functional performance can be achieved if the surface is analysed in 3D space. 3D surface measurement can then be analysed in a manner similar to 2D (i.e. form removal moves from regression line to regression plane) or employed to characterise properties impossible in 2D (such as directionality and areal representations).

3.5 Currently published 3D surface parameters

There has been some work done on 3D surface parameters but nowhere near as much research as has been done on 2D parameters. There are essentially three research groups who have done work relating some aspect of 3D surface topography to functional performance. The work is reviewed below.

The first major proposal came from an EU funded project led by Birmingham University. In the final report, a primary set of fourteen parameters (the "Birmingham 14") were proposed which used the letter "S" to mean surface

as opposed to "R" parameters for profiles. The complete list of Birmingham parameters is reported in Table 3.1 below [Dong et al 1994], while their mathematical definitions are contained in Appendix 1.

Name	Type	Description / Functional Characteristics
Sq	Amplitude (2D Extension)	Root Mean Square Deviation of the Surface. This is a dispersion parameter defined as the root mean square value of the surface departures within the sampling area. Statistically it the standard deviation of the height distribution.
Sz	Amplitude (2D Extension)	Ten Point Height of the Surface. This is an extreme parameter defined as the average value of the absolute heights of the five highest peaks and the depths of the five deepest pits or valleys (eight neighbours method) within the sampling area. Please refer to Table A1.1for the mathematical definition, and section A1.5 (appendix1) for a more detailed description.
Ssk	Amplitude (2D Extension)	Skewness of Topography Height Distribution. This is the measure of asymmetry of surface deviations about the mean plane. This parameter can effectively be used to describe the shape of the topography height distribution. For a normally distributed surface, which has a Symmetrical shape for the surface height distribution, the skewness is zero. For an asymmetric distribution of surface heights, the skewness may be negative if the distribution has a longer tail at the lower side of the mean plane. It will be positive if the distribution has a longer tail at the upper side of the mean plane. This parameter can give some indication of the existence of "spiky" features.
Sku	Amplitude (2D Extension)	Kurtosis of Topography Height Distribution. This is a measure of the peakedness or sharpness of the surface height distribution and characterises the spread of the height distribution. A normally distributed surface has a kurtosis value of 3. A centrally distributed surface has a kurtosis value larger than 3 whereas the kurtosis of a well spread distribution is smaller than 3. By a combination of the skewness and the kurtosis, it may be possible to identify surfaces, which have a relatively flat top and deep valleys.
Sds	Spacing (2D Extension)	Density of Summits of the Surface. This is the number of summits of a unit sampling area (eight neighbours method)
Str	Spacing (AACF)	Texture Aspect Ratio of the Surface This is a parameter used to identify texture strength i.e. uniformity of texture aspect. It is defined from auto-correlation function (AACF). Str can be defined as the ratio of the fastest to the slowest decay for a correlation length, 0.2 in the AAFC. In principle, the texture aspect ratio has a value between 0 and 1. Larger values indicates uniform texture in all directions. Smaller values indicates an increasingly strong directional structure or lay
Sal	Spacing (AACF)	The Fastest Decay Auto-correlation Length. This is a parameter in length dimension used to describe the auto-correlation character of the AACF. It is defined as the horizontal distance of the AACF, which has the fastest decay to 0.2. In other words the Sal is the shortest autocorrelation length that the AACF decays to 0.2 in any possible direction. For an anisotropic surface Sal is in a direction perpendicular to the surface lay. A large value of Sal denotes that the surface is dominated by low frequency (or long wavelength) components. While a small value of the Sal denotes the opposite situation.
Std	Spacing (Fourier)	Texture Direction of the Surface. This is the parameter used to determine the most pronounced direction of the surface texture with respect to the y axis within the frequency domain, i.e. it gives the lay direction of the surface.
$S\Delta q$	Hybrid	Root mean square value of surface slope within the sampling area
Ssc	Hybrid	Arithmetic Mean Summit Curvature of the Surface. This is defined as the average of the main curvatures on the summits within the sampling area. The sum of the curvatures of a surface at a point along any two orthogonal directions is equal to the sum of the principal curvatures.
Sdr	Hybrid	Developed Interfacial Area Ratio. This is the ratio of the increment of the interfacial area of a surface over the sampling area. Large values of the parameter indicates the significance of either the amplitude or the spacing or both.
Sbi	Functional (Bearing Area)	Surface Bearing Index. This is the ratio of the Sq parameter over the surface height at 5% bearing area. A larger surface-bearing index indicates a good bearing property.
Sci	Functional (Bearing Area)	Core Fluid Retention Index. It is the Sc normalised also to Sq. Larger Sci indicates a good fluid retention. For a normally distributed surface, this index is about 1.56.
Svi	Functional	Valley Fluid Retention Index.

	(Bearing Area)	It is the Sv normalised also to Sq. Larger Svi usually indicates a good fluid retention in the valley zone.
Sm	Functional (Volumes)	Material Volume of the Surface. The material volume is defined as the material portion enclosed in the 10% bearing area and normalised to unity. The material volume may reflect wear and the running-in properties. A surface with a rapid increase in the material volume ratio shows good running-in properties whereas those with a slow increase of the functions indicates that the top part of the material is easily worn.
Sc	Functional (Volumes)	Core Void Volume of the Surface. The void volume enclosed between 10% and 80% of the Abbot-Firestone curve (AFC) and normalised to the unit sampling area.
Sv	Functional (Volumes)	Valley Void Volume of the Surface. The valley void volume enclosed between 80% and 100% of the AFC and normalised to the unit sampling area.

Table 3.1 - Birmingham 14 - The primary set

These "Birmingham 14" (B14) parameters are mostly 3D extensions of existing 2D parameters. Several are novel in that they describe some aspect of surface patterns or texture: these are Str, Sal and Std. The suitability of these parameters for describing sheet metal deformation during deep drawing will be assessed during this research programme.

The Belgium Steel Industry Research Association tested these 14 parameters with automotive panel pressing performance and also proposed two further 3D parameters. They found that none of the B14 parameters showed much correlation with pressing performance. This is perhaps not surprising because the B14 parameters were not developed for forming but rather as general-purpose parameters. They did propose two new parameters, Vr, and WR, which are illustrated in Figure 3.4 and Figure 3.5. These two parameters describe some features of the EBT surfaces [Vermeulen et al 1995] and are calculated from the designed pattern (not the measured surface as for all the other surface parameters). In particular:

- WR is the ratio of the captured oil area (Aw) to the open area (Ad). Because of the hexagonal deterministic pattern, those two areas can be calculated from simple trigonometry as shown in Figure 3.4.
- Vr represents the potential oil retention volume per unit cell area. Mathematically it is the ratio between the total surface (Asc) and the valley volume (V_0). Once more, thanks to the deterministic pattern of EBT surfaces, it can be calculated by using simple trigonometry as shown in Figure 3.5.

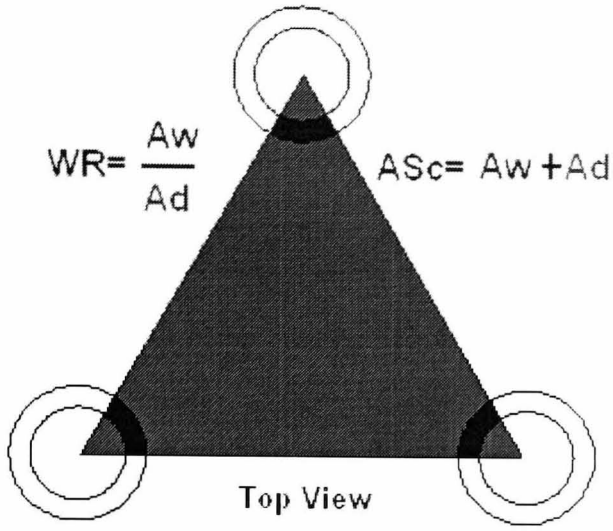

Figure 3.4 – WR definition for EBT surfaces

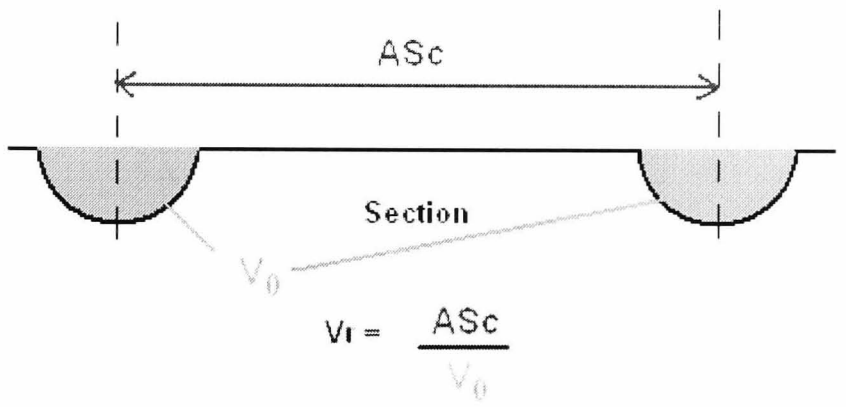

Figure 3.5 – Vr definition for EBT surfaces

Vermeulen et al [1995] found these parameters good candidates to describe steel sheets pressing performance.

Thirdly a German research group from the University of Erlangen-Nuremberg suggested parameters (α_{cl}, α_{op}, α_{clm} exemplified in Figure 3.6), which define fluid retention properties [Pfestorf et al 1998]. These parameters were presented as good candidates to describe pressing performances, although no detailed results on experimental applications could be found.

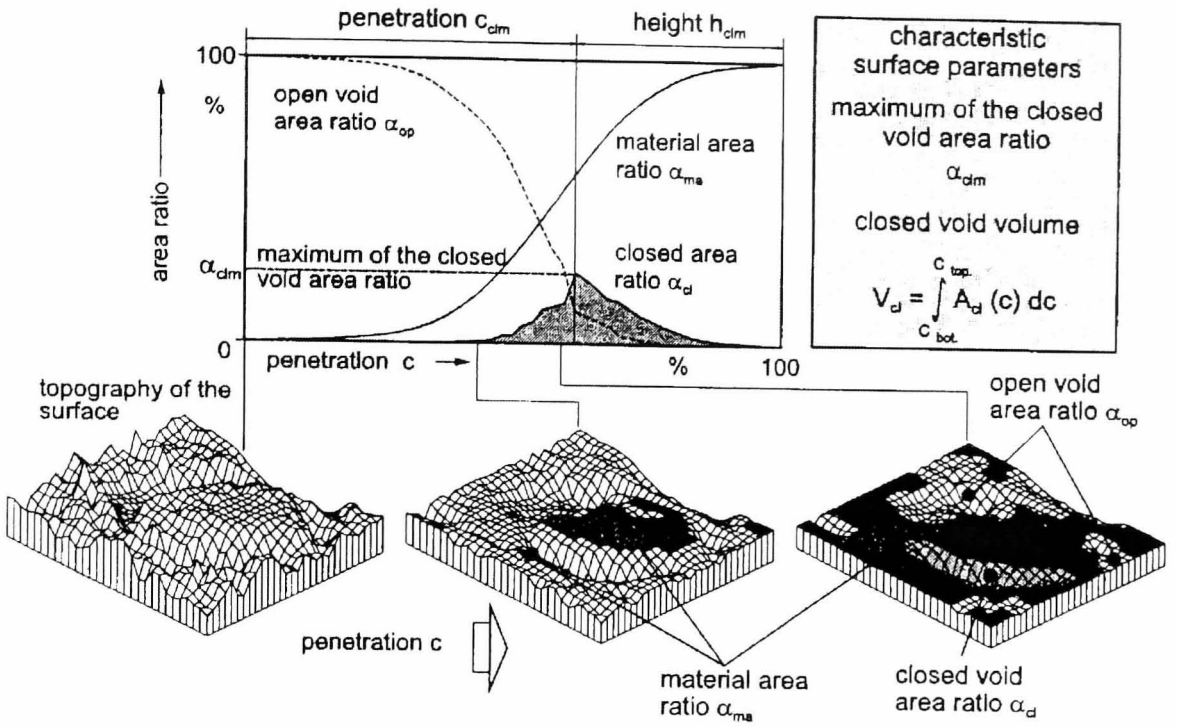

Figure 3.6 - Void Volume Parameters

3.6 Previous experimental work with the "Birmingham 14"

A major study of the "Birmingham 14" applied to the prediction of friction had been performed by [Jonasson et al 1998]. Jonasson employed a special "bending under tension" test. The only correlations he could find were those with the core roughness parameter (Sk) and the reduced summit parameter (Spk), although no detailed statistical proof could be read from the paper.

Another study of the "Birmingham 14" parameters (with respect to automotive sheet metal frictional behaviour) was undertaken by OCAS [Vermeulen et al 2001]. Vermeulen attempted a description of friction phenomenon trough a number of parameters. Once more, the paper lacked statistical details.

All the above work was concerned with isotropic (or near isotropic) surfaces so it is no surprise that no correlations were reported with texture parameters like the texture aspect ratio (Str) or the texture direction (Std). However, [Griffiths 1998] shows that when drawing steel sheets with strongly anisotropic textures there is a relationship between texture and friction. Thus, for these anisotropic surfaces Std is a good parameter for defining

directionality. However, in this case, the surfaces were produced by abrasion and the surfaces were strongly anisotropic so there is little relevance to sheet metal work. It must be said that the trend in sheet metal deformation is to go to deterministic or semi-deterministic surfaces as provided by the latest electron beam texturing techniques.

Thus, from the above discussion, it can be concluded that only a few of the "Birmingham 14" parameters are relevant to pressing performance.

[Vermeulen et al 1995] presents some examples, which show that of the (only) two surfaces tested, higher values of Vr and WR give superior tribological behaviour. Hence, a deep study of oil retention on sheet steel surfaces was necessary to better understand the influence of steel surface upon deep drawing (the work is presented in the following chapter).

The above parameters that show some potential of a correlation with pressing performance will be included in the parameters investigated during this investigation.

3.7 Novel surface parameters tested during this work

The surface parameters developed during this work (by this author) mainly relate to the "Spatial" (areal distribution) category.

Within this category, perceived was the need to characterise the typical dimensions of peaks and valleys, therefore taking further the work of [Pfestorf et al 1998], [Vermeulen et al 1995] and [Schmoeckel et al1997] who found that the closed-valley-areas (α_{clm}) parameter was able to identify tribological behaviour.

In fact, the valley area dimensions were perceived to influence lubricant movement (both the oil retention and dynamic lubrication during friction). On the other hand, peak areas were perceived to influence the contact between surfaces either trapping oil on their micro-asperities or simply wearing out.

The above descriptions and expectations led this researcher to include these parameters in this research work. A robust definition of "peak" and "valley"

had to be made and the following parameters could then be easily defined [Sacerdotti et al 2000(c)]:

- Spa (m^2) – The average peak area protruding above a given plane.
- Sva (m^2) – The average valley area protruding below a given plane.
- Spd (#peaks/m^2) – The number of peaks per unit area above a given plane.
- Svd (#valleys/m^2) – The number of valleys per unit area below a given plane.

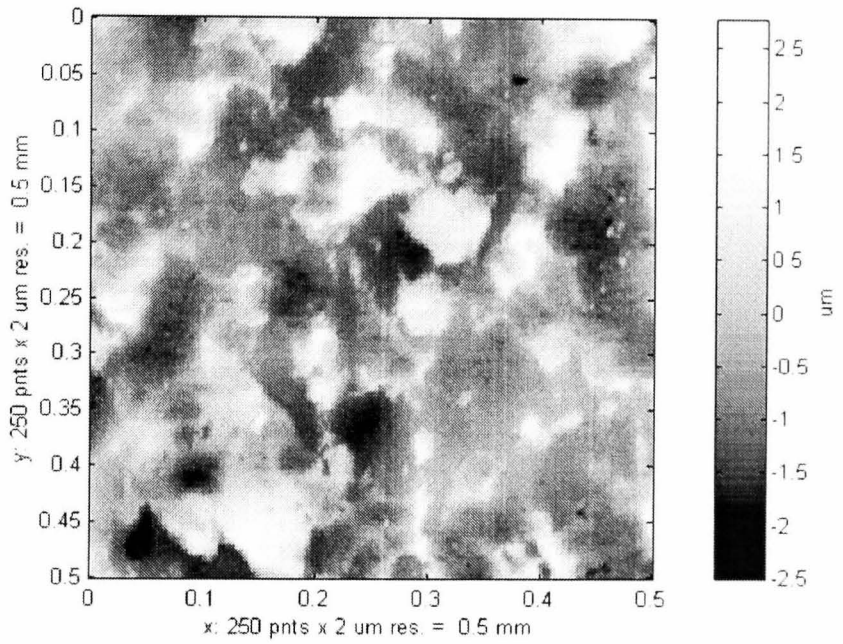

Figure 3.7 - EDT reference surface for the following example

Sva and Spa can be defined as follows: when the surface (such as the one shown in Figure 3.7) is sectioned at a particular height, there will be closed regions pertaining to peaks (black areas in Figure 3.8) as well as valleys (white areas in Figure 3.8). The peak-closed regions are the load bearing areas between die and sheet. The valley-closed regions are the oil retention areas. Closed and open area definitions and calculation methods for these surface parameters are given in Appendix 2.

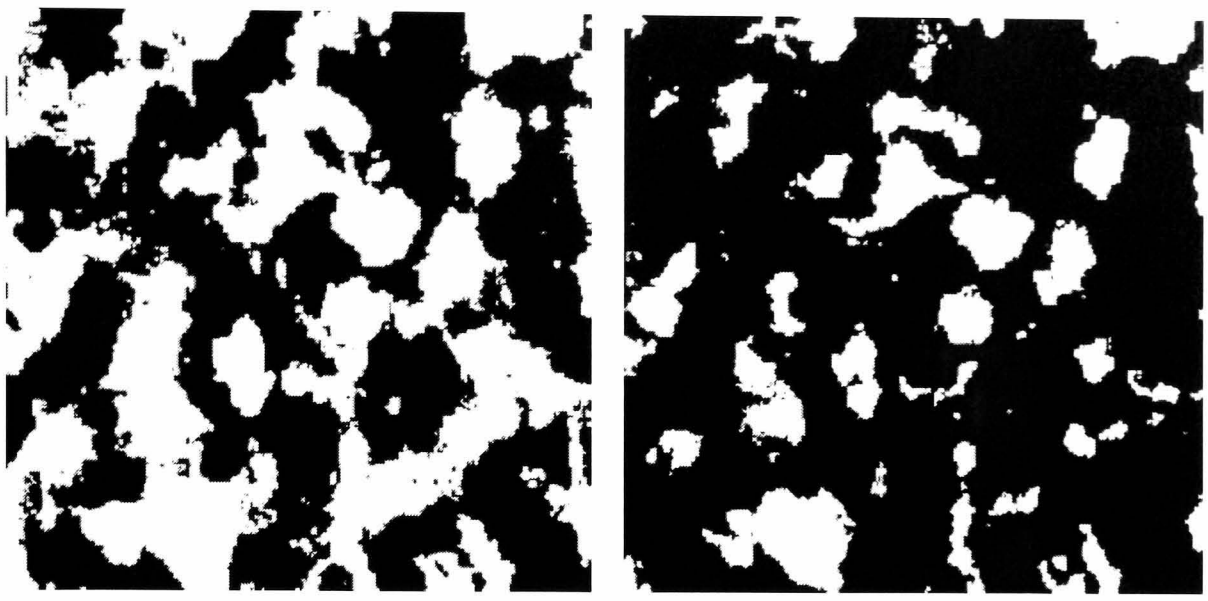

(a) (b)

Figure 3.8 - Reference Surface intersected at 0 um (a) and +0.7 µm (b)

In the following chapters, these new "Autosurf" surface parameters, will be employed along with the "Birmingham 14" and other relevant parameters to test the characterisation of the surface topographies of the steel sheets under forming tests. Correlation analysis between test results and the various surface parameters measured will guide us towards an improved description of the autobody manufacturing processes.

3.8 Summary

- ✓ The surface topography measuring devices can be divided into two categories:
    - Stylus – the most common, slow but reliable
    - Optical – faster but sensitive to dust and dirt

  Both the types of devices are capable of and have been used to measure the steel sheets of the autobody manufacturing processes.

- ✓ Nowadays, 3D measurements of a surface topography can be taken very easily by measuring multiple parallel 2D profiles; hence only 3D characterisation will be employed in this thesis.

- ✓ Roughness (the higher frequency signal of a surface profile) is the only characteristic of interest for this work.

- ✓ The currently employed 3D surface parameters are known as the "Birmingham 14". These parameters are "general-purpose", hence they do not correlate with steel sheet deep forming parameters and will not be investigated here.

- ✓ Taking further the work of several researchers (i.e. Vermeulen, Jonasson etc) novel 3D spatial parameters were proposed in addition to the "Birmingham 14". These will be investigated here.

- ✓ The work of the mentioned researchers indicated the study of oil retention as the next required step for the understanding of friction and hence forming of autobody panels.

4. Oil retention

4.1 Introduction

This chapter is concerned with a study of the ability of a steel sheet to retain oil on its surface such that the surface can resist corrosion and there is sufficient lubricant present during subsequent forming of an autobody panel.

Oil starvation on the surface of a steel sheet used in autobody manufacture is a very important factor in industry production. When oil migrates across a surface it will cause dry spots to form where there is no oil present. There are severe implications for the presence of "dry" spots on sheets with respect to spoiled appearance and galling. The appearance of the autobody panel will be seen to be unacceptably poor if there are spots of corrosion damage on the sheet surface. Also, the dry spots will cause welding between the punch and the sheet such that surface discontinuities form. This phenomenon is called "galling". Not only are galling discontinuities unsightly but also they cause an increase in friction and wear. Thus, dry spots are to be avoided in autobody manufacture.

This chapter is essentially in two parts. Firstly, a short description of the limited previous work that has been published on oil retention and secondly, a description of a test programme undertaken as part of this programme of work aimed at improving and predicting the ability of a surface to retain oil.

4.2 Previous work on oil retention

A literature review found that there was very little published on oil retention. This at first sight is perhaps surprising because, there must be a significant body of knowledge "out there", particularly "locally" within the automotive industry. However, because each manufacturer tends to work in isolation, they do not want their information "discovered" because it might give their rivals a market advantage. Hence the manufacturers are secretive and do not publish information on such things. Although this is unfortunate, it is understandable and, of course it is a fact that we have to live with it.

The literature survey and a discussion with the "Autosurf" partners only identified one paper and one report, those of Zaccone et al [1998] and Holtkamp [1999(a)]. These are reviewed below.

Although it was stated above that manufacturers do not report on their experiences of oil retention, it was a surprise to find one paper published by Zaccone et al [1998] which appears to be a Ford Motor Company research report. Zaccone et al [1998] report on an industrial investigation of the oil migration phenomena on pre-lubricated sheets. Furthermore, no mention was given to the effect of surface topographies upon the observed oil migration. The work described by Zaccone mainly concentrated on understanding how the oil migrates over time. The findings showed that after a number of weeks of storage the oil would re-distribute over the sheet surface moving from the centre to the sides of the coil. Furthermore, 30% of the migration happens in the first 4 days storage and 49% in the following 4 weeks. Finally, the remaining migration happens over in the following 6 weeks (no further measurements afterwards were taken). Thus, the merit of Zaccone et al's work is that they provide information on the time involved in migration.

The other person to have done work on oil migration is Holtkamp who was working for Corus (formerly know as Hoogovens Staal), one of the Autosurf consortium partners. The Corus company (in cooperation with other Autosurf partners such as OCAS) was involved in the oil retention studies and Holtkamp from their research department was charged with developing an oil migration test rig and procedure. Vermeulen developed the initial testing idea in cooperation with Holtkamp. The latter performed a series of tests with different tools, loads and application times and presented his results in the form of a report [*Holtkamp 1999(a)*]. The object of his research programme was to determine the best laboratory test to simulate real life oil migration conditions. He wanted to develop a test that lasted only hours yet which was representative of the days determined by Zaccone et al. Also, he wanted to simulate two situations, firstly when short steel sheet lengths are stacked and secondly when a long length is rolled. He conducted a series of tests and found that the best conditions to simulate migration in industry are a migration time of 5 hours and the use of a tool with a flat end having rounded corners pressing down on a pile of sheets. This set-up was found to satisfactorily simulate the weight of the pressing sheets in either a stack or a

roll. Holtkamp only wanted to develop a satisfactory test because the intention was for Autosurf to use this test to investigate the relationship between topography and migration.

The literature survey on oil retention concluded that apart from Zaccone et al [1998] and Holtkamp [1999(a)], there is no published information on the relationship between migration (or indeed retention) and surface topography, hence the following work can be considered absolutely novel.

4.3 The "Autosurf" oil retention test programme

4.3.1 The surface parameters under test

Surface tension plays a major element in oil retention since, when a oil is applied to a steel sheet (even in small quantities), the oil is not expected to completely fill or "drain" into the valley area. This is because firstly, the real surface slopes are usually small (up to 10^0 according to Scheers [1999(b)]) and secondly because of surface tension. This means that in all cases, even when a lubricated surface is "pressed", some lubrication action should be observed.

All the above discussion begs the question as to which surface topography features and/or parameters influence oil retention and migration. This author suggests that there are two things related to the surface that are significant and which need to be borne in mind when designing an oil retention test programme. These are the resistance offered to the migrating oil due to the roughness of the surface in general acting as a barrier and the ability of the surface to hold and retain the oil in the valleys. These can be related to two aspects of the surface, the surface "finish" or "roughness" which provides the resistance to oil movement and the valley dimensions, which keep the oil in the surface pools. Both these aspects can be related to 3D surface parameters, see the diagram in Figure 4.1 below for a schematic of the surface form.

With regard to the "resistance" the surface offers to oil migration, this will depend on the average across the complete surface rather than any particular area since oil drains off all the edges of a sheet. Thus, it is thought that the best descriptor would be the average surface finish or roughness of a sheet

rather than the extremes of roughness since these are likely to be localised. This author suggests that the "best" parameter to consider is the parameter considered by the topography fraternity to be the most statistically significant average parameter. This is the root-mean squared (RMS) roughness [Sacerdotti et al 1999]. In three-dimensions this is given by the Sq parameter which is one of the "Birmingham 14" parameters. Thus, in this test programme, the influence of the parameter **Sq** on oil migration will be tested.

With regard to the pools of oil retained on the surface in the valleys, there are two aspects or features that could be significant. These are the **valley volume** and the **pool surface area**. The valley volume represents the total amount of oil on the surface, i.e. the oil captured within the valleys and hence retained. The pool area is the area of the surface that is exposed to the atmosphere and hence, when related to the total area is that fraction of the surface covered by oil.

The valley volume is the volume of the "pools" on the surface in which the oil will be trapped. It is therefore the total volume of the trapped oil. The higher the volume, the more the oil will be kept in the valleys and not move across the surface. The surface parameter associated with this mechanism could be the "Birmingham 14" parameter **Sci**. This parameter can be calculated as the ratio between the difference of valley volume at 5% and 80% bearing area and the amplitude parameter Sq (functional, see Appendix 1 for full definition).

The valley surface area represents the area on the surface covered by oil that is seen by the contacting surface when sheets are stacked in a pile. The smaller the valley area, the less oil will move off the surface.

With regard to the valley area, there is no standard surface parameter, of say the "Birmingham 14" set, which describes any aspect of this exposed surface valley area. This means that a parameter needs to be calculated and given a new "S?" designation. The parameter used is the parameter designed by the author and designated the "valley area" (i.e. "va") parameter and is termed "**Sva**". It is the area of the valley "pools" seen when the surface is sectioned at particular levels. This begs the question concerning what level to section the surface at.

All the areal surface parameters need to be calculated at a given height. Recent studies at OCAS report that the flattening of the asperities due to die contact is typically 25% of the peak to valley height [Scheers et al 1998]. However, the real peak deformation or flattening produced during deep drawing or during these experiments is unknown because it will vary depending upon the operating conditions. Therefore Sva will be calculated at several heights ranging from 0 (50% of the bearing area, or mean surface line) to +Sq (25% of the bearing area circa). Thus, there needs to be a section level used in the parameter description. The designation used is to put the level in brackets after the parameter. For example, if the section level is at the mean line, the designation is Sva(0). This parameter has been described in the previous chapter and the method used to calculate it at the relevant level is described in Appendix 2.

Note that the diagram of Figure 4.1 below is in 2D. Hence the parameter shown on the diagram in Figure 4.1 is in reality the 2D equivalent which would be termed Rva or more correctly Rva(0) referring to the section level.

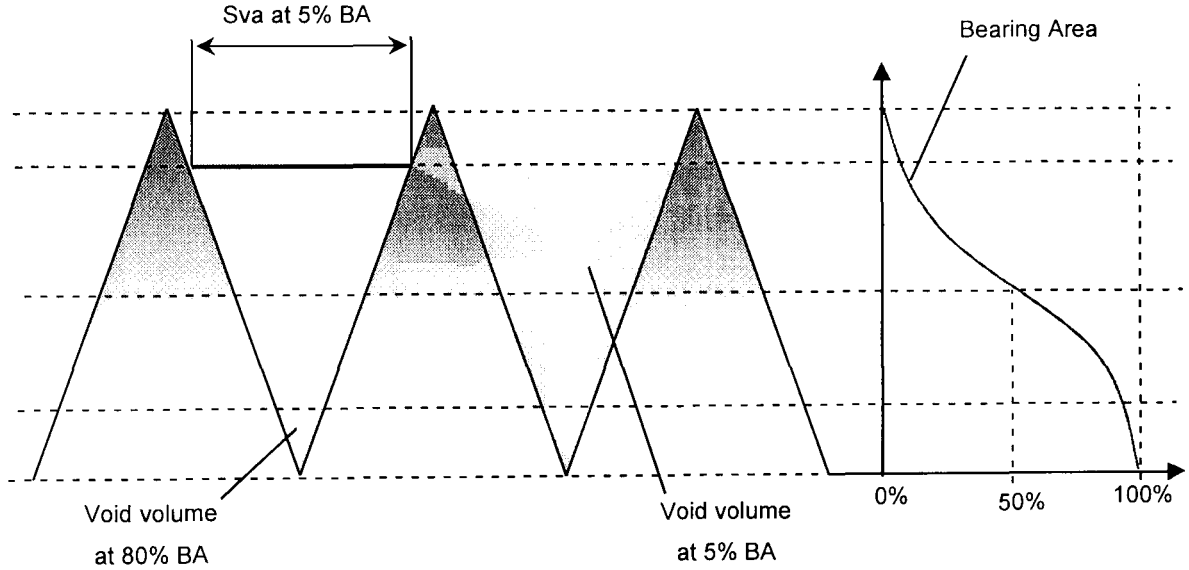

Figure 4.1 – Schematic representation of Sva and void volumes

For the standard sheet steel surfaces produced by the eleven manufacturing processes described in the previous chapter, the values for Sq, Sci and Sva are given in Table 4.1. Please note that the "CRS" coating type in Table 4.1 below simply indicates "uncoated material" (CRS is the commonly accepted acronym of "Cold Rolled Steel").

Name	Texturing	Coating	Yield Strength [MPa]	Sq [µm]	Sci [m^2]	Sva(0) [m^2]
N1	EDT	CRS	156	2.902	6.57E-09	2.187E-06
N2	EDT	CRS	165	2.740	4.81E-09	7.600E-07
H14	EDT	GA	221	1.099	4.02E-09	3.086E-07
H1	EDT	GI	166	1.380	8.75E-09	2.798E-07
H2	EDT	GI	162	0.897	6.54E-09	3.389E-07
S2	EBT	ELO	157	1.402	3.63E-09	1.816E-06
S3	EBT	ELO	163	2.147	4.08E-09	1.616E-07
S5	EBT	GI	157	1.718	3.22E-09	1.126E-06
S6	EBT	GI	165	2.416	4.26E-09	3.470E-08
S8	EBT	GA	155	1.825	5.64E-09	2.985E-06
S9	EBT	GA	171	2.229	4.36E-09	1.199E-06

Table 4.1 - Topographic characterisation

4.3.2 Test description

In order to study the effect of surface topography on oil migration, a series of experiments was undertaken as part of this work. These experiments were modelled on the recommendations of Holtkamp [1999(a)] i.e. a migration time of 5 hours and a flat tool with rounded corners. The particular experimental configuration is illustrated in Figure 4.2 to Figure 4.5.

In each test, oiled sheets in groups of two (Figure 4.2) were sandwiched together (Figure 4.3). The sheets were A4 sized and oil was placed between each group of two identical sheets. They were placed in a compression test machine and pressed between a flat table and the tool (see Figure 4.4).

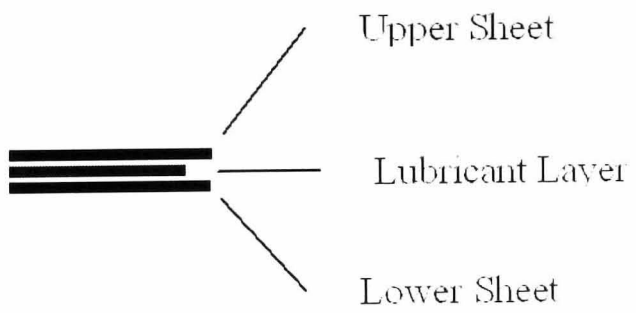

Figure 4.2 – Oil is positioned only between sheets of identical material

Since no oil leakage could be observed during initial tests, several sheets "sandwiches" (such as the one in Figure 4.2) could be placed one on another enabling several material-oil combinations to be tested at the same time (as shown in Figure 4.3).

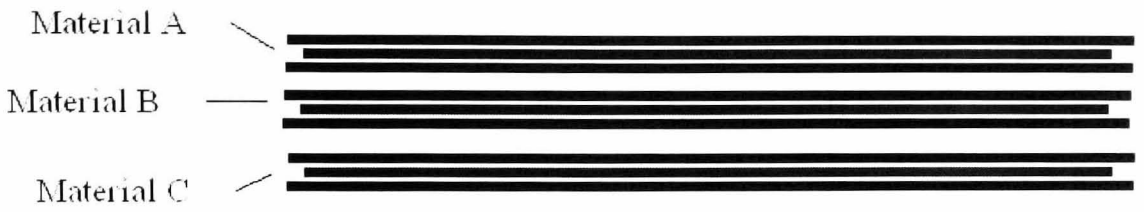

Figure 4.3 – Sandwiches of different materials were piled up and tested at the same time

The stack of "sandwiches" was compressed with a flat tool (width 210 and length 297 mm) having rounded corners with radii of 4 mm for a period of 5 hours, as shown in Figure 4.4. The flat with rounded corners tool shape was chosen because of its ability to replicate the pressure distribution within the coil of steel sheet as suggested by Holtkamp [1999(a)].

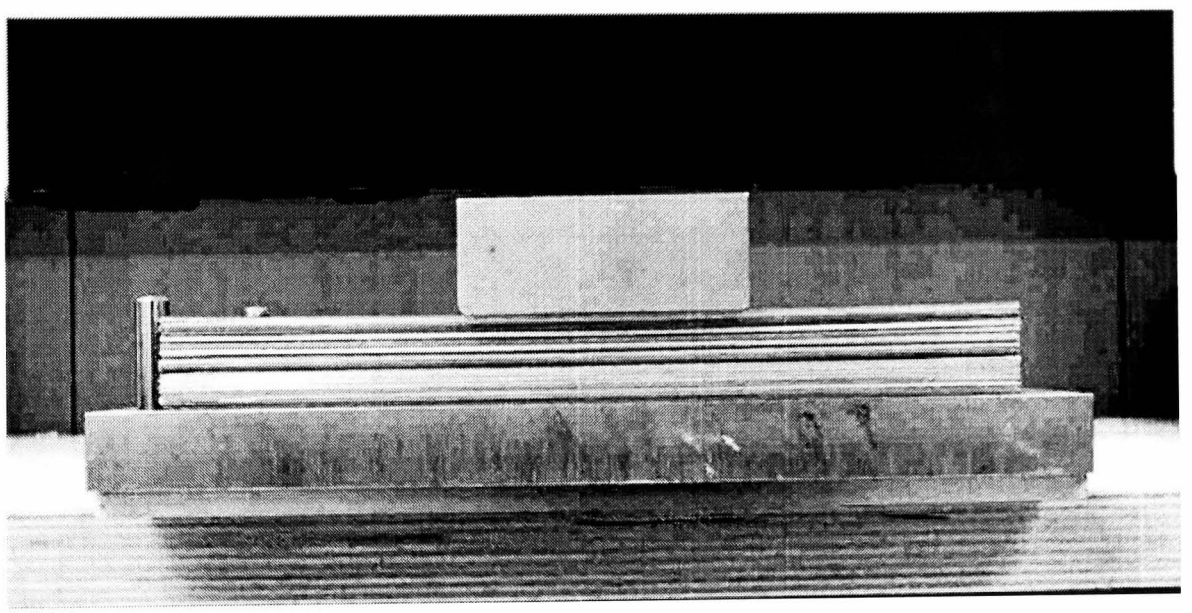

Figure 4.4 – Tool shape adopted for the experiment

The experimental work included 11 different materials (a total of 13 "sandwiches" – one material was repeated in three stack positions), in terms of:

- Coating: Uncoated (or **CRS**), **ELO**, **GI** and **GA**
- Texturing techniques: **EBT** or **EDT**

In order to speed up the tests, a set of 26 coupled samples were stacked. The top 13 were oiled with the thicker oil, the lower 13 with the thinner one.

Three different stacks were formed using 3 different amounts (0.7, 1.5 and 2.5 g/m^2).

The two oils (low viscosity and high viscosity) where chosen because of their use in the automotive industry, the former is used for pressing and the latter as rust prevention.

These three amounts were chosen for the following reasons:

- rust prevention: a minimum of 0.5-0.7 g/m^2 is usually applied. Hence the lower amount chosen for these experiment was 0.7g/m^2
- pressing: a minimum of 1g/m^2 is usually applied, increased up to 2-3 g/m^2 when the part is very "difficult" to manufacture [Fredin 1999].

The two oils employed are the following table:

Description		Unit	ARAL Ropa VOV6	FUCHS 4107S
Density (15oC, 1 atm)	ρ	[g/ml]	0.878	0.887
Cinematic viscosity (20oC, 1 atm)	v	[mm^2/s]	13.9	112
Dynamic viscosity (20oC, 1 atm)	η	[Pas]	0.0122042	0.099344

Table 4.2 - characteristics of the oils employed

A total of 156 steel sheets were tested (2 sheets per sandwich, 26 sandwiches per experiment, 3 oil amounts – one per experiment) and a total of more than 2000 measurements of oil retention were performed. A summary of the testing procedure is shown in Figure 4.5.

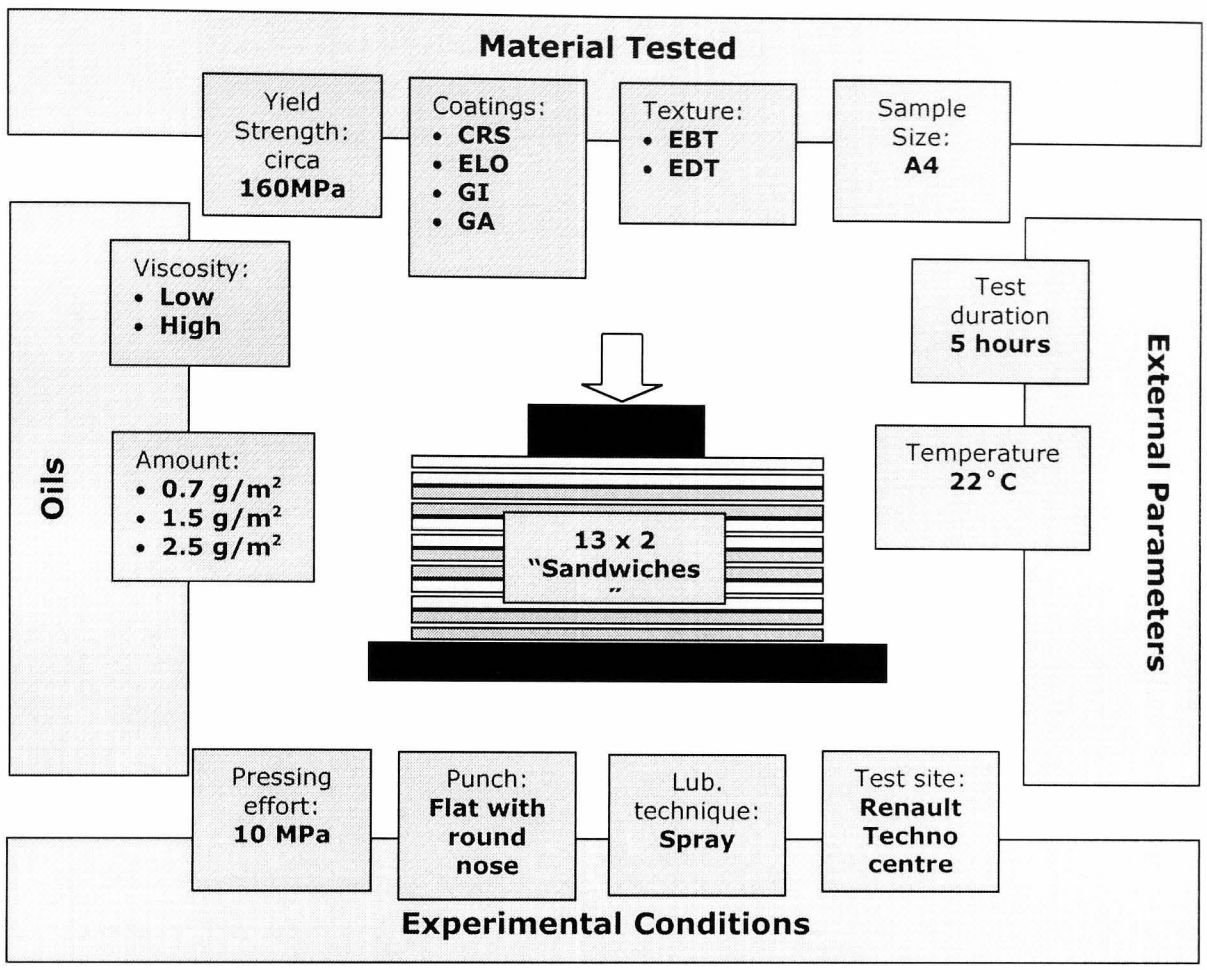

Figure 4.5 – Experimental conditions

After pressing the stack, each sheet was measured for the amount of oil remaining in the positions shown in Figure 4.7. Measurements were taken using a Fischer Betascope MMS module [Betascope 2000]. This device consists of a sensing probe that generates beta radiation, placed in contact with the lubricated sheet (see Figure 4.6). The measured oil thickness is a function of the radiation backscatter. Further details on the Betascope are given in Appendix 3.

Unfortunately, when the probe is removed from the surface, some oil is dragged away with it. This was always the case and there was no way to prevent it. Because of this problem only a few measurements could be taken from every sheet and the limit was the number of times the probe (shown in Figure 4.6) fits in the sheet without overlapping. If there is overlapping one reading will disturb another due to the dragging and both overlapping results will be invalidated.

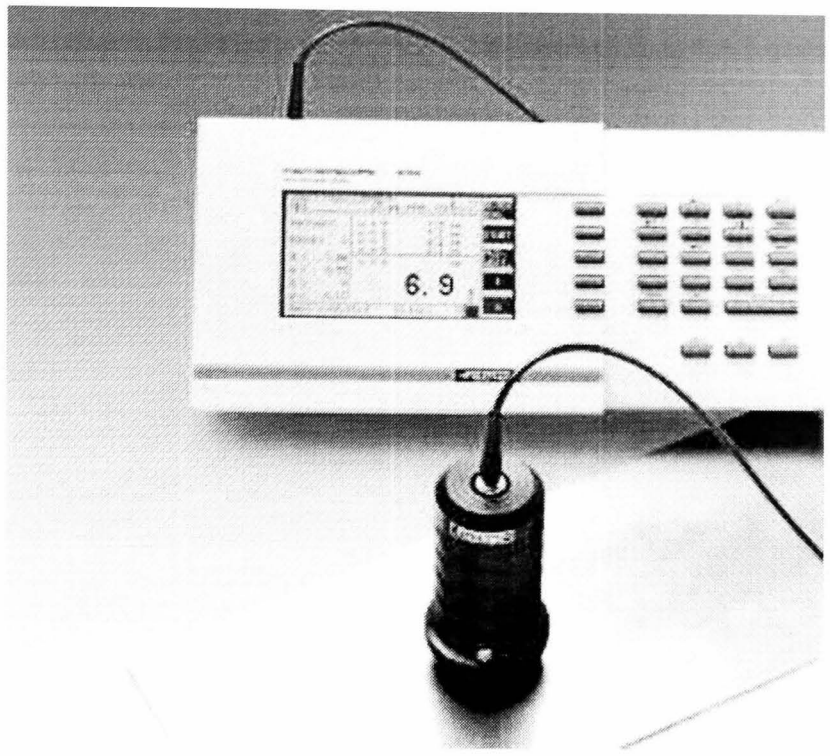

Figure 4.6- The Betascope probe measuring a oil film [Betascope 2000]

Figure 4.7 is a photographic representation of a sheet where:

- Measurements (probe position) are represented by black circles;
- Every circle position is numbered from 0 to 4 (the number is a rank distance from the centre of the sheet)
- Tool position is the marker-shaded area at the centre.

The results showed that the final amount of oil was mainly a function of the distance from the tool. Therefore a rank numbering of the measurements was adopted.

Comparing the shaded area with the circles, it is also possible to notice that:

- Two circles (labelled "0") fall within the shaded area;
- Six circles (labelled "3" and "4") fall outside the shaded area;
- Six circles (labelled "1" and "2") are in the transition region.

Circles "0" and "1" will be used to study oil behaviour under "High Pressure" while the others will be used to study oil behaviour at "Low Pressure".

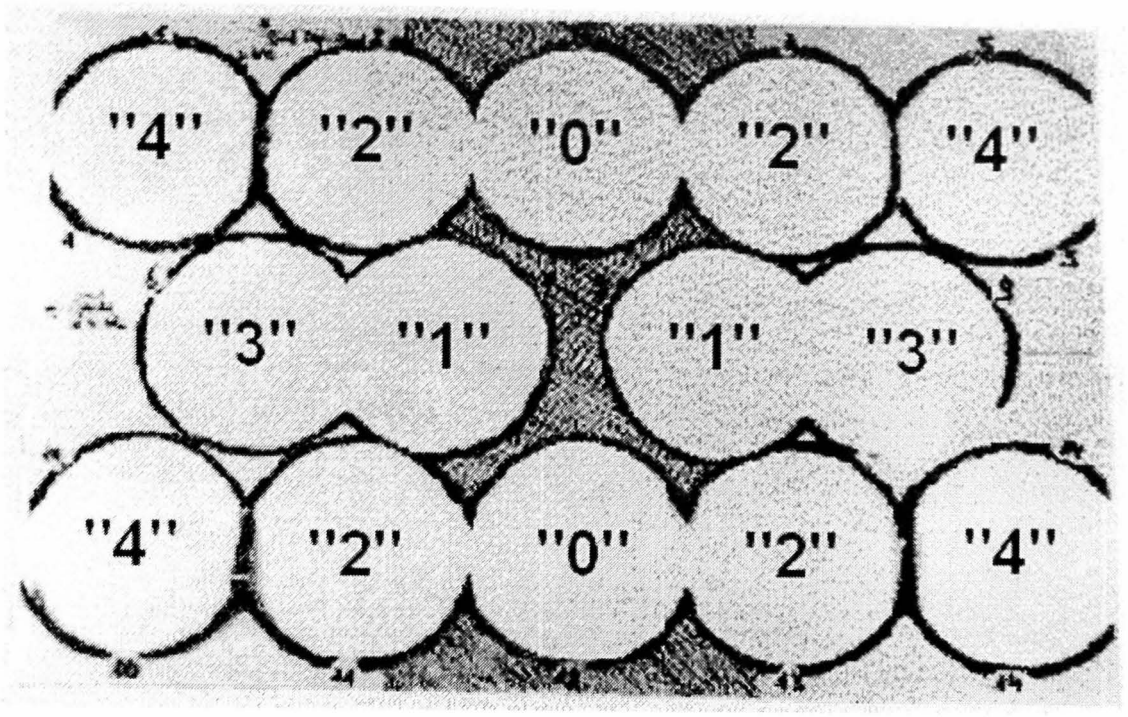

Figure 4.7 – Probe positions and respective numbering (sheet size 210x297 mm²)

With respect to sensitivity, the Fisher Betascope is considered to be able to resolve a thickness to an accuracy of 5 atomic layers, although sensitivity experiments showed a confidence interval usually better than 15% of the measurement for oil amounts higher than 0.5 g/m² (see Appendix 3). By precision weighing sheets prior to testing it was also verified that the real initial oil amount always fell within a range of 5% of the target value.

4.3.3 Experimental design

A number of investigations were undertaken with the materials available. An initial full factorial experiment (see Appendix 4) was attempted to test the influence of zinc coating type upon oil retention. This experiment included the following factors:

Control Factor	Level 1	Level 2	Level 3	Level 4	Level 5
A – Coating type	CRS	ELO	GA	GI	
B – Oil type	Low Viscosity	High Viscosity			
C – Oil initial amount	0.7 g/m²	1.5 g/m²	2.5 g/m²		
D – Position on the sheet	0	1	2	3	4

Table 4.3 – DOE for the initial investigation on stack position effect upon oil movement

Then followed three full factorial Design of Experiments (or DOE), one for each coating type, with the following control factors:

- A - Material (all the surfaces available)
- B - Oil type (2 levels)
- C - Oil initial amount (3 levels)
- D - Measuring position (5 levels)

4.4 Analysis of test results

Statistical analyses were performed on all the experimental designs that it was possible to undertake. For convenience a summary of the results is presented below while the complete list of the statistical results is shown in Appendix 5.

4.4.1 Coating type

After pressing, the Betascope-measured (average) oil amount was found to be significantly lower than the amount initially applied (average 13% loss), although neither leakage nor weight loss was ever observed. This phenomenon was considered significant and it was decided to perform additional tests to confirm the results. Some experiments were repeated and sheets were both precision weighted and measured with a Betascope. The results were exactly the same again! The average results for all conditions are shown in Figure 4.8. This is a plot of the average oil amount found on the sheets for all the different coating types and oil amounts.

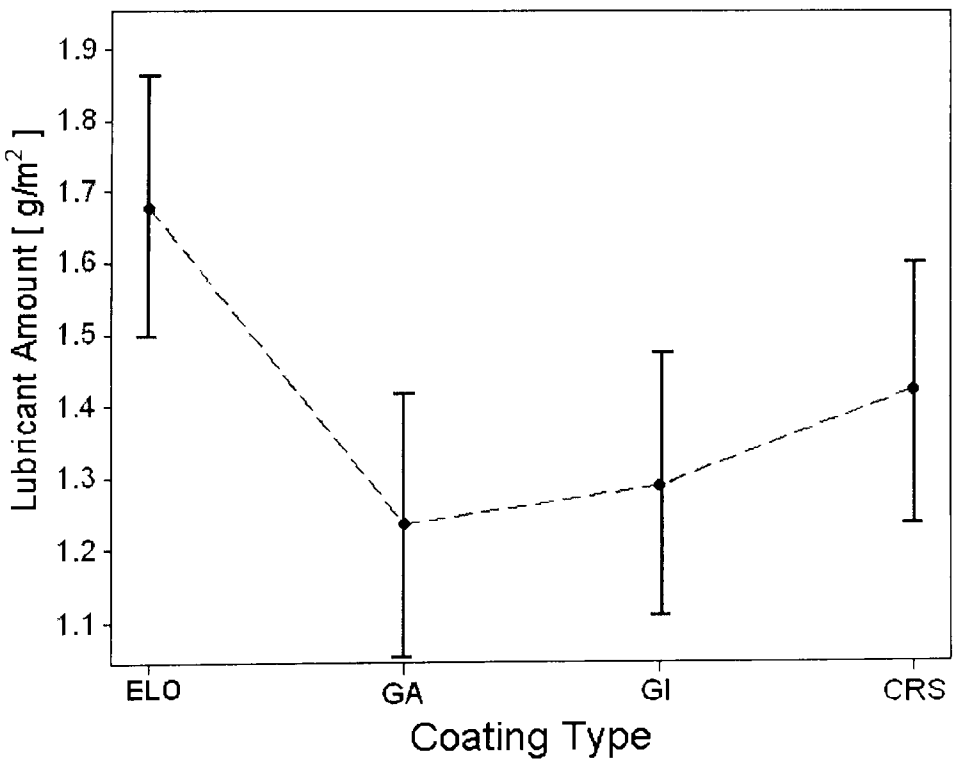

Figure 4.8 – Mean plot of final oil amount vs. coating type on EBT materials

The blue vertical line represents the measurement uncertainty (99.7% confidence interval). Since the confidence intervals of GA and GI compared to ELO do not overlap it means that the former are significantly lower than ELO. Obviously there can be no loss of oil and there must be an explanation since oil does not vanish into thin air! The loss could be due to the inaccuracies of the Betascope itself but an accuracy test on the instrument gave an offset of -0.074 g/m^2 (at 1.5 g/m^2) and a precision of ± 0.15 g/m2 (99.7% confidence interval averaging 8 measurements). These results indicate that the loss cannot be due to instrument inaccuracies. There will obviously be a loss of some volatile oil components but not sufficient to explain the differences in Figure 4.8. There could also be a lower chemical affinity of ELO compared to the "hot-dip" family (GA and GI) but since the coatings are all zinc, again this could not explain the big difference. This observation is obviously a problem since it implies that some oil had actually disappeared, which is impossible [Karila 2000], as shown in Appendix 3. Thus, the amount of loss on average could not be accounted for, for any of the above and another explanation needs to be found.

It is significant that the amount "lost" is high for the GA surfaces (average 25%), and almost zero for the ELO surfaces (average 3%). This indicates that the loss is due to the nature of the surfaces. The GA surface, and to a lesser extent the GI surface, is complex with many cracks, re-entrant angles and micro-porosity (as shown by the numerous black spots in Figure 4.9b). These cracks and the pores are smaller than the stylus tip dimensions so a surface finish measuring instrument cannot characterise them although they can be seen in the optical photographs of Figure 4.9. Thus, it is thought that the oil is held beneath the surface within the structure by surface tension such that the Betascope cannot register it and it therefore appears to be "hidden". Conversely, because the ELO surface is not crystalline, there are no re-entrant angles and or micro-porosity so the Betascope can see the majority of the oil.

This trapping of the oil on GA surfaces is significant since the oil is retained within the structure and will not migrate across the sheet because of surface tension. This is an advantage because there will be no dry spots with GA whereas, because the oil on the ELO sheet is literally sitting on the surface, it will easily flow across the surface due to gravity or pressure and may leave dry spots. On the other hand, the oil on the ELO surface will be immediately

available for lubrication because it simply sits on the surface (assuming no prior migration). This will not be the case for the GA surfaces since the "trapped" oil will not be freely and immediately available for lubrication. On the other hand, when the GA surface is deformed, the trapped oil will be squeezed out and will then only then provide lubrication.

Looking at the experimental results on friction (see following chapter) it can be seen that GA coated materials always act as they were "poorly lubricated" although they were oiled with the same amount as the others. This is coherent with the results from lubricant migration (i.e. GA "hides some of the lubricant" and GA act as it was "poorly lubricated") and it is considered a result of great value.

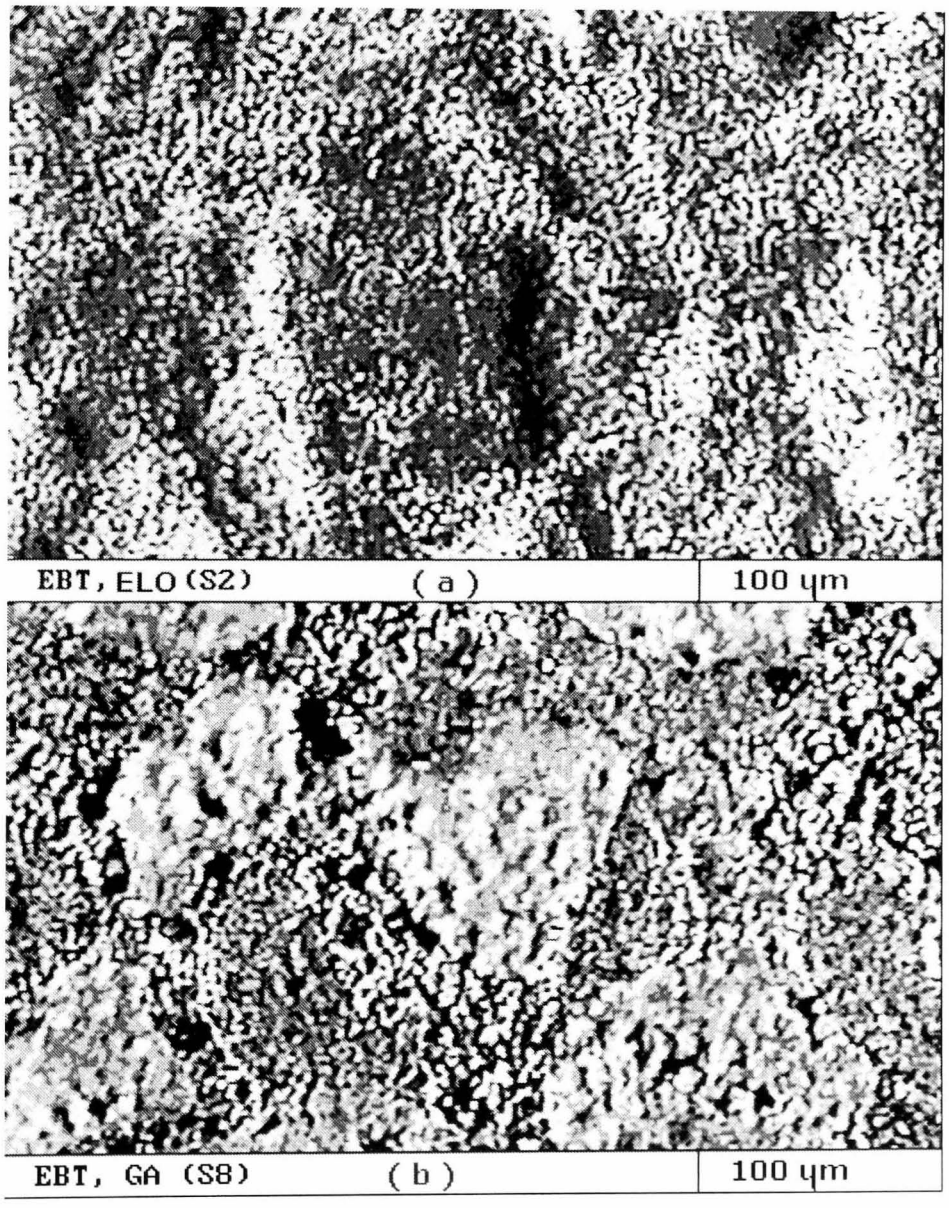

Figure 4.9 – Optical image of an EBT ELO coated (a) and GA coated (b) surface topographies

Nevertheless, in order to better clarify the reason of such a "dry" behaviour of "hot-dip" zinc coatings further research is needed. In particular, it would be of great interest to explore the chemical affinity and the surface tension of different oils and additives with the named zinc coatings. This needs to be the subject of future work.

4.4.2 Distance from the punch

As expected, the measured oil amount retained on the surface was greatly affected by the distance from the centre of the sheet (the numbering is described in Figure 4.7). The migration phenomenon could be described as a smoothened reaction to the tool pressure as represented in Figure 4.10.

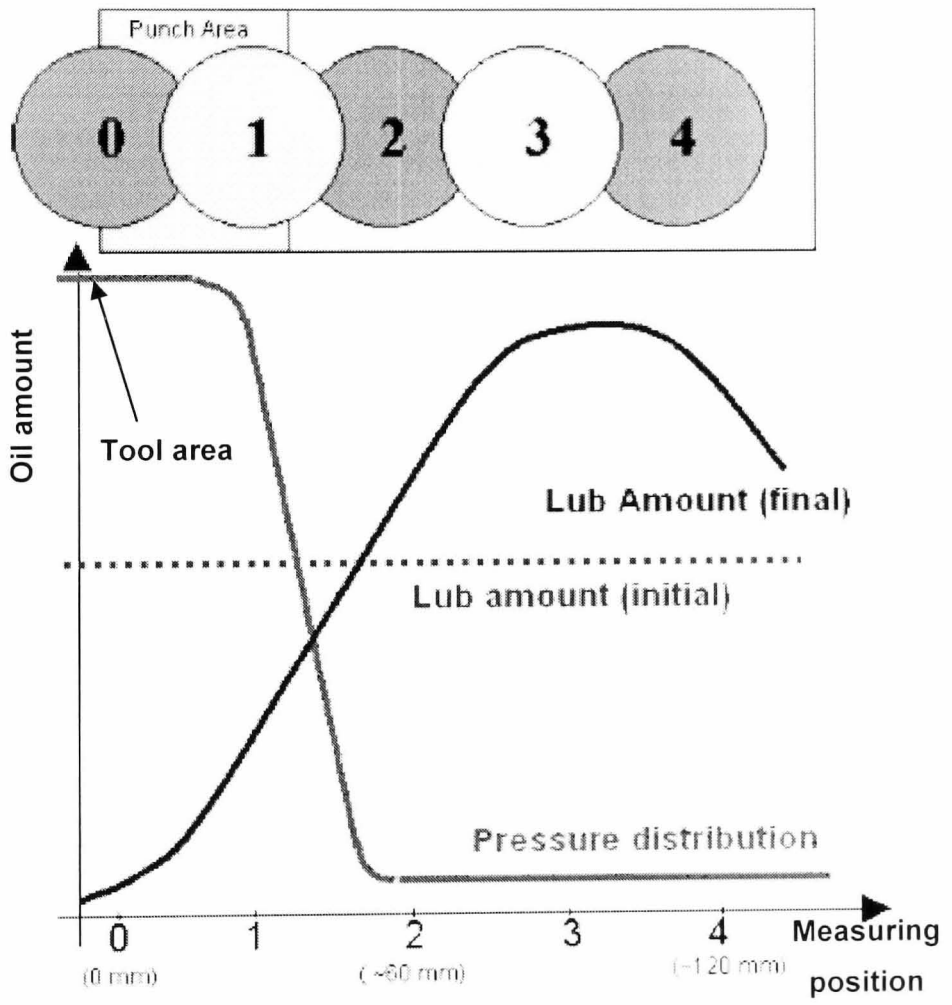

Figure 4.10 - Oil amount vs measuring position (theoretical)

The experimental behaviour of oil distribution versus distance from the tool always presented an "S-shaped" curve of the form shown schematically in Figure 4.11. Some features of this curve were found affected by the surface

parameters presented. Now, the problem was to quantify the amount of oil movement.

This problem was solved by proposing a migration index according to the mechanism expected, those being:

- **High pressure** – the high-pressure region is under the tool (bottom-left circle in Figure 4.11). In this area the curve generally exhibits linear behaviour and the adopted migration index (MI_H – see Equation 4.1) was the difference between the oil amount in position "1" and amount in position "0" (centre of the sheet):

$$\mathbf{MI_H = LA(1) - LA(0)}$$

Equation 4.1 - Migration index at high pressure

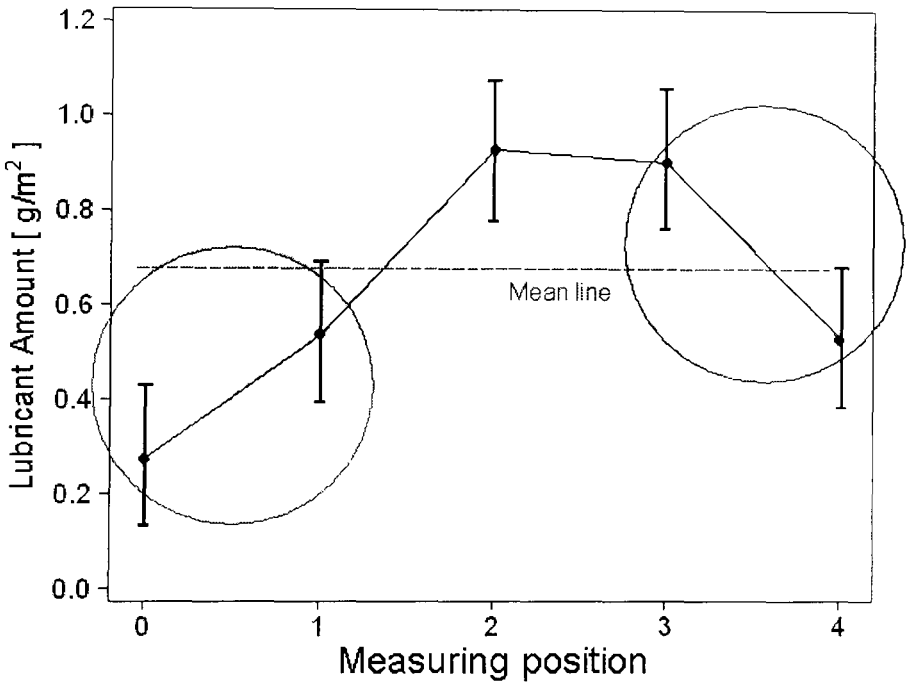

Figure 4.11 - Oil amount vs measuring position (experimental – average of different EBT materials at 0.7 g/m² initial oil amount)

- **Low pressure** – the low-pressure region is far from the tool (top-right circle in Figure 4.11). In this area the final oil amount curve generally presents exponentially smoothed behaviour and the adopted migration index (MI_L – see Equation 4.2) was the logarithm of the difference of amount in the oil between the last two positions in the sheet:

$$MI_L=LOG10(LA(4)-LA(3))$$

Equation 4.2 - Migration index at low pressure

Linear and exponentially smoothed behaviours are very frequent in nature. The former represents a system's reaction to a constant force (i.e. punch), while the latter to an impulse (squeezed oil moving because of inertia). Further, these approximations are usually employed for "first attempts" when no previous knowledge is available, as is the case here.

4.4.3 Oil migration under the punch (high pressure region)

The high pressure area is directly under the punch and can represent the behaviour of oil when pressing the panel. For this reason only the oil used in pressing operations was considered of interest and tested for correlation. Because of the power of modern computers a commercial programme (MiniTab) was used. The oil migration results were correlated with every conceivable 3D roughness parameter that has been suggested and combinations of relevant parameters but paying particular attention to the parameters thought to be significant as described above in section 4.3.1. The results showed that in this high pressure region of the sheet, the oil migration showed a high correlation with the surface topography parameter Sva calculated at surface level zero (annotated as Sva(0)), as shown in Figure 4.12.

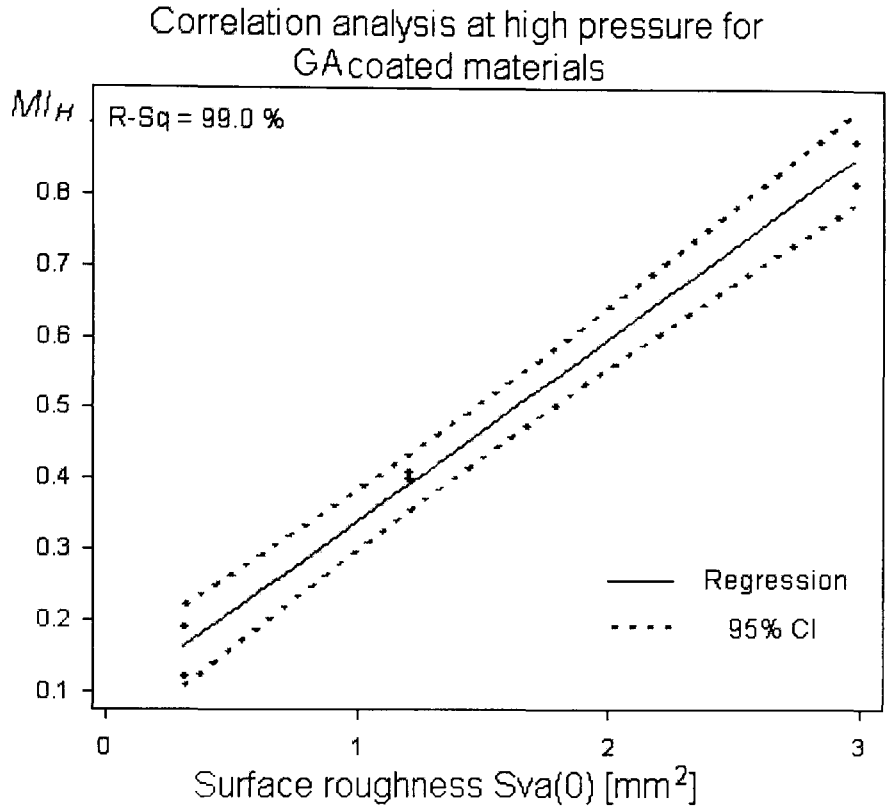

Figure 4.12 - Correlation between the closed area surface parameter Sva(0) and the oil migration index under the tool for GA coated materials

A theoretical explanation of the phenomenon could be as follow: the stochastic misalignment of void valley areas (Figure 4.13) enables oil migration across the sheet because oil can move from one valley to the next because of the overlaps. The greater is the average valley area, the higher the expected area overlapping one another, thus the higher the migration. This is shown in the schematic diagrams of Figure 4.12. The right hand diagram has more overlaps than the left hand one and hence there are more escape paths for the oil to pass along. Although these diagrams are shown in 2D, the pattern of overlapping valleys will be in 3D and thus the 3D parameter will show a stronger correlation than the equivalent 2D (Rva(0)) which was the case. Thus, only the 3D parameter correlation of (Sva(0)) is shown because it had the highest correlation of all the parameters and combinations investigated.

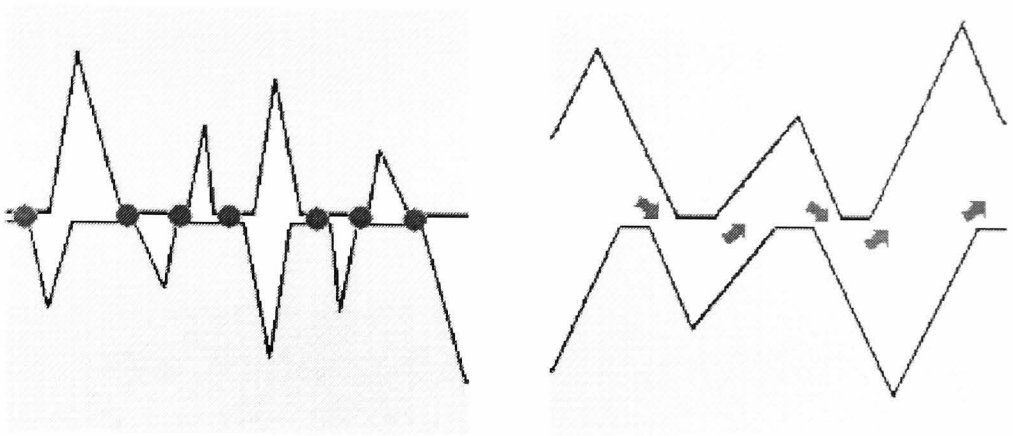

Figure 4.13 - Closed Areas migration mechanism (smaller closed area overlapping leads to less oil migration)

4.4.4 Oil migration outside the punch (low pressure region)

This area is away from the punch and was thought to be more representative of the behaviour when storing the material prior to pressing. For this reason only the oil with rust preventing properties was considered of interest and tested for correlations with parameters. The rust preventing oil is the one showing lower viscosity. Lower viscosity lubricants are normally employed for this purpose because they are easier to wash away.

Under these low-pressure conditions, the oil migration results showed that there was not one universal 3D parameter that correlated with oil migration but rather two parameters. One was the valley area parameter Sva and the other was the average roughness Sq. The former applied to all oil migration tests using the coating GA and the latter to all the tests using the coating GI. It was unfortunate that no correlation tests could be performed using the other coating (ELO) or the uncoated steel (CRS). The reason for this unfortunate situation is that the organisation required to get all the materials to the right place at the right time was sometimes very difficult due to factors like production pressures, delivery failures and simple misunderstandings. For a variety of reasons, there was a shortage of CRS sheets and ELO coated sheets delivered in time for the oil migration tests. Some sheets were included in the programme but unfortunately due to the combination of available materials, there were not sufficient repetitions performed to allow a correlation analysis on coatings CRS and ELO. There were only two sets of

results generated, which is insufficient for a reliable correlation test. Further research work on these two coating types is therefore recommended.

With regard to the GA coating, the migration phenomenon appeared to be driven by the size of the closed valleys (Sva at level 0, i.e. Sva(0), which is the level at 50% of the bearing area curve). Conversely, for GI coated materials it appears that the migration is driven by the average roughness of the sheet surface. In this case the "best" average roughness correlation was with the RMS parameter Sq. Figure 4.14 shows the correlation between the MI_L on GA materials and the Sva(0) parameter. Figure 4.15 shows the correlation between MI_L on GI materials and the Sq parameter.

At low pressure, beside minor spots, no peak deformation should be observed. This means that Sq (height distribution of the surface) should well describe the peaks opposing the lubricant movement as observed for GI coated materials. Nevertheless, GA coated seems to behave similarly to the high pressure. This might well be due to lack of experimental data for the named coated materials.

Due to the combination of available materials, there were not sufficient repetitions to perform a correlation analysis also on CRS and ELO. Further research work on these two coating types is therefore recommended.

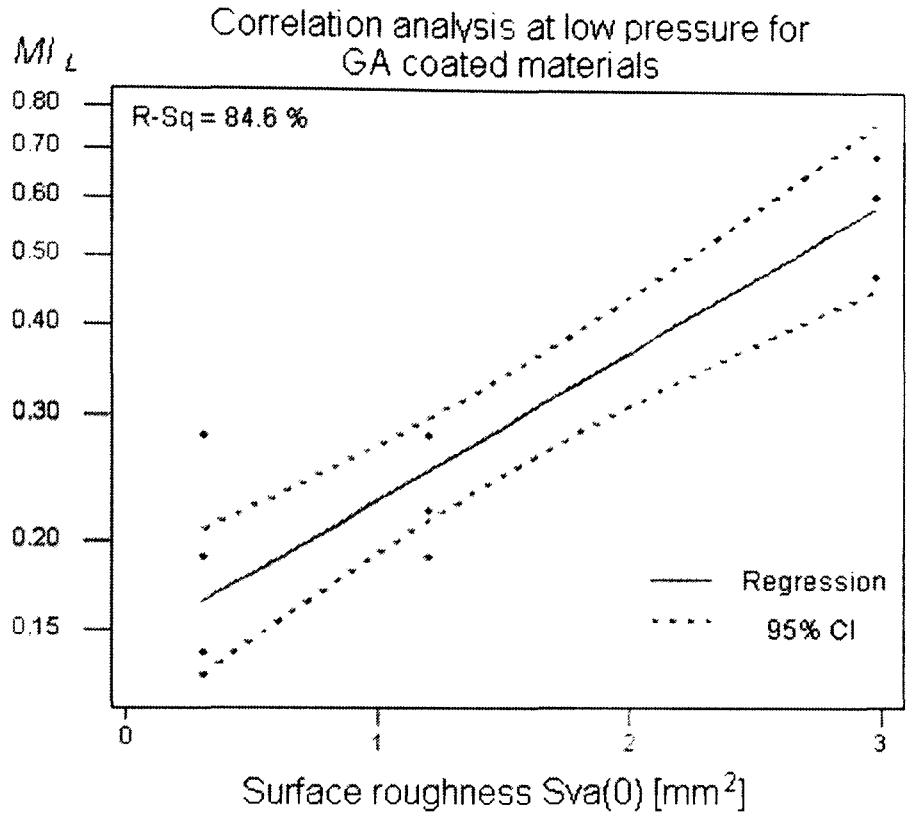

Figure 4.14 - Correlation between the closed area surface parameter Sva and oil migration index outside the tool for GA coated materials

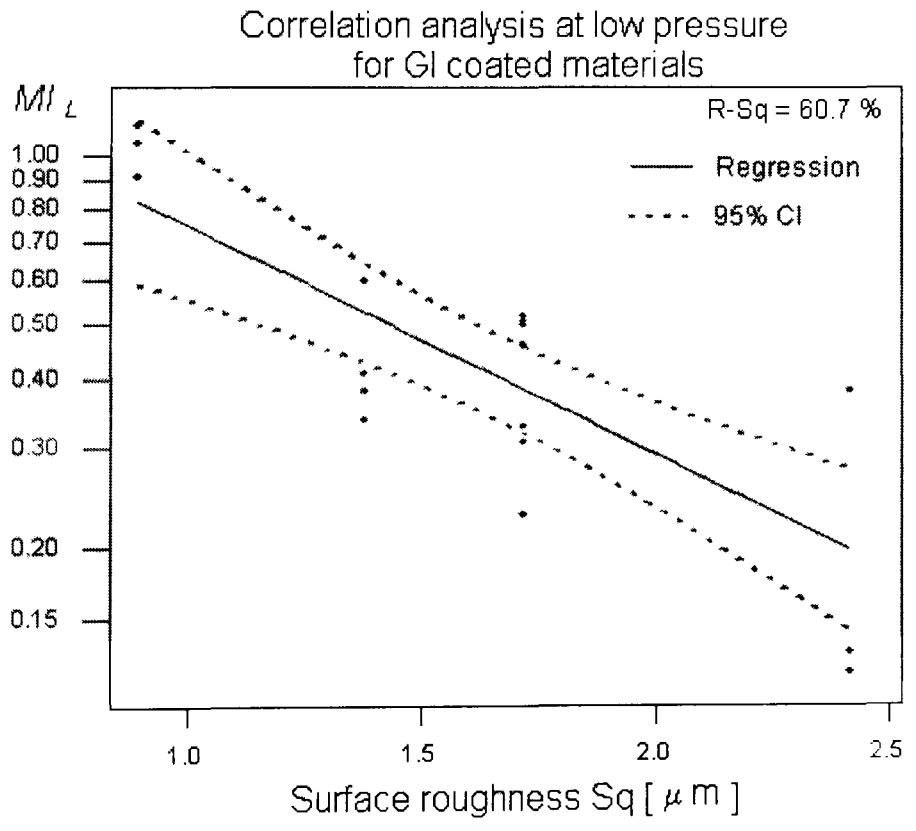

Figure 4.15 - Correlation between the surface parameter Sq and oil migration index outside the tool for GI coated materials

4.5 Summary

- ✓ Oils are used in the automotive industry to protect the metal from corrosion and improve its performance during forming.

- ✓ Besides the work of [Zaccone et al, 1998 and Holtkamp, 1999], describing the oil re-distribution over the sheet after different storage times, no work could be found in the field of oil migration for the automotive industry.

- ✓ Because of this lack of previous knowledge, a novel experimental procedure was deployed in order to study the phenomenon.

- ✓ This experimental procedure is based on a compression-testing machine, compressing a stack of lubricated sheets for 5 hours at a pressure of 10MPa.

- ✓ This test configuration proved to be effective in relating surface topography effects upon oil retention.

- ✓ There was a high correlation found between the migration index (difference of two consecutive measurements of oil amount) and the surface parameter Sva.

- ✓ In fact, the larger the average valley area (Sva), the larger the expected oil migration (see Figure 4.12).

- ✓ At lower pressures (far from the tool area) it was found that different coatings behaved in different ways.

- ✓ At low pressure, GA coated materials continued behaving in the same way as described for high pressure, while GI coated materials appeared to be influenced by the surface parameter Sq.

The study of the effect of surface parameters upon deep drawing can now be taken further. In the next chapter lubricated surfaces will be tested for behaviour under a rotation friction experiment.

5. Friction in sheet metal forming

5.1 Introduction

In the previous chapter, the subject of oil migration on steel sheets during autobody panel processing was covered in terms of the previous work and the description of a research programme. In this chapter the same approach will be adopted but with respect to friction in autobody panel manufacture.

The chapter will start with a description of the relevant previous work published on the subject of friction. This will be followed by the description of a test programme that aims to simulate the friction conditions existing in forming autobody panels. Finally, the results of the friction tests will be related to 3D surface roughness parameters.

5.2 The historical laws on friction

5.2.1 Friction on moving dry surfaces

Amonton presented three laws (although the third is implicit in the first two) for dry friction between relatively moving objects in the year 1699 [Wihlborg 2000]:

1) The ratio of friction stress (F_T) to the normal stress (F_N) is commonly known as the coefficient of friction (μ). This law is also known as **Coulomb's law** (linear relation between the forces shown in Figure 5.1).

$$F_T = \mu \cdot F_N$$

Equation 5.1 - Coulomb's law

Coulomb's law states that friction only depends on the nature of the two surfaces and not on the size of the nominal contact area. Because of surface roughness, there is a difference between the nominal and real contact areas. Therefore, as long as an increase in real contact area is proportional to an increase in surface load, Coulomb's law remains true. However, when the surface load increases above a given level such that surface and sub-surface deformation occurs, this proportionality ends, see Figure 5.1.

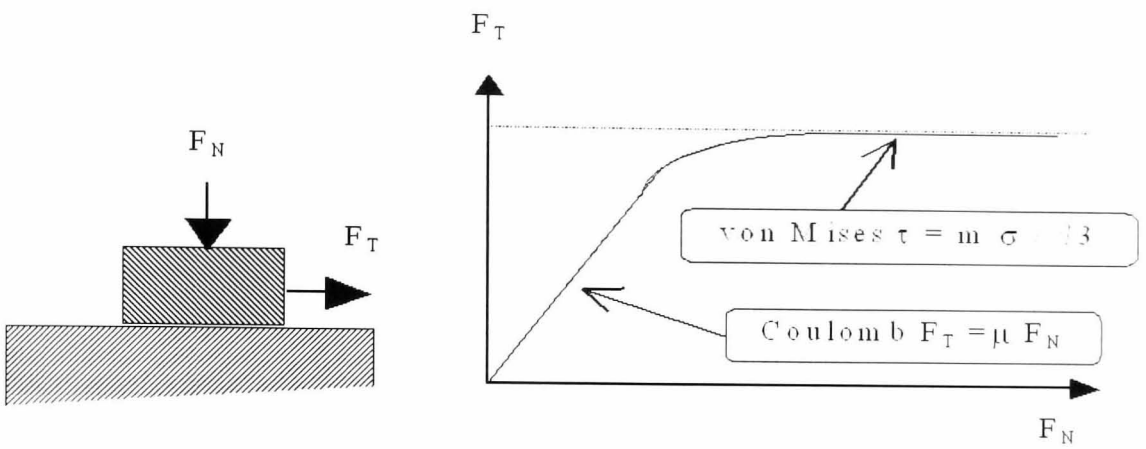

Figure 5.1– Un-lubricated friction mechanisms

2) At high surface loads the frictional resistance of the material (shear strength) is a fraction of the strength of the material in the surface layer. This law is known as **von-Mises's** law:

$$\tau = m \cdot \frac{\bar{\sigma}}{\sqrt{3}}$$

Equation 5.2 - Von-Mises's law

Where "τ" is the friction stress, "$\bar{\sigma}$" is the material shear strength and "m" a constant. In this region, the real contact area is very close to the nominal contact area and the movement takes place by shearing of surface layers.

3) The friction force is independent of sliding velocity. This third law is also attributed to **Coulomb**, and applies to both Coulomb's and von-Mises's regions.

Therefore, the classic Coulomb's friction law gives a coefficient of friction that is independent of speed and contact area. This is approximately true for non-lubricated surfaces at relatively low surface pressures. For lubricated friction however, the effects are considerably different. Emmens [1988] has shown that under the conditions relevant to autobody panel forming, the coefficient of friction turns out to be dependent upon speed, normal load and lubricant viscosity. If we are going to consider the friction in forming, we must consider the lubricated case.

5.2.2 Friction on moving lubricated surfaces

At the beginning of last century, a scientist named Stribeck described what happens between lubricated surfaces. He pointed out the difference between classic non-lubricated friction conditions and lubricated friction conditions. He states things like [Jonasson 1995]:

1. "The friction coefficient varies dramatically depending on the lubrication conditions between the steel surfaces. It appears that, when little lubricant amount is applied, sliding velocity is slow and the pressure between the surfaces is high, the (tribological) system follows the von-Mises's law".
2. "Under conditions of increasing velocity and decreasing pressure, the lubricant film becomes active and reduces the real contact area between the contacting surfaces. Thus, the friction coefficient reduces dramatically".
3. "Under conditions of high velocity and low pressure it appears that friction is influenced only by the lubricant viscosity. Lubricant viscosity is perceived to increase the importance of the lubricant film thickness".

Stribeck's experiments were based upon a shaft rotating at high velocity in a lubricated bearing. Upon reaching a stable high speed, an increasing radial load was applied to the shaft. This caused the speed to reduce because of the effect of friction. He found that under different operating conditions he could always identify three lubrication regimes when friction was plotted against operating conditions (eg velocity, viscosity and pressure). Another scientist named Hersey [*Jonasson 1995*] found that the Stribeck curve could be simplified if a parameter was used that subsumed three things: the oil viscosity, the pressure and the velocity. This parameter is called the "Hersey" parameter and is given by:

$$H = \eta \cdot \frac{v}{P}$$

Equation 5.3 - Hersey parameter

Where "v" is the surface velocity, "P" the surface pressure and "η" is the lubricant's kinematic viscosity.

A typical schematic Stribeck curve is shown in Figure 5.2 in which friction (μ) is plotted against the log of the Hersey parameter (H).

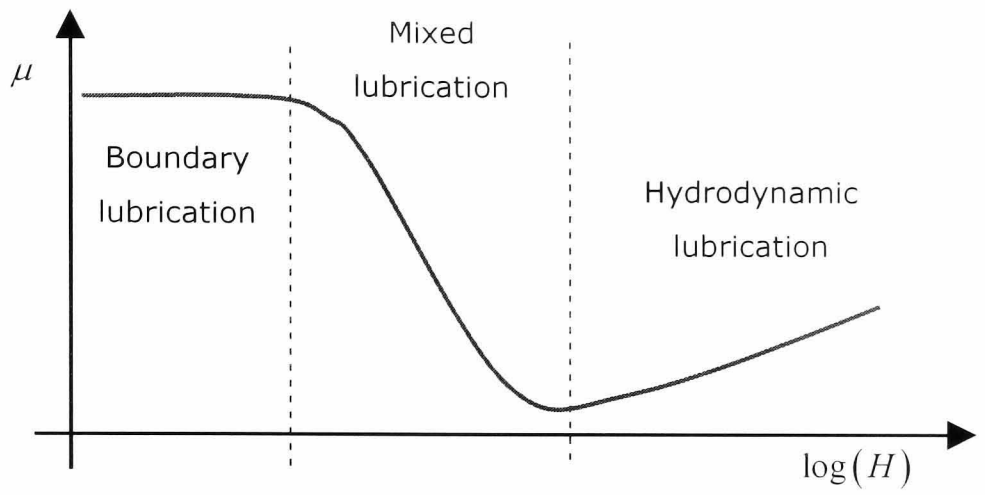

Figure 5.2 – Typical Stribeck curve

Stribeck showed that the curve could be divided into three different lubrication regimes, which he named "Boundary", "Mixed" and "Hydrodynamic". These lubricated friction regimes can be graphically represented [ASME 1995] as shown in Figure 5.3 below:

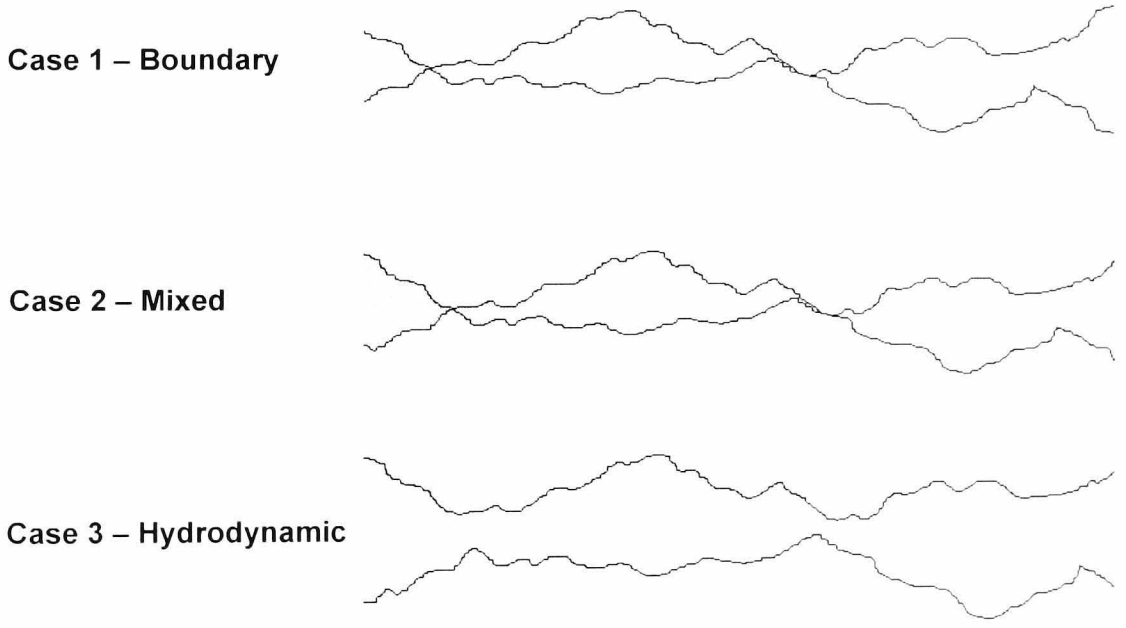

Figure 5.3 – Lubrication regimes

The first regime is boundary lubrication (case 1). It is characterised by a thin layer of lubricant covering the surfaces. When the lubricant is applied in this amount, it never fills the valleys and rarely prevents contact between the two

surfaces. The third regime is hydrodynamic lubrication (case 3) where oil completely fills the valleys as well as the interface and prevents the metal surfaces from coming into direct contact. The second regime is mixed lubrication (case 2) and it is, as its name implies, the intermediate regime between boundary and hydrodynamic.

Applying the principles of the three lubrication regimes to sheet metal forming in general and deep drawing in particular, all three regimes have been observed. The hydrodynamic regime exists where the pressure is low and the velocity is high. Such conditions can exist during deep drawing but they are rare. Hydrodynamic conditions certainly do not exist at those points on a die surface where there is a change in geometry because the local pressure will be high and the velocity low. At sharp changes in geometry, like small radii, there is very likely to be boundary lubrication conditions and possibly mixed [Skade 1994]. The situation is complicated by the fact that a sheet travels through the die as it is formed.

For example, consider the cup drawing case shown in Figure 1.1. An element on the sheet surface will pass along the flat portion horizontally under the blank holder, flow over the die radius and be pulled vertically as it is transformed into the cup wall. As the sheet undergoes this shape transformation, it is subjected to very different interfacial conditions under the boundary and/or mixed lubrication regimes. For example, Ter Haar [1996] observed that most deep-drawing processes operate either in the boundary or at the beginning of the mixed lubrication regime.

The complexities of even the simplest deep drawing operation mean that it is very difficult to model the process and thus, the approach adopted here will be to model friction using a specially designed rig and then relating the results to deep drawing and the lubrication regimes. This underlines the importance of correctly characterising these regions. Thus, the experimental work on friction was performed with a focus on the characterisation of the mixed and boundary lubrication regions (see Appendix 6 for experimental details).

5.3 The friction experimental procedure

Over the years, many friction test devices have been proposed and used. The first friction-testing device appears to be the one developed by Leonardo da Vinci (Florence, circa 1495). This device is sketched in Figure 5.4. He used this device to show that friction force is dependent on the force pressing two bodies together but independent of the apparent area of contact [ASM 1995]. This device contains the basic elements used in any friction test device.

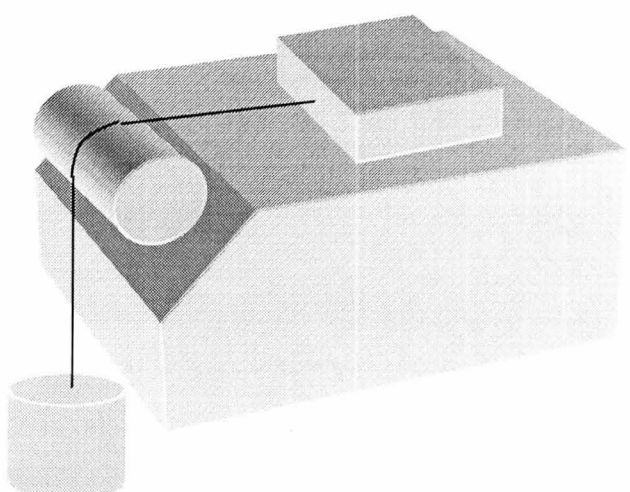

Figure 5.4 - Leonardo da Vinci's friction test device

A comprehensive survey of friction and wear test devices has been undertaken by the American Society of Lubrication Engineers [ASLE, 1976]. All devices in the ASLE survey contained in some manner or other the basic elements used by Leonardo da Vinci. These are: a means of providing movement, of controlling pressure and of measuring friction. They found that one of the simplest devices and one of the most common was the "pin-on-disk" type. In their classification, this is a type E device. In a pin-on-disk device, the force applied to the pin gives the interfacial pressure, the disk speed of rotation gives the velocity and a torque transducer measures the friction. Since this is such a standard and common device, it was the one selected for use in this work. It is also significant that Emmens [1988], one of the foundational workers in friction measurement as applied to industrial deep drawing testing, also use the pin-on-disk approach.

5.3.1 The friction testing device

The test adopted during this work (shown in Figure 5.5), is a pin-on-disc type with three pins rubbing against a disc (class E of the American Society of Lubrication Engineers) [ASLE 1976]. It is of the same type as the one used by

Emmens first [1997] then Holtkamp [1999] within the Hoogovens organisation who are one of the Autosurf partners.

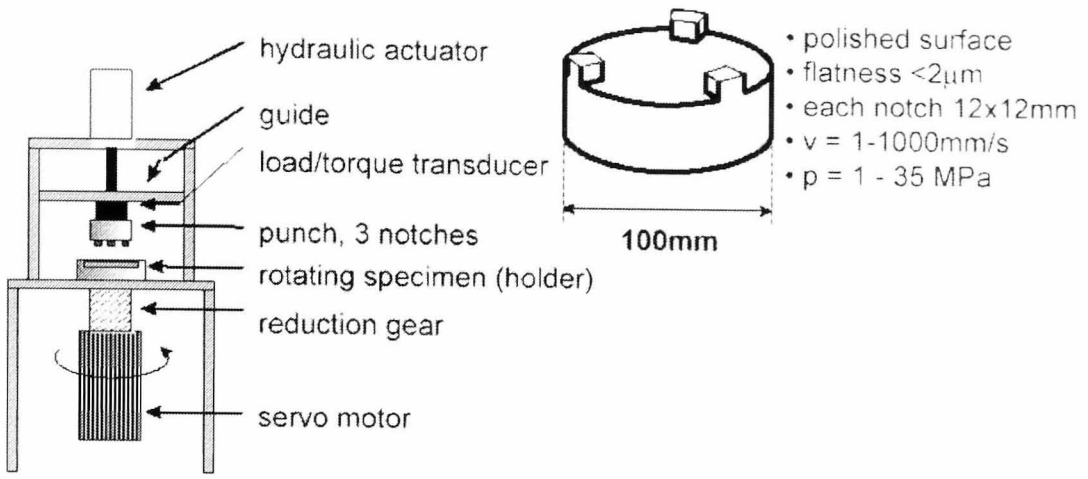

Figure 5.5 - Rotational friction tester at Hoogovens

5.3.2 The materials tested

Every coated material available was tested during these tests. The procedure adopted produced eight points on the Stribeck curve, which had eight equidistant H values. Every testing combination was repeated at least 4 times (plus one "dummy" to warm up the device). The full list of tested materials was as follows:

Name	Yield Strength [MPa]	Coating type	Texture	Sq [μm]
B1	257	ELO	EDT	1.63
B2	182	ELO	EDT	2.29
B3	135	ELO	EDT	1.93
B5	167	GI	EDT	1.57
B8	261	GA	EDT	1.73
H1	166	GI	EDT	1.69
H2	162	GI	EDT	1.31
H11	150	GA	EDT	2.79
H14	221	GA	EDT	2.4
H17	387	GA	EDT	1.94
S1	128	ELO	EBT	1.39
S2	157	ELO	EBT	1.81
S3	163	ELO	EBT	2.51
S4	178	GI	EBT	1.78
S5	157	GI	EBT	1.23
S6	165	GI	EBT	2.43
S8	155	GA	EBT	2.05
P2	168	GI	ECD	1.84

Table 5.1 – List of materials employed for friction testing

5.3.3 The experimental conditions

The eight H values were obtained by the following factors combination:

4. two lubricants of different viscosity (one thick and one thinner, the same two as in Chapter 4, section 4.3)
5. two sliding velocities (2 and 200 mm/sec) – these two velocities were though to be the minimum and maximum velocities that can be observed in a typical deep drawing operation [Holtkamp 1999(b)]
6. two clamping pressures (1 and 10 MPa) – similar to the velocity, the typical pressure expected to be exerted on steel sheets during deep drawing operations range from 1 to 10 MPa [Holtkamp 1999(b)].

By combining these three control factors it is possible to obtain the eight Hersey values, these being:

Setting	Lubricant Viscosity [Pa]	Velocity [m/s]	Pressure [Pa]	H [m/s]	Log H
1	12.2E-3	2E-3	10E6	2.44E-12	-11.61
2	99.3E-3	2E-3	10E6	1.99E-11	-10.70
3	12.2E-3	2E-3	1E6	2.44E-11	-10.61
4	99.3E-3	2E-3	1E6	1.99E-10	-9.702
5	12.2E-3	200E-3	10E6	2.44E-10	-9.612
6	99.3E-3	200 E-3	10E6	1.99E-09	-8.702
7	12.2E-3	200 E-3	1E6	2.44E-09	-8.612
8	99.3E-3	200 E-3	1E6	1.99E-08	-7.702

Table 5.2 – Settings for Stribeck Measurement

For information, the complete testing procedure is presented in Appendix 6, and the Stribeck curves are presented in Appendix 7.

5.3.4 Contact between the steel sheet and the tool

In any rubbing situation, the lubrication regime shown in Figure 5.3 above will depend upon the surface topography of both surfaces in contact. Since we wish to investigate only the effect of the autobody sheet surface texture on the interfacial conditions, we need to measure the effect of the sheet on friction and not the die. We can do this by making the die surface finish as smooth as possible in comparison to the sheet. Thus, the tool surface was polished to a finish of at least 0.05μm Ra. This is a "mirror" finish. This compares to a typical sheet surface finish of 1 to 2 μm Ra. Thus, the die surface finish is an order of magnitude better than the sheet surface finish. It was felt that this was sufficient to ensure that we were only measuring the

effect of the sheet topography and not the die. To maintain this smooth surface finish, the tool surface was polished between each experiment and re-measured to check it was less than the 0.05 μm Ra value.

Because of this constant tool polishing, one can assume that tool roughness is negligible in comparison to the material roughness. Therefore, as a first approximation, the material surface could be considered as interacting with a nominally flat surface.

5.4 Surface topography and friction

There has been much research work done on the influence of surface topography on forming forces, friction, lubrication and wear. The number of books published on the subject typifies this. The most recent publications and the ones most relevant to deep drawing are as follows. As a means of understanding the lubrication regimes in deep drawing, Emmens [1997] found a correlation between the 2D surface parameter "Ra" and the point of inflection between the boundary and mixed lubrication regimes on a typical Stribeck curve. In the same vein, Scheers et al [1998] used the transition point between boundary and mixed regimes to discriminate the influence of different surface topographies upon friction. Other representations of the relationship between coefficient of friction and surface topography were also undertaken. For instance, [Schipper 1988] proposed a model where the friction coefficient is a function of the average roughness (Ra), lubricant viscosity (η), sliding velocity and pressure. In his studies, he stated that the transition between regimes depends upon the combined roughness of the two sliding surfaces. [Holtkamp 1994] presented a similar model where the coefficient of friction is function of surface average roughness (Ra). This representation assumes that the surface topography follows a Gaussian distribution. Westeneng in 1996 and Gelink in 1999 further developed this last model [Holtkamp 1999(b)]. Although these results are very useful, there is a problem with them in that in all cases, the relationship with topography was in terms of 2D parameters. Also, workers assume a Gaussian surface topography since this can be conveniently represented mathematically. Few surfaces are truly Gaussian and certainly not the very structured ones produced by deterministic processes such as EBT. Thus, although there has

been significant previous work, it is not that helpful in relation to the search for 3D parameters to model deep drawing performance.

In the context of relating the 3D topography to friction, we can seek to link aspects of the process with the surface texture and this is attempted in the following section.

5.4.1 Hypothesis on surface parameter effects upon friction

Vermeulen [2001] has suggested a lubrication mechanism during deep drawing. His suggestion is that, when a surface is lubricated, only some peaks are in contact with the tool and therefore we should observe the boundary lubrication regime. The activation of the mixed regime should be due to lubricant dragged from surface's micro-valleys (see Figure 5.6) rather than the hydrostatic pressure build-up due to activation of the lubricant reservoir inside the valleys [Vermeulen 2001].

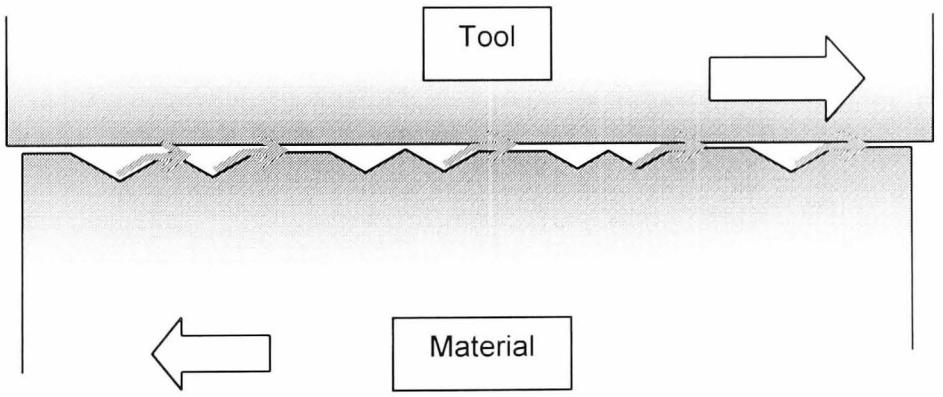

Figure 5.6 – Lubricant dragged by the movement

Thus, the contact area of the peaks against the die must be an important factor. This seems to be the case since the published literature correlates this phenomenon with surface topography using the number of peaks per unit of measured area [Pfestorf 1998]. This surface parameter is named "Peak Count", which in 2D is Pc. The fact that there is a proven correlation between Pc and drawability [Beherens 2000] shows that this mechanism is a reasonable one. Thus, since a forming operation is inherently a 3D one, the 3D equivalent of the peak spacing (Pc) is the peak density Spd. The 3D definition of Spd can be found in Appendix 2.

It is postulated that the 3D peak density is related to friction since as the peak count (Spd) increases, the peaks get smaller and the friction should decrease. This is the natural extension of the 2D case with the correlation with Pc. However, a better parameter to use is the average peak area since this is the actual area of the average peak that must be lubricated to prevent dry contact. In theory, the distance the oil must be dragged is less if the peak area is small rather than large. The average peak area is given by the 3D parameter Spa whose definition is given in Appendix 2. Simply put, it is the bearing area at a particular height divided by the peak density (Spd). Thus, this Spa will be investigated as part of the friction experimentation.

When the **surface is almost dry**, it is assumed to follow the Coulomb's law. Coulomb's law postulates that (see Equation 5.1), an increase of normal load (F_N) should lead to an increase of the tangent load (F_T) therefore keeping the friction coefficient (μ) constant. The increase of F_T is due to the growth of the real area of contact between the two surfaces. The real contact area is frequently addressed in the literature dimensionless as "Area Fraction of Contact" (also known as "α"), and it is defined as [Klimczak et al 1994]:

$$\alpha = \frac{A_{Real}}{A_{App}}$$

Equation 5.4 – Area fraction of contact

Note that "α" equals in definition the bearing area value at a given height (see section A1.3 of Appendix 1). Thus, the bearing area fraction will also be investigated as part of the friction experimentation.

Both these parameters depend upon the depth of deformation since the real contact area depends on the amount of tool penetration into the steel sheet's surface (which is unknown). Thus, in the analysis of the friction results, the values of "α" and Spa are calculated at different heights, which is the equivalent of different tool penetration depths determined from statistical analysis.

Because it is impossible to calculate the parameters at an infinite number of heights, for convenience of analysis, a selection of different heights is used based on statistical values. These are:

1. at the mean line [$h_{0.5}$],
2. at an average top of the peaks height which is given by 95% of the profile height [S95p],
3. at a height equivalent to half the distance from "average" top of the peaks to the mean line [S95p/2]

To explain these further, an example of an EBT surface is used. The heights are presented for convenience, through the bearing area curve for the EBT – GA coated material (named "S3") below (Figure 5.7).

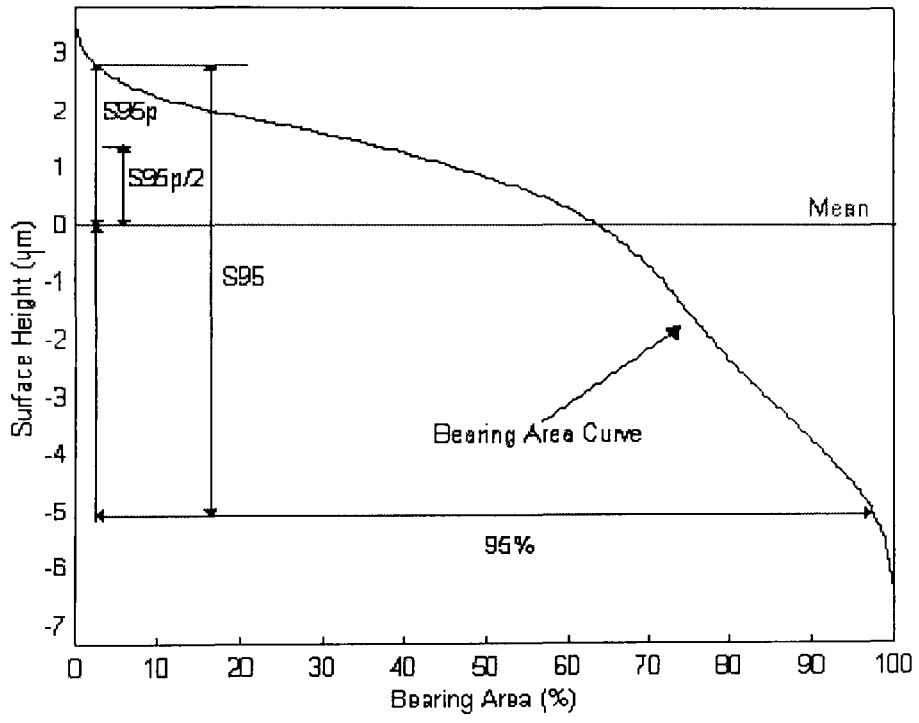

Figure 5.7 - Different height compared to the bearing area curve for the material S3

1. **$h_{0.5}$** (mean line, 50% of the bearing area) – this height represents the lowest possible level reached by the tool during any contact if no material is removed from the surface.
2. **S95p/2** (half of the distance between the mean line and the 95% of the surface's peaks) – this height is usually higher than h1g (defined below in point 4) and equals the 25% peak crush proposed by [Scheers et al 1998]. If the surface heights were normally distributed, S95p/2 would represent surface density's standard deviation (which

also equals Sq). For generally distributed surfaces it represents a surface "collapsing" by plastic deformation to half of its height above mean line.

3. **S95p** (the height covering 95% of the peaks) – this height represents the higher possible height reached by the tool during any contact. This height, if the surface heights were normally distributed, would represent twice the standard deviation (Sq). For generally distributed surfaces it represented a surface collapsing to only 2.5% of its original height.

A further height needs to be defined which relates to the amount of lubricant present on the surface. It is a fact that in some lubrication situations, the amount of lubricant applied is insufficient to fill the valleys completely with the result that the surface is not completely covered with oil. In this case, the amount used will only fill the valleys up to some common height. This height is termed "h1g" by this author. Thus, another height needs to be used in the experimentation:

4. **h1g** – this height represents the lower possible height reached by the tool prior to the onset of the hydrodynamic regime. It is the height at which the valley volume surface parameter $V_V(h1g)$ = 1.02ml (equivalent to 1 g/m^2).

In the friction testing experimentation, described below, the value of the parameters at the above heights will be used.

5.5 Analysis of tests results

Statistical analyses were performed on all possible factorial combinations for the available materials. A summary of the results is presented below (fully detailed analysis is available in Appendix 8). The results fell into two broad classes, which were those that follow the standard Stribeck's model and those that did not. The two types were strongly correlated to the coating type.

5.5.1 Zinc coating effect upon Stribeck curve

During the friction experiments, all the materials were lubricated with the same amount of lubricant (1 g/m^2). However, depending upon the experimental conditions used, the results fell into the two classes

characterised by two differently shaped curves, one following the Stribeck pattern and one not. The results are typified by the curves of Figure 5.8. This shows the different behaviour of two differently coated materials ("H14" is GA coated and "S2" is ELO coated) both were tested with the thinner lubricant (Aral Ropa VOV6).

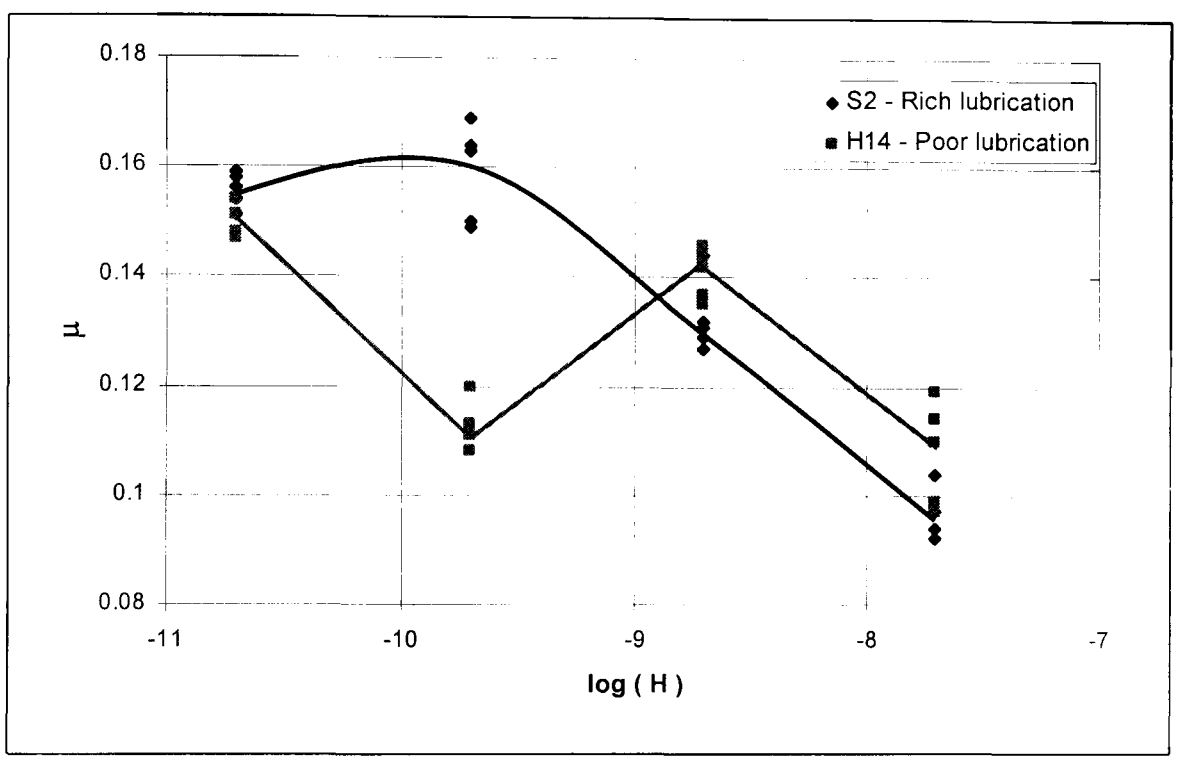

Figure 5.8 - Poor and rich lubrication behaviour

It is believed that the different curves are related to the ability of the surface coatings to provide lubrication. The amount of lubricant dispensed is 1 g/m^2, irrespective of the coating. Some of this amount might be trapped inside surface porosities or cracks that cannot be measured (i.e. GA coating effect in Chapter 4 Figure 4.8), hence this "trapped" lubricant is not available to generate mixed or hydrodynamic regimes, see chapter 5.5.3 below. The two classes of Stribeck and non-Stribeck results typified in Figure 5.8 could be described by:

- **"Poor" lubricated surfaces** – when the lubricant amount was insufficient to lead to Stribeck behaviour. During this "dry-surface" condition the material did not necessarily behaved accordingly to Coulomb's law. GA coated materials frequently showed this condition.

- **"Rich" lubricated surfaces** – when the lubricant amount appeared to be enough to lead to friction behaviour accordingly to the Stribeck theory. ELO coated materials frequently showed this condition.

GI coated materials showed both Stribeck and non-Stribeck behaviour.

It is thought the reason why the GA coating always showed poor lubrication is related to a very low h1g value. Inspection of the surface showed there was little oil coating the surface. This is supported by the oil retention results of Chapter 4 (see Figure 4.8). It is known that the GA coating has a structure which is complex consisting of many micro-cracks and micro-porosity, recesses and caverns similar to coral. This is caused by the annealing process, which creates a crystalline structure [Carless 2001]. The oil dispensed on the surface enters the crystalline structure and due to surface tension within the structure, there is little oil available for lubrication. Hence, the friction tends to be less dependent on speed. In fact these surfaces never switch to mixed or hydrodynamic regime.

Conversely, the ELO surface always appeared "oily" supported by the Chapter 4 oil retention results. The ELO surfaces do not have the same crystalline structure but rather the equivalent of a series of hemispheres caused by the growth of the electrolytic deposition process [Carless 2001]. The oil gathers in the resulting pockets and does not disappear "within" the coating. The oil is therefore available for lubrication. The friction tends to be lower and speed dependant, hence achieving the lubrication conditions described by Stribeck.

The GI friction results sometimes fell into one class and sometimes into another. The GI coatings are created as a result of dipping the sheet into molten zinc, hence the coating is cast onto the sheet surface. There follows an annealing process. However, the different GI operating conditions used are different and this creates slightly different surface structures which are variously crystalline [Carless 2001]. It is therefore thought that in those cases where the fiction is high, the surface is more crystalline and therefore the friction results are similar to the GA coating results. In other cases, the GI coating is not particularly crystalline and the results are similar to the ELO results. What is needed is for the various GI coated surfaces to be classified as to whether they are crystalline or not and then for the friction results to be

re-evaluated. Unfortunately, there was insufficient time and material available to test this theory and it has to be left to future work.

5.5.2 Lubricant effect on Stribeck curve

During his original studies, Emmens [1988] employed only base mineral oils with no additives. This enabled him to explore a wide range of Hersey values by simply changing the lubricant (viscosity), rather than the speed and load. In a similar manner, we decided to create a wide Stribeck curve by performing the same velocity-pressure experimental combinations using two lubricants and the ELO coating. Unfortunately, the results did not align themselves as per Emmens results. The reason for this is that both the lubricants used here contained additives with the result that the two plots could not be combined. A typical example of this behaviour for material "S2" tested at all Velocity-Pressure combinations with both lubricants is illustrated in Figure 5.9.

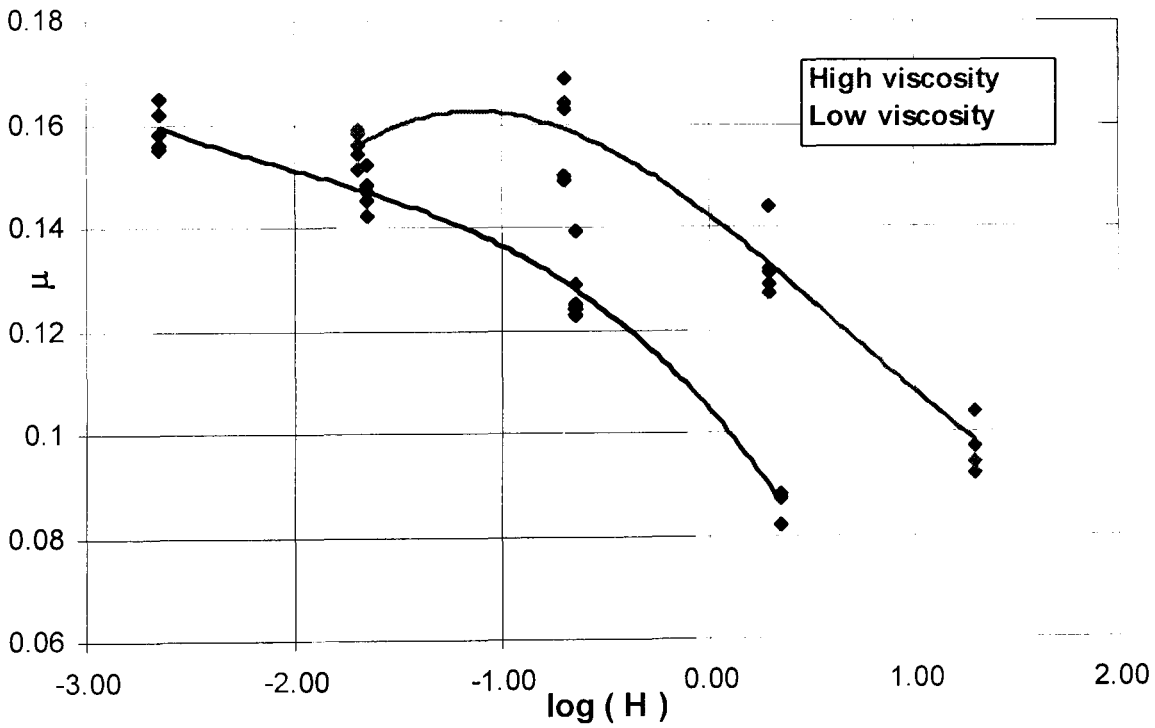

Figure 5.9 - Stribeck curves with different lubricants on the "S2" material

The full set of results can be seen in Appendix 7. The two sets of results show clear Stribeck behaviour but the curves are different. They are both of the same form but the low viscosity curve is shifted to the left in comparison to the high viscosity one. The relationship of the two curves is as expected in that as the viscosity increases, the entire curve shifts because the mixed

regime occurs later. This behaviour was exhibited with all ELO coated surfaces, irrespective of their surface finish. It would appear therefore that the ELO coating mostly creates the mixed lubrication regime. Some of the GI coating results showed this behaviour but it is significant that none of the GA coating results did. All the GA results showed a non-Stribeck curve, as did some of the GI ones. A typical curve for material H14 having a GA coating is shown in Figure 5.10.

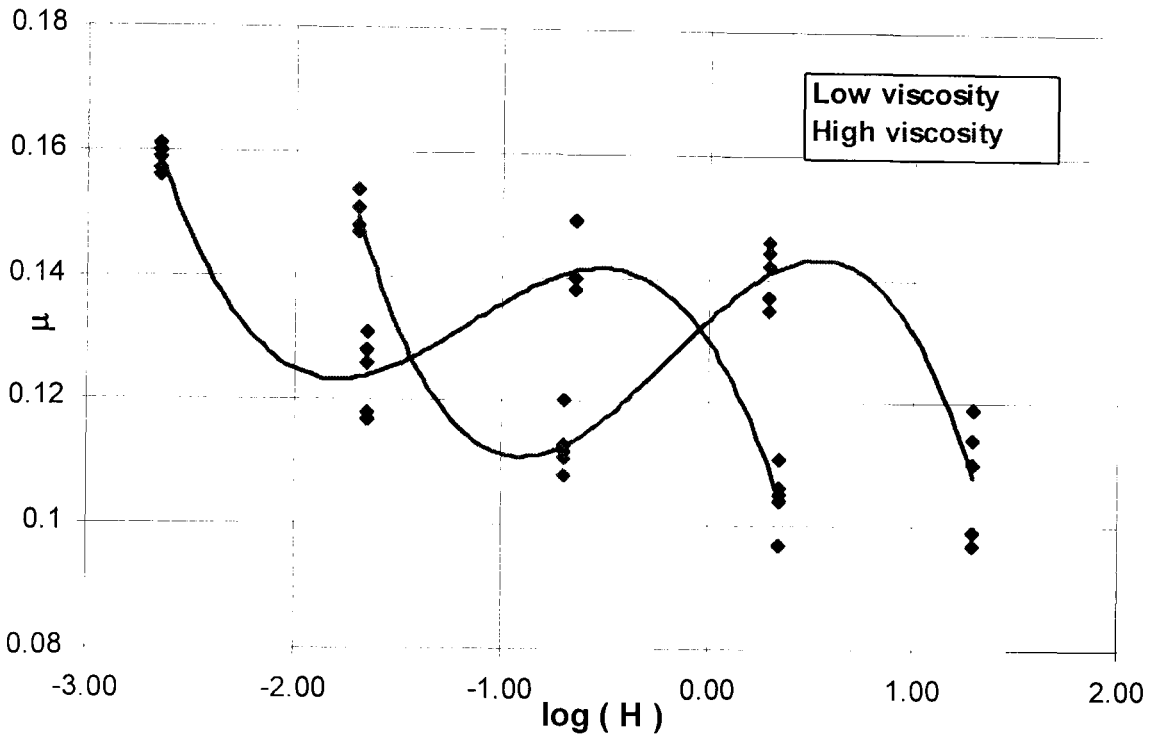

Figure 5.10 - Stribeck curves with different lubricants on the "H14" material

The full set of results is shown in Appendix 7. These curves are clearly non-Stribeck but like the Figure 5.9 curves, they follow the typical trend in that the low-pressure curve is to the right of the high pressure one. The reason for the undulations is that the two high points on each one are for the high-pressure test results and the two low points are for the low-pressure results. They do not seem to produce one continuous curve but rather undulations. One wonders if three pressures had been used rather than two whether the results would have produced two curves? Thus one can question whether there are four curves. Only further testing would prove this. However, what is clear is that these GA results are non-Stribeck and therefore the lubrication regime is boundary. It is thought the reason for this is the porous nature of the GA coatings in that the lubricant is held in the crystalline structure beneath the surface and cannot leach out to provide enough lubricant to

reach the mixed regime. However, there is some lubricant present because the two curves are shifted in relation to one another.

It is confusing that in some cases the GI coating results follow the Figure 5.9 curves and sometimes the Figure 5.10 curves. It is thought the reason for this is to do with the slightly differing structures of the GI coating. The GA coating is cast and then annealed whereas the GI coating is just cast, there is no annealing. Surface inspection indicates that, depending on the hot-dip conditions, sometimes the GI coating is closer in structure to the GA coating and at other times it is closer to the ELO coating. Thus, the friction test results will tend towards either the GA friction results or the ELO results. This means boundary or mixed lubrication regimes respectively. More testing needs to be undertaken to confirm this.

5.5.3 Correlation analysis with surface topography

Because of the interaction between lubricant type and zinc coating type (presented above), different correlation analysis had to be performed for the different coating-lubricant combinations. These various tests will now be described in turn.

GA coated materials

Friction data for GA materials frequently showed the "Poor Lubrication" regime, and the coefficient of friction (μ) was found to be dependant on the clamping pressure. In fact it was found that μ actually increases with pressure instead of remaining constant as stated per Coulomb (see section 5.2.1)

From the statistical analysis (the ANOVA table is shown in full in paragraph A8.1 of Appendix 8) it could be noticed that the most influential factors were pressure, velocity and surface texture but not the lubricant type. The same statistical results can be read from Figure 5.11 below. In this graph, every box plots the average values of friction coefficient for each of the control factors. In this case, the pressure seems to have more of an effect than velocity since the slope of the line is steeper.

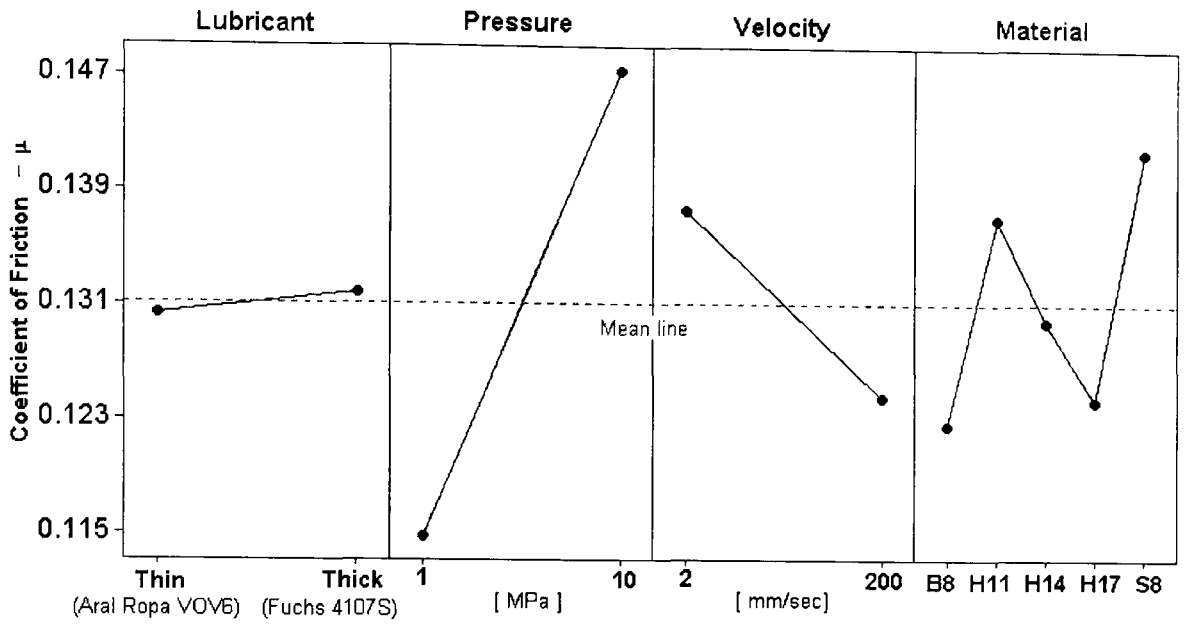

Figure 5.11 - Main effect plot of means for GA coated materials

As one can see, while the different values of pressure, velocity and the different materials tested lead to a very different average coefficient of friction, the two lubricants lead to similar ones (in fact they are very close to the mean line). This in turn means that the correlation analysis between the material surface topography and friction had to be performed separately for each combination of pressure-velocity. It is to be expected from all the above results that the pressure and the velocity will have an effect on friction. What is significant in our search for a topography descriptor or parameter that the surface finish or topography also has a significant effect on friction. The next stage is to investigate the influence of topography on friction.

For convenience, only one correlation analysis is presented in this section. The full GA correlation analysis can be found in section A8.2 of Appendix 8. The testing condition for this correlation analysis was 10MPa pressure and 2mm/s velocity, used because these conditions represent those present at the critical deformation points in a deep drawing process. Correlation showed that, in this situation it was found that the coefficient of friction depends on two things. Firstly, the bearing area fraction of contact (α) - the higher the value of α, the higher the coefficient of friction. Secondly, the sheet mechanical properties - the higher the yield strength the smaller the tool's penetration hence smaller friction. For all these results, the best-fit equation is given by Equation 5.5:

$$\mu = 0.144 - 0.000091 \cdot YS + 0.0695 \cdot \alpha(h1g)$$

Equation 5.5 – Correlation for GA materials, low velocity and low pressure

Where YS is the yield strength of the substrate material and α(h1g) is the area fraction of contact calculated at the "h1g" height defined in paragraph 5.4.1. It is not surprising that YS is in the equation because it is one the things that determines the peak's deformation. The αh1g is the total area of the peaks resisting the deformation at a height corresponding to the lubricant fill depth. This is an important depth (or indeed height) in that it is the depth of deformation at which the lubricant begins to be pressurised and hence will be available for lubrication. The effect of substrate material upon friction in GA zinc coated steel sheets was rationalised in the following way: since the coating is far harder than the substrate [Wrentik 2001], the peak deformation will be controlled only by the substrate yield strength.

In Figure 5.12 one can see the correlation plot of equation 5.5 where μ is plotted against value of equation 5.5.

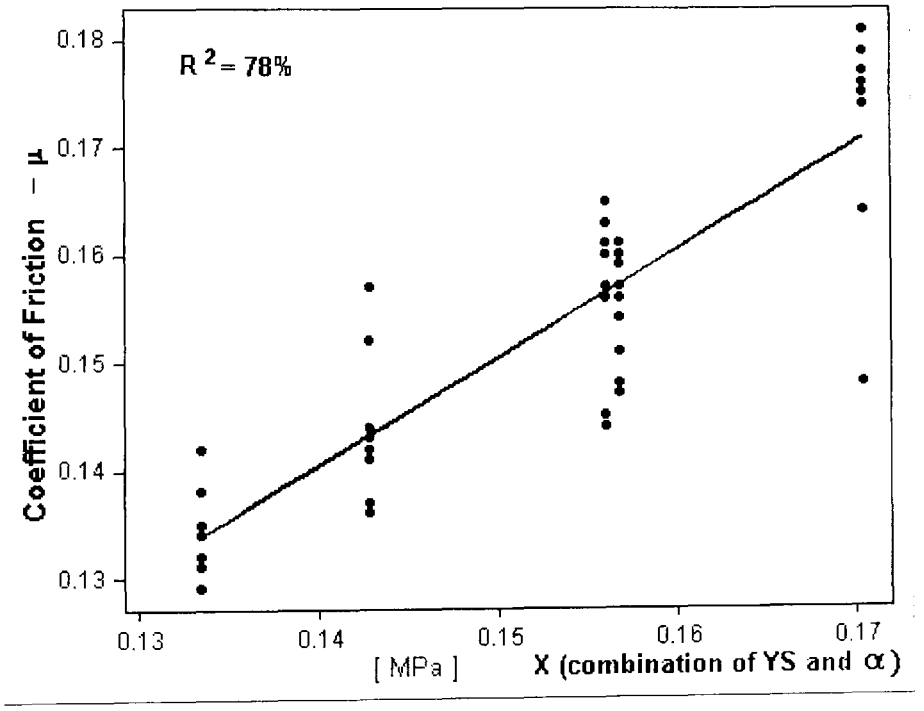

Figure 5.12 - Correlation between coefficient of friction and equation 5.5.

The correlation index (R^2) is 0.78. The higher the R^2 the better is the correlation (maximum 100%). The 0.78 is a high correlation and shows that one can place confidence in the fact that the material yield strength and the topography influence friction. We will return to topography and friction later.

ELO coated materials

All the ELO coated materials exhibited Stribeck behaviour, i.e. the "rich lubrication" condition of Figure 5.8, which means the lubrication regime was mixed rather than boundary. However, we need to explore the effect of the various operating conditions on friction for the ELO coating as we did for the GA coating (above). Thus, a similar set of tests was undertaken for the ELO coating. The full results are given in paragraph A8.3 of Appendix 8. The interactions of pressure, velocity, lubricant and material for these tests can be seen in the mean plots of Figure 5.13.

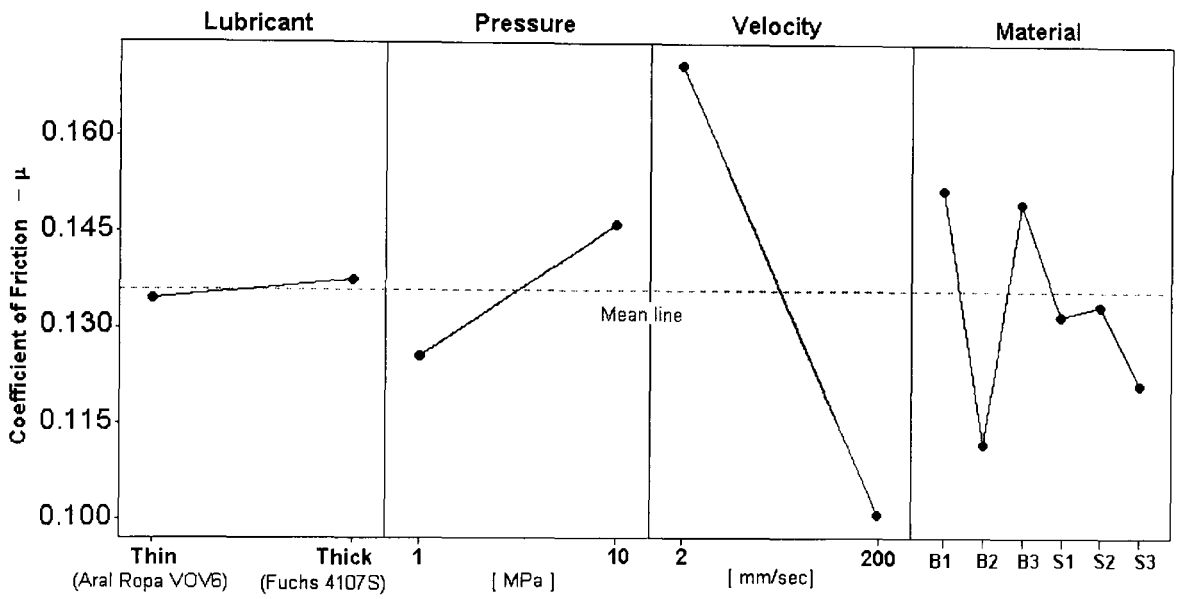

Figure 5.13 – Main effect plot of means for ELO coated materials

This ANOVA plot (and the statistical analysis) showed very similar results, as was the case with GA: a strong effect of pressure (second box), velocity (third box) and material type (fourth box) but not the lubricant type (first box). The lubricant result is the same as that noted above with GA in that lubricant seems to have a minimal effect. However, there was a difference between these ELO results and the GA results in that, although pressure and velocity each had a significantly effect, in this ELO case, the velocity seems to have more of an effect than pressure because the slope of the line is much steeper. This was the opposite to the GA results (Figure 5.11), which showed pressure to have more of an influence than velocity.

These primary results show that lubricant had little effect, however, there was an important interaction between material type and velocity, which was not

seen with GA and needs to be presented here. This interaction is shown in Figure 5.14.

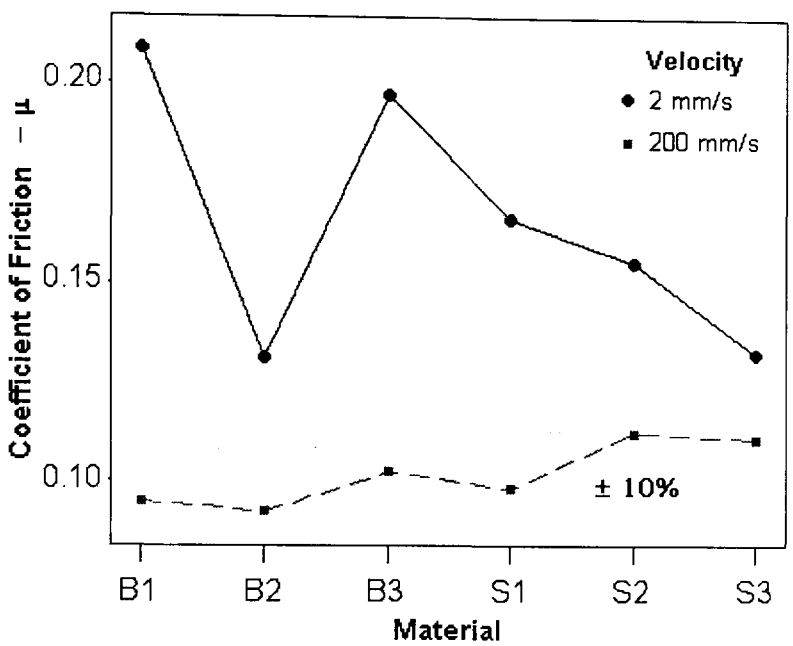

Figure 5.14 - Non-parametric interaction plot. Material name and velocity for ELO coated materials

At high velocity, the friction was always of a low value, in the order of 0.1, and it only varied by ±10%. This indicates mixed and possibly hydrodynamic friction. In this case, topography will have little effect on friction. With low velocity, the friction varied with material and had a much higher value, with a variation of about ±100%. This is probably boundary lubrication and it illustrates that there is interfacial contact with the die. In this case, if topography has an influence, it will be most likely to be seen at this low velocity since this is the velocity at critical places such as the die radius. Thus, in the search for a correlation with topography, we need to concentrate on the low velocity case.

In an attempt to find a correlation between a 3D surface parameter and the friction coefficient, a programme was written to compare the range of 3D parameters (mentioned above) with friction. This was the same programme used with the GA tests above, so we are comparing like with like. The full set of ELO results is shown in Appendix 9, section b.2. The highest correlation was for the average peak area "Spa", calculated at the "S95p/2" height. Figure 5.15 shows a typical set of results for 10MPa and 2mm/s. This

correlation coefficient was the highest of all the set of 3D parameters and was R^2 = 0.66 and was given by equation 5.6:

$$\mu = 0.125 + 3.94 \cdot S_{pa}\left(\frac{S95_p}{2}\right)$$

Equation 5.6 - Correlation for ELO materials, low velocity and low pressure

The graph for this equation is shown in Figure 5.15 below:

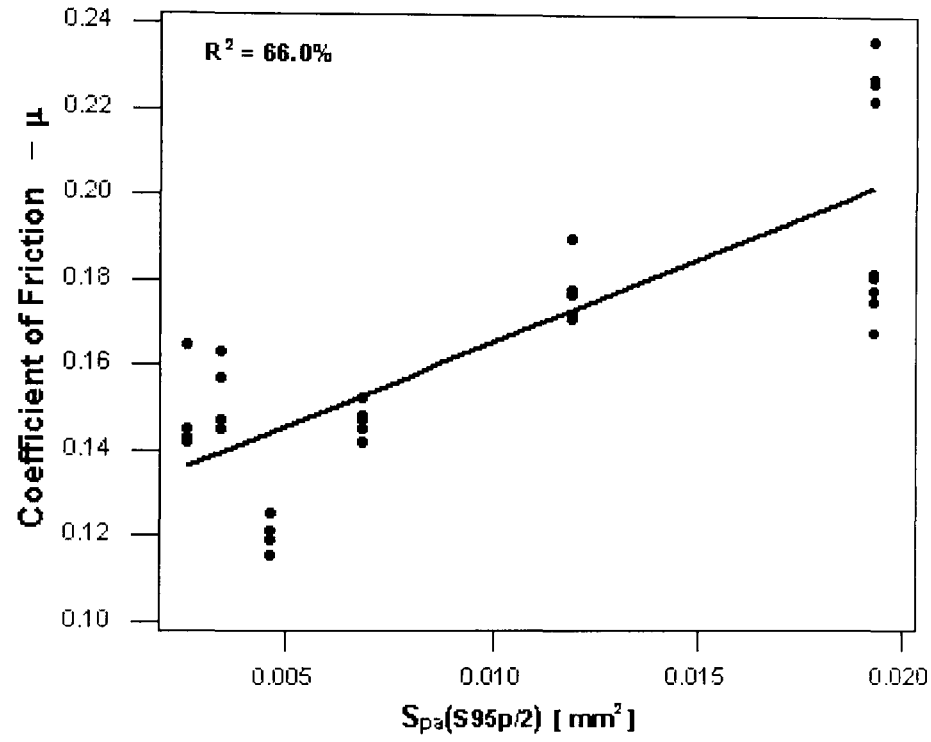

Figure 5.15 - Correlation between friction and surface topography for ELO

This is a very encouraging result in that it proved what this author had thought from the beginning, which is that when the surface finish is represented by a 3D "functional" parameter, there will be a correlation with things such as friction.

The results shown by equation 5.6 and Figure 5.15 proved the best correlation to be with the average peak area "Spa", calculated at the "S95p/2" height. One wonders why the correlation was best at this particular height and not another one such as the h1g as was the case for GA materials (given in equation 5.5). The reason for this is that, as noted by Scheers [1998], this height represents for ELO materials, the plastic deformation height or the

"collapsing" height (noted above in chapter 5.4.1) because it is only the very tops of the peaks that are deformed. For the majority the ELO materials, the h1g height was less than the S95p/2 height, thus, the deformation of the top of the peaks is never of such a magnitude that the h1g height is reached. Thus, if the h1g height is never reached there is unlikely to be much of a correlation with the Spa value at the h1g height and much more with the S95p/2 height value.

GI coated materials

A similar series of ANOVA tests were undertaken for the GI coated materials as had been used for the GA and ELO materials. The ANOVA table is shown in full in paragraph A8.3 of Appendix 8. The main effects plot is shown in Figure 5.16 below.

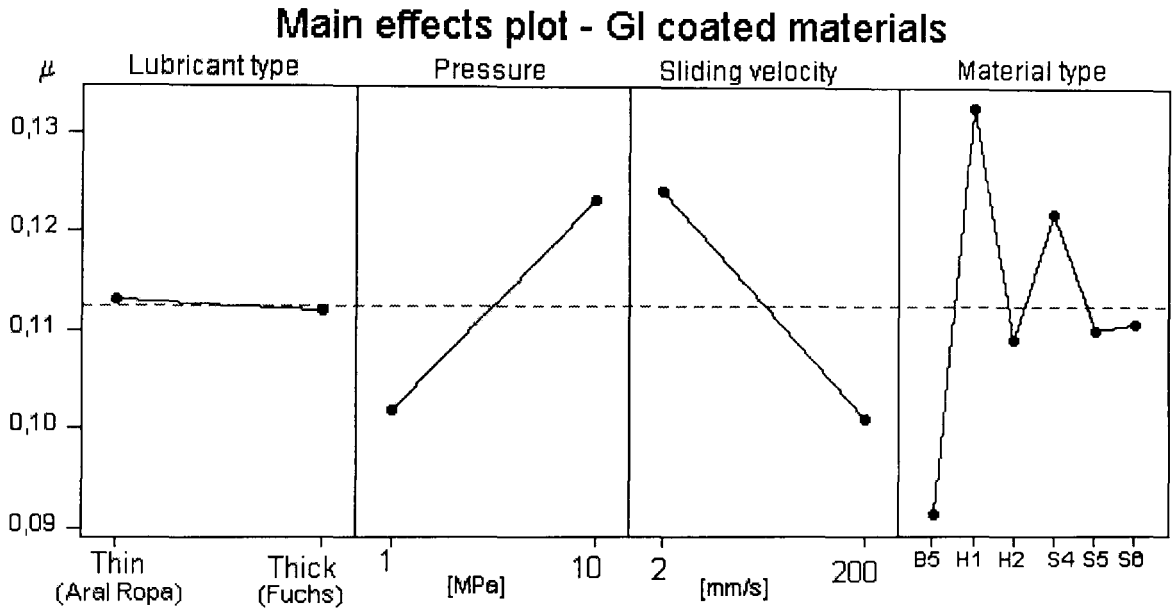

Figure 5.16 - Main effect plot of means for friction experiments on GI coated materials

These GI results show very similar trends to the GA and ELO results in that the most influential factors were pressure, velocity and surface texture but not the lubricant type. Indeed, for these GI coatings, the pressure and velocity seemed to have an almost equal effect because the slopes of the two lines in Figure 5.16 are equal (but opposite) which was not the case for the GA and ELO results. The main effects plot for GA coatings (Figure 5.11) showed that pressure was more influential than velocity whereas the main effects plot for the ELO coatings (Figure 5.13) showed that velocity was more influential than pressure. Here pressure and velocity have almost equal effects.

However, what is significant is that all the three coating tests followed the same trend in that in the lubricant has little effect whereas the velocity, pressure and topography all have a significant effect. It would appear therefore that whatever the coating used, the material is experiencing the same interfacial conditions during all the friction tests.

In the above friction experiments using the GA and ELO coated materials, tests were conducted to see if there were correlations between the friction coefficient and any of the surface area parameters. As has been explained above, the results showed correlation's between friction and the parameters α(h1g) and Spa(S95p/2) for GA and ELO coated materials respectively. When it came to testing the GI coated material results, an identical procedure was followed but with unfortunate results. No significant correlations were found between friction and any of the "R" (2D or "roughness") or "S" (3D or "surface") parameters covered above. Indeed, the GI friction results seemed not to follow any form of uniform behaviour. In some cases the results indicated "Poorly Lubricated" behaviour as per the situation described in section 5.5.1 above. This was the case for the H1, S4 and S6 materials. In other cases there was "Richly Lubricated" behaviour. This was the case for the materials named B5, H2 and S5. It thus appears that the GI materials do not conveniently fit into either the "GA" or the "ELO" friction categories. However there was no overall relationship between friction coefficient and any "R" or "S" type parameter, each one of the GI results either followed the GA or the ELO trends. Sometimes it seems that a GI result agreed with the GA trend and sometimes with the ELO trend, i.e. there was relationship between friction and α(h1g) or Spa(S95p/2) but not with any other parameter. It was noted in section 5.5.2 above that with respect to the Stribeck curves, the GI results sometimes followed the GA results (Figure 5.9) and sometimes the ELO results (Figure 5.10). It was suggested that the reason for this is to do with the slightly differing structures of the GI coating. The GA coating is cast and then annealed, whereas the GI coating is just cast (there is no annealing). Surface inspection indicates that, depending on the hot-dip conditions, sometimes the GI coating is closer in structure to the GA coating and at other times it is closer to the ELO coating. Thus, the friction test results will tend towards either the GA friction results or the ELO results. It would appear that the friction results follow the same pattern in that

sometimes the friction follows the GA trends and sometimes the ELO trends, never anything else. It seems logical to ascribe the difference to the way in which the GI structures are sometimes similar to the GA structure and at other times similar to the ELO structure. It is thought that this could be clarified by a further experiment. Which would involve dividing the whole set of GI friction results into one of two classes. One class would be those GI surfaces that resembled a GA coating structure and the other those GI surfaces that resembled an ELO structure. If analyses were then run to test the friction coefficient correlation with the parameters α(h1g) and Spa(S95p/2), it is suspected that correlation's would be seen. However, this would need to be the subject of a further investigation because it was not undertaken here.

5.6 Conclusions and discussion

The results on friction experimental work proved that the Stribeck model for friction of lubricated surfaces lacks accuracy when trying to describe the zinc coated materials used in metal forming.

The interaction between lubricant type and zinc coating confirmed the results found during the lubricant retention work. In fact, looking at Figure 4.8 in Chapter 4, it is possible to notice that ELO coated materials exhibit the higher amounts of retained oil after testing, while GA coated materials lower. In the same way, during the friction experiments, the GA coated materials behaved as "Poorly" lubricated while ELO coatings always behaved as "Richly" lubricated, although they were lubricated with the same amount of oil. Therefore, the two different friction behaviours could only be rationalised by employing two different surface topography parameters.

The coefficient of friction of the materials exhibiting "Poor" lubricated behaviour (GA coatings) was found to be dependant on the area fraction of contact as described by the Coulomb law (see Figure 5.12). This means that, the larger the area fraction of contact, the higher the microscopic forces between the sliding surfaces and hence the higher the friction. Although, the materials with lower yield strength were found deviate even more from Coulomb's law, as shown in Figure 5.17.

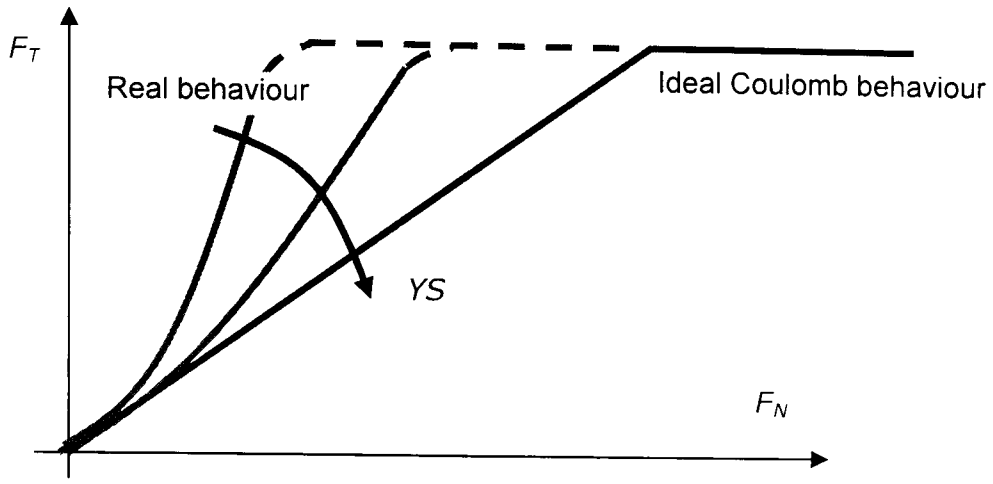

Figure 5.17 - Schematic representation of "poor" lubricated surface behaviour

The coefficient of friction of the materials exhibiting "Richly" lubricated behaviour (ELO coated) was found to be dependant on the average closed peak area. For these materials, the proposed friction model describes the lubrication of the peaks to be due to a dragging of the lubricant oil onto the sliding surfaces (see Figure 5.6).

The larger the peak dimension, the more difficult it will be to lubricate them with this dragging. Indeed, when the velocity is increased to 200mm/s the dragging phenomenon appears to become so important as to obscure any other effect (including the surface topography effect). This interaction between surface topography and velocity can be schematised by the graph shown in Figure 5.18.

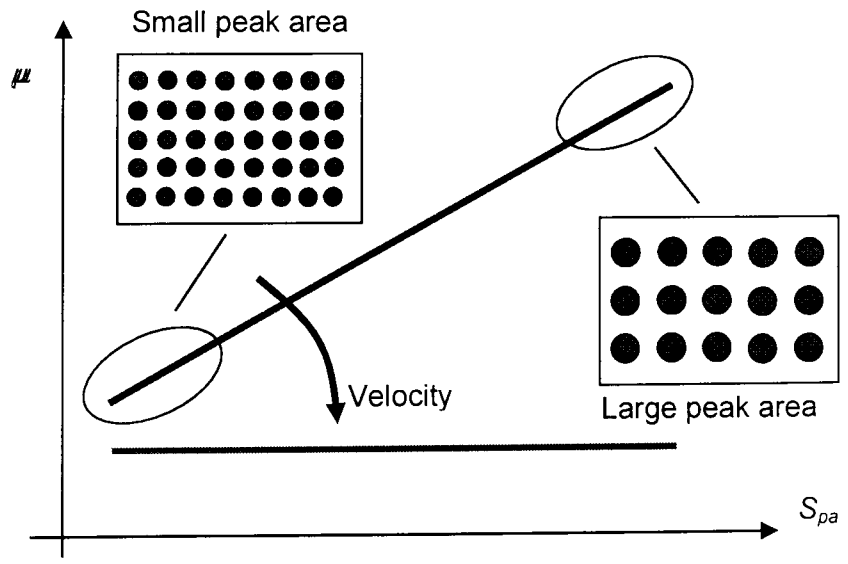

Figure 5.18 - Schematic representation of "rich" lubricated surface behaviour

Finally, the GI coated materials could not be described by any surface topography parameter but it was suggested that there may be a means of separating the tests into two classes such that relationships do exist but different ones for each of the two classes. This will have to be the subject of further research.

5.7 Summary

- ✓ The historical laws on friction were presented to set the scene, those being:
  - Dry friction – Coulomb's and von Mises's laws
  - Lubricated friction – Stribek curve

- ✓ During the eighties a scientist named [Emmens 1988] conducted work on tribology (friction) of steel sheets for the autobody manufacturing processes. He showed possible correlations between 2D surface parameters and features of the Stribek curve.

- ✓ Emmens's work was taken further in this chapter trying to describe the autobody tribological system by employing 3D surface parameters.

- ✓ Because of different affinity with the lubricants, the coatings had to be correlated separately with surface topography:

- ✓ ELO coated materials showed Stribeck behaviour, and their coefficient of friction correlated with the surface parameter Spa(S95p/2) (average closed peak area). Larger areas exhibited higher friction coefficients.

- ✓ GA coated materials showed dry behaviour, and their coefficient of friction correlated with the surface parameter α(h1g) (area fraction of contact). The larger the contact area, the higher the coefficient of friction.

- ✓ GI coated materials showed no correlation with surface topography

6. Deep drawing processes

6.1 Introduction

The previous two chapters have shown significant differences between the surfaces investigated and their ability to retain oil and to lower friction. The differences were thought to be due to the different surface structures and the topography as defined by certain 3D parameters related to valley area and peak area. In particular, the coating GA acted in a manner different from ELO and the GI surfaces sometimes acted like GA and at others like ELO.

In the oil migration tests, the ELO coated materials had a superior ability to exhibit lubrication. The friction tests seemed to support these findings in that the GA coated surfaces behaved as if they were unlubricated (i.e. Coulomb-like behaviour) while ELO behaved as they were well lubricated (i.e. Stribeck-like behaviour). It was concluded that the ELO coated surfaces, due to their structure and their topography, retained oil in such a manner as to reduce friction. However, the friction tests were "in the laboratory" and the aim of this chapter is to conduct controlled deep drawing tests to see if the general conclusions concerning oil retention and oil distribution are applicable in real production sheet metal forming.

The test employed to study the deep drawing process is called the "modified stretch drawing" (MSD) test. The MSD test combines drawing and stretching actions in order to emulate a real deep drawing process under controlled conditions. It enables the parts of the deep drawing process to be partially separated so that the ability of the sheet material to be both stretched and formed over a die can be isolated. The MSD test will be described in more detail below after a description of the material combinations used.

As has been explained above, due to production problems and material availabilities, it was not always possible to obtain material so that every combination of base material and coating could be investigated. The materials tested during this investigation were chosen from those available, in an attempt to answer the following questions:

- ***What is the effect of the texturing techniques and coating types upon drawability?***

  To answer this question one experimental set was performed including four materials using GA and ELO coatings with all the surface topographies available.

- ***What is the effect of substrate material upon deep drawing?***

  In order to answer this question two experimental sets were performed including GA and GI coatings, coated over sheets prepared with two of the three texturing techniques available, i.e. EBT and EDT. Note that no MSD experimental work was possible on the Pretex (ECD) texture due to a fire in the manufacturing plant.

The list of materials employed was the following:

Name	Yield Strength [MPa]	Coating type	Texture	Sq [μm]
B2	182	ELO	EDT	2.29
B3	135	ELO	EDT	1.93
B5	167	GI	EDT	1.57
B6	152	GI	EDT	1.80
B8	261	GA	EDT	1.73
H14	221	GA	EDT	2.40
H17	387	GA	EDT	1.94
H5	350	GI	EDT	1.38
H8	256	GI	EDT	2.20
S2	157	ELO	EBT	1.81
S3	163	ELO	EBT	2.51
S5	157	GI	EBT	1.23
S6	165	GI	EBT	2.43

Table 6.1 - List of the material tested during the deep drawing experiments

6.2 Previous work on deep drawing

Surface characteristics are perceived to strongly affect steel sheet drawability by influencing the friction conditions at the interface between tool and sheet material. Many authors [for example *Siekirk 1986* and *Staeves et al 2001*] perceived the most important surface characteristics to be coating type, surface topography and lubrication. Indeed, the initial friction tests of Chapter 5 seem to support this since interfacial friction has been related to particular surface structures and topographies. Thus, it would seem likely that the same surface structures and topographies, which reduce friction, would produce superior deep drawing.

No surface is geometrically perfect; therefore the contact between die and workpiece is a limited portion of the total (apparent) area. Surface irregularities and their behaviour during sliding, together with the lubricant and the surface chemistry are key factors for controlling friction during the deep drawing process [*ASM 1995*]. Therefore it is expected that the surface parameters found relevant in the friction tests described in Chapter 5 (i.e. Sva and Spa) will be relevant in deep drawing too.

Emmens [*Emmens 1997*], performing deep drawing tests, stated that the influence of roughness upon drawability could be observed only when the lubricant is sufficient to induce a "mixed" (see chapter 5) lubrication regime. During this work he found that higher roughness leads to higher punch load. Although, Emmens concentrated on uncoated cold-rolled steel (CRS), hence, although being helpful in pointing out trends, his results are not directly applicable to this work where we are particularly interested in coated steels. Also, his work used 2D surface roughness parameters and these are limited in their use for the 3D approach we are trying to adopt here. Thus, it is unfortunate that there is almost no previous 3D parameter work on coated steels that can help us in this particular investigation.

6.3 The experimental procedure

6.3.1 Test description

The test used in this research programme is the so-called Modified Stretch Drawing (MSD) test. It is based on the common Swift round nose cup test [*Haberfield et al 1974*], further developed at the Welsh Technology Centre in early 1970's. During this test, sets of disc samples are formed to failure under a range of blankholder loads in highly controlled (in terms of speed and loads) conditions. The deeper a material can be drawn (see Figure 6.1) without breaking the better is its forming ability (or drawability) [*Sy-Wei et al 1998*].

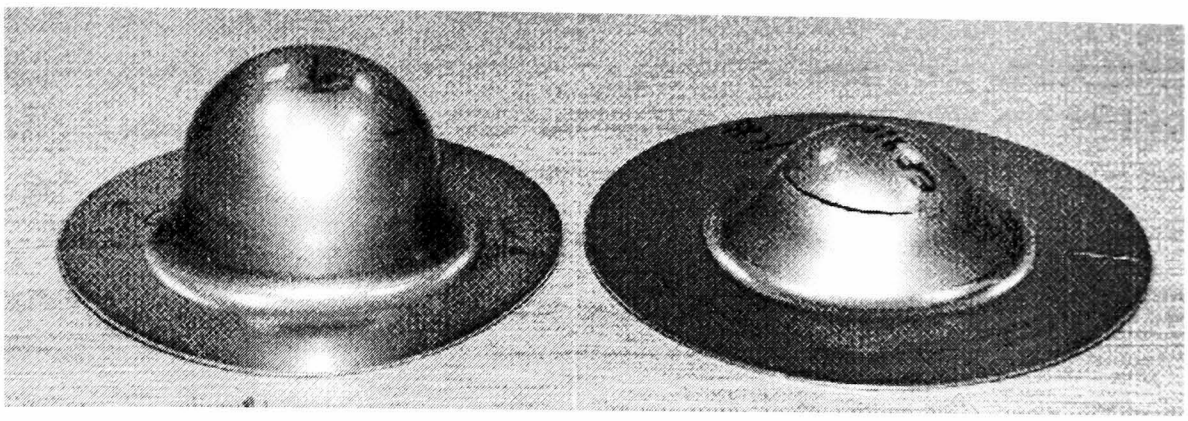

Figure 6.1 – Cup test samples with different drawing ability

In early stretch drawing tests, the surface effect upon formability could not be separated from the effect of substrate mechanical properties. As developments in sheet steel coatings and surface topography progressed, it became necessary to isolate the effects of surface from the substrate mechanical properties. In an attempt to remove the effect of mechanical properties from the results, Elliot and Boyle [*Elliot et al 2000(b)*] suggested the test could be modified by the addition of polyethylene sheets (0.2 mm thick) placed on either side of the steel sheet. Since this was a modification of the conventional stretch drawing test, the new test became known as the Modified Stretch Drawing test. It is able to monitor and (partially) isolate material property and surface contributions over a wide range of forming regimes, as will be shown later in this chapter.

The MSD test involves the deformation of a set of circular samples, under a range of blankholder forces. A 60-ton hydraulic press was chosen because it was known to be more than adequate for the forming tests. The punch velocity was a constant 2 mm/s because this was the same speed as was used in the friction test and is typical of industrial deep drawing.

6.3.2 Drawability values and indexes

Several drawability measurements can be taken from the formed samples or from deformation loads. When studying the effect of surface upon forming, the friction between the tool and the steel is of interest. In similar testing, Emmens estimated the friction coefficient between tool and material by comparing punch force and blankholder force [*Emmens 1997*]. During the test described here no coefficient of friction could be estimated by employing Emmens's approach since, in the industrial trails, only two blankholder loads

were explored and this would lead to estimation uncertainty. Since this was not possible, other measures had to be used. Two other measures were used which are related to formability. When a cup is drawn two things happen, firstly, the cup increases in height and secondly, the flange decreases in diameter. These two aspects lead to "formability" values and they are as follows:

- The cup **fracture height** (FH – see Figure 6.2). This is the easiest measurement that can be taken. This is the height the cup can be drawn to before fracture. Obviously, the higher the better since large values of FH indicate good drawability.

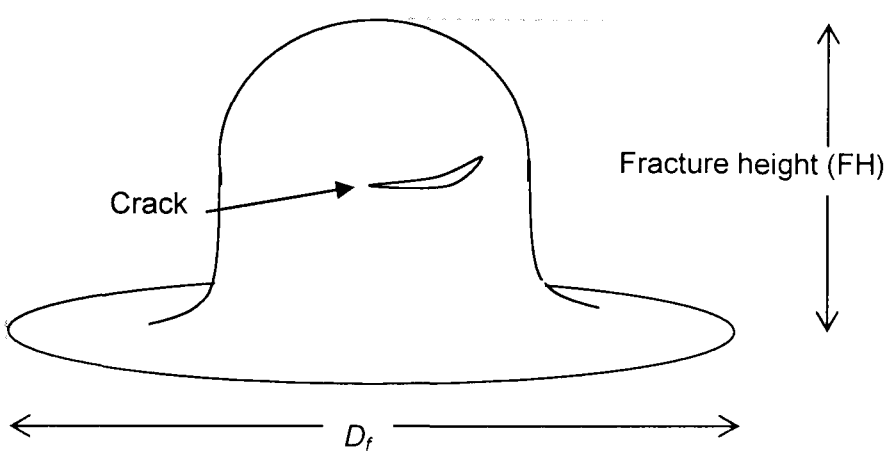

Figure 6.2 – Schematic representation of the formed cup

- A second measurement on the sample is the **percentage draw** of the flange at fracture. The percentage draw is the actual flange reduction to maximum flange reduction. This can be calculated as shown by Equation 6.1.

$$\%Draw = \frac{C_0^2 - C_f^2}{C_0^2 - C_d^2} \times 100$$

Equation 6.1 - Percentage draw of the flange

Where *Co* is the initial circumference of blank, *Cd* is the circumference of the die and *Cf* is the final diameter of the flange.

The higher the *%Draw* the better, since it implies more deformation before failure.

During a deep drawing operation, as the cup is drawn and the cup height increases, the flange will move radially inwards and the flange diameter will decrease. One would expect there to be some relationship between the two albeit there will be things like stretching of the cup and thickening of the flange which distort the picture. To test the relationship and in order to see which is the best forming parameter to use, a series of tests were undertaken to see the correlation between fracture height (FH) and %Draw. The results are shown in Figure 6.3. They are for a range of conditions of sheet materials and of coatings, which are shown in Appendix 9.

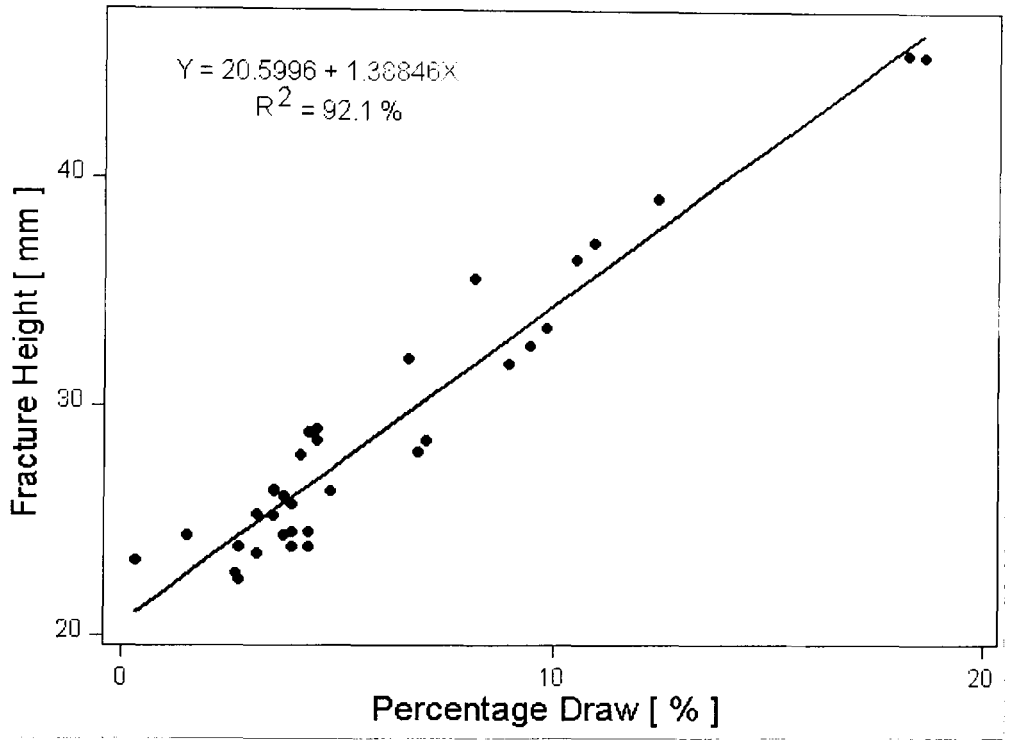

Figure 6.3 - Correlation between Fracture Height (FH) and %Draw

The results showed that the fracture height (FH) and percentage drawn (%Draw) correlated very well at 92.1%. This was expected since, in any deep drawing process, as the cup gets higher, the flange diameter must get smaller. Some scatter can be seen in the Figure, which can probably be attributed to the discontinuities caused by things like the sheet stretching in the cup region and thickening in the flange region. The fact that FH and %Draw correlate very well means that there is no need to measure them both since they give identical information. In general, the FH value will be used during the remainder of this study because it is by far the easier of the two to measure.

Another method of analysing the formability is by trying to remove friction from the system. This might appear impossible but if polythene sheets are placed on either side of the steel sheet prior to forming, the friction at the sheet and punch/blankholder interfaces will be reduced significantly. Although this does not entirely remove friction from the system, it does permit one to see the effect of minimising friction. If the results of testing with "polythene" sheets and "non-polythene" sheets are compared, the trends will enable one to postulate what is the effect of friction. This allows one to almost isolate interfacial friction from formability.

To test the usefulness of this technique, another series of tests were undertaken using a variety of materials, coatings and topographies. The overall results can be seen in Appendix 9. The results showed a general pattern, which was repeatable across the conditions used. The overall results seemed to fit a clear pattern, which is shown schematically in Figure 6.4.

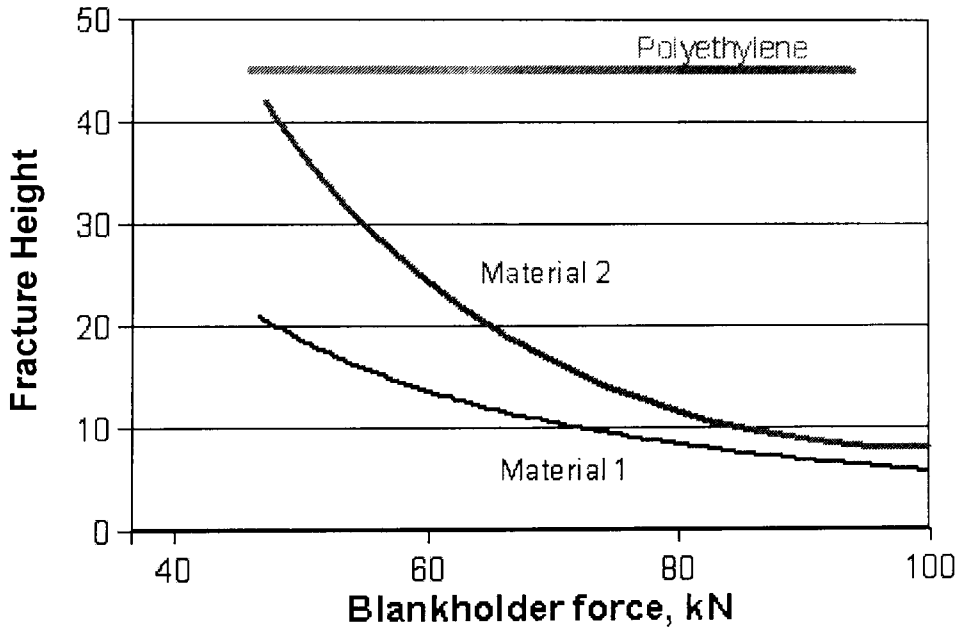

Figure 6.4 - Typical outcome from MSD test

The schematic shows three lines on the graph that are representative of three conditions. Here the "**material 1**" designation is representative of those material/coating combination results which showed high friction. The "**material 2**" designation is representative of those material/coating combinations which showed low friction. The "**polyethylene**" line is representative of the tests in which polythene sheets were used to minimise friction.

The three sets of lines follow a trend, which is related to the interfacial friction. The lower the friction, the higher the curve on the graph. When the friction is minimal (with the polythene sheets), the line is very high and horizontal. The line is lower for the low friction cases and is no longer horizontal because the blankholder pressure has an increasing effect. The line is even lower for high values of friction. Of interest is that at very high pressures the two "friction" results converge.

The **polyethylene results** for every condition produced a horizontal straight line, parallel to the blankholder axis. The fact that this line is horizontal is a significant result because it points to the fact the blankholder force had no effect on the drawability of a sheet. The logical conclusion is that the friction is of such a low value that it is insignificant with respect to the blankholder forces used. There seems to be no falling away of the line at high blankholder values indicating that friction really is minimal. It is therefore suggested that, as a first approximation, the horizontal lines represent the ideal case where the deformation is limited by the material bulk deformation and not surface effects. If this is the case, the "polythene" result of any test must be close to the maximum deep drawing deformation that can be achieved. It therefore represents a base value with which other values can be compared. Thus, from the results, another measurement can be used which is conveniently a dimensionless ratio. It is the:

- **Normalised fracture height**. When drawing a material blank with polyethylene sheets on the top and bottom faces of the steel sheet as opposed to oil lubricants, a larger cup is formed. The maximum drawn height of the oil-lubricated cup is always smaller than the polyethylene one, due to friction. The fracture height of any normally lubricated cup (FH_L) may be normalised (Normalised Fracture Height – NFH) against the fracture height of the polyethylene-lubricated cup (FH_P) to obtain a percentage of the maximum achievable cup height. This has the advantage of being a dimensionless ratio. This assumes that the fracture height obtained by employing the polyethylene "lubricant" is the highest possible for the given material since almost no friction should be present; see Equation 6.2:

$$NFH\% = \left(1 - \frac{FH_P - FH_L}{FH_P}\right) \cdot 100$$

Equation 6.2 – Normalised Fracture Height

6.3.3 Experimental design

A number of experiments were undertaken with the materials available. An initial fractional factorial experiment (see Appendix 4) was performed to test the influence of zinc coating type upon NFH%. An initial factorial test was used because there were insufficient materials available for a full factorial test. This experiment included the following factors:

Control Factor	Level 1	Level 2	Level 3
A – Coating type	ELO	GA	GI
B – Oil type	Low Viscosity	High Viscosity	
C – Blankholder load	36KN	107KN	

Table 6.2 – DOE for the initial investigation on coating type effect upon NFH

Then followed three fractional factorial Design of Experiments (or DOE), one for each coating type, with the following control factors:

- A - Material (all the surfaces available)
- B - Oil type (2 levels)
- C – Blankholder load (2 levels)

Finally, a regression analysis between NFH% and μ (measured during the friction experiments) was carried out.

6.4 Results analysis

Statistical analyses were performed on all the designed factorial combinations for the selected materials. A summary of the results is presented below (fully detailed analysis is available in Appendix 9).

6.4.1 Results on normalised fracture height

A further series of tests were undertaken to investigate the effect of the different materials, coating (and therefore topography) and oil types on FH and MFH%. The full results can be seen in Appendix 9. The set of results may be summarised using the ANOVA test methodology. The full set of results may be summarised by the two diagrams shown in Figures 6.5 and 6.6. The

former is the main plot for the coating type and the latter the main effect plot for all the other factors. This graph shows the results for the low velocity and high pressure since this is the critical regime for things like the die corners and other high deformation areas.

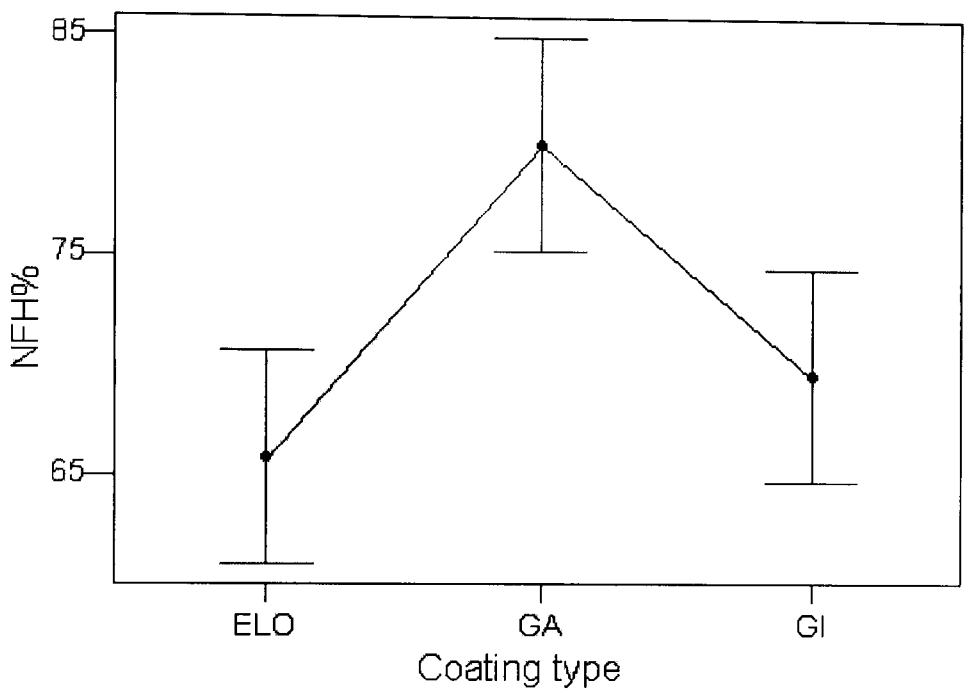

Figure 6.5 – Initial investigation - Coating effect

With reference to Figure 6.5, it can be seen that the ELO coated interval never overlaps the GA interval and the GA never overlaps the GI interval. This means that one can say with certainty that in this treatments combination, the GA coating is the superior. This is surprising because the above work has shown the GA coating does not exhibit Stribeck behaviour. It is thought this is due to the more porous nature of the GA and GI coatings. It was noted in chapter 4 above that oil was "lost" (Figure 4.8) but not lost in the conventional sense of the word but held within the coating structure, which, in the case of GA, is crystalline with many undercuts and sub-surface voids, similar to coral. It is thought that under the high-pressure conditions, which exist in the example of Figure 6.5, the pressure is such that the crystalline structure is deformed so much as to squeeze the "hidden" oil out of the sub-surface structure and hence it is available to reduce friction at the interface. This is supported in this case by the fact that the NFH% is higher with GA than GI. The GA coating is heat-treated (annealed) and therefore has a more porous structure than the GI, which is not annealed. The GA coating is thus likely to be more crystalline and therefore likely to "hide" or trap more

lubricant within the structure. Figure 4.8 shows that this because GA seems to "hide" more lubricant than GI.

Turning now to the main effect plots, the complete set of results is shown in Appendix 9. All the plots for the different coatings show the same trends and therefore we need only consider one and a typical one is shown in Figure 6.6. It shows that of the three, the lubricant type seems to have little (still measurable) effect. The most important ones are the blankholder force and the material type. The latter is a combination of the substrate material and the topography.

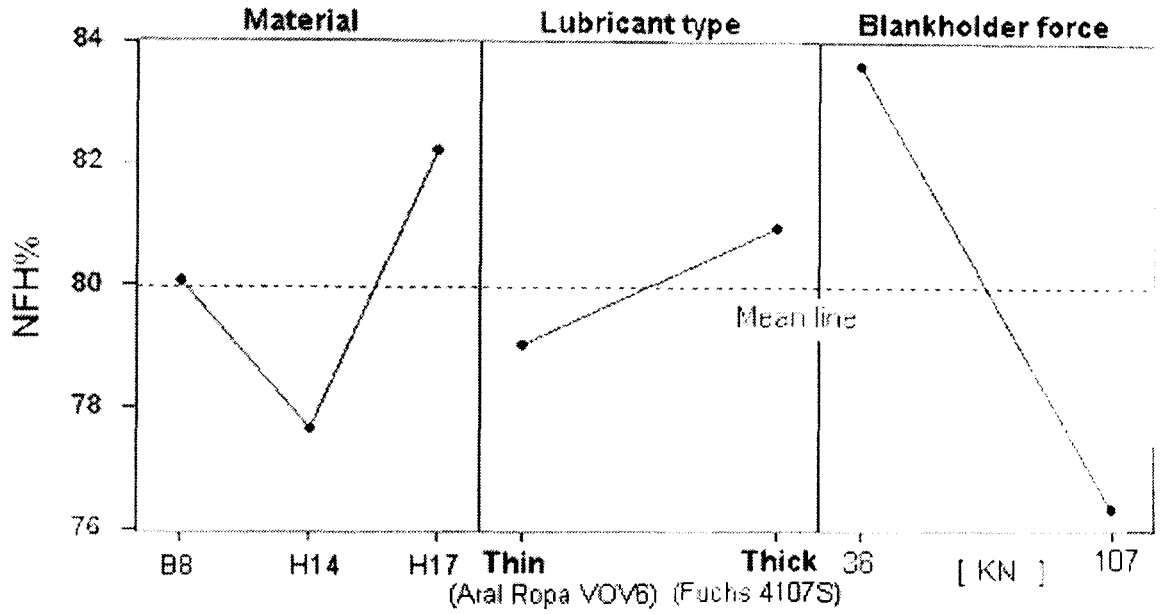

Figure 6.6 - Main effect plot for GA coated materials statistical analysis

It is to be expected that the blankholder force has a major effect since this produces the interfacial pressure, which determines friction. This confirms the friction results of Chapter 5, i.e. Figure 5.12.

The "material" results are a combination of the substrate material (i.e. yield strength) and the topography. This is encouraging in that one would expect the yield strength to influence drawability and this result implies that the topography too influences drawability and hence a definition of topography (i.e. an "S" parameter) is likely to show a correlation with drawability and hence friction.

The fact that the oil viscosity has little effect compared to the others is due to the fact that in this high-pressure regime, the pressure is so high that oil is squeezed out of the subsurface and the type of oil is irrelevant. This is supported by the results shown in Figure 5.11 where it was shown that lubricant type was not significant.

Figure 6.6 shows the effect, amongst other things of the GA material on NFH%. A problem with the previous material graph is that the materials are ordered by name. To investigate the effect of material hardness, they need to be ordered by strength. Figure 6.7 shows the effects of the different GA materials on the blankholder force where the materials are ordered by their yield strength value rather than their names. This is a typical interaction plot.

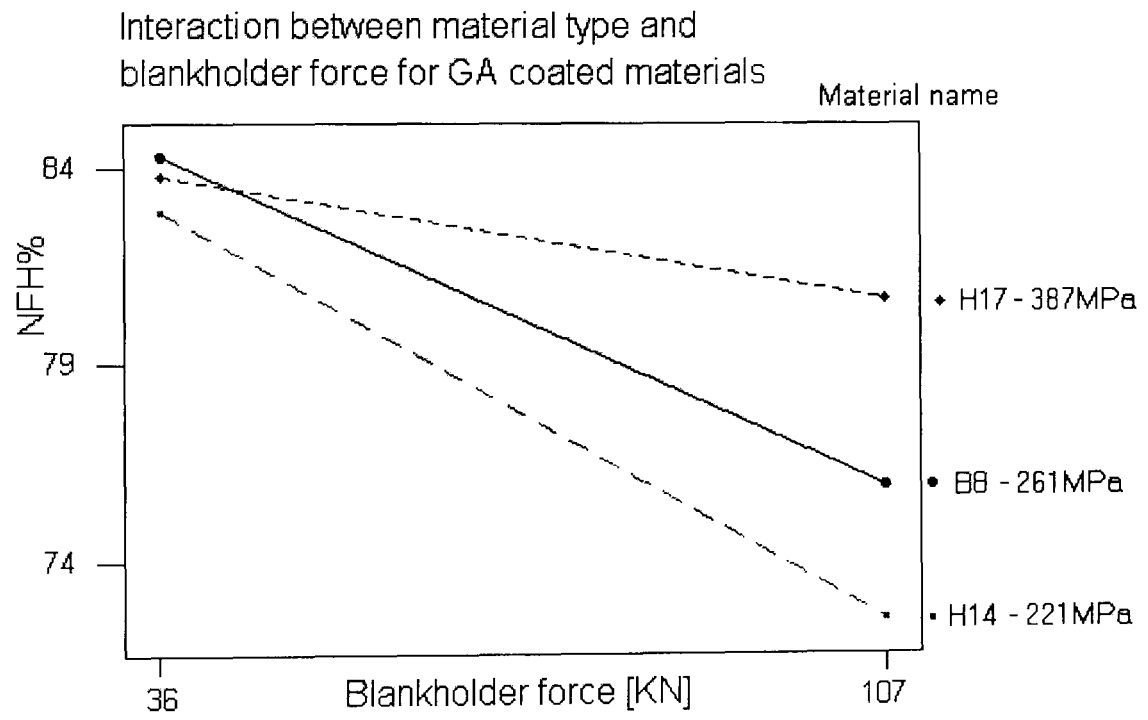

Figure 6.7 – Interaction between BHF and YS for GA coated materials

This Figure shows that the blankholder force has only a small effect on the drawability of the harder material (H17) whereas it has a significant effect on the drawability of the softer materials (B8 and H14). This is thought to be due to the fact that the peaks of the harder materials are more resilient to deformation and the contact area is little changed by blankholder force. However, the softer materials are more easily deformed and hence as the "clamping" force increases, the peaks deform and the contact area increases, hence reducing the formability.

This interaction between drawability and mechanical properties was found similar to the results on friction experiments presented in Equation 5.5 in that the hardness has a reducing effect on friction whereas the topography has a an increasing effect (the negative and positive signs respectively in the equation). With a hard material, the effect of topography is hardly changed because the material deforms very little whereas with a softer material, there is more of a conjoint effect of material and topography.

6.4.2 Correlation with friction experiments

In the above work (section 6.4.1), because of the effect of mechanical properties on the NFH% drawability index, it was not possible to separate out the effect of the yield strength and topography. Chapter 5 showed that both topography and substrate material influence friction. In this chapter we are interested in drawability and we know from the above Figures 6.6 and 6.7 that the substrate material hardness influences drawability, yet it is not unreasonable to assume that friction also influences drawability which is related to material hardness and topography. Thus, we have a very complex and interrelated system between drawability, topography and substrate material hardness. We therefore need to have a technique where we can analyse the problem further and test any relationship between topography and material with respect to drawability.

The above implies that any final equation relating topography and material to drawability will be extremely complicated and the problem is that we do not have sufficient test results to enable us to do this, hence we need to use a technique, which does allow some form of solution. One way to try to do this is by the use of differentials and this will now be attempted. This led to the technique whereby one compares the "increment of NFH" to the "increment of coefficient of friction".

In fact, if we imagine that NFH is due to the work performed by friction and the deformation work of the substrate properties, at every given blankholder force we could describe it with an equation similar to the following:

$$NFH = C + W(friction) + W(deformation)$$

Therefore, if we subtract the NFH values at different blankholder loads (2 – higher blankholder loads, 1 – lower blankholder loads) we will find something like the following:

$$NFH(2) - NFH(1) = W\left[friction(2) - friction(1)\right] + W\left[deformation(2) - deformation(1)\right]$$

The differential work performed by friction is therefore expected to be a function of the coefficient of friction. The differential work of deformation is expected to be a function of some material properties (i.e. Yield Strength).

Hence, the equation we are going to use for a test of correlation is:

$$NFH(2) - NFH(1) = K + f\left[\mu(2) - \mu(1)\right] + g\left[YS\right]$$

where f_1 and f_2 are different functions.

Therefore the NFH and friction increments or differentials need to be defined and they are as follows:

- Decrease of fracture height – $Diff_H = NFH(36KN) - NFH(107KN)$ where this is the difference between NFH at blankholder forces of 36 and 107kN.
- Increase of coefficient of friction – $Diff_F = \mu(1MPa) - \mu(10MPa)$ where this is the difference between the friction coefficients produced when the pressure (during the friction tests) was 1 and 10Mpa.

Thus, we are trying to incorporate the friction results from chapter 5 into the drawability results from this chapter 6, to advance our understanding of the conjoint effect of topography and material on drawability.

This correlation analysis is possible because the two test sets (MSD and friction test) used almost the same test conditions. These conditions are that the same lubricants, the same materials, the same topographies and the same velocity (2mm/s) were used for a range of substrate materials as well as coatings. However, the blankholder loads were not exactly close enough to give confidence in the comparison. These are shown in Table 6.3:

Blankholder Force	Contact Area	Blankholder Pressure	Friction experiment Pressure
36KN	$0.011m^2$	3.2MPa	1MPa
107KN	$0.011m^2$	9.8MPa	10MPa

Table 6.3 - Blankholder pressures on MSD

These "differential" measurement tests were then undertaken and the full results are shown in Appendix 9. Figure 6.8 typifies the results.

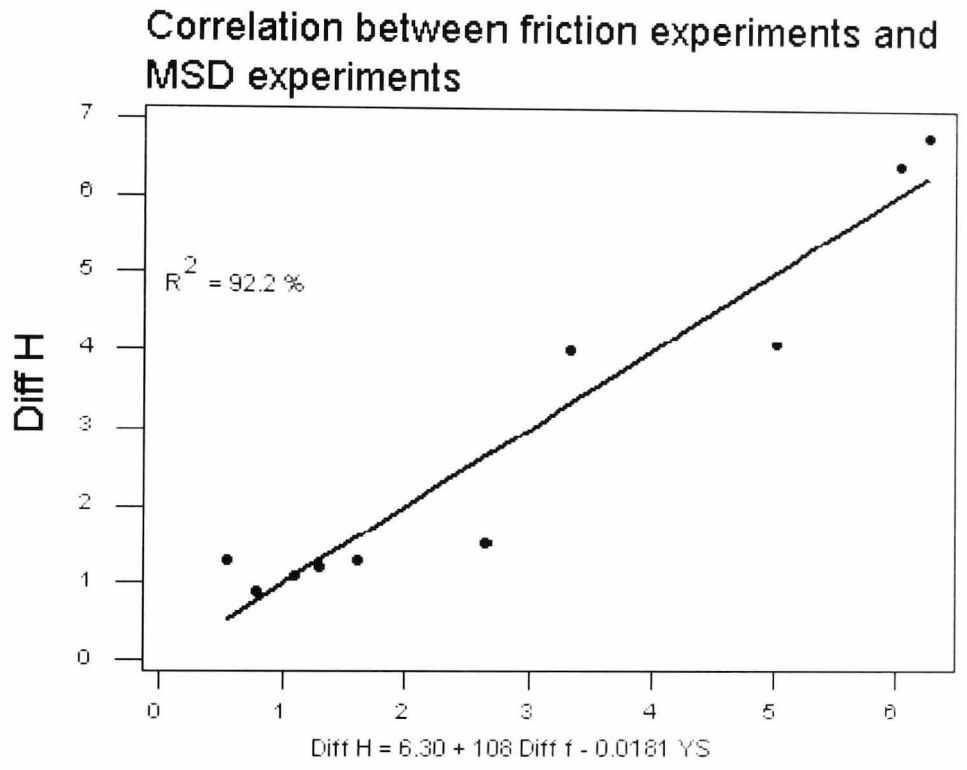

Figure 6.8 – Correlation between MSD and Friction experiments

This Figure shows that in difference terms, there does indeed appear to be a direct relationship between friction and drawability and the relationship can be represented by the equation:

$$Diff_H = 6.3 - 108 \cdot Diff_f - 0.0181 \cdot YS$$

Equation 6.3 - Regression equation between MSD and Friction

This shows that whenever there is a decrease in drawability (*DiffH*), there is an increase in the coefficient of friction (*Difff*). This correlation further proved

that the substrate mechanical properties influence NFH% since Yield Strength (YS) had to be added to Equation 6.3.

From Figure 6.8 one can see that the harder the substrate material is, the lower will be the coefficient of friction, irrespective of the coating used. Thus, these results apply to GA, ELO and GI coatings on any of the substrate materials.

Since a yield strength effect was found to drive the friction experiments in section 5.5.3, the substrate mechanical properties appear even more important in deep drawing performance as has been shown in this chapter 6. This is significant because we have combined the friction results of Chapter 5 with the drawability results of Chapter 6 and made progress with the separation of topography and material hardness. Although we have not made any quantitative progress since we are using differences, we have made progress in that we can now say that the material hardness and the topography both have a significant effect on drawability but that the effect of material is more significant than topography. Since material hardness and topography influence friction, (chapter 5) and from this chapter 6 we have found that friction and substrate material hardness influence drawability, we can conclude that as a first order effect, the material hardness has twice the effect on drawability as does topography. This is a significant conclusion and a major contribution to the subject knowledge because, although this was suspected, nobody had proved it.

6.5 Conclusions and discussion

The results from the MSD experiment on drawability proved to be affected by friction as shown in Figure 6.8. Unfortunately, no direct correlation between surface topography and drawability indexes could be found. This is most likely due to the fact that the drawability index (NFH) is still influenced by the substrate mechanical properties.

Analysing these results using a "differences" approach, it was found that the harder the substrate material was, the lower was friction and therefore the higher was the drawability (see Figure 6.7).

6.6 Summary

- ✓ [*Emmens 1997*] performing deep drawing tests stated that the influence of roughness could be observed only when the lubricant was sufficient to induce a mixed lubrication regime.

- ✓ The testing device adopted here is a modified Swift round nose. The specimen is a round sheet drawn into a common "cup-shape".

- ✓ The drawability indexes adopted where: fracture height (FH), %Draw and normalised fracture height (NFH).

- ✓ Initial statistical analysis proved that FH and %Draw results correlated. Only FH was therefore employed in later analysis.

- ✓ Similarly to the friction results of chapter 5, it has been demonstrated that a high yield strength (YS) resulted in less of an NFH sensitivity to normal load (see Figure 6.7)

- ✓ Unfortunately, no direct correlation between drawability and surface topography could be found. Although a correlation between friction and NFH variations proved that a high friction coefficient was associated with lower NFH values and softer materials.

- ✓ Using a "differences" approach, it has been found that as a first order assumption, one can say that the substrate material hardness (or the yield stress) has about twice the effect on drawability as does topography.

7. Conclusions

The experimental data collected can be a precious heritage for further process improvement whether that be surface topography or coating or process design and assessment. For this reason, all the experimental results and raw surface data have been collected in a large database. This will enable the results to be used in future for further analysis, which could lead to future novel parameters and filtering techniques being developed. This is available in the form of a CD-ROM and has been distributed to all the Autosurf partners.

Much experimental work was undertaken in this programme that proved that many factors are important with respect to friction, drawability and oil retention. These are as follows:

1. ***The metal sheet substrate mechanical properties.*** - The yield strength (or hardness) of the panel has been shown to have a major influence on friction and drawability but little effect on the oil retention. Furthermore, with respect to drawability, the hardness had a variable effect in that the effect of blankholder force was negligible for the harder materials but had a significant effect with the softer materials. These conclusions are significant to the automotive industry because it has started to employ higher strength steels (i.e. YS 160MPa and higher) in an attempt to reduce body-weight and improve structural integrity. Therefore, these conclusions are significant for those concerned with planning body-panel forming processes.

2. ***The surface topography.*** – The work showed that the panel topography had a major effect on friction, drawability and oil retention. With respect to friction and drawability, the effect was less significant than the material but important all the same. The areal surface roughness parameters developed during this research project describes the lubricant migration and the friction during forming, see chapters 4 and 5. The surface topography valleys (closed) as described by **Sva** need to be small in order to prevent lubricant from moving across the panel. The peaks need to be small in size (low **Spa**) and high in number (high **Spd**) in order to reduce friction during forming. These are the 3D-parameter guidelines that can now be followed in the automotive industry.

3. ***The zinc coatings.*** – The work showed that the panel coating had a major effect on friction and oil retention but less of an effect on drawability. However, with respect to friction and drawability, there is an interaction between the coating and the lubricant. The coating type can either enhance lubrication and hence reduce friction (see ELO effect in sections 4.4.1, 5.5.1) or reduce lubrication and hence increase friction (see GA effect in the same sections). The results for the GI coatings were confusing in that sometimes the results followed the GA coating trends and sometimes the ELO trends. Further work needs to be done with respect to the GI coatings to provide a classification with respect to friction. However, the conclusion is that coating has a major influence in the forming process.

This research programme has produced a large mass of results, which are very complex, and at times confusing in that there are significant interactions and many exceptions. This has made it very difficult to give order to all the results but some general trends have become evident. For example, although it has not been possible to quantify all the conditions, one can say that with respect to drawability, the material substrate has much more of an effect than sheet topography. Using such a qualitative approach, one can start to draw general conclusions from the mass of results. A chart showing qualitative relationships can represent these general conclusions is shown in Figure 7.1. Here, the effect of the "input" factors of material, lubrication, and operating conditions are related to the experimental categories of oil retention, friction and drawability. In this case a solid circle means that there is a significant relationship, a half-filled circle means there is a medium relationship and an open circle means there is a minimal relationship.

		Oil retention	Friction	Drawability
Material	Substrate	○	◐	●
	Coating	●	●	◐
	Topography	●	●	◐
Lubricant	Viscosity	◐	●	○
	Additives	○	●	●
	Amount	○	◐	●
Conditions	Velocity	N/A	●	N/T
	Pressure	●	●	●

● there is a significant relationship

◐ there is a medium relationship

○ there is a minimal relationship

N/A Not Applicable

N/T Not Tested

Figure 7.1 – Qualitative relationship found between input and experimental work

The Figure 7.1 table shows the overall results of this research programme, which it is hoped, will be of interest to the automotive industry as well as the general metal forming industry. Certainly, all the results have be disseminated to the Autosurf partners in the form of a final report [Sacerdotti, 2001] which is available from the Brussels Secretariat.

8. References

- *Altan T, Ahmetoglu M, Brouwers D, Shulkin L, Taupin L, Kinzel G, 1995, "Deep Drawing of Round Cups from Tailor-Welded Blanks", Journal of Material Processing Technology 53*
- *Amici E, Vermeulen M, Fredin K et alt, 2001, internal CSM report for Autosurf, Task 4.3 (CSM PR 10467R 01)*
- *AMSA (American Metal Stamping Association) 2022,1970, Technical Research and Standard Committee, Metal Stamping Design Guide – Data Sheet No. 2022*
- *Amer. Soc. Lubrication Engrs, 1976, "Catalogue of Friction and Wear Devices"*
- *ASM International, 1995, "ASM Handbook of Friction, Lubrication and Wear Technology" (ISBN 0-87170-380-7) pp81-99, p45*
- *Aspinwall DZ, Wise MLH, Stout KJ, Goh THA, Zhao FL, El-Menshawy MF, 1992, "Electrical discharge texturing"; Int. J. Mach. Tools Manufact. Vol. 32, pp183-193*
- *Behrens B, 2000, personal communication about Pretex topography on behalf of Salzgitter AG held at Brunel University June 2000.*
- *Benati F, Tan Z, Holtkamp H, Vermeulen M, 1999(a), internal Brunel report for Autosurf, Task 2.2 (BRU TR ASS 1001202)*
- *Benati F, Butler C, Gatti S, Sacerdotti F, Yang QP, 1999(b) "Trimming Tool Optimisation for the Autobody Manufacturing Process" Proceedings of the 15th International Conference on Computer-Aided Production Engineering, 1999 Durham (UK)*
- *Benati F, Butler C, Gatti S, Sacerdotti F, Yang Q, 1999(c), "A Robot-based Burr Measurement System for the Automotive Industry", Proceedings of the IMTC99*
- *Benati F, Fredin K, Broggiatto G, 1999(d), internal Brunel report for Autosurf, Task 2.1 (BRU TR ASS 2001102)*
- *Benati F, 2000, internal Brunel report for Autosurf, Task 2.3 (BRU TR ASS 1001301)*
- *Benati F, Sacerdotti F, Gatti S, Kang H, 2000(b), "Development of a Hand-Held Burr Measurement System for Statistical Process Control of the Trimming Process", Proceedings of the 17 Instrumentation and Measurement Technology Conference, Baltimore (USA), pp1420-1423*

- *Benati F, Griffiths B, Sacerdotti F, Butler C, Karila JM, Vermeulen M, Holtkamp H, Gatti S, 2001(a), "Correlation Between Surface Topography and Lubricant Migration in Steel Sheets for the Autobody Manufacturing Process", Submitted to the Journal of Phisics*
- *Benati F, 2001(b), internal Brunel report for Autosurf Task 1.7 - 2.5 (BRU TR ASTR 0001702)*
- *Benati F, 2001(c), internal Brunel report for Autosurf Task 1.7 – 2.4 (BRU TR ASTR 0001602)*
- *Burrows JM, Griffiths BJ, 1998, "A vector modelling technique for the representation of 3-Dimensional surface topography", International journal of machine tools & manufacture, Vol.38, No.5-6, pp.537-542*
- *Carless S, 2001 "The Influence of Steel Strip topography on the Quality of Galvannealed Coatings", PhD Thesis at University of Swansea (UK), pp1-10*
- *DIN 4776, 1990, "Measurement of Surface Roughness; Parameters Rk, Rpk, Rvk, Mr1, Mr2 for the description of the Material Portion in Roughness", German Standard*
- *Dong WP, Sullivan PJ, Stout KJ, 1994, "Comprehensive study of parameters for characterising three-dimensional surface topography", Internal Report, Birmingham University*
- *Elliott L, 2000(a), internal report for Autosurf Task 2.5 (WLAATN C651923/1/2000R)*
- *Elliott L, Boyles M, 2000(b), "Experiences in the use of a combined drawing and stretching test for assessing the formability of sheet steel products", Proceedings of IDDRG Congress 2000, pp181-186*
- *Emmens WC, Vegter H, Janssen E, 1986, "Roughness and Formability", Proceedings of the 14th IDDRG Congress 1986, Koln, Germany pp398-399*
- *Emmens WC, 1988, "The Influence of Surface Roughness on Friction", 15th Biennal Congress-IDDRG, Dearborn, USA, pp63-70*
- *Emmens WC, Monfort G, 1990, "The Influence of Process Conditions and Surface Characterisation on friction at low Pressure", 3rd International Conference on Technology of Plasticity, Kyoto, pp1277-1284*
- *Emmens WC, 1997, "Tribology of Flat Contacts and its Application in Deep Drawing", PhD Thesis, University of Twente, (ISBN 90-3651028-7)*
- *Fredin K, 1999, private conversation during an Autosurf workshop in London*

- *Galilei G, approx 1611, "Notes on Motion", folio (page) 85v, Biblioteca di Firenze (Italy), also available on-line*
  http://www.imss.fi.it/ms72/DHTML/D202SD4.HTM
- *Gillespie LK, 1996, "The Battle of the Burr: New Strategies and New Tricks", Manufacturing Engineering, Vol. 116 No 2, p6*
- *Gillespie LK, 1998, Inspecting for Burrs, Manufacturing Engineering, Vol. 120 No 4, p70-74*
- *Griffiths BJ, 1998, 'Surface Integrity, Functional Performance & Standards', Proceedings of the Conference/Workshop on Engineering Surfaces, held at Grenoble, France, 24 & 25 June 1998. Also published in 'Engineered Surfaces', published by Kogan Page, 1998.*
- *Haberfield B, Boyles MW, Chilcott HS, 1974, "Development of a Laboratory Simulative Test for the Prediction of Sheet Metal Formability under Combined Stretching and Drawing Conditions", 8th Biennal IDDRG Congress, Gothemburg, 1974*
- *Holtkamp H, 1994, "Effect of surface roughness on traction in elasto hydrodynamic lubrication", MSc report, University of Twente, the Netherlands*
- *Holtkamp H, 1999(a), internal Corus report for Autosurf Task 2.3 (HOO TP 10142701)*
- *Holtkamp H, 1999(b), internal Corus report for Autosurf Task 2.4 (HOO TP 101427 01)*
- *ISO4287, 1996, Geometrical Product Specifications (GPS) –Surface Texture – Profile method – Terms, definitions and parameters of surface texture*
- *ISO4288, 1996, Geometrical Product Specifications (GPS) –Surface Texture – Profile method – Rules and procedures for assessment of surface texture.*
- *ISO12085, 1996, Geometrical Product Specifications (GPS) – Surface Texture – Profile method – Motif parameters*
- *Jonasson M, 1995, "3D Surface Topography Applied to Forming and Painting of Autobody Panels", PhD Thesis, Chalmers University, Gothemburg, Sweden, p19-20*
- *Jonasson M, Wihlborg A and Gunnarsson L, 1998, 'Analysis of Surface Topography Changes in Sheet Steel Strips during Bending under Tension Friction Test', INT.J.Mach.Tools & Manufacture, Volume 38, No 5 & 6, 1998 p459-467*

- *Karila JM, 1999, internal Renault report for Autosurf Task 2.3 (REN OR JMK001 01)*
- *Karila JM, 2000, internal Renault report for Autosurf Task 2.3 (REN OR JMK004 11)*
- *Klimczac T, Jonasson M, 1994 "Analysis of real contact area and cange of surface texture on deep drawn steel sheet", Wear No. 179 pp129-135*
- *Kondo K, 1989, "recent Developments of Shearing in Japan" Int. J. Mach. Tools Manufact. Vol. 29, No 1, pp29-38*
- *Lange K, Pohlandt K, 1985, "Handbook of Metal Forming", MacGrawHill, New York pp24.5-24.37*
- *Liu Y, 1996, "Effect of Coating Characteristics on Friction and Formability of Zn-Fe Alloy Electroplated Sheet Steel", Journal of Material Engineering and Performance, Vol. 5 pp469-477*
- *Mardia KV, 1972, "Statistics of Directional Data", Academic Press London and New York, pp6*
- *Mia S, 1998, "Autobody Panels' Burr Measurement", MSc Main Project Report, Imperial College, London*
- *Montgomery DC, 1997, "Design and Analysis of Experiments", John Wiley & Sons Inc., pp255-281*
- *Muraki M, Ide H, Takagawa K, Nakamura T, 1995, "The effect of Lubricant on Deep Drawability of Zinc-Coated Steel-Sheets" Lubrication Science No 7-3 pp273-283*
- *Nakagawa T, 1993 "Recent Developments in Auto Body Panel Forming Technology", Annals of CIRP, Vol. 42/2/1993 pp717-722*
- *Pfestorf M, Engel U, Geiger M, 1998, "3D Surface Parameters and their Application on Deterministic Textured Metal Sheets", University Erlangen-Nuremberg, Germany (and published also in Machine Tools and manufacture, Vol. 38 No 5-6, pp607-614)*
- *Porrino A, Sacerdotti F, Visentin M, Benati F, 2000, "Applications of Gram-Schmidt Filtering technique to Electron-Beam-Textured Surfaces", p442-446, Proceedings of the 17 Instrumentation and Measurement Technology Conference, Baltimore (USA)*
- *Power R, 1997, Part "B2" of the EU Autosurf (BE-97-4140) proposal*
- *Rosen BG, 1999(a), internal Chalmers report for Autosurf, Task 1.1 (CHA TR 9804200003)*
- *Rosén BG, Ohlasson R, Westberg J, 1999(b), "Interactive Surface Modelling, An Implementation of an Expert System for Specification of*

Surface Roughness and Topography", Chalmers University, Sweden, Int. J. Mach. Tools Manufacture Vol35, No 2, p317-324

- *Sacerdotti F, Griffiths BJ, Benati F, Butler C, 1999, "The Variability of Three-Dimensional Amplitude Roughness Parameters for Electron-Beam and Electro-Discharged Textured Surfaces ", Proceedings of Landamap Conference 1999, WITpress, p287-296*
- *Sacerdotti F, Griffiths BJ, Benati F, Butler C, 2000(a), "The variability of Functional and Amplitude three-dimensional roughness parameters for Electron-Beam and Electro-Discharged textured Surfaces", Measurement Science and Technology, 11 No 3 (March 2000) pp171-177*
- *Sacerdotti F, 2000(b), internal Report for Autosurf Project, Task 1.6 "Formulate 3D parameters" (BRU TR ASS1001200)*
- *Sacerdotti F, Griffiths BJ, Benati F, 2000(c), "Closed Regions: A proposal for spacing parameters for areal surface measurements", Submitted to Measurement Science and Technology*
- *Sacerdotti F, Griffiths BJ, Benati F, Butler C, 2000(d), "Mathematical Modelling of three-dimensional surface topography in autobody manufacture - The State of the Art", Proceedings of the Institution of Mechanical Engineers, Vol 214 (2000), Part B, B03499*
- *Sacerdotti F, Griffiths B, Benati F, Butler C, Autosurf Consortium, 2000(e), "Software Variability in the Three-Dimensional Measurement of Autobody Steel Panel Surfaces" Proceedings of Chemnitz Conference, Feb 2000*
- *Sacerdotti F, Griffiths BJ, Benati F, Butler C, Autosurf Consortium, 2000(f), "Hardware Variability in the Three-Dimensional Measurement of Autobody Steel Panel Surfaces", Proceedings of the 8th international Conference on Metrology and Properties of Engineering Surfaces, April 2000*
- *Sacerdotti F, Autosurf Consortium, 2001, "Final Report of the Autosurf Project"*
- *Schedin E, 1993, "Control of Friction in Sheet Metal Forming can Result in More Stable Production", Material & Design, Butterworth-Heinemann, Vol. 14 No. 2, p127-129*
- *Scheers J, deMare C, 1998, "Study of the Frictional Behaviour of Steel sheets surfaces during deep drawing by use of Design of Experiments", Proceedings 20th International IDDRG Congress, 1998, pages 59-67*
- *Scheers J, Vermeulen M, 1999(a), internal report for Autosurf Task 2.3 (OCA PRJ AS9904B01)*

- *Scheers J, 1999(b), internal Ocas report for Autosurf, Task 1.2 (OCA TRJ AS9811B01)*
- *Schipper DJ, 1988, "Transitions in the Lubrication of Concentrated Contacts", PhD-thesis, University of Twente, the Netherlands*
- *Scott PJ, 2000, "An Algorithm to Extract Critical Points from Lattice Height Data", Proceedings of the 8th international Conference on Metrology and Properties of Engineering Surfaces, April 2000*
- *Scott PJ, 2001, private conversation during Autosurf meeting in Rome*
- *SEP 1940, February 1997, "Measurement of roughness average Ra and peak count RPc on cold rolled steel sheet with stochastic surface textures", ECISS*
- *Siekirk JF, 1986, "Process Variable Effects on Sheet Metal Quality", Journal of Applied Metalworking, Vol. 4 No 3 pp262-269*
- *Skade S, 1994, "Engineering of Surface Topographies", Ph.D. thesis Institute of Manufacturing Engineering, Technical University of Denmark*
- *Staeves J, Filzek J, Schmoeckel D, 2001, "Surface qualification in the sheet metal domain" Institute for Production Technologies and Forming Machines, Darmstadt University of Technology, Petersenstr. Germany.* http://www.ptu.tu-darmstadt.de/forschung/tribologie/shemet/shemet.htm
- *Stout KJ, Sullivan PJ, Dong WP, Mainash E, 1991, "Analysis of 3-D surface topography questionnaire", EC Report, University of Birmingham*
- *Stout KJ, Sullivan PJ, Dong WP, Mainsah E, Luo N, Mathia T and Zahouani H, 1993, "The development of methods for the characterization of roughness in three dimensions" Report EUR 15178EN (Kogan Page)*
- *Surfstand, 1996, EU commission DGXII from 1996 to 2000 under contract SMT4/CT95/2018.*
- *Suzuki S, Totsuka N, Kurisu T, Ichida T, Mouri T, 1992, "Development of Self-Lubricating Steel Sheet", Kawasaki Steel Giho, report no. 27*
- *Sy-Wei L, Jing-Yeong L, 1998, "Optimum Blank Shapes for Prismatic Cup Drawing – Consideration of Friction and Material Anisotropy", Transaction of the ASME, Vol. 120 pp306-315*
- *Szeri AZ, 1980, "Friction, Lubrication and Wear", Hemisphere Publishing, p2*
- *Taguchi G, 1987 "System of Experimental Design", Kraus International Publications (UNIPUB), Vol. 1 pp147-152*
- *Taupin E, Breitling J, Wu WT, Altan T, 1996, "Material Fracture and Burr Formation in Blanking, results of FEM simulations and comparison with*

experiments", Journal of Material Processing Technology, Vol. 59 No. 1-2, pp68-78

- *Ter Haar R, 1996, "Friction in Metal Forming – The influence of local contacts in deformation", PhD Thesis, Univesity of Twente, The Netherlands*
- *Timmerbeil W, 1956 "Der Einflib der Scheidkantenabnutzung auf den Schineidvorgang am Blech Werkstattechnik", Machinnebau, Vol. 46, p58-66*
- *Tressel AR, 1977, " In plant Standard on Burrs", SME Technical Paper series MR, No. MR77 – 467 p12*
- *VDI 2906, 1994, General Guideline of German Institute of Engineers on: "Quality of Cut Faces of (sheet) metal parts after cutting, blanking, trimming or piercing"*
- *Vermeulen M, Scheers J, De Maré C and De Cooman B, 1995, "3D Characterisation of EBT Steel Sheet Surfaces", Int. J. Mach. Tools and Manufacture. Volume 35, No. 2, pp273-280*
- *Vermeulen M, 1999, internal Ocas report for Autosurf task 2.3 (OCAS PR JAS9904B 01)*
- Vermeulen M, Hoebeke H, Antonissen J, 2001, "Mixed Lubricated Plastic Contact Phenomena in EBT Textured Steel Sheet", Proceedings of the 9th International Conference on Sheet Metal, Leuven, Belgium, pp415-424
- Vermeulen M, De Boeck A, Claessens S, Antonissen J, Scheers J, 2001(a), "Sheet metal processing, texturing anc coating methods in view of application manufacturing steps", Proceedings of the 9th International Conference on Sheet Metal, Leuven, Belgium, pp3-26
- *Werbeagentur ZM, 1998, "Manufacturing Programme and Applications", for Fuchs Lubritech GmbH, pp25-38*
  http://www.fuchs-lubritech.de/untern_e.htm
- *Whitehouse D, 1982, "Parameter Rash, Is There A Cure?" Wear, Vol. 83, pp75-78*
- *Whitehouse DJ, 1994, "Handbook of Surface Metrology", IOP publishing, pp376-531*
- *Wihlborg AH, 2000, "The influence of steel sheet surface-topography on friction in stamping", PhD Thesis, Chalmers University, 2000 (ISSN 1100-7524), pp19-20*
- *Wilson WRD, 1997, "Tribology in Sheet Metal Forming", Journal of Manufacturing Science and Engineering, Vol. 119 pp695-698*

- *Wrentik DJ, 2001, private conversation during an Autosurf workshop in London*
- *Zaccone DC, Elko RG, Horgart DJ, Oltean JW, Grimmet MW, Shi MF, Bodnar JJ, Grivna JM, 1998, "A study on Uniformity of Pre-Applied Lubricants from Mill Application to Draw Die", SAE Special Publications, v 1322, pp7-15.*
- *SCOUT 2000 – Surface Characterisation Open-Source Universal Toolbox, Version 2000.05.24*
  http://www.brunel.ac.uk/research/scout/
- Betascope 2000 – Fischer Instrumentation Electronique
  http://www.helmut-fischer.com/us/produkte/mms6.htm
- *Autosurf 1998 – Surface Topography Optimisation for the Automotive Industry – EU Funded AUTOSURF – BE-97-4140 Project*
  http://www.autosurf.org/
- *Surfstand 1998 – Development of a basis for 3D Surface Topography Standard – EU funded SURFSTAND – SMT4 CT98-2209 Project*

APPENDIXES

A1. Surface topography parameter definitions

Statistical characterisation is widely used both in academia and industry. Since surfaces can be represented as two sets of data ("x" and "y") in 2D and three sets of data ("x", "y" and "z") in 3D. It is natural and meaningful to apply statistics in order to characterise them. The data sets can be analysed in a variety of ways and the resulting parameters can be divided into various classes, such as: heights, height distribution, hybrid and spatial [Griffiths, 2001]. The published 3D surface roughness parameters are now presented based on these classes.

A1.1 Amplitude and amplitude distribution parameters

The amplitude parameters describe some form of peak-to-valley characterisation. Several amplitude parameters are currently standard in 2D and their natural extension in 3D is now widely employed (the most important are presented in Table A1.1). The amplitude parameters are: dispersion (Sa, Sq), extremes (Sz).

The amplitude distribution parameters describe the shape of the heights distribution. The distribution parameters are: asymmetry (Ssk) and sharpness (Sku).

These are now described mathematically in the following table, where:

$z_{ij} = z(x_i, y_j)$ where $i = 1..n$ and $j = 1..m$

$$M = \frac{1}{mn}\sum_{ij} z_{ij} = 0$$ (Surface referred to mean plane)

Parameter	Definition	Unit
Sq	$\sqrt{\frac{1}{mn}\sum_{ij} z_{ij}^{\,2}}$	µm
Sa	$\frac{1}{mn}\sum_{ij} \lvert z_{ij} \rvert$	µm
Ssk	$\frac{1}{mn}\sum_{ij} z_{ij}^{\,3} \Big/ S_q^{\,3}$	pure number
Sku	$\frac{1}{mn}\sum_{ij} z_{ij}^{\,4} \Big/ S_q^{\,4}$	pure number
St	$Max(z_{ij})-Min(z_{ij})$	µm
Sz	*Avg(5 Max)-Avg(5 Min)*	µm

Table A1.1 – Amplitude parameters

The 3D surface (z_{ij} in Table A1.1) can be represented as a matrix of height. Every column or row can be interpreted as a 2D profile. Every 2D profile of the matrix is composed of a number of sampled heights.

A1.2 3D Spatial characterisation

Spatial properties of surfaces are the most difficult to characterise because of random and multi-wavelength components of surfaces and high sensitivity to the sampling interval. The main current techniques include:

- **Auto-correlation.** The areal auto-correlation function (AACF or "R") describes the "repeatability" of a surface at different positions. This function is calculated averaging two copies of the same surface displaced in all possible overlapping combinations. When the calculated AAFC exhibit values close to 1 (100% auto-correlation), it means that the surface is "repeating" itself [*Porrino et al 2000*].

$$R(\tau_x, \tau_y) = E[z(x, y) \cdot z(x + i\Delta_x, y + j\Delta_y)] =$$

$$= \frac{1}{(m-|i|)(n-|j|)} \sum_{k=k_1}^{k_2} \sum_{l=l_1}^{l_2} z(x_k, y_l) \cdot z(x_{k+i}, y_{l+j})$$

where $\tau_x = i\Delta_x$, $\tau_y = j\Delta_y$ and

$i \in [-(m-1), +(m-1)]$, $j \in [-(n-1), +(n-1)]$

$k_1 = \max[0, -i]$, $k_2 = \min[m-1, m-1-i]$

$l_1 = \max[0, -j]$, $l_2 = \min[n-1, n-1-i]$

In the example below (Figure A1.1) it can be noticed that the maximum auto-correlation is when the two surfaces are perfectly overlapped (the centre of the diagram shows a peak of the auto correlation function – the dark spot).

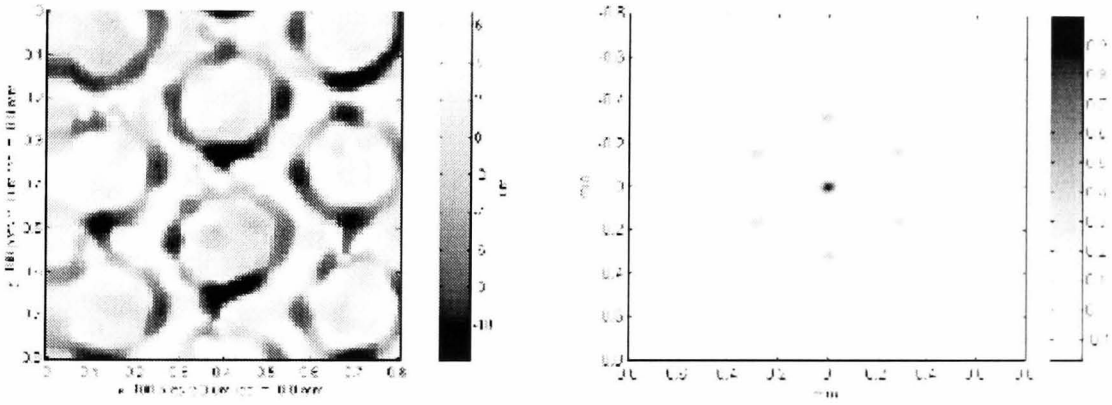

(a) (b)

Figure A1.1- A surface (a) and its AACF (b)

- **Density of peaks**. In 2D, this parameter is given by the number of peaks (per mm or cm), which project through a line that is parallel to the mean line but displaced a distance above it. It is termed RHSC but since the displacement is set arbitrarily this parameter is not standardised, even in two dimensions. The 3D parameter is the number of peaks that project through a plane. However, in 3D there is a problem of how a peak is defined which is a problem of how neighbourhood rules described in appendix 2 are applied.

- **Geometrical**. Wherever there is a predominance of deterministic features in a surface, as in EBT sheet, information can be retrieved using plain Euclidean geometry characterisation such as: depth of the crater, diameter of the island, distance between two craters parallel or perpendicular to the rolling direction. Such descriptors are simply average dimensions of features and are not standardised. They have been mainly defined by Vermeulen et al [1995].

A1.3 3D functional characterisation

This is a set of techniques, which are proven to relate to particular functional properties of surfaces, e.g. fluid levels. The main disadvantage is that due to the wide range of functional requirements, it is impossible to find a universal function model, so there are potentially as many parameters as there are functions. The main functional descriptors are as follows:

- The **Abbott-Firestone** curve (AFC) or bearing area curve is defined as a percentage of surfaces above a given height. It is a standard in 2D profiles and widely employed to characterise fluid retention properties, mechanical resistance and load carrying capacity [*ISO 4287, 1996 and DIN 4776, 1990*]. Although an extension of the AFC for areal surfaces seems natural and meaningful, there is no current specification of areal filtering in the literature. Parameters that can be derived are: core roughness depth Sk, reduced peak height Spk, reduced valley depth Svk, bearing area points Sr1 Sr2, as illustrated in the Figure A1.2 [*Sacerdotti et al 2000(d)*].

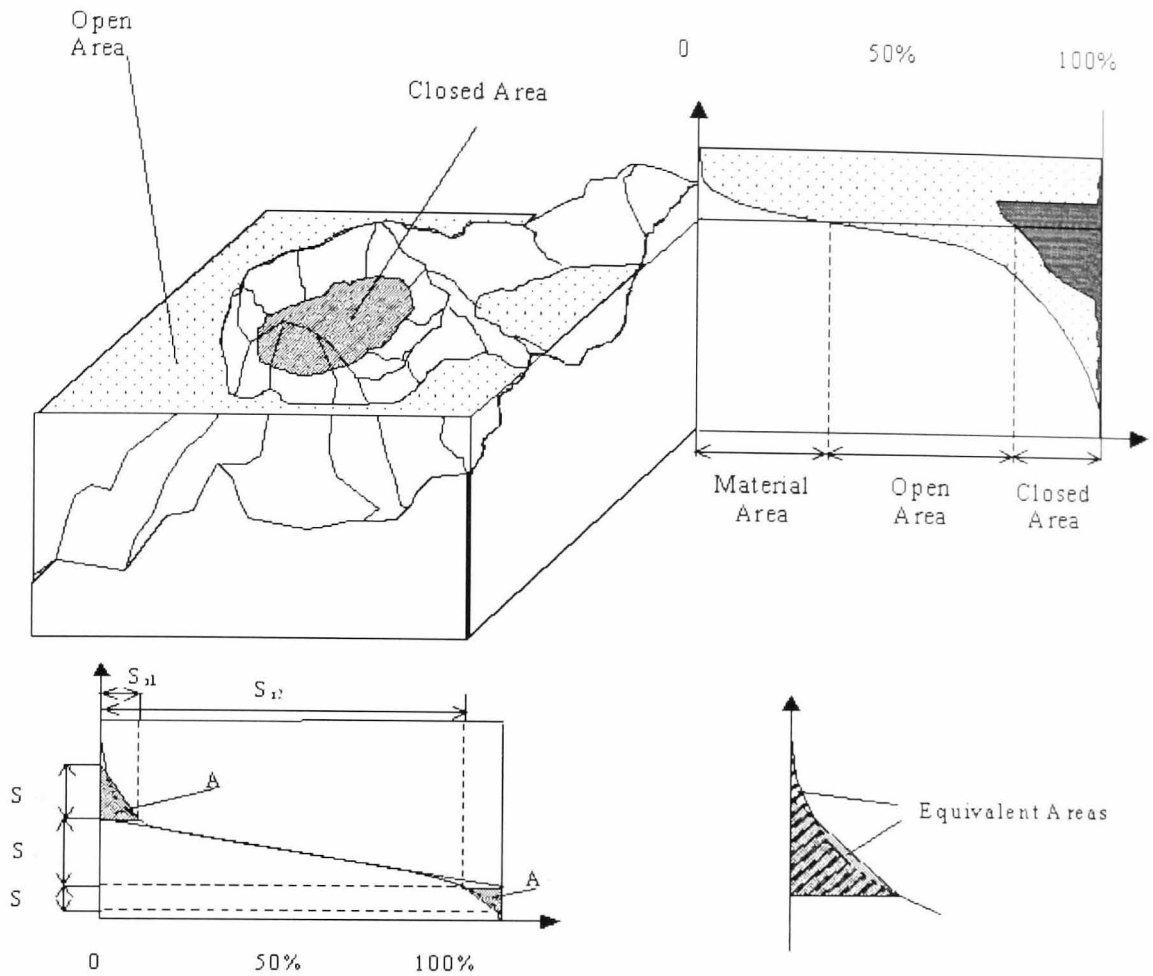

Figure A1.2 – AF Curve and void areas

- **Volumetric** characterisation is becoming increasingly used, since fluid retention and flow properties relate to empty volumes. Particular attention is given to the distinction between open and closed volumes [*Pfestorf et al 1998*], since closed volumes support lubricant pressure build-up in forming. For volumetric parameter definition please refer to the following part of this appendix (Volumetric Family of the "Birmingham 14") and section 3.5.
- **Motif parameters** are currently 2D standard for functional performance in autobody panels [*ISO 12085, 1997*]. There is neither a standard nor a stable algorithm for calculating them in 3D [*Scott, 2000*].

A1.4 3D hybrid techniques

Every method, which is the result of combining two or more of the previously classified techniques, is known as hybrid. Many hybrid parameters have been generated, such as: the root-mean square slope of surface SΔq, the

arithmetic mean peak curvature of the surface Ssc, and the interfacial area ratio Sdr [*Sacerdotti et al 2000(d)*].

A1.5 The "Birmingham 14" (+3)

A major European research programme was centred at Birmingham University between 1996 and 2000 [Surfstand, 1996]. It was the first research to concentrate on 3D surface parameters and it made recommendations for parameters that should be standardised. Fourteen parameters were recommended, hence the title the "Birmingham 14". Since then a second research or continuation project, run by the same team but now based at Huddersfield University re-recommended the 14 parameters and added another 3 parameters (the last three of the list – the "Functional Volume Family"), hence the title the "Huddersfield 17"! These are the foundational parameters since the research team have made significant progress and are certainly the world leaders. These parameters will now be introduced in the following sections.

A1.5.1 AMPLITUDE PARAMETERS

Four parameters are used for characterizing the amplitude property of surfaces. They are classified into four categories, dispersion (1), extreme (2), asymmetry of the height distribution (3) and sharpness of the height distribution (4) [Surfstand, 1996].

(1) Root-mean-square deviation of the surface *Sq*

This is a dispersion parameter defined as the root mean square value of the surface departures within the sampling area.

$$S_q = \sqrt{\frac{1}{mn}\sum_{ij} z_{ij}^2}$$

where, "m" is a number of points per profile, "n" is the number of profiles (this definition applies to all the other equations in this section). *Sq* is a very general and widely used parameter. In statistics, it is the sample standard deviation.

(2) Ten point height of the surface *Sz*

This is an extreme parameter defined as the average value of the absolute heights of the five highest peaks and the depths of the five deepest pits or valleys within the sampling area.

$$S_z = \frac{\sum_{k=1}^{5} |z_{pk}| + \sum_{k=1}^{5} |z_{vk}|}{5}$$

where z_{pk} and z_{vk} are the five highest surface peaks and lowest surface valleys respectively, which rely on eight nearest neighbour peaks presented in appendix 2.

(3) Skewness of topography height distribution *Ssk*

This is the measure of asymmetry of surface deviations about the mean plane.

$$S_{sk} = \frac{1}{mn \cdot S_q^3} \sum_{ij} z_{ij}^3$$

This parameter can effectively be used to describe the shape of the topography height distribution. For a Gaussian surface, which has a symmetrical shape for the surface height distribution, the skewness is zero. For an asymmetric distribution of surface heights, the skewness may be negative if the distribution has a longer tail at the lower side of the mean plane or positive if the distribution has a longer tail at the upper side of the mean plane. This parameter can give some indication of the existence of "spiky" features.

(4) Kurtosis of topography height distribution *Sku*

This is a measure of the peakedness or sharpness of the surface height distribution.

$$S_{ku} = \frac{1}{mn \cdot S_q^4} \sum_{ij} z_{ij}^4$$

This parameter characterizes the spread of the height distribution. A Gaussian surface has a kurtosis value of 3. A centrally distributed surface has a kurtosis value larger than 3 whereas the kurtosis of a well spread distribution is smaller than 3. By a combination of the skewness and the kurtosis, it may be possible to identify surfaces which have a relatively flat top and deep valleys.

A1.5.2 SPATIAL PARAMETERS

Four parameters are used to characterize spatial properties (1), density of peaks (2), texture aspect ratio (3), directionality of surface lay and fastest decay auto-correlation length (4).

(1) Density of peaks of the surface *Sds*

Sds is the number of peaks per unit sampling area. The peak definition is based on the 8 nearest neighbours rule. In other words, a peak is defined of it only if and only if it is higher than its 8 nearest neighbours as defined in appendix 2.

$$s_{ds} = \frac{\#summits}{(m-1)\cdot(n-1)\cdot\Delta x\cdot\Delta y}$$

where Δx and Δy are respectively the spacing between two samples in the x-direction and the y-direction.

(2) Texture aspect ratio of the surface *Str*

Str is a parameter used to characterise texture strength (i.e. uniformity of texture aspect). It is defined through the areal auto-correlation function (AACF). *Str* can be defined as the ratio of the fastest to the slower decay when AACF is 0.2.

$$S_{tr} = \left.\frac{\min\left(\sqrt{\tau_x^2+\tau_y^2}\right)}{\max\left(\sqrt{\tau_x^2+\tau_y^2}\right)}\right|_{R(\tau_x,\tau_y)\le 0.2}$$

In principle, the texture aspect ratio has a value between 0 and 1. Larger values, say *Str*>0.5, of the ratio indicates uniform texture in all directions i.e. no defined lay. Smaller values, say *Str*<0.3, indicates an increasingly strong directional structure or lay. Since the size of the sampling area is finite, it is possible that the slowest decay of the AACFs of some anisotropic surfaces never reach 0.2 within the sampling area. In this case the longest distance of the AACF along the slowest decay direction can be used instead.

(3) The fastest decay auto-correlation length *Sal*

This is a parameter in length dimension used to describe the auto-correlation character of the AACF. It is defined as the horizontal distance of the AACF

which has the fastest decay to 0.2. In other words the Sal is the shortest auto-correlation length that the AACF decays to 0.2 in any possible direction.

$$S_{al} = \min\left(\sqrt{\tau_x^2 + \tau_y^2}\right)\Big|_{R(\tau_x,\tau_y)\le 0.2}$$

For an anisotropic surface *Sal* is in a direction perpendicular to the surface lay. A large value of *Sal* denotes that the surface is dominated by low frequency (or long wavelength) components. While a small value of the *Sal* denotes the opposite situation.

(4) Texture direction of the surface *Std*

This is the parameter used to determine the most pronounced direction of the surface texture with respect to the y axes within the frequency domain, i.e. it gives the lay direction of the surface. A unified definition of the texture direction of a surface is given through an angle. By this definition, when the measurement trace direction is perpendicular to the lay (this is a very common case) the texture direction is 0° .

$$S_{td} = \begin{cases} -\beta & \beta \le \dfrac{\pi}{2} \\ \pi - \beta & \dfrac{\pi}{2} \le \beta \le \pi \end{cases}$$

where, β is the maximum value of the angular spectrum.

$$\beta = tg^{-1}\frac{\mathrm{Re}\left[F_{pq}\right]}{\mathrm{Im}\left[F_{pq}\right]}\Bigg|_{\max\left(\sqrt{\left(\mathrm{Re}\left[F_{pq}\right]\right)^2+\left(\mathrm{Im}\left[F_{pq}\right]\right)^2}\right)} \quad \text{and} \quad F_{pq} = \Delta x\cdot\Delta y\sum_{k=1}^{m-1}\sum_{l=1}^{n-1} z_{pq}\cdot e^{-j2\pi\left(\frac{p\cdot k}{m}+\frac{q\cdot l}{n}\right)}$$

A1.5.3 HYBRID PARAMETERS

The hybrid property is a combination of both amplitude and spacing. Any changes that occur in either amplitude or spacing may have an effect on the hybrid property. Three hybrid parameters are calculated here.

(1) Root-mean-square slope of the surface $S_{\Delta q}$

This is the root-mean-square value of the surface slope within the sampling area.

$$S_{\Delta q} = \sqrt{\frac{1}{(m-1)(n-1)}\sum_{j=1}^{m}\sum_{i=1}^{n}\rho_{ij}^2}$$

where $\rho_{ij} = \sqrt{\left(\frac{\partial z_{ij}}{\partial x}\right)^2 + \left(\frac{\partial z_{ij}}{\partial y}\right)^2}$

(2) Arithmetic mean peak curvature of the surface *Ssc*

This is defined as the average of the principal curvatures of the peaks within the sampling area. Since the sum of the curvatures of a surface at a point along any two orthogonal directions is equal to the sum of the principal curvatures.

$$S_{sc} = -\frac{1}{2} \cdot \frac{1}{n} \sum_{j=1}^{m} \sum_{i=1}^{n} \left(\frac{\partial^2 z_{ij}}{\partial x} + \frac{\partial^2 z_{ij}}{\partial y} \right)$$

This parameter can only be calculated after the peaks.

(3) Developed interfacial area ratio *Sdr*

This is the ratio of the increment of the interfacial area of a surface over the sampling area.

$$S_{dr} = \frac{\sum_{i=1}^{n-1} \sum_{j=1}^{m-1} A_{ij} - (m-1)(n-1) \cdot \Delta x \Delta y}{(m-1)(n-1) \cdot \Delta x \Delta y} \cdot 100\%$$

where the interfacial area of the unit surface (quadrilateral) is

$$A_{ij} = \frac{1}{4} \cdot \left[\sqrt{\Delta y^2 + \left(z_{ij} - z_{ij+1}\right)^2} + \sqrt{\Delta y^2 + \left(z_{i+1j+1} - z_{i+1j}\right)^2} \right] \cdot$$

$$\left[\sqrt{\Delta x^2 + \left(z_{ij} - z_{i+1j}\right)^2} + \sqrt{\Delta y^2 + \left(z_{ij+1} - z_{i+1j+1}\right)^2} \right]$$

The developed interfacial area ratio reflects the hybrid property of surfaces. A large value of the parameter indicates the significance of either the amplitude or the spacing or both.

A1.5.4 FUNCTIONAL PARAMETERS

- **INDEX FAMILY**

The functional indexes proposed here are applicable to all kinds of typical engineering surfaces (highly stressed or ordinary).

(1) Surface bearing index *Sbi*

This is the ratio of the root mean square deviation (Sq) over the surface height at 5% bearing area.

$$S_{bi} = \frac{S_q}{z(AFC = 0.05)} = \frac{1}{h_{0.05}}$$

Where $h_{0.05}$ is the height reached at AFC=5%, AFC being defined in section A1.3 above. Note that a larger Sbi indicates a good bearing property.

(2) Core fluid retention index *Sci*

Sci is defined as the void volume V_v, calculated including all voids between two planes at 80% and 5% of the AFC. Sci is then normalised to the root mean square (Sq) and the unit sampling area.

$$S_{ci} = \frac{1}{S_q} \cdot \frac{V_v(h_{0.05}) - V_v(h_{0.80})}{(m-1)(n-1) \cdot \Delta x \Delta y}$$

where $V_v(h_{0.05}) = \sum_{i=1}^{n} \sum_{j=1}^{m} \sum_{k=h_{0.05}}^{h_{1.00}} f_{ijk}$ and $f_{ijk} = \begin{cases} 0 & k < z_{ij} \\ 1 & k \geq z_{ij} \end{cases}$

A larger *Sci* indicates a good fluid retention. For a Gaussian surface, this index is about 1.56.

(3) Valley fluid retention index *Svi*

Svi is defined as the void volume calculated including all voids between two planes at 100% (void volume zero) and 80% AFC. Svi is then normalised to the root mean square (Sq) and the unit sampling area.

$$S_{vi} = \frac{1}{S_q} \cdot \frac{V_v(h_{0.80})}{(m-1)(n-1) \cdot \Delta x \Delta y}$$

where $V_v(h_{0.80}) = \sum_{i=1}^{n} \sum_{j=1}^{m} \sum_{k=h_{0.80}}^{h_{1.00}} f_{ijk}$ and $f_{ijk} = \begin{cases} 0 & k < z_{ij} \\ 1 & k \geq z_{ij} \end{cases}$

A larger *Svi* should indicate a good fluid retention in the valley zone.

- **VOLUME FAMILY**

The material volume and void volume in the surface bearing area is a naturally geometrical descriptor of a surface topography. The material volume and void volume enclosed in the contacting surface of the material, they may

have a very close relation with functional properties of the surface, such as bearing, wear, running in and fluid retention. Three volume parameters, are presented here to characterize the functional properties of surfaces.

(1) Material volume of the surface *Sm*

The material volume is defined as the material portion enclosed at the first 10% of the AFC and normalised to the unit sampling area.

$$S_m = \frac{V_m(h_{0.10})}{(m-1)(n-1)\cdot\Delta x\Delta y}$$

where $V_m(h_{0.10}) = \sum_{i=1}^{n}\sum_{j=1}^{m}\sum_{k=h_{0.00}}^{h_{0.10}} f_{ijk}$ and $f_{ijk} = \begin{cases} 0 & k > z_{ij} \\ 1 & k \le z_{ij} \end{cases}$

The material volume and the material volume ratio are not only geometrical descriptors of the surface, but also have significant functional implications. The material volume may reflect wear and the running-in properties. On the other hand, for a "flat-topped" surface, such as a honed surface, the material volume ratio may increase quickly, whereas for a spiked surface, such as a bored surface, the function shows a slow increase with the truncation level. Thus functionally, the material volume reflects the resistance against wear and friction. Surfaces with a rapid increase in the AFC show good running-in a property whereas those with a slow increase in the AFC indicates that the top part of the material is easily worn.

(2) Core void volume of the surface *Sc*

Sc is defined as the void volume calculated including all voids between two planes at 80% and 10% AFC. Sc is then normalised to the unit sampling area.

$$S_c = \frac{V_v(h_{0.10}) - V_v(h_{0.80})}{(m-1)(n-1)\cdot\Delta x\Delta y}$$

where $V_v(h_{0.10}) = \sum_{i=1}^{n}\sum_{j=1}^{m}\sum_{k=h_{0.10}}^{h_{1.00}} f_{ijk}$ and $f_{ijk} = \begin{cases} 0 & k < z_{ij} \\ 1 & k \ge z_{ij} \end{cases}$

(3) Valley void volume of the surface *Sv*

Sv is defined as the void volume calculated including all voids between two planes at 100% and 80% of the AFC. Sv is then normalised to the unit sampling area.

$$S_V = \frac{V_v(h_{0.80})}{(m-1)(n-1)\cdot \Delta x \Delta y}$$

where $V_v(h_{0.80}) = \sum_{i=1}^{n}\sum_{j=1}^{m}\sum_{k=h_{0.80}}^{h_{100}} f_{ijk}$ and $f_{ijk} = \begin{cases} 0 & k < z_{ij} \\ 1 & k \geq z_{ij} \end{cases}$

The void volume has the aim to provide a direct inspection of lubrication and fluid retention of surfaces. It represents the fluid retention capacity of a highly worn surface. For a flat-topped surface, such as a honed surface, the core void volume may decrease quickly with the truncation level, whereas for a spiked surface, such as a bored surface, the function shows a slow decrease. Thus functionally, the void volumes reflect the fluid retention property.

A2. The closed regions parameters (Sva and Spa)

This appendix is concerned with defining new 3D parameters proposed by this author which provide a model, related to the situation existing in deep drawing, of firstly how oil is retained on a surface and secondly, how the peaks protruding above the surface plane contact an opposing surface. This means the volume of void existing below the mean line and the volume of peaks protruding above the mean line need to be characterised.

The objective of the proposed parameters is to characterise the peaks and valleys protruding above and below a plane intersecting a surface. In concept the analysis is the same for both these cases and we will start with the definitions appropriate to the peaks' volumes protruding above the mean line. Lattice height data is obtained from a discrete areal measurement of an engineering surface z_{ij} where "i" ranges from 1 to "n" and j from 1 to "m" and spacing $\Delta x, \Delta y$.

The surface can be sectioned with a horizontal plane at whatever height (h) is required. The Figure A2.1(a) below shows a typical electro discharge textured (EDT) engineering surface and a 2D profile obtained at the section shown by the horizontal white line. The extracted profile (Figure A2.1) is then sectioned at a given height.

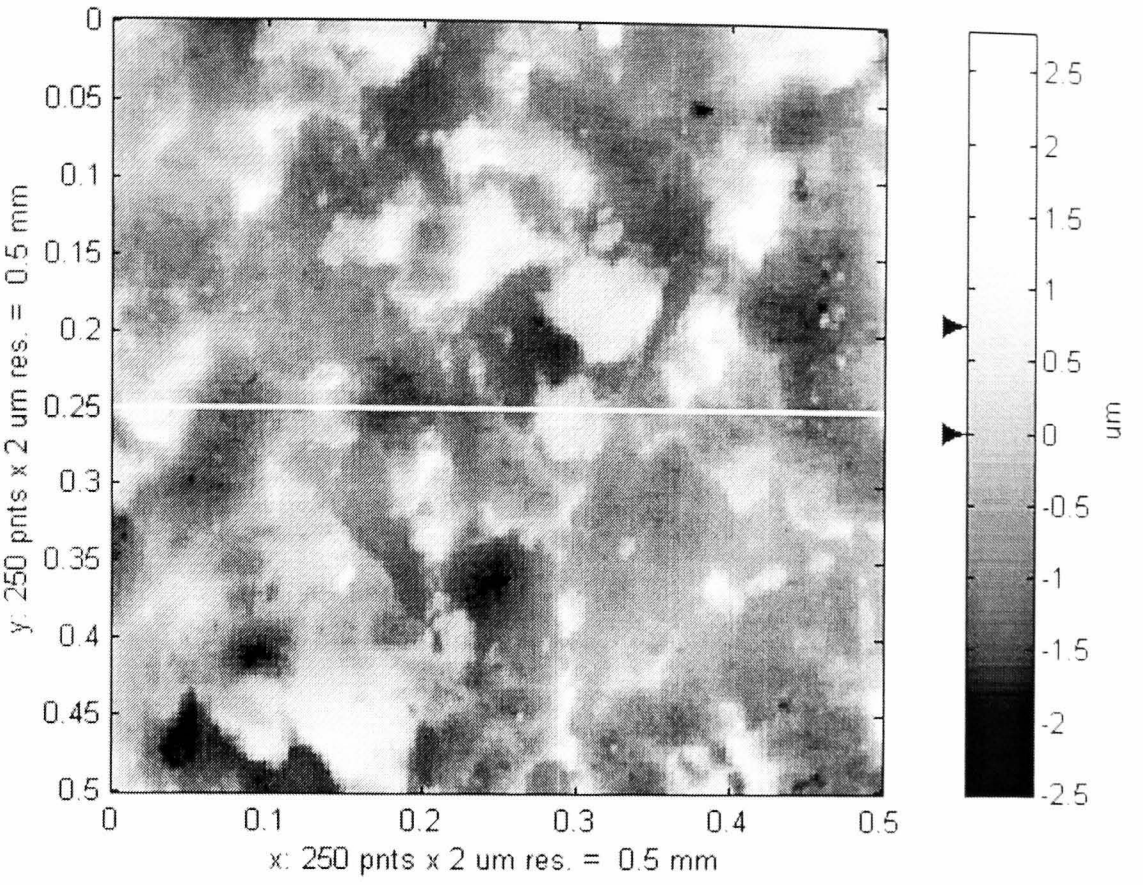

(a)

(b)

Figure A2.1 - Reference surface (a) and extracted profile (b).

The section line in Figure A2.1(b) above is for illustrative purposes only since in reality we are talking about a plane and so the "profile" approach needs to be extended to a "surface". Also, the plane can be defined for any height above the mean plane and this is shown in the Figures A2.2 and A2.3 below where two sections are determined at *h=0* and *h=0.7* μm, which are respectively the mean line and the value of the Sq parameter for this surface. In those Figures A2.2 and A2.3, the peaks (white regions) and valleys (dark

regions) can be observed. Regions (peaks and valleys), which are composed of interconnected points, will be referred to as ***closed regions***.

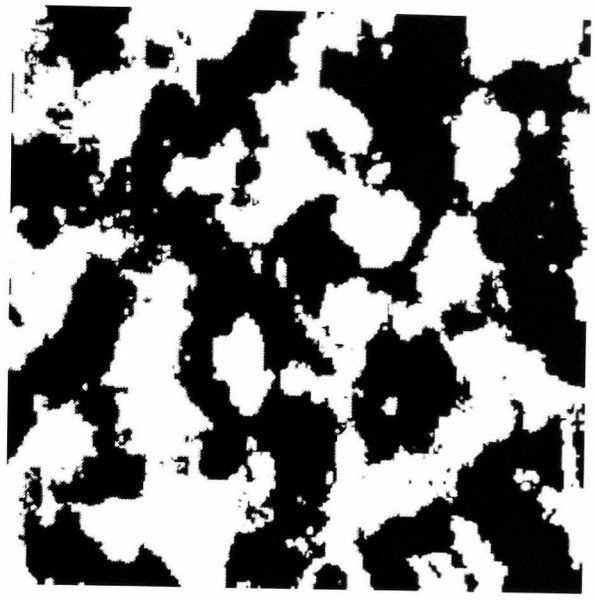

Figure A2.2 - Reference surface intersected at 0 um

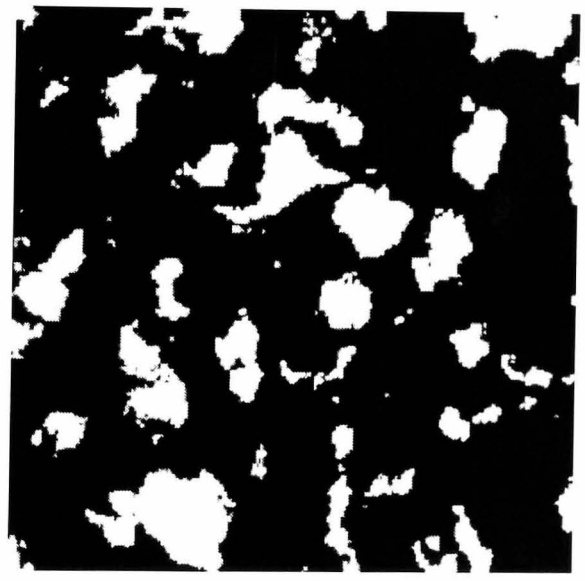

Figure A2.3 - Reference surface intersected at +0.7 µm

Once the desired height of the horizontal intersecting plane (h) is defined, then the characterisation is implemented as follows:

Step 1 - $L_h = \{A_1, A_2 \ldots A_k \ldots A_w\} = NC(z_{ij} \geq h)$

L_h is a list of closed regions above the intersecting plane (peaks). A_k represents the area in m^2 measured with a given neighbouring criterion (NC).

In the definition of a peak, one has to ask how a peak is defined in relation to its neighbours. Traditionally, this begs the question as to which are the important neighbouring heights/peaks. This is a fundamental question [Scott, 2000] and there are two classic cases, which are the 4 and 8 nearest neighbour criteria. These are shown in below, Figure A2.4 is the "4" and Figure A2.5 is the "8" nearest neighbour situations, [Scott 2000]. Here, the "X" represents a point above the given height, "O" below and "-" equal. In Figure A2.4 and Figure A2.5 it is possible to notice the tested points for the given criterion because they are circled and connected to the centre. Note that the points tested in those Figures can not be defined "peaks" for neither of the NCs.

During our experiments, no appreciable difference was found between the two criteria and the 8 neighbours was therefore adopted as the standard criterion because it was more exhaustive.

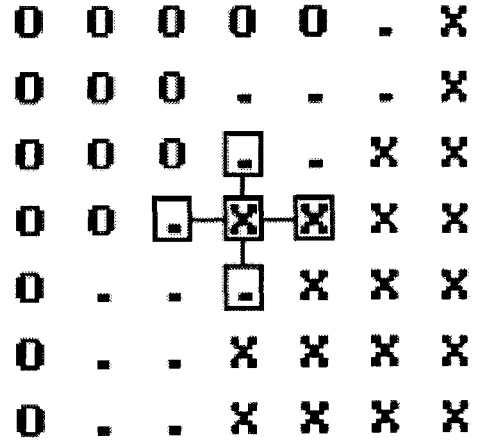

Figure A2.4 - Four neighbours proximity criteria

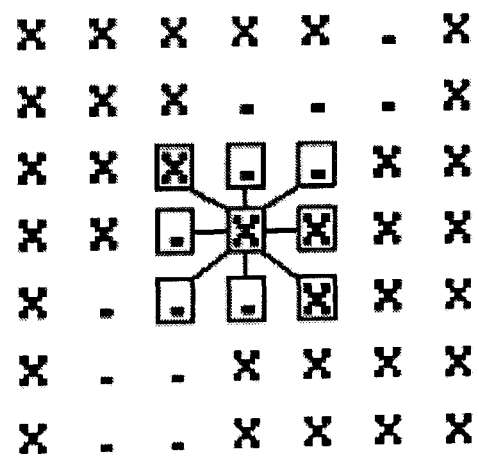

Figure A2.5 - Eight neighbours proximity criteria

Step 2 - $L_h = PC\left(L_h\right)$

The list is pruned of closed regions that can be considered as noise (see Figure A2.6 and Figure A2.7).

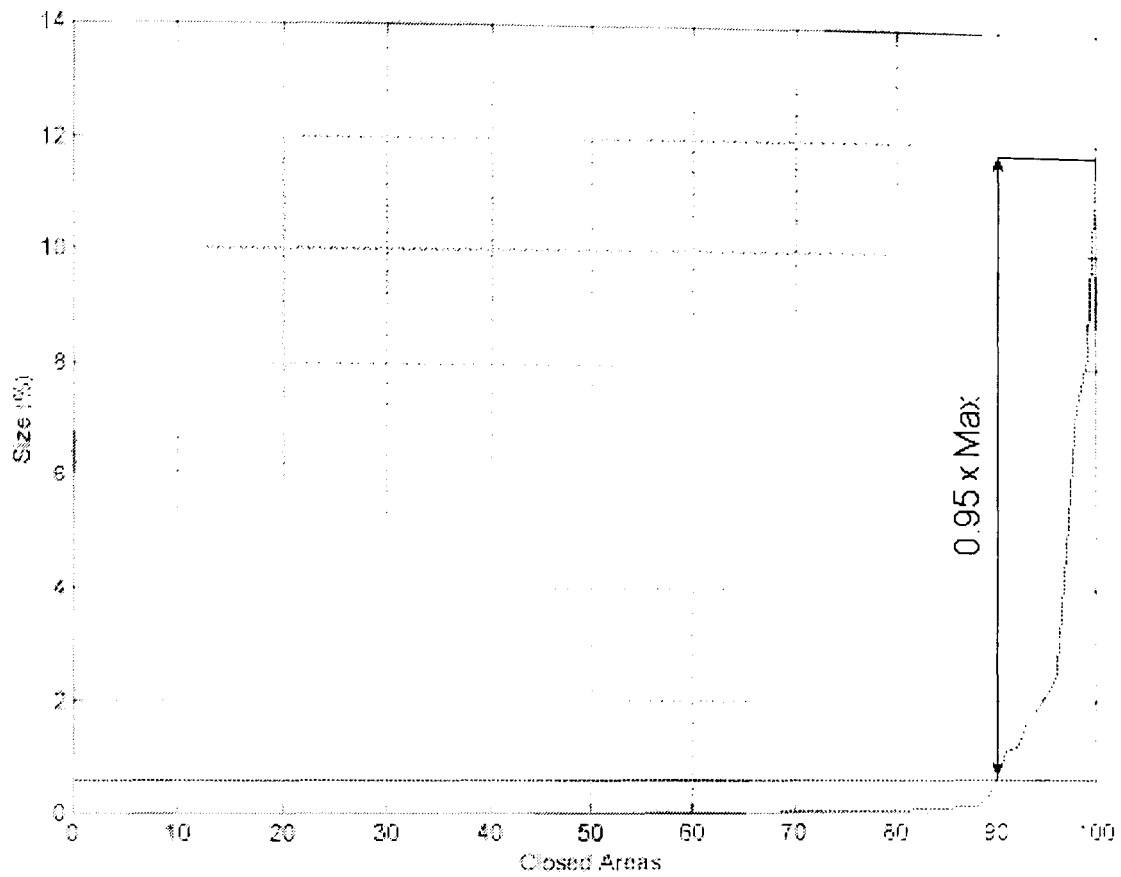

Figure A2.6 - Closed regions list before pruning

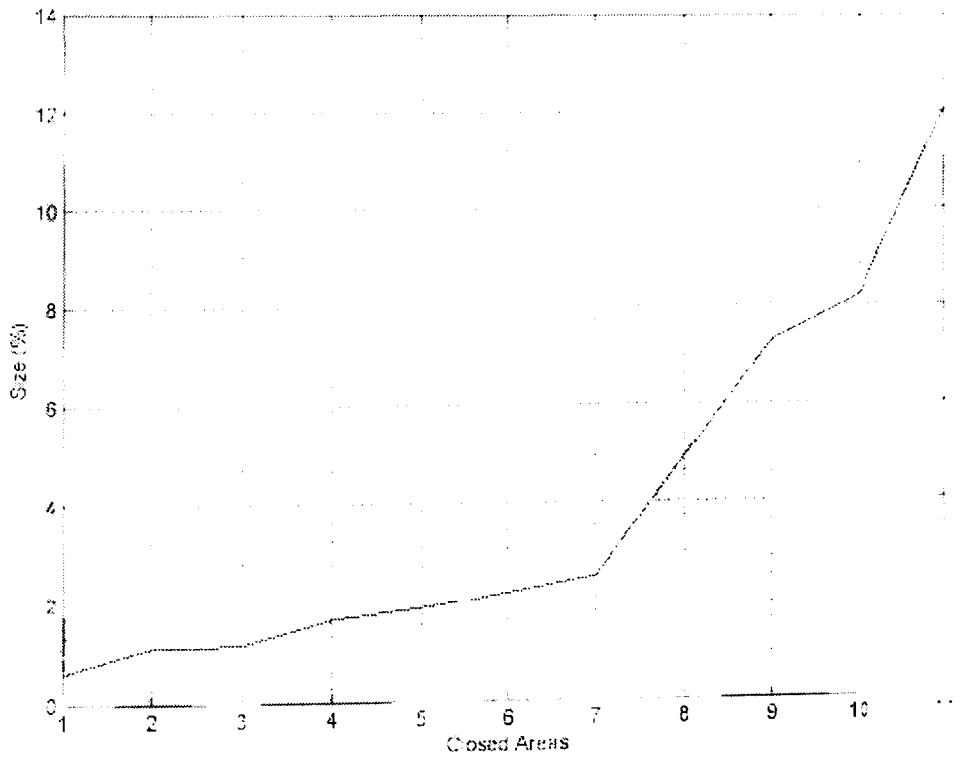

Figure A2.7 - Closed regions list after pruning

This has been done by excluding all regions whose area is less than 5% of the maximum one.

The justification for this particular pruning criterion is that when dealing with physical phenomena such as friction or fluid retention peaks/valleys of a smaller order of magnitude are expected to have a negligible effect. In fact, as one can read in Chapter 4, larger valley areas lead to higher lubricant migration (i.e. Figure 4.12). In the same way, larger peak areas lead to higher friction forces as explained in Chapter 5 (i.e. Figure 5.15).

Step 3 - $S_{pa} = \overline{L_h}$

The closed peak area parameter is defined as the average areas of the pruned regions list.

Step 4 - $S_{pd} = \frac{1}{S_{pa}} \cdot \frac{1}{(n-1)(m-1) \cdot \Delta x \Delta y} \sum L_h$

The closed peak density parameter is defined as the ratio between the overall closed area and Spa divided by the total area.

The same calculation process applied to the closed regions below the intersecting plane ($Z_{ij} <= h$) leads to the definition of the average valley area (Svd) and valley density parameter (Svd). The above definition presents many similarities with standard 2D spacing parameters [*SEP 1940*]. As it can be observed in Figure A2.1, when intersecting the surface at the mean line *(h=0)*, the closed region area parameters (Spa and Sva) definition is comparable to the 2D mean spacing parameter (Sm). Further, when considering the profile protruding above a given band, the closed region density parameters (Spd and Svd) are comparable to the peak count (Pc).

A3. Fischer Betascope MMS

This instrument is used to determine the amount of oil retained on an autobody sheet surface. It is used to provide quantitative values for the oil migration tests described in chapter 4. In this appendix, the "Fischer" instrument is described as well as a test programme to determine its accuracy and repeatability.

A3.1 Working principle

This sensor is based on the measurement of reflected beta particles. Figure A3.1 below shows the principle of operation. Beta particles (electrons) are emitted by a radioactive isotope and reflected back from the sample being irradiated. The intensity of the reflected beam depends, among other factors, on the thickness Th of the coating on the substrate.

The instrument can be calibrated using known standards and an uncoated substrate to accurately measure the coating thickness [*Betascope 2000*]. The main disadvantage is the need for a radioactive isotope. In fact, even if it the isotope exhibits very low power, it is classified and regulated by the "Ionising Radiations Regulations" which strictly control (and limits) its use [Karila 2000].

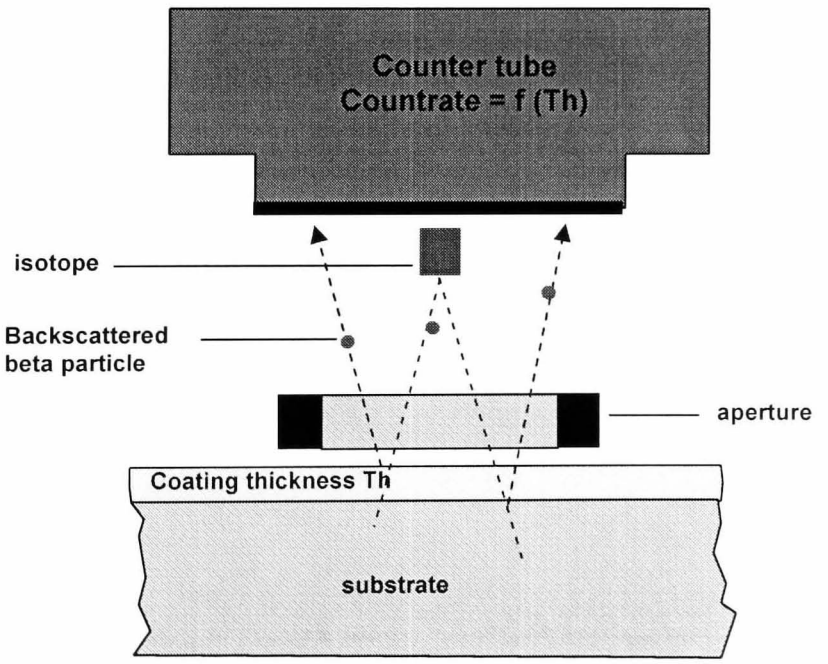

Figure A3.1 - Beta backscatter method

The MMS BETASCOPE employs the beta backscatter method to measure the thickness of coatings consisting of practically any material on any substrate under the condition that there exists a difference of at least 5 atomic numbers between the coating and substrate materials. Typical applications of the MMS BETASCOPE are:

- Measurements of the thickness of conformal coatings, SnPb, Au or Ni coatings in the PC-board industry. Note that the photograph in Figure A3.2 is from the manufacturer's information pack and shows the instrument as part of a test rig being used to measure the thickness of a coating on a PCB board.

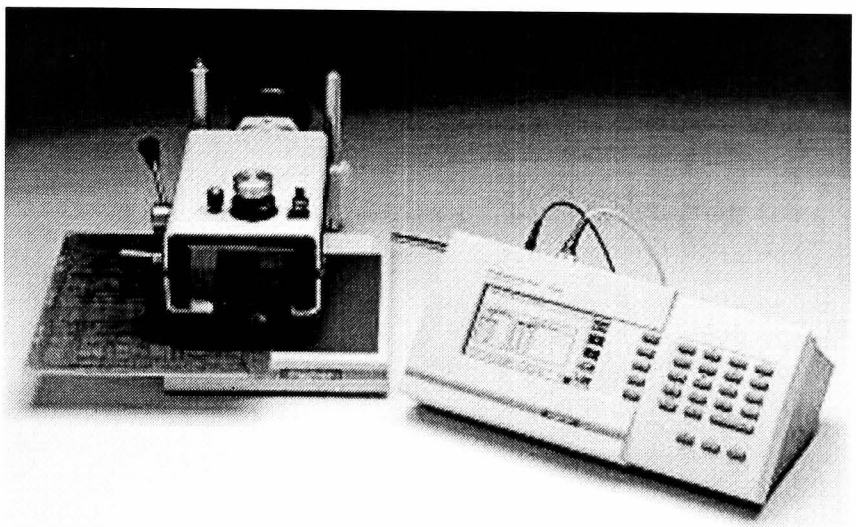

Figure A3.2 - Measurement of electro deposited coatings on a PC-board

- Measurement of oil films and "Bonazinc" coatings in sheet metal production. The unit measures the oil thickness underneath the "probe" when placed on the steel sheet (see at the photograph of Figure A3.3). Note that the photograph of Figure A3.3 is from the manufacturer's information pack and shows the unit being used in "free-standing" mode where it is simply placed on a surface and the coating thickness is measured. It is in this configuration that the unit was used in this research programme. Nevertheless, the measurement positions were decided in advance for our experiments and they are shown in Figure 4.7.

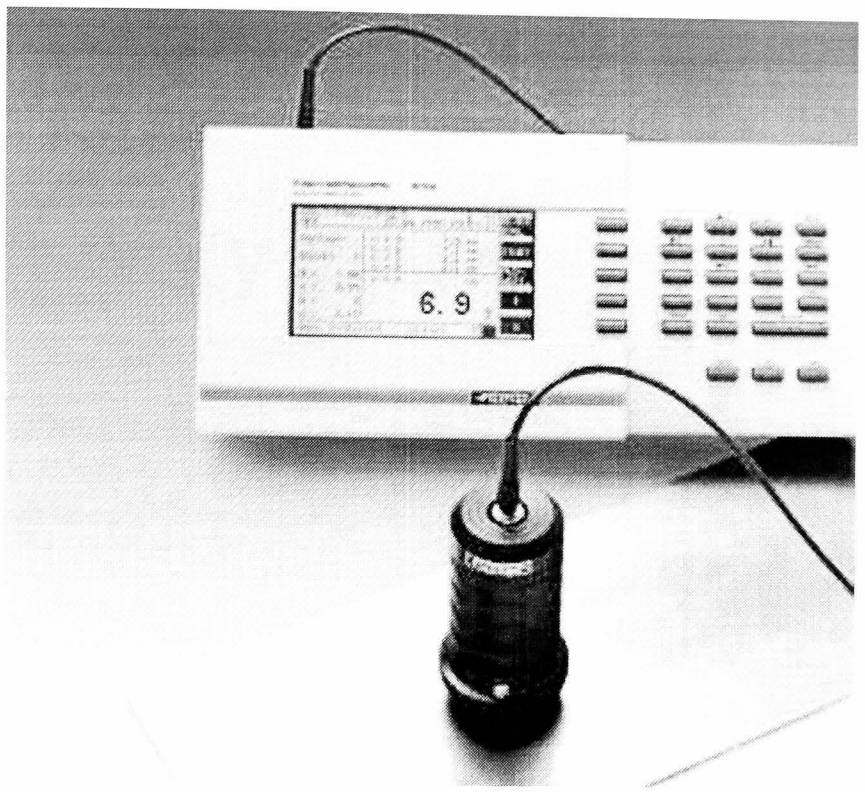

Figure A3.3 - Contact free measurement of a thin oil film

The manufacturers information says the Betascope accuracy (from the calibration report [Karila 2000] is:

- Between 0 and 10 g/m^2 → ±0.00007 g/m^2
- Between 10 and 50 g/m^2 → ±0.00013 g/m^2

However, it was thought it would be inappropriate to just accept these values so in order to be able to use the instrument confidently, it was decided to conduct a series of tests to check the accuracy and repeatability of the instrument.

A3.2 Description of the Betascope accuracy experiment

A test programme was devised to test the accuracy of the instrument. This involved depositing a known amount of oil on a sheet surface and comparing the results form weighing and form the Betascope. The full test procedure is described below.

1) Steel sheets where produced in a square format measuring 60mm by 60mm. This size was chosen because the end of the Betascope probe is 55mm in diameter although the area measured by the probe is only 35mm diameter.

2) The sheets were degreased in an ultrasonic bath to remove all prior traces of oil from the surface.
3) Oil was then applied to the sheets by careful metering with target amounts of 1.5, 1.0, 0.7, 0.5 and 0.3 g/m^2.
4) The actual oil amount was found by weighing the sheets and the results are as follows

Nominal [g/m^2]	Real [g/m^2]	Weight (60x60 mm^2) [g]
1.5	1.522	0.00548
1.0	1.002	0.00361
0.7	0.691	0.00249
0.5	0.508	0.00183
0.3	0.355	0.00128

Table A3.1 – Accuracy tests measuring conditions

5) The oil amount was then determined using the Betascope and the results are given in the following table:

Target	1.5	1	0.7	0.5	0.3
Measured (weighing)	**1.522**	**1.002**	**0.691**	**0.508**	**0.355**
Measured with Betascope [g/m^2]	1.48	0.955	0.563	0.545	0.298
	1.53	1.01	0.639	0.467	0.118
	1.48	0.96	0.67	0.365	0.173
	1.39	0.852	0.621	0.391	0.238
	1.43	0.948	0.642	0.376	0.207
	1.38	1	0.644	0.412	0.094
	1.41	0.894	0.592	0.407	0.23
	1.44	0.994	0.627	0.52	0.267
Mean	1.448	0.9649	0.6344	0.4387	0.1989
Offset	-0.074	-0.0371	-0.0566	-0.0693	-0.1561
Standard Deviation	0.045122	0.054755	0.034923	0.059051	0.061328
Confidence Interval	0.270732	0.328529	0.20954	0.354305	0.367966
CI%	3%	6%	6%	13%	31%

Table A3.2 – Accuracy tests results for Betascope [g/m^2]

These results show that, for the amount of oil of our interest (always above 0.7g/m^2) the Betascope does exhibits an accuracy of 6% at the worst (usually better). This accuracy was regarded as sufficient for our experimental work since no other devices were found able to measure "locally" oil thickness with better accuracy.

Although we understand that this 6% accuracy on the single measurement is above the expectation, this instrument allowed us to explore for the first time the "green field" of lubricant migration on textured surfaces. These initial

results will therefore be challenged soon by other research thanks to advancement in instrumentation accuracy and further experimental work.

Nevertheless, the opportunity given by this instrument of attempting lubricant migration studies makes us confident of the intrinsic value of the results.

Appendix 3

A4. The experimental design (DOE)

This appendix describes the practices and features of "design of experiments" methodology that are used in general and how they relate to this programme. The actual design of experiments applicable to the main themes of oil retention, friction and formability are then addressed in appendices A5, A8 and A9 respectively. Appendix 6 is the sequence of activities and procedures related to the friction experimental work and Appendix 7 contains all the Stribeck plots from the friction experiments.

A4.1 Full and fractional design of experiments

The primary goal in scientific research is to demonstrate the relationships between control factors and measured outputs (the dependent variable/s). In order to do this, there is a need for a full exploration of all the possible combination of factors and analysis of data with statistical tools. This needs to be done in order to quantify the significance of the effect an individual factor or a combination of factors has on the dependent variable of interest. This typically leads to a full factorial experimentation, called a "full factorial".

On the other hand, in industrial research, the primary goal is usually to extract the maximum amount of information on how to control the manufacturing processes from as few observations as possible. This is usually driven by cost. This is done by pruning the full test programme the "less promising" experimental conditions. Hence there is a reduction in the number of tests undertaken. Since this means that only a proportion or fraction of the full test set is used, the technique is called a "fractional factorial".

Both the full factorial test and the fractional approaches are based on the same statistical rules (named "Design of Experiments") but they are applied in different ways.

During this research programme, both these approaches were used either in order to satisfy the needs of Universities (obtain knowledge and publish papers) and industry (obtain solutions fast and cheap), or because there was a lack of supplies of material/coating combinations due to operational reasons.

A4.2 Analysis of variance

The purpose of analysis of variance (ANOVA) is to test for significant differences between mean values. ANOVA is the natural extension of the statistical t-test to a more-than-two groups of observations.

ANOVA was invented by Ronald Fischer in 1922 to study the effect of different fertilizers on the productivity of his field. Fisher, in order to test for statistical significance between means discovered that it was actually necessary to compare observation's variances.

In fact, the total variance of the observations is composed of the variances of single effects. Defined SS_{TOT} the sum of squares of a number of observations, it can be demonstrated that we can partition it into sum of squares of the control factor (SS_F) and sum of square of the phenomenon's natural variability (SS_E): $SS_{TOT} = SS_F + SS_E$

If we call "*N*" the total number of observations and "*a*" the total number of groups of observations, we can define the following:

$$df_{TOT} = df_F + df_E$$

where $df_F = (a-1)$ and $df_E = (N-a)$ hence $df_{TOT} = (a-1) + (N-a) = N-1$

$$MS_F = SS_F / df_F = SS_F / (a-1)$$

$$MS_E = SS_E / df_E = SS_E / (N-a)$$

It is possible to demonstrate that, if the effect of a control factor is null, then the number $F = \left(MS_F / MS_E \right)$ follows a Fisher statistical distribution. Hence, if "F" reaches "highly improbable" values it means that the effect of our control factor is different from zero. This approach can be repeated for a large number of control factors altogether.

A4.2.1 Interaction between factors

If there is more than one control factor under test, a further effect may appear which is the interaction between factors. The interaction can be

interpreted as the following: given two factors, when their values are varied altogether the total effect "differs from the sum" of their single effects.

If we imagine representing the response of an experiment as a hyper surface, the single factor effects can be interpreted as linear effects. In the same representation, interaction can be interpreted as higher order polynomial combinations of the factors. For instance, in a 2^2 full factorial design, the response function (y) can be represented as:

$$y = \mu + \beta_1 \cdot x_1 + \beta_2 \cdot x_2 + \beta_3 \cdot x_1 \cdot x_2 + \varepsilon$$

where β_1 and β_2 are the main effects of each of the two control factors, and β_3 is the effect of the combination of the two. The "order" of the interaction is the order of the equivalent polynomial equation.

Second (two-factors) and third (between three-factors) order interactions are frequently non-null in scientific research.

Higher order interactions are rarely statistically significant and industry does not pay attention to them because they are difficult to control. Hence during experimental design the study of high-order interactions is frequently discarded to reduce experimentation overall costs.

A4.2.2 The ANOVA table

The ANOVA table is the classical representation of the statistics used to evaluate whether factors or interactions are statistically significant or not. One example of an ANOVA table is shown in Table 4.1.

Source	df	Seq SS	Adj SS	Adj MS	F	P
FactorA	2	1.4462	0.9717	0.4858	1.16	0.319
FactorB	**2**	**54.8658**	**43.8479**	**21.9240**	**52.44**	**0.000**
FactorC	1	0.1157	0.0545	0.0545	0.13	0.719
FactorD	**4**	**98.4808**	**98.4808**	**24.6202**	**58.89**	**0.000**
A*B	4	1.4011	1.0257	0.2564	0.61	0.654
A*C	2	0.3296	0.2528	0.1264	0.30	0.740
A*D	8	1.0418	1.0418	0.1302	0.31	0.959
B*C	2	0.1092	0.0563	0.0281	0.07	0.935
B*D	**8**	**25.3680**	**25.3680**	**3.1710**	**7.58**	**0.000**
C*D	4	0.8657	0.8657	0.2164	0.52	0.723
A*B*C	4	0.5767	0.4439	0.1110	0.27	0.899
A*B*D	16	2.3126	2.3126	0.1445	0.35	0.990
A*C*D	8	1.1190	1.1190	0.1399	0.33	0.950
B*C*D	8	0.4180	0.4180	0.0522	0.12	0.998
A*B*C*D	16	2.2874	2.2874	0.1430	0.34	0.990
Error	72	30.1022	30.1022	0.4181		
Total	161	220.8396				

Table 4.1 - Example of ANOVA table: the stack verification test

This table was created from the experimental data obtained during the initial experiment on lubricant retention in order to understand whether the stack position on the pile (Factor A) was important or not.

In this case, it can be seen that the experimental design employed a full factorial with four factors (A, B, C, D shown in first column) where A and B have 3 levels (hence 2 degrees of freedom), C has 2 levels (hence 1 *df*) and D has 5 levels (hence 4 *df*). The degrees of freedom (*df*) are shown in the second column. The third column contains the sums of squares (*SS*). The fourth column shows the adjusted sum of square (*Adj. SS*). Adjusted sum of squares differs from *SS* only when some experimental data are discarded from the statistical computation. The fifth column shows the number $MS = SS / df$ necessary to calculate the sixth column (our statistic $F = MS / MS_E$). Finally, the column *P-value* shows the probability to obtain the *F-value* on its left hand side if *F* follows a Fisher distribution. This means that, when the *P-value* is lower than say 0.01 (ie 1%, which is a typical value for a large number of factors such as applies to the ANOVA table above), it means that the relative *F-value* is highly improbable, hence this factor / interaction is non-null.

Thus, from the data in the ANOVA table of Figure A4.1, we can conclude that that Factor B, Factor D and the interaction between these two are the only statistically important effects upon or output because the P value is less than 0.01 (i.e. 1%) in these cases.

A4.3 The P value employed

P value is the critical value to choose since it relates to the "power" of the test to spot abnormal behaviour. On one hand, if one chooses very low P-values (less than say 5%) might not be able to recognise abnormal behaviour (effects) hence reduce the **sensitivity** of the test. On the other hand, if one chooses a very high P-value (more than say 5%) he might wrongly identify normal behaviours as effect reducing the **power** of the test.

The **typical P-value adopted is** therefore around **5% for a single statistical test** (i.e. correlation analysis) **and 1% for a multiple statistical test** (i.e. DOE).

If more than one statistical test is performed on the same set of sampled data in fact, it is good practice to reduce the single test P value (reduce sensitivity) in order to keep the overall P value (power) at an acceptable level. The way overall P value and the single P value relate to each other can be explained with the Bonferroni method presented below.

A4.4 Calculation of confidence intervals

The Fisher test described above enables one to determine whether a control factor or combination of factors significantly influences the dependant variable. The confidence interval is usually employed to point out which setting of the given control factor (value) stands out with respect to the other values. In other words, Fisher is used to point out which control factor affects the results and – subsequently – the confidence interval is used to explore this effect further by pointing out which settings of the given control factor is doing what.

There are several ways to calculate the confidence intervals for more than one comparison per time. The most common is named after the statistician "Bonferroni". Bonferroni states [Montgomery 1997] that, if simultaneous multiple interval estimations are desired with an overall confidence coefficient 1-α (being "α" the probability of failure), one can construct each interval with confidence coefficient (1-α/g), where "g" is the number of intervals to calculate. In particular, the confidence interval C_i can be calculated with the following equation:

$$C_i = t_{\frac{\alpha}{2c}} \cdot \sqrt{\frac{MS_E}{n}}$$

where MS_E is the mean square error calculated for the ANOVA table, "n" is the number of repetitions of each experimental set and "t" is a value coming from the t-student distribution calculated with α probability (usually 5%) and degrees of freedom equals to twice the number of comparisons (2 times c).

The Bonferroni technique is an extremely powerful statistic since it can be employed even when the number of observations varies between treatments, although the confidence interval is usually larger than other statistics (i.e. Scheffe and Tuckey [Montgomery 1997]).

Confidence intervals were frequently employed in most of the data analysis simply in the form of a vertical line inside the graphs (i.e. Figure 4.8). Thus, whenever two confidence intervals do not overlap, it means that the two values are significantly different.

A4.5 Full factorial design

Factorial designs are widely used in experiments involving several factors where it is necessary to study the total effect of the factors on the response. Full factorial design means that the experiment involves K control factors studied at different groups (also called "levels") of observations, each with all their possible combinations.

One particular full factorial design is named 2^k, which means that all the K factors are studied at only two levels. The 2^k designs are particularly useful in the early stages of experimental work, when there are likely to be many factors to be investigated.

The main restriction of this approach is related to the number of levels available for each factor (only two levels) hence we must assume that the response is approximately linear over the range chosen for the factor levels. The statistical model for a 2^k design would include:

- K factors (each at two levels);
- $\binom{k}{2}$ Two-factors interactions;
- $\binom{k}{3}$ Three-factors interactions;
- ...
- One k-factors interaction.

The full factorial experimental design was employed in the majority of our experimental work. This was the preferred one in this programme since it gives the highest confidence. A full factorial was used for the following tests:

1. **The oil retention tests –** (chapter 4) - this set of experiments were based on three full factorial DOE (one for each coating type) with 4 factors:
    - Lubricant type (2 levels)
    - Lubricant initial amount (3 levels)
    - Measuring position (5 levels)
    - Material (a number of surface topography and mechanical properties)

2. **Friction experiments** – (chapter 5) **-** one 2^3 DOE repeated for each of the materials available. This full factorial experimental design included:
    - Sliding Velocity (2 levels)
    - Pressure (2 levels)
    - Lubricant type (2 levels)
    - Material (a number of surface topography and mechanical properties)

A4.6 Fractional factorial design

When it is not possible to run the entire set of the possible experiments because of reasons of time or cost, it is possible to reduce the number of runs whilst minimising the loss of information. This experimental approach is known as "Fractional Factorial" since only a "fraction" of the entire set of tests are performed.

The larger the fraction of the total number of experiments required, the higher is the resolution of the experimental design. When designing a fractional factorial design it is not possible to predict which test to do or to leave out since this is not a function of the mathematical models. This decision must be down to the intuition of the researcher and their previous experience in the field. Obviously, the accuracy of the final results will be dependent on the wisdom of the selection. Running a fraction of the experiment will thus only return a fraction of the possible information and it is

important to correctly "predict" what will be the information of interest. A good design should take account of some of the unexpected since to high "pruning" can obviously be dangerous!

The fractional factorial mathematical convention is to numerate the Design resolution by employing a roman numeral below the exponential of the design. For example, the resolution R can be expressed in the form: 2_R^{k-p} where k is the number of factors, p is the number of prunes and R is the obtained resolution. In this case "obtained resolution" means the following bearing in mind that "resolution I" and "resolution II" experimental designs are never employed.

Resolution III

- Main effects are aliased with two-factor interaction.
- Two-factor interaction may be aliased within each other.

Resolution IV

- Main effects are not aliased with any other effect (two or higher order interactions).
- Two-factor interactions are aliased with each other.

Resolution V

- Main effects are not aliased with any other effect (two or higher interactions).
- Two-factor interactions are aliased with higher interactions.

Usually, interactions 3 and above are preferred for pruning, i.e. aliasing them with each other. For convenience of testing, Resolution IV or V is recommended and during this work, no resolution lower than IV was used.

A fractional factorial experimental design was employed for all the drawability experiments described in Chapter 6. These were three 2_{IV}^{3-1} experimental designs, one for each coating.

A4.7 Regression analysis (correlation)

Regression analysis is a measure of the correlation between two or more sets of data. A simple linear regression assumes that the observed data follows a mathematical model such as:

$$y = \beta_0 + \beta_1 \cdot x + \varepsilon$$

If we have n pairs of data such as (x_1, y_1) (x_2, y_2) ... (x_n, y_n) we may estimate the regression model parameters β_0 and β_1 by minimising the least square function $L = \sum_{i=1}^{n} \varepsilon_i^2 = \sum_{i=1}^{n} (y_i - \beta_0 - \beta_1 \cdot x_i)^2$ on noise.

In order to state that a correlation exists, we can employ a standard Fisher test. Defining sum of square for residuals $SS_E = \sum_{i=1}^{n} e_i^2 = \sum_{i=1}^{n} (y_i - \hat{y}_i)^2$, the regression sum of square can be written as $SS_R = \sum_{i=1}^{n} (\hat{y}_i - \bar{y})^2$.

Thus, similarly to the ANOVA analysis, the corrected total sum of square $S_{YY} = \sum_{i=1}^{n} (y_i - \bar{y})^2$ can be partitioned as $SS_{YY} = SS_R + SS_E$.

We can then use the Fisher statistical distribution to test the hypothesis $\beta_1 \neq 0$ by comparing the statistic $F_0 = \dfrac{SS_R / 1}{SS_E / (n-2)} = \dfrac{MS_R}{MS_E}$ with a Fisher distribution with 1 and (n-2) degrees of freedom. Regression analysis was performed on all the experimental results.

A4.7.1 Model Adequacy Checking in Simple Linear Regression

Lack of fit test (LOF)

Regression models are often fitted to data when the true functional relationship is unknown. This test verifies whether the order of the model tentatively assumed is correct.

H_0: The model adequately fits the data

H_1: The model does not fit the data

This test involves partitioning of the error of residual sum of squares into the following two components:

$SS_E = SS_{PE} + SS_{LOF}$

PE = Pure Experimental error
LOF = Lack Of Fit to the model

The coefficient of determination (R^2)

It is defined Coefficient of Determination the quantity:

$$R^2 = \frac{SS_R}{SS_{YY}} \quad \text{Where } 0 \leq R^2 \leq 1$$

This quantity is often used to judge the degree of correlation, ie the adequacy of a regression model.

If the regressor x is a random variable, so that y and x may be viewed as jointly distributed random variables, then R is just the simple correlation between y and x. If x is not a random variable but a control factor, which is the most frequent situation, then the concept of R is undefined. A possible interpretation is that R^2 represent the percentage of variability in the data accounted for the model.

This quantity must be used very carefully since it is always possible to make R^2 unity by simply adding enough terms to the model: we can obtain R^2 very close to 1 simply fitting n data points with a polynomial model of n – 1 order.

Using regression analysis we must be really careful, since misuses are very frequent. For instance, regression relationships are valid only for values of the regressor variable within the range of the original data.

A4.8 Residual analysis

A residual analysis (sometimes called an "analysis of residuals") is an important aspect of any experiment. A normal probability plot of the residuals should always be performed. All the experiments performed in this thesis

were subject to a residual analysis and in no case was anything of significance found. Hence, residuals will not be discussed any further here.

Appendix 4

A5. Statistical analysis of the oil retention

A5.1 The effect of the coating on oil retention

The aim of this test was to assess whether:

- zinc coating type or
- any interaction between the zinc and oil (type and initial amount)

would change the final oil amount in the five positions of the sheet.

This experimental work was performed on a number of materials with similar surface topographies (all of them EBT textured with 2μm Ra) and different coating types. The list of control factors is presented below. The DOE was a full factorial.

Control Factor	Level 1	Level 2	Level 3	Level 4	Level 5
A – Coating type	CRS	ELO	GA	GI	
B – Oil type	Low Viscosity	High Viscosity			
C – Oil initial amount	0.7 g/m^2	1.5 g/m^2	2.5 g/m^2		
D – Position on the sheet	0	1	2	3	4

Table A5.1 - DOE table for oil retention initial investigation

The output from the test (the response) was the final oil amount (g/m^2) in each of the five positions. The ANOVA table for these tests is shown in table 5.2 below. In Appendix 4, mention was made about "P" values of less than 0.01 being significant. Note that when a "P" value in this table is less than 0.01, the row is highlighted.

Source	df	Seq SS	Adj SS	Adj MS	F	P
A	3	10.777	9.7798	3.2599	9.81	0.000
B	1	0.7363	0.4041	0.4041	1.22	0.271
C	2	183.32	128.16	64.082	192.8	0.000
D	4	173.70	135.54	33.886	101.9	0.000
A*B	3	3.0040	2.7920	0.9307	2.80	0.040
A*C	6	10.408	5.5676	0.9163	2.75	0.013
A*D	12	9.6013	8.4868	0.7072	2.13	0.015
B*C	2	0.4761	0.3349	0.1674	0.50	0.605
B*D	4	1.1183	1.4211	0.3553	1.07	0.372
C*D	8	69.5325	61.701	7.7127	23.2	0.000
A*B*C	6	1.7975	1.5206	0.2534	0.76	0.600
A*B*D	12	3.5740	3.5740	0.2978	0.90	0.551
A*C*D	24	6.0663	6.4156	0.2673	0.80	0.731
B*C*D	8	2.3931	2.5649	0.3206	0.96	0.463
A*B*C*D	24	7.0143	7.0143	0.2923	0.88	0.630
Error	300	99.674	99.674	0.3322		
Total	419	583.20				

Table A5.2 - ANOVA table for oil retention initial investigation

With reference to the three highlighted rows, rows A, C and D, the ANOVA table shows that zinc coating type (factor "A") influences the average final oil amount. This can be interpreted as an ability of the coating to "hide some of the oil" after applying pressure. In the same way, the initial oil amount (factor "C") changes the final average amount and the oil amount in different positions (factor "D") is different from the average.

Since the former is nothing unexpected (the more oil at the beginning, the more oil in the end) no further exploration will be performed. On the other hand, the factor D effect is interesting in terms of "shape" of the final distribution. Further, at different initial oil amounts, the distribution of oil changes shape (interaction "C*D"). This final aspect of oil distribution will be the object of visual investigation.

The above has outlined the main three factors and these will now be investigated in more detail.

A5.1.1 Main plot for zinc coating effect ("A")

In order to understand which zinc coating type leads to a higher (or lower) final oil amount, a plot of the final (average over the five positions) oil amount was drawn (see Figure A5.1). The confidence intervals (CI) around the single point of the plot was calculated employing Bonferroni (95% confidence).

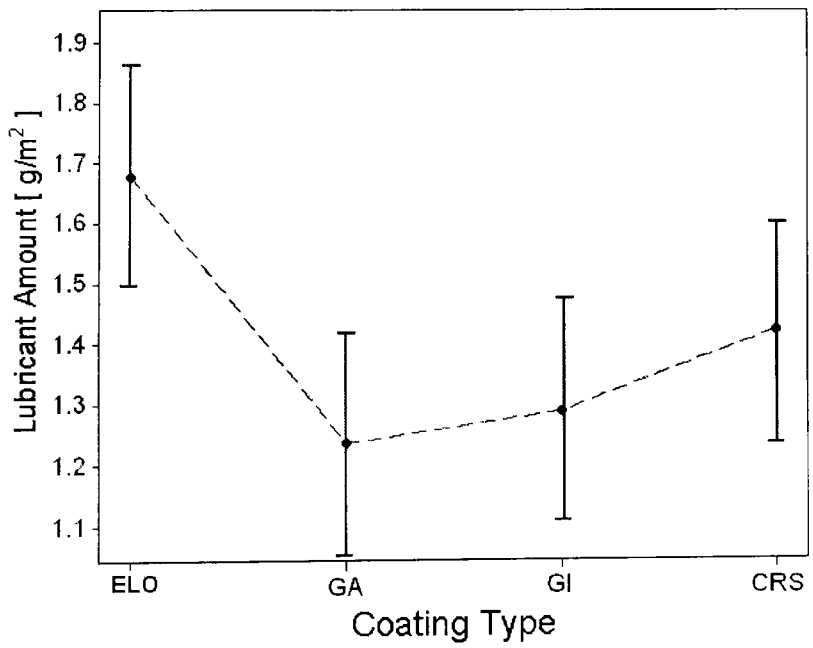

Figure A5.1 – Initial investigation – zinc coating effect upon final lubricant amount

Since the confidence intervals of GI, GA and ELO do not overlap, we can conclude that the **statistical evidence shows that the** GI and GA coatings shows less average oil amount than ELO. It also shows that there is no evidence that CRS show less retention than ELO.

A5.1.2 Description of the oil distribution ("D" and "C*D")

In order to understand how the oil re-distributes over the sheet, a plot of the final oil amount (the average for all the materials and the entire initial oil amount) on the different measuring positions is shown in Figure A5.2.

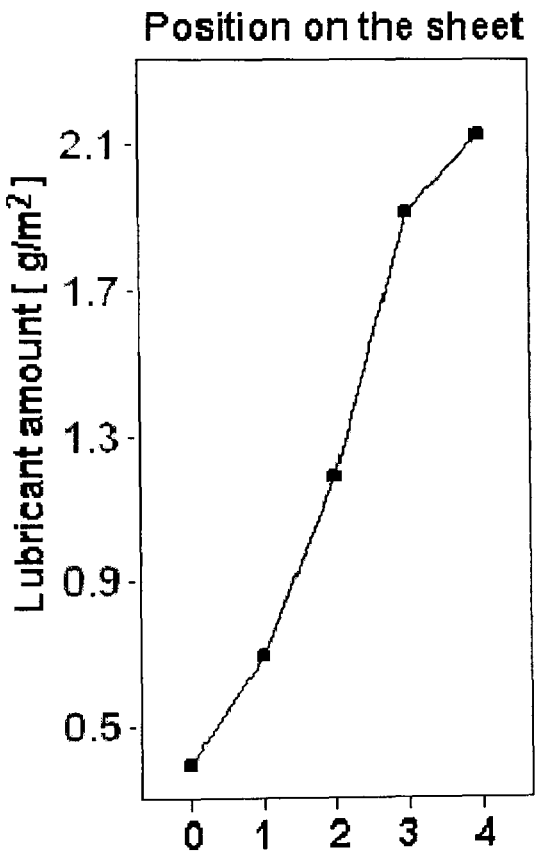

Figure A5.2 –Initial investigation– measuring position effect upon final lubricant amount

The shape can be investigated further by examining the different behaviors at different initial oil amounts (interaction "C*D"). This plot is presented in Figure A5.3.

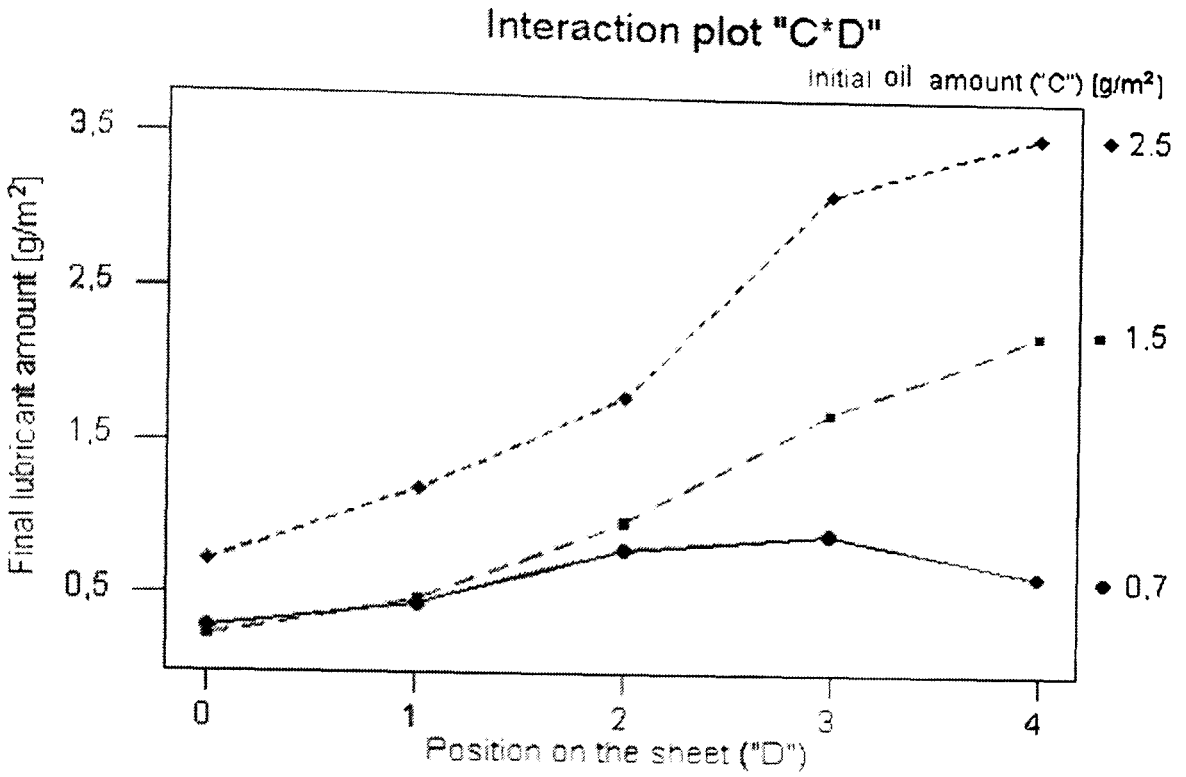

Figure A5.3 –Initial investigation– interaction plot for initial oil amount and position on the sheet

Reading the plot, one can see that with 0.7 g/m^2 initial oil amount the distribution reaches the maximum value at position 3 whilst for higher initial oil amounts, the plot shows the maximum is at position 4.

For all the different initial amounts, the final oil distribution is roughly an "S-shape".

A5.2 Main investigation on surface topography effects

The aim of this experimental work was to assess whether the surface topography (roughness) changes the distribution of oil on the sheet.

A5.2.1 GI zinc coated steel sheets

This statistical analysis was performed on the full range of the GI zinc coated materials. These materials exhibit different roughness. The surface parameter chosen to represent the roughness is Sq (described in Appendix 1).

Control Factor	Level 1	Level 2	Level 3	Level 4	Level 5
A – Surface roughness (Sq)	0.87 µm (H2)	1.38 µm (H1)	1.72 µm (S2)	2.42 µm (S3)	
B – Oil type	Low Viscosity	High Viscosity			
C – Oil initial amount	0.7 g/m^2	1.5 g/m^2	2.5 g/m^2		
D – Position on the sheet	0	1	2	3	4

Table A5.3 - DOE table for oil retention GI coated materials

The output from the test (the response) was the final oil amount (g/m^2) in each of the five positions. The ANOVA table for these tests is shown in table A5.4 below. In Appendix 4, mention was made about "P" values of less than 0.01 being significant. Note that when a "P" value in this table is less than 0.01, the row is highlighted.

Source	df	Seq SS	Adj SS	Adj MS	F	P
A	3	0.4034	1.1614	0.3871	1.02	0.384
B	1	0.1564	0.0191	0.0191	0.05	0.823
C	2	159.35	104.22	52.113	137.1	0.000
D	4	248.83	194.27	48.569	127.8	0.000
A*B	3	2.3141	1.6346	0.5449	1.43	0.232
A*C	6	3.6814	2.2411	0.3735	0.98	0.436
A*D	12	8.2203	5.9600	0.4967	1.31	0.212
B*C	2	5.1064	2.7475	1.3738	3.61	0.028
B*D	4	1.5889	1.7039	0.4260	1.12	0.346
C*D	8	88.0686	76.208	9.5260	25.07	0.000
A*B*C	6	1.8038	1.2075	0.2012	0.53	0.786
A*B*D	12	3.5502	3.5502	0.2958	0.78	0.673
A*C*D	24	10.8851	10.604	0.4419	1.16	0.273
B*C*D	8	1.3003	1.0679	0.1335	0.35	0.945
A*B*C*D	24	8.9672	8.9672	0.3736	0.98	0.487
Error	384	145.89	145.89	0.3799		
Total	503	690.13				

Table A5.4 - ANOVA table for oil retention GI coated materials

This ANOVA table shows the significant factors to be C and D and their interaction (C*D) and these rows are highlighted. Of significance is that row A shows that there is no surface topography effect. However, row D shows that there is a positional effect. When one investigates this further, it is reasonably to divide the sheet area into two regions (named respectively "low" and "high" pressure regions – see Figure 4.11). These two regions exhibit very different migration process as shown by the following analysis where a relationship between topography and migration was observed for both regions.

A5.2.1.1 Low pressure – GI coated materials

A regression analysis was performed between surface topography and the migration index at low pressures. The best performing surface parameter for GI coated materials at low pressure was found to be Sq.

This correlation analysis was performed on the results of the following materials:

- H1 – Sq 1.38 μm
- H2 – Sq 0.89 μm
- S5 – Sq 1.72 μm
- S6 – Sq 2.42 μm

The ANOVA table below shows the regression to be statistically significant and therefore it is highlighted (P value less than 5% as shown in section A4.2.3).

Analysis of Variance

Source	DF	SS	MS	F	P
Regression	1	3.8609	3.8609	27.81	0.000
Residual Error	18	2.4987	0.1388		
Total	19	6.3597			

Regression equation found:

$$MI_L = 0.652 - 0.939 \cdot Sq$$

Predictor	Coef	StDev	T	P
Constant	0.6520	0.3083	2.12	0.049
Sq	-0.9392	0.1781	-5.27	0.000

S = 0.3726 R-Sq = 60.7% R-Sq(adj) = 58.5%

Table A5.5 – regression analysis for GI coated materials at low pressure

The Lack of fit test (also described in Appendix 4) proved that this correlation fits well only within the tested Sq range (0.89–2.42μm). The correlation plot is presented in Figure A5.4.

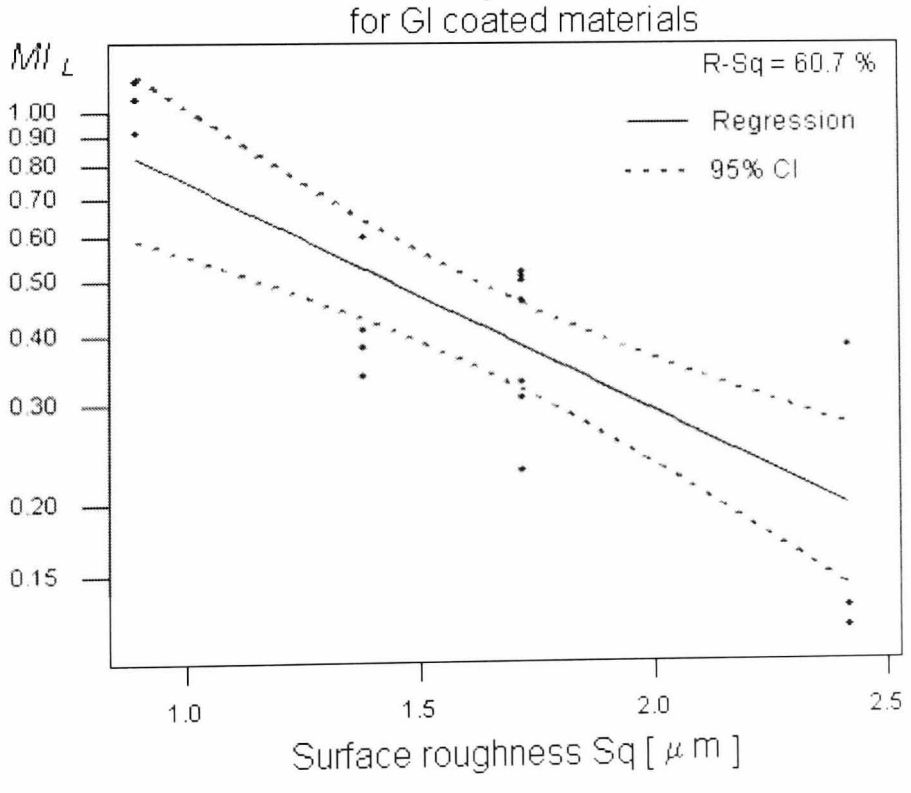

Figure A5.4 – GI coated materials – correlation analysis at low pressure

A5.2.1.2 High pressure – GI coated materials

The regression analysis was performed between a surface topography parameter and the migration index at high pressure. The best performing surface parameter for GI coated materials at high pressure was found being Sva(0). This correlation analysis was performed on the results of the following materials:

- H1 – Sva(0) 0.28 mm^2
- H2 – Sva(0) 0.34 mm^2
- S5 – Sva(0) 1.13 mm^2
- S6 – Sva(0) 0.03 mm^2

Once more, in the ANOVA table below the statistically important factors are highlighted (P value less than 5% as shown in section A4.2.3).

Analysis of Variance

Source	DF	SS	MS	F	P
Regression	1	0.20184	0.20184	7.53	0.021
Residual Error	10	0.26806	0.02681		
Total	11	0.46989			

Regression equation found:

$$MI_H = 0.0807 + 0.336 \cdot Sva(0)$$

Predictor	Coef	StDev	T	P
Constant	0.08071	0.06046	1.33	0.211
Sva0	0.3357	0.1223	2.74	0.021

S = 0.1637 R-Sq = 43.0% R-Sq(adj) = 37.2%

Table A5.6 – regression analysis for GI coated materials at high pressure

The Lack of fit test proved that this correlation fits well and it is a good candidate to describe the phenomenon also outside the tested Sva(0) range (0.03–1.13mm^2). The correlation plot is presented in Figure A5.5.

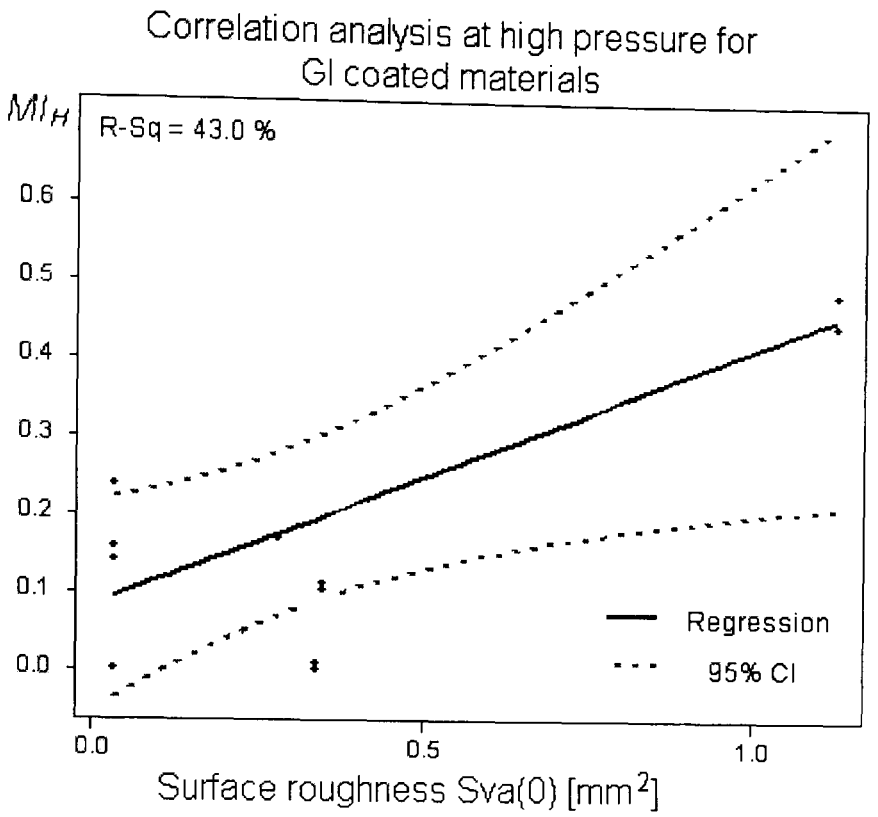

Figure A5.5 – GI coated materials – correlation analysis at high pressure

A5.2.2 GA zinc coated steel sheets

This statistical analysis was performed on the full range of the GA zinc coated materials. These materials exhibit different roughness. The surface parameter chosen to represent the roughness is Sq (described in Appendix 1). The list of control factors is presented in Table A5.7.

Control Factor	Level 1	Level 2	Level 3	Level 4	Level 5
A – Surface roughness	1.10 µm (H14)	1.82 µm (S8)	2.23 µm (S9)		
B – Oil type	Low Viscosity	High Viscosity			
C – Oil initial amount	0.7 g/m^2	1.5 g/m^2	2.5 g/m^2		
D – Position on the sheet	0	1	2	3	4

Table A5.7 - DOE table for oil retention GA coated materials

The response was the final oil amount (g/m^2) in any of the five positions. For convenience, in the ANOVA table below all the statistically important factors are highlighted (P value less than 1%).

Source	DF	Seq SS	Adj SS	Adj MS	F	P
A	2	4.1812	3.5129	1.7564	6.83	0.001
B	1	2.8014	1.6716	1.6716	6.50	0.012
C	2	141.15	105.57	52.786	205	0.000
D	4	54.984	54.984	13.746	53.4	0.000
A*B	2	4.2544	5.0016	2.5008	9.73	0.000
A*C	4	6.4846	6.5116	1.6279	6.33	0.000
A*D	8	0.7603	0.7603	0.0950	0.37	0.935
B*C	2	0.7495	0.7218	0.3609	1.40	0.249
B*D	4	1.2989	1.2989	0.3247	1.26	0.287
C*D	8	37.737	37.737	4.7171	18.3	0.000
A*B*C	4	13.470	13.077	3.2693	12.7	0.000
A*B*D	8	3.0916	3.0916	0.3865	1.50	0.160
A*C*D	16	3.8940	3.8940	0.2434	0.95	0.517
B*C*D	8	2.4518	2.4518	0.3065	1.19	0.307
A*B*C*D	16	3.7211	3.7211	0.2326	0.90	0.565
Error	162	41.633	41.633	0.2570		
Total	251	322.66				

Table A5.8 - ANOVA table for oil retention GA coated materials

The ANOVA table shows the important factors to be A, C and D and the interactions A*B, A*C, C*D and A*B*C. In this case, there is statistical evidence to show that the steel sheet roughness (factor "A") influences the average final oil amount. This can be interpreted as an ability of the coating to "hide some of the oil" after applying pressure. Also, the initial amount changes the final average amount (factor "C") and the oil amount in different positions is different from average (factor "D"). Also the interaction between these two factors appears important ("C*D"). Since this effect is similar to the initial tests, no further investigation is required for these two factors and their interaction.

On the other hand, the surface roughness appears to interact both with the oil type ("A*B") and the initial oil amount ("A*C"). Finally, the third order interactions with surface roughness ("A*B*C") was found difficult to interpret. The surface topography effects will now be examined in more detail for factor A and the interactions A*B and A*C.

A5.2.2.1 The effect of surface roughness ("A")

In order to understand which roughness leads to a higher (or lower) final oil amount for the coating GA, a plot of the final (average over the five positions) oil amount was drawn, see Table A5.9 The confidence intervals (CI) around the single point of the plot was calculated employing the Bonferroni method (95% confidence).

Topography Effects:

Bonferroni 95.0% Simultaneous Confidence Intervals

H14 reference value:

```
 Lower Centre Upper-+---------+---------+---------+-----
S8 -0.082 0.1175 0.317    (-------*-------)
S9 -0.386 -0.1860 0.014 (-------*-------)
   -+---------+---------+---------+-----
   -0.50 -0.25 0.00 0.25
```

S8 reference value:

```
 Lower Centre Upper-+---------+---------+---------+-----
S9 -0.503 -0.3035 -0.103 (-------*-------)
   -+---------+---------+---------+-----
   -0.50 -0.25 0.00 0.25
```

Table A5.9 – Confidence interval for factor A – GA coated ANOVA

There is statistical evidence to state that S9 material (Sq 1.82μm) shows more average oil amount than S8 (Sq 1.82μm). The surface topography parameter Sq does not control this behavior. If it would control it then the retention values could be ranked coherently to the Sq values.

A5.2.2.2 Description of the oil distribution ("A*B" and "A*C")

In order to visualize how the different oil types behave on different surface topographies ("A*B"), a plot of the final oil amount (average for all the materials and all the initial oil amount) is presented in Figure A5.6.

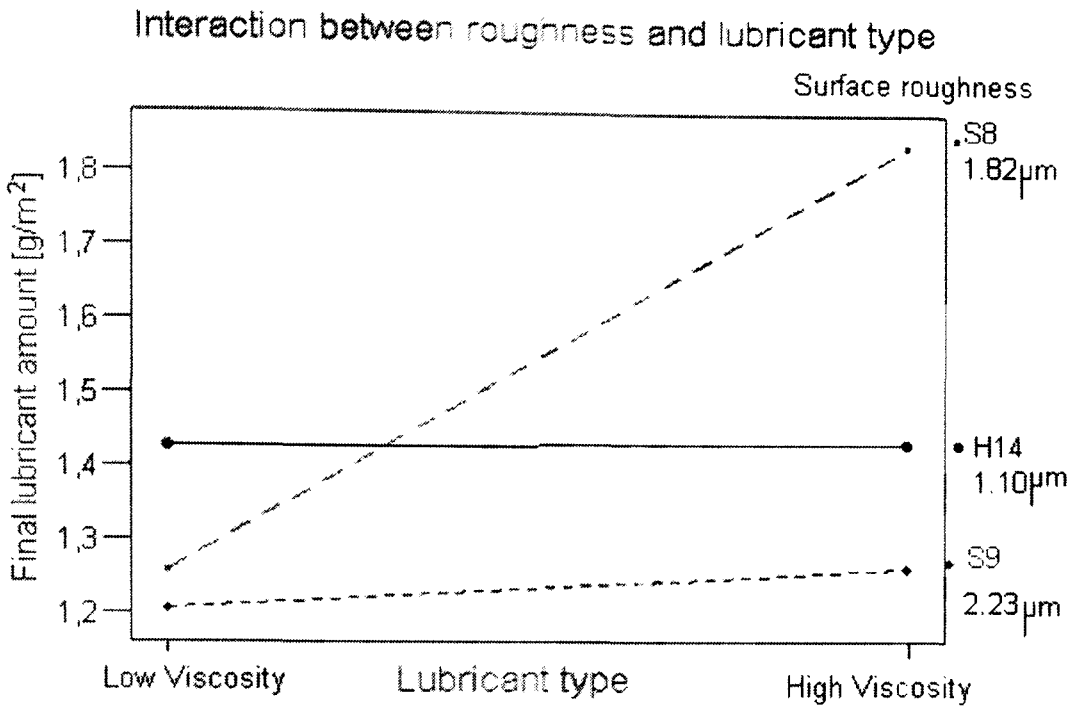

Figure A5.6 – GA coated materials – interaction plot for oil type and surface roughness

Looking at the interaction plot above, the material named "S8" (Sq roughness 1.82µm) shows that more oil is retained with the high viscosity oil.

The other interaction plot ("A*C") could not be interpreted statistically and shows that the surface parameter Sq is inadequate to describe oil behaviour over a GA coated steel sheet.

The search for the best surface parameter able to describe oil behaviour will be performed with the correlation analysis below.

A5.2.2.3 Correlation with surface topography

The oil distribution was sectioned into two areas:

- Low pressure – represented by points 3 and 4 on the sheet
- High pressure – represented by points 0 and 1 on the sheet

The oil migration indexes (MI) for the two different areas were therefore defined as follow:

- Low pressure – MI_L
- High pressure – MI_H

as described in chapter 4.

A5.2.2.4 Low pressure – GA coated materials

The regression analysis (methodology described in appendix 4) was performed between a surface topography parameter and the migration index at low pressure. The best performing surface parameter for GA coated materials at low pressure was found being Sva (0).

This correlation analysis was performed on the results of the following materials:

- S8 – Sva(0) 2.98 mm^2
- S9 – Sva(0) 1.19 mm^2
- H14 – Sva(0) 0.31 mm^2

Once more, in the ANOVA table below the statistically important factors are highlighted (P value less than 5% as shown in section A4.2.3)

Analysis of Variance

Source	DF	SS	MS	F	P
Regression	1	3.3623	3.3623	54.84	0.000
Residual Error	10	0.6131	0.0613		
Total	11	3.9755			

Regression equation found:

$$MI_L = -1.95 + 0.0476 \cdot Sva(0)$$

Predictor	Coef	StDev	T	P
Constant	-1.9535	0.1198	-16.30	0.000
Sva0	0.047562	0.006423	7.41	0.000

S = 0.2476 R-Sq = 84.6% R-Sq(adj) = 83.0%

Table A5.10 – regression analysis for GA coated materials at low pressure

The lack of fit test proved that this correlation fits well and it is a good candidate to describe the phenomenon also outside the tested Sva(0) range (0.31–2.98mm^2). The correlation plot is presented in Figure A5.7.

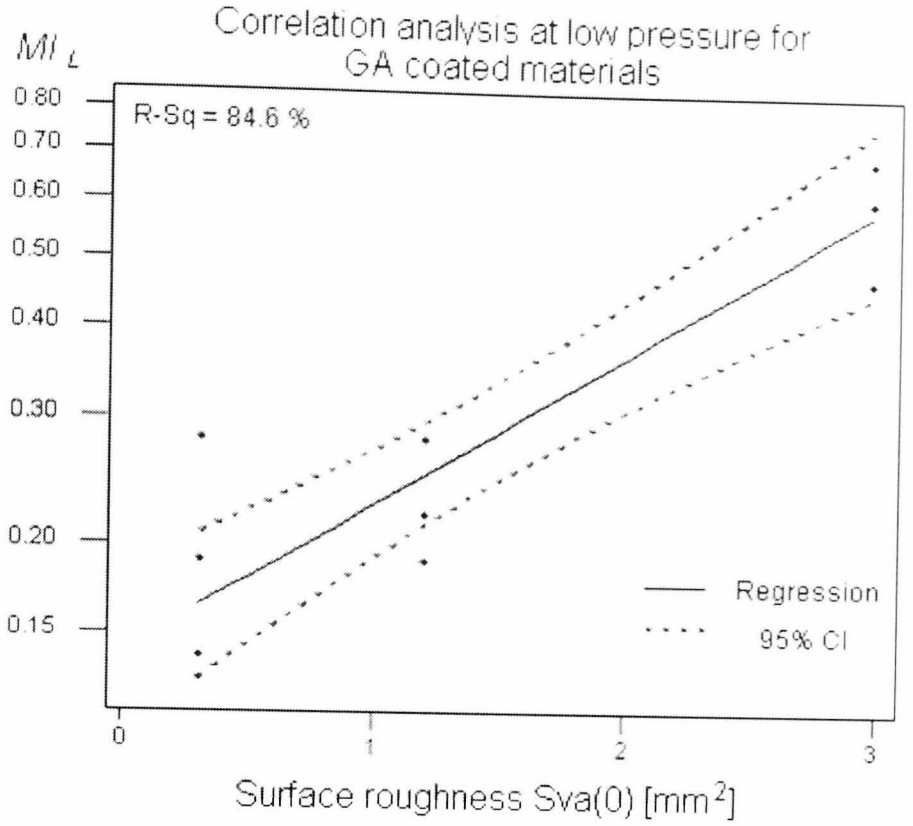

Figure A5.7 – GA coated materials – correlation analysis at low pressure

A5.2.2.5 High pressure – GA coated materials

The regression analysis was performed between a surface topography parameter and the migration index at high pressure. The best performing surface parameter for GA coated materials at high pressure was found to be Sva (0). This correlation analysis was performed on the results of the following materials:

- S8 – Sva(0) 2.98 mm^2
- S9 – Sva(0) 1.19 mm^2
- H14 – Sva(0) 0.31 mm^2

In the ANOVA table below the statistically important factors are highlighted (P value less than 5% as shown in section A4.2.3).

Source	DF	SS	MS	F	P
Regression	1	0.49525	0.49525	417.02	0.000
Residual Error	4	0.00475	0.00119		
Total	5	0.50000			

Regression equation found:

$MI_H = 0.0834 + 0.258\ Sva(0)$

Predictor	Coef	StDev	T	P
Constant	0.08335	0.02359	3.53	0.024
Sva0	0.25815	0.01264	20.42	0.000

S = 0.03446 R-Sq = 99.0% R-Sq(adj) = 98.8%

Table A5.11 – regression analysis for GA coated materials at high pressure

The Lack of fit test proved that this correlation fits well and it is a good candidate to describe the phenomenon also outside the tested Sva(0) range (0.31–2.98mm^2). The correlation plot is presented in Figure A5.8.

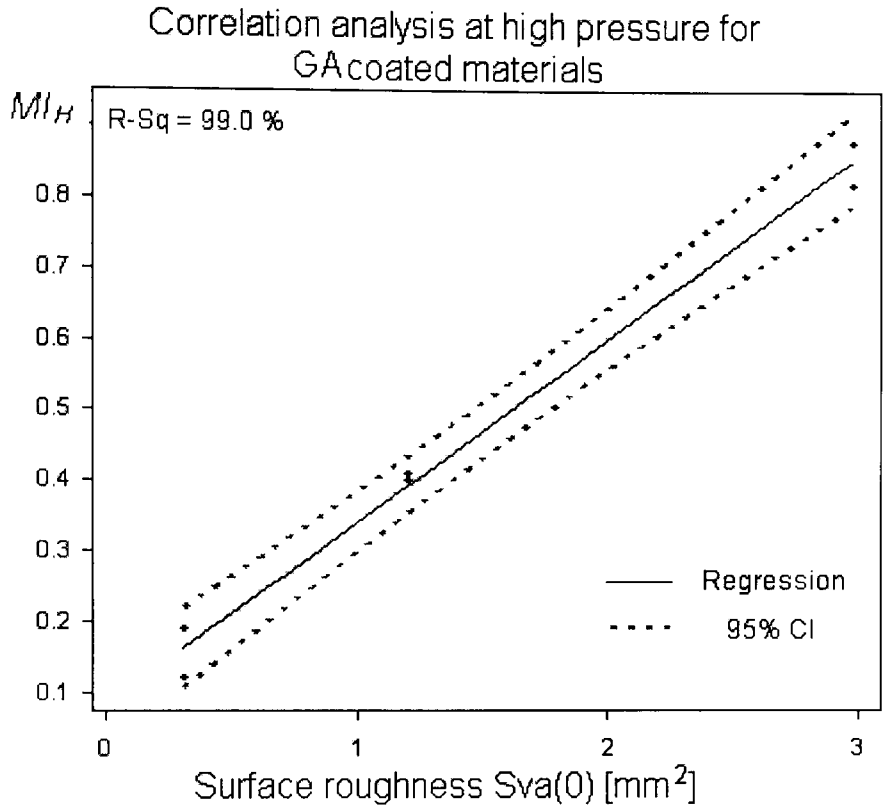

Figure A5.8 – GA coated materials – correlation analysis at high pressure

A6. Details of the friction experimental procedure

1) **Lubricants** employed:
   a. Thinner - Aral Ropa VOV6 (12.2mPa kinematic viscosity)
   b. Thicker – Fuchs 4107s (99.3mPa kinematic viscosity)
2) **Sheet steel lubrication**:
   1 ± 0.5 g/m^2 sprayed
3) **Repetitions**:
   Every experiment was repeated at least 4 times (plus one "dummy" test employed to warm up the device).
4) **Stribeck curve characterisation**:
   The Stribeck curve was measured through 8 points of the Hersey parameter H, by employing the following scheme:

Setting	Lubricant Viscosity [Pa]	Velocity [m/s]	Pressure [Pa]	H [m/s]	Log H
1	12.2E-3	2E-3	10E6	2.44E-12	-11.61
2	99.3E-3	2E-3	10E6	1.99E-11	-10.70
3	12.2E-3	2E-3	1E6	2.44E-11	-10.61
4	99.3E-3	2E-3	1E6	1.99E-10	-9.702
5	12.2E-3	200E-3	10E6	2.44E-10	-9.612
6	99.3E-3	200 E-3	10E6	1.99E-09	-8.702
7	12.2E-3	200 E-3	1E6	2.44E-09	-8.612
8	99.3E-3	200 E-3	1E6	1.99E-08	-7.702

Table A6.1 - Settings for Stribeck measurement

The 8 named Hersey values cover all of the boundary and mixed lubrication regimes and some part of the hydrodynamic lubrication regime [Holtkamp 1999(b)].

5) **Experimental order**:
   All the materials were tested following a random order. Within the same material a special order was employed to minimise experimental costs and influences between control factors. The order was the following:
   a. Run all the experiments with the thinner oil, then the thicker
   b. Within the same oil, start with the lower Hersey value to the higher
   c. Run first the "dummy" experiment then the 4 friction measurement

6) **The tool material**:

it was decided to manufacture the tool with a common 12% Cr tool steel. This tool material is widely used for small and complex deep drawing dies or inserts in larger cast iron dies. This steel exhibited an hardness of about 58-62HRC.

7) **The tool roughness**:

Circa Ra =0.05 μm. This was achieved by hand polishing the tool with fine abrasive paper. Abrasion was performed following the same direction of motion during the test.

8) **Temperature**:

Room temperature, i.e. circa 20°C. It is important to keep the temperature at this level, since the viscosity of the two lubricants differs by exactly a factor ten at this temperature. This is only true for 20°C (viscosity -temperature relation is different for the two oils oil). An automatic heating/cooling system ensured the temperature remained within + and – 5°C.

9) **Sample preparation**:

a. Specimen edges were grounded with a file or grinding paper in order to remove eventual burrs created while cutting of the strips.
b. Specimen were cleaned in an ultra sonic bath with petroleum ether for 3 minutes, then rinsed with acetone or spirit and immediately dried with air.
c. Spray lubrication and weight sample
d. Immediately run the test (no storage for more than 4 hours or the specimen might attract dust or the lubricant evaporate)

10) **Between tests**:

a. The tool surface was cleaned with a cloth drenched in acetone or another solvent, after each specimen test to avoid extra-lubrication.
b. The tool surface was polished with a very fine abrasive paper (similarly to point 7) to remove any zinc built-up and smoothing tool's roughness

11)**The measured data**:

a. Average coefficient of friction (calculated excluding the first and the last 20mm of tool movement).
b. Measured velocity (when possible)
c. Measured pressure (when measured)
d. Date and time of the experiment
e. Temperature of the laboratory (when measured).

A7. Experimental results - the Stribeck graphs

The work on friction described in chapter 5 was based on the results from the analysis of friction with respect to velocity, pressure and lubricant type/viscosity. The results from all the test combinations are given here in the form of Stribeck curves. Each includes the following information, which provides the test details:

- **Title**: includes the "name" of the material (i.e. "B1" - full list of materials available in Chapter 5 section 5.3.1) followed by the lubricant employed (i.e. "Aral" for Aral Ropa VOV6 – the low viscosity one). Note that two different graphs for the two oils were plotted in line with the explanation given in Chapter 5 section 5.5.1
- **Y-axis**: represents the friction coefficient (**μ**). This value is dimensionless hence units are displayed
- **X-axis**: in the typical Stribeck curve the x-axis is the Hersey parameter in logarithmic scale. Instead of the Hersey value, in these plots it was decided to use the treatment combination number, also "Setting". Every setting value correspond to a specific Hersey value, as explained by Table A6.1 in Appendix 6 and reported below for convenience.

Setting	Lubricant Viscosity [Pa]	Velocity [m/s]	Pressure [Pa]	H [m/s]	**Log H**
1	12.2E-3	2E-3	10E6	2.44E-12	**-11.61**
2	99.3E-3	2E-3	10E6	1.99E-11	**-10.70**
3	12.2E-3	2E-3	1E6	2.44E-11	**-10.61**
4	99.3E-3	2E-3	1E6	1.99E-10	**-9.702**
5	12.2E-3	200E-3	10E6	2.44E-10	**-9.612**
6	99.3E-3	200 E-3	10E6	1.99E-09	**-8.702**
7	12.2E-3	200 E-3	1E6	2.44E-09	**-8.612**
8	99.3E-3	200 E-3	1E6	1.99E-08	**-7.702**

Table A7.1 - Settings for Stribeck curves

The following plots are also presented in 3 different sections, one for each zinc coating available. Finally, the Pretex (material named P2) Stribeck curve is also presented. Note that, due to a fire at the Salzgitter manufacturing plant,

the experiments on P2 were performed several months later than all the other experiments and on a differently arranged test set-up. This is unfortunate and means that we are not confident that we are comparing like with like and hence, these comparisons are not included in this analysis.

Appendix 7

A7.1 ELO zinc coated materials

All these Stribeck curves can be clearly associated with the "Rich lubrication" behaviour presented in Chapter 5 section 5.5.1 with the exception of B3 lubricated with the high viscosity oil (Fuchs 4107S).

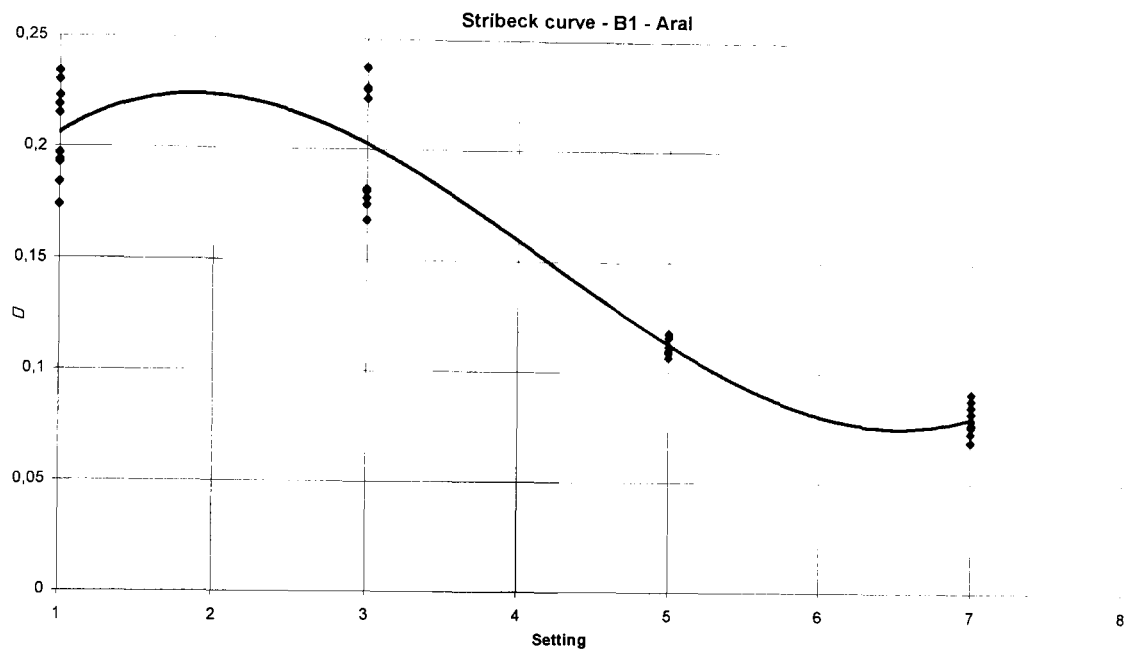

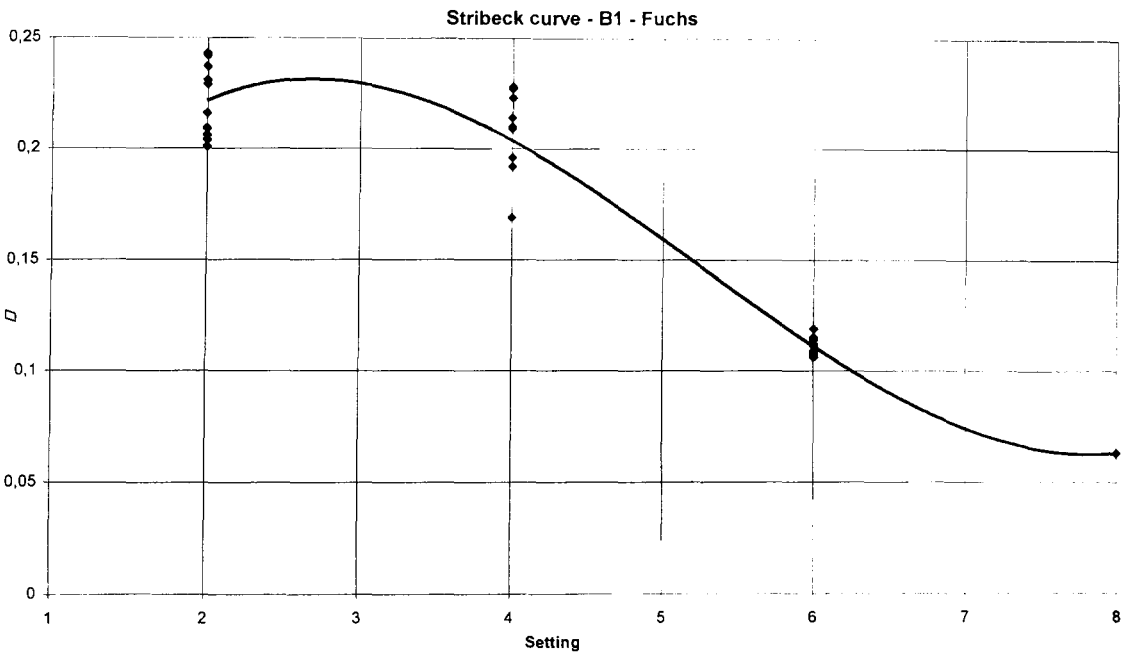

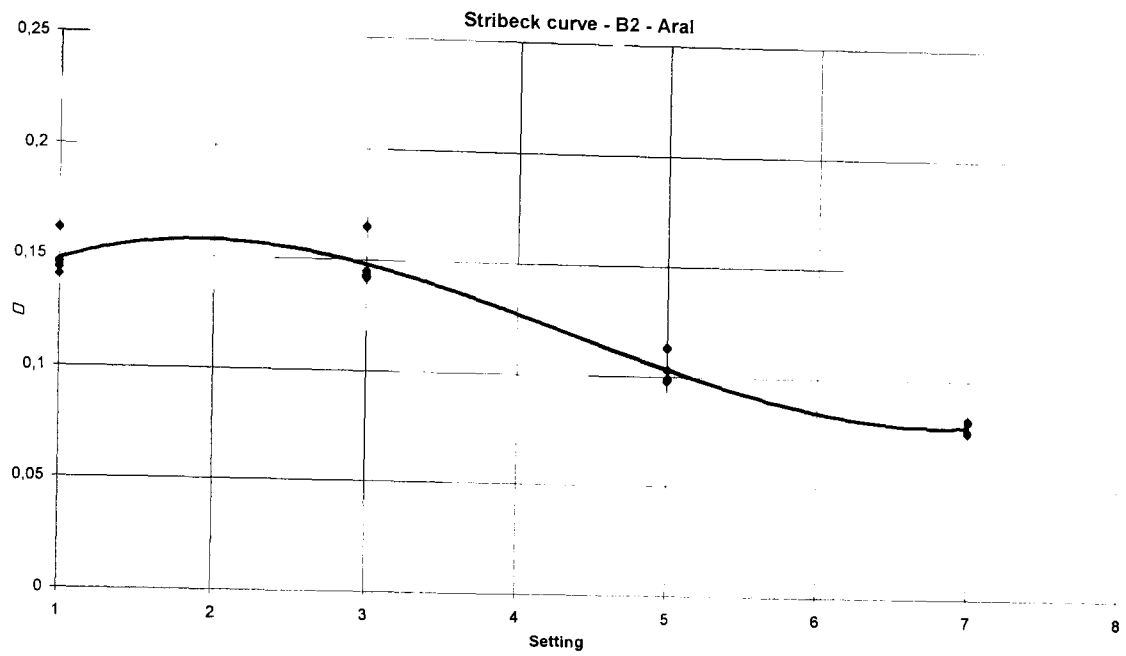
Stribeck curve - B2 - Aral
0,25
0,2
0,15
0,1
0,05
0
D
1
2
3
4
5
6
7
8
Setting

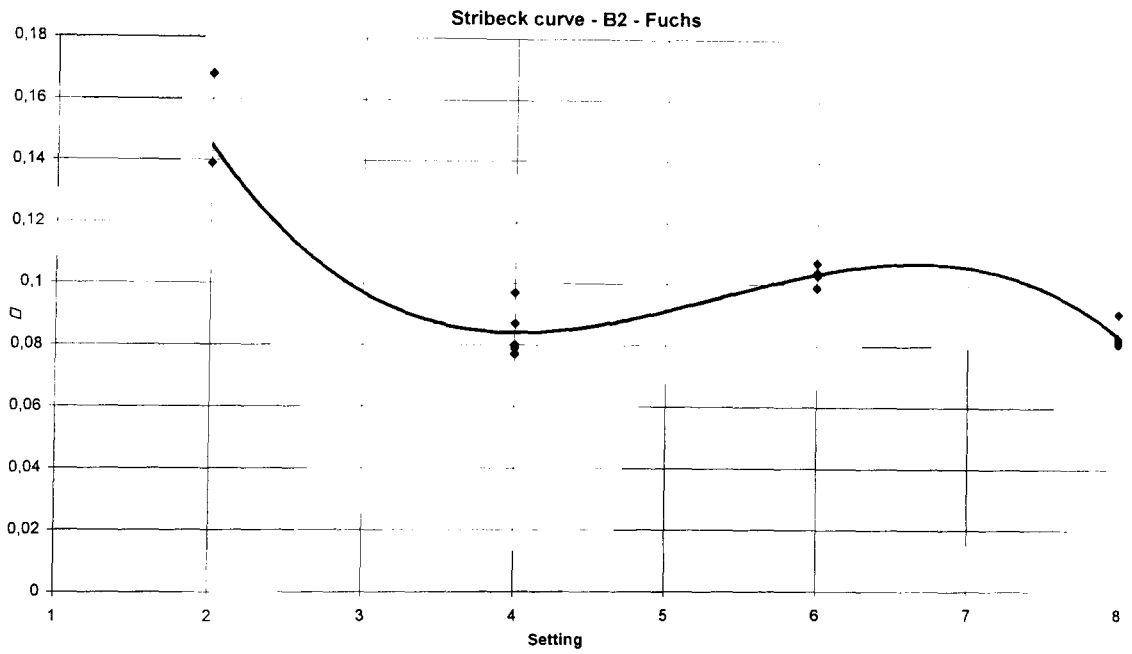
Stribeck curve - B2 - Fuchs
0,18
0,16
0,14
0,12
0,1
0,08
0,06
0,04
0,02
0
D
1
2
3
4
5
6
7
8
Setting

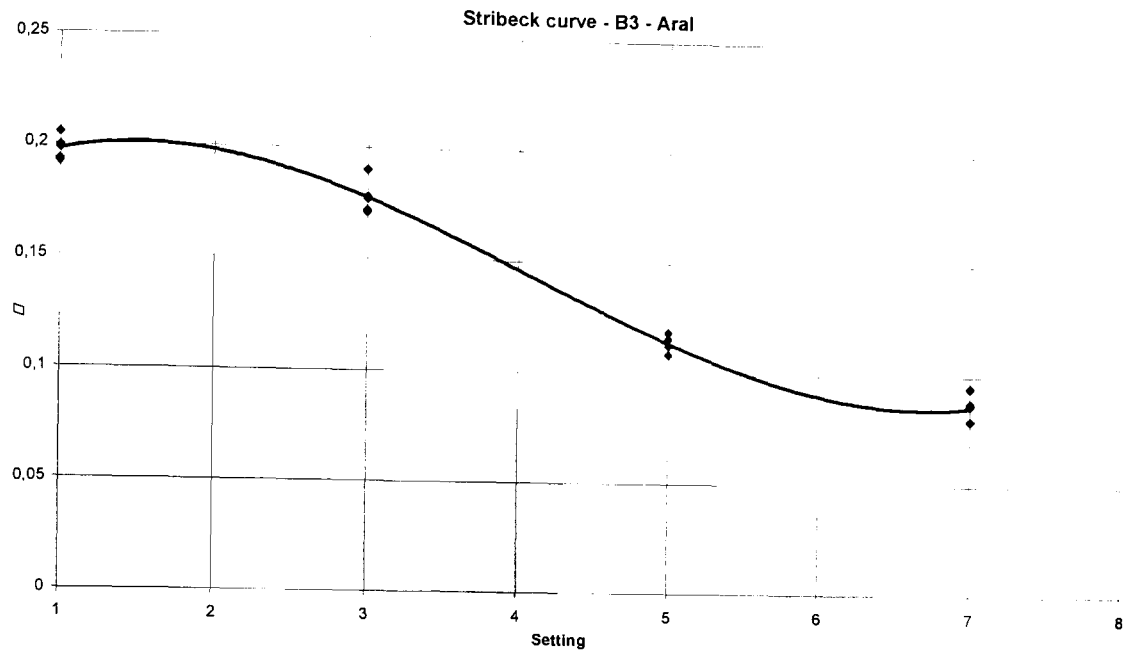
Stribeck curve - B3 - Aral
0,25
0,2
0,15
0,1
0,05
0
1
2
3
4
5
6
7
8
Setting

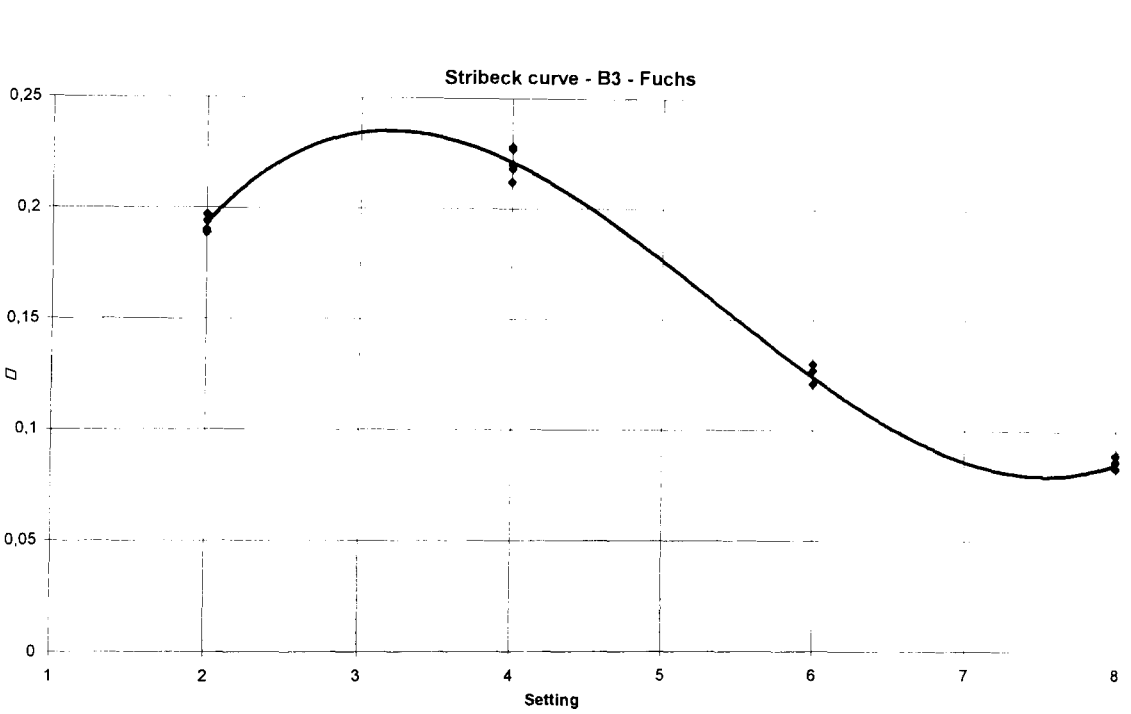
Stribeck curve - B3 - Fuchs
0,25
0,2
0,15
0,1
0,05
0
1
2
3
4
5
6
7
8
Setting

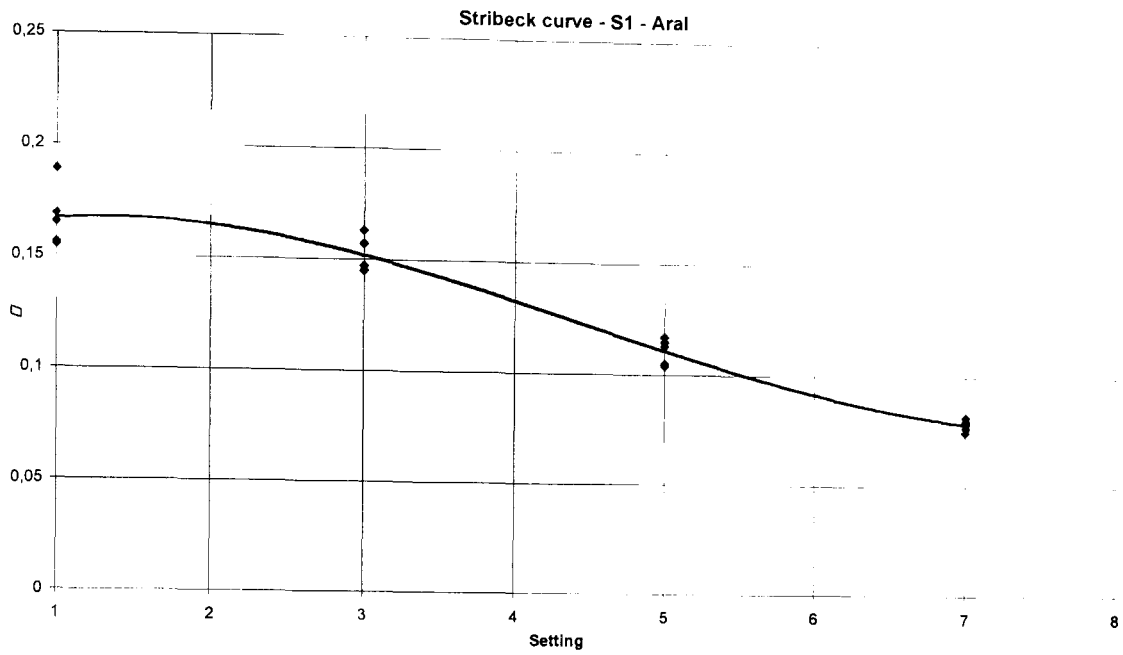
Stribeck curve - S1 - Aral
0,25
0,2
0,15
0,1
0,05
0
D
1
2
3
4
5
6
7
8
Setting

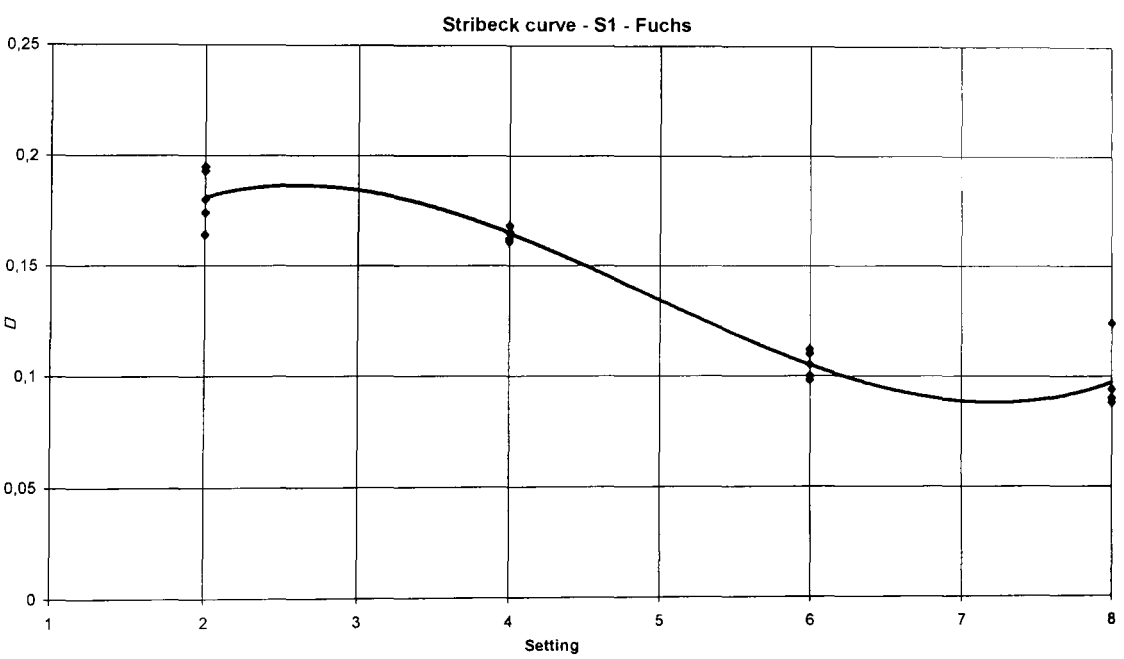
Stribeck curve - S1 - Fuchs
0,25
0,2
0,15
0,1
0,05
0
D
1
2
3
4
5
6
7
8
Setting

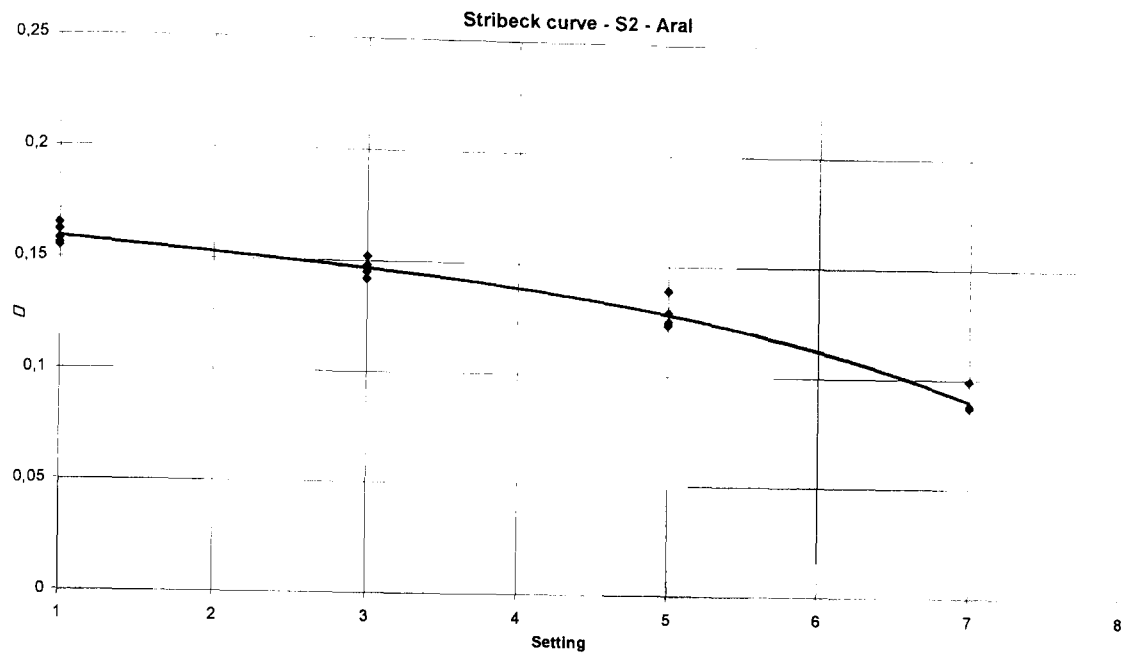
Stribeck curve - S2 - Aral
0,25
0,2
0,15
0,1
0,05
0
D
1
2
3
4
5
6
7
8
Setting

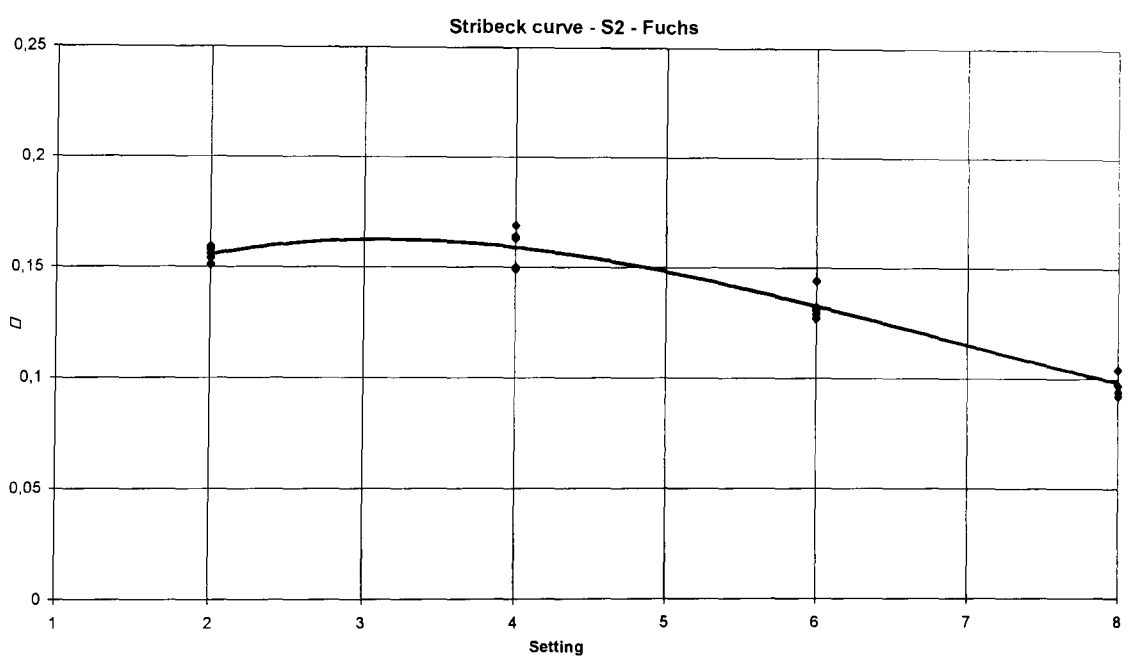
Stribeck curve - S2 - Fuchs
0,25
0,2
0,15
0,1
0,05
0
D
1
2
3
4
5
6
7
8
Setting

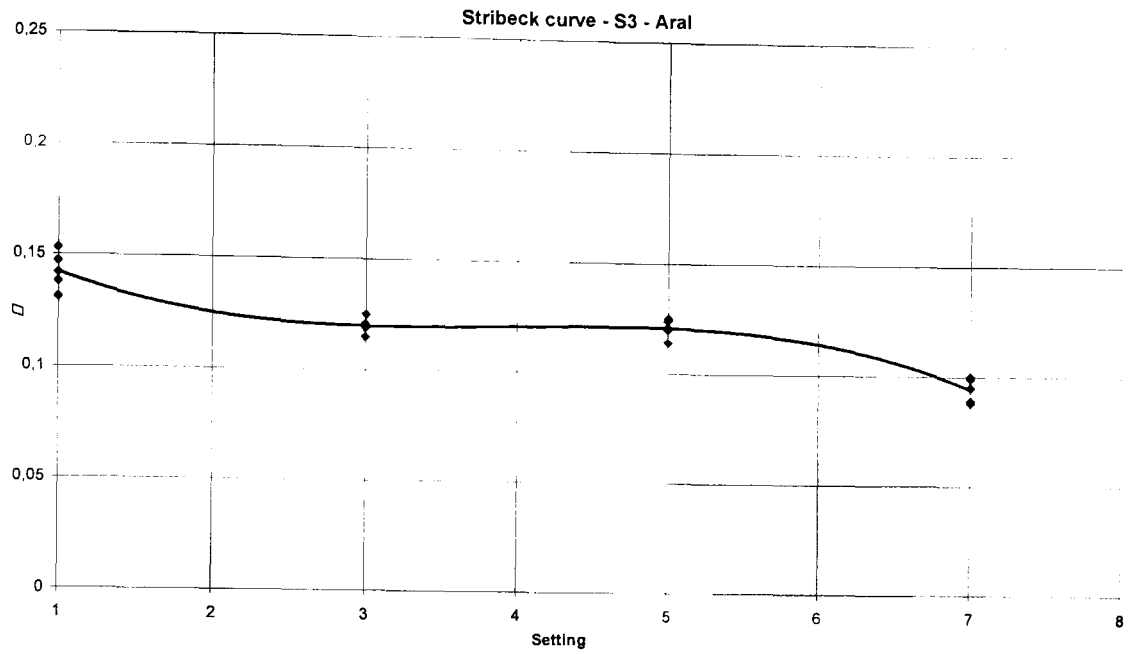
Stribeck curve - S3 - Aral
0,25
0,2
0,15
0,1
0,05
0
1
2
3
4
5
6
7
8
Setting

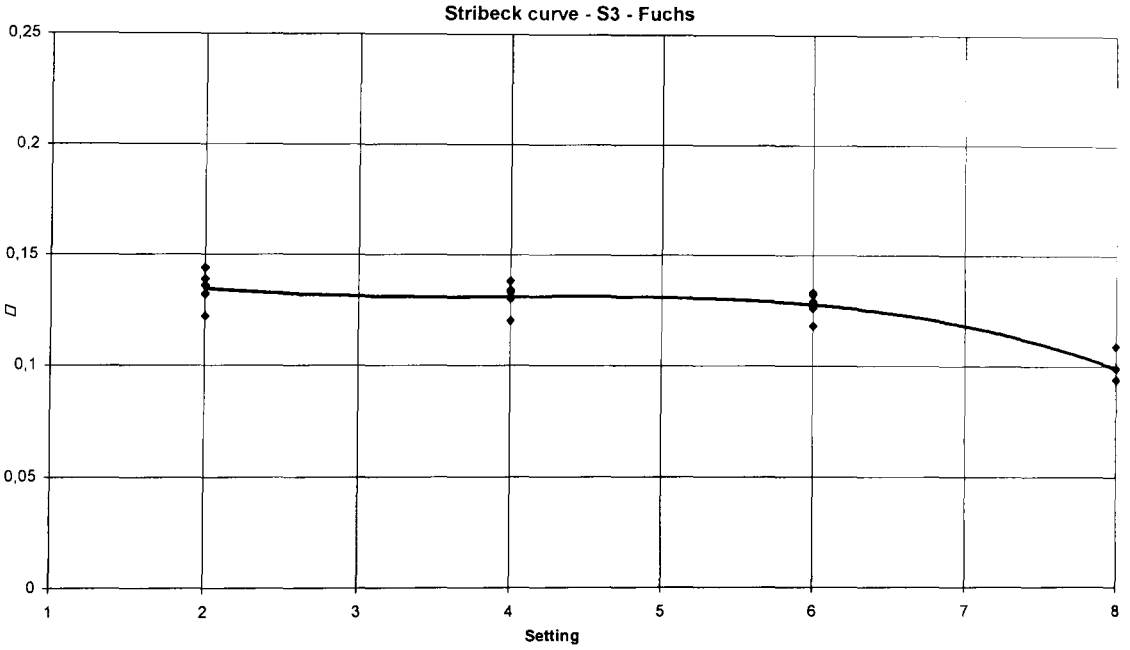
Stribeck curve - S3 - Fuchs
0,25
0,2
0,15
0,1
0,05
0
1
2
3
4
5
6
7
8
Setting

A7.2 GI zinc coated materials

These Stribeck curves cannot be clearly associated to either of the lubrication behaviour presented in Chapter 5 section 5.5.1. In fact the materials named:

- H1, S4 and S6 clearly behaved as "Poorly lubricated" while
- B5, H2 and S5 seems to behave as "Richly lubricated".

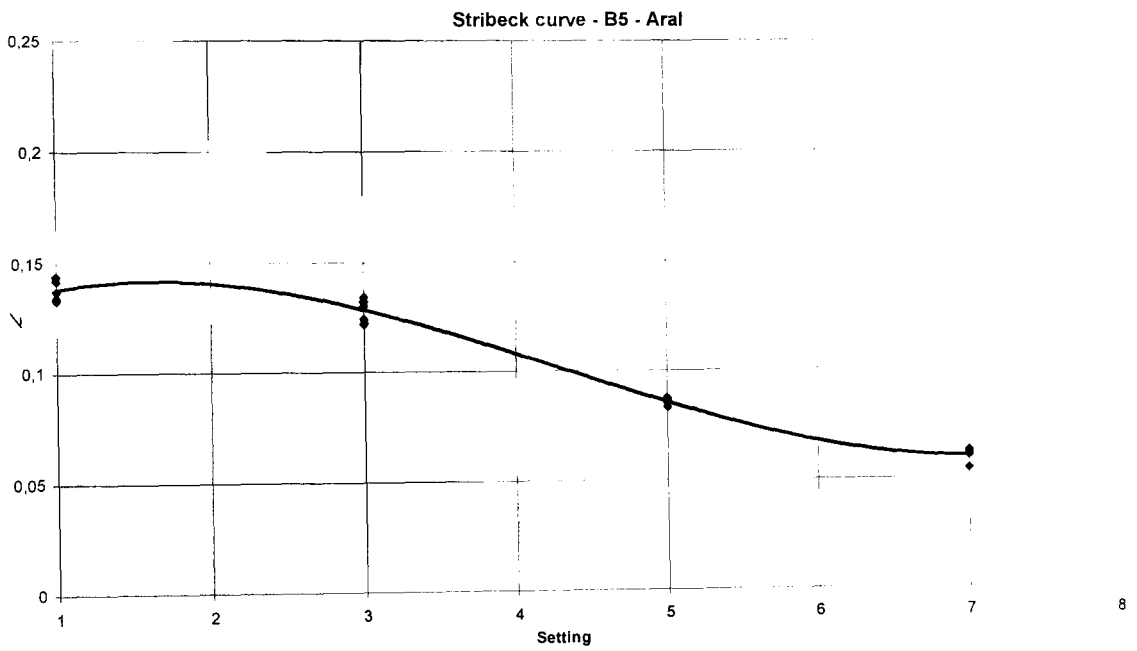

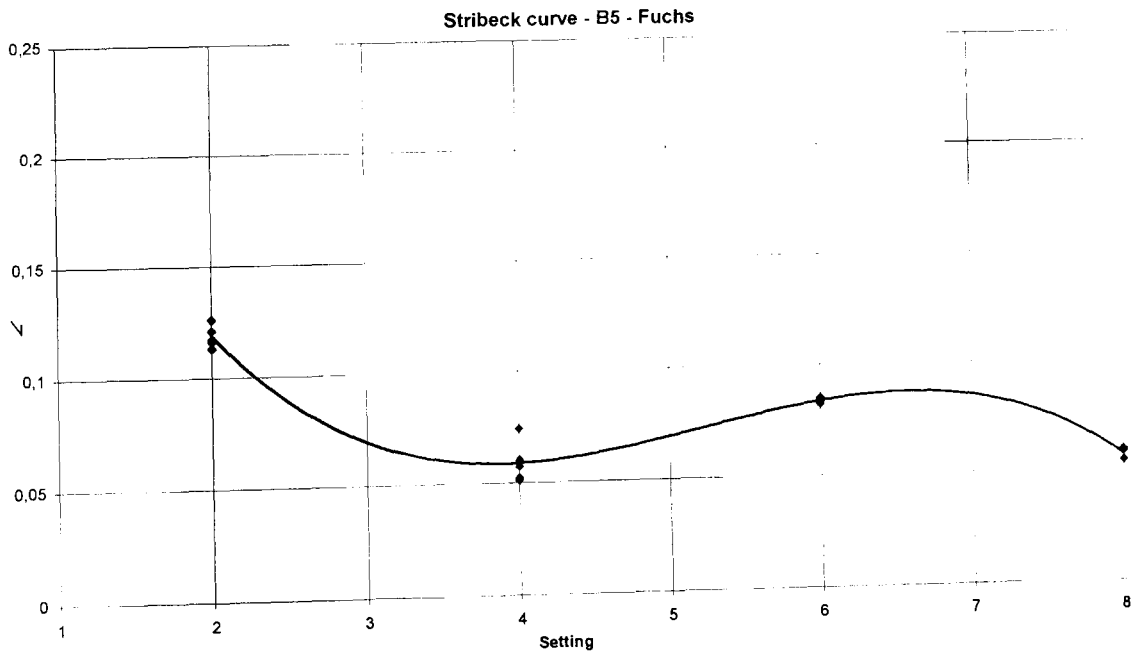

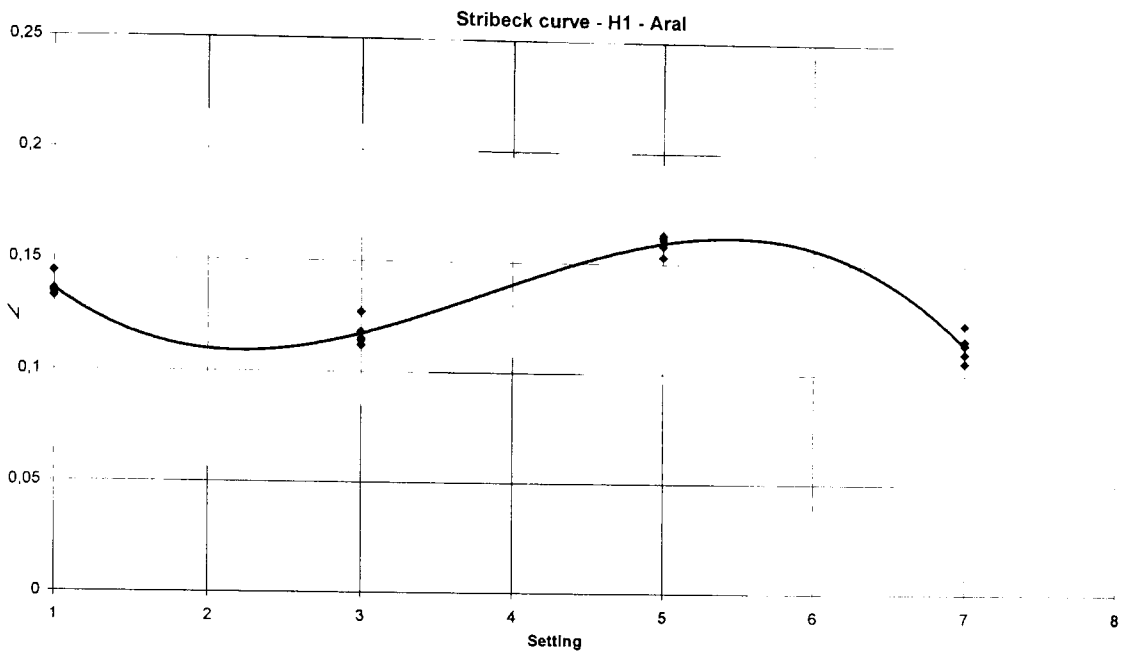
Stribeck curve - H1 - Aral
0,25
0,2
0,15
0,1
0,05
0
1
2
3
4
5
6
7
8
Setting

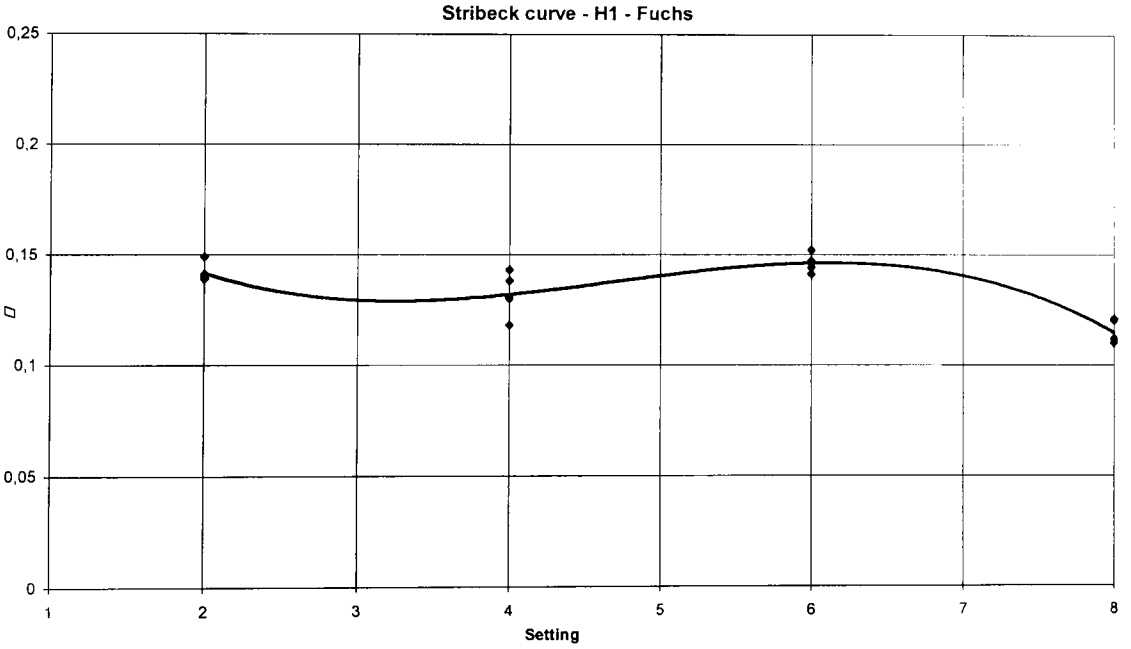
Stribeck curve - H1 - Fuchs
0,25
0,2
0,15
0,1
0,05
0
1
2
3
4
5
6
7
8
Setting

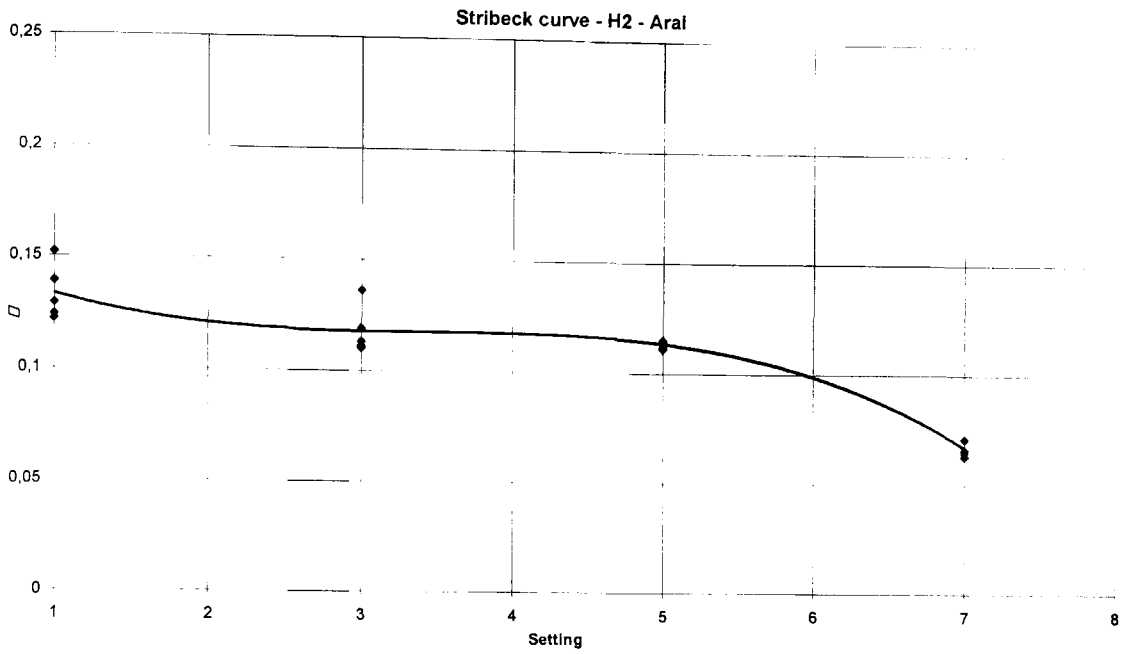
Stribeck curve - H2 - Aral
0,25
0,2
0,15
0,1
0,05
0
D
1
2
3
4
5
6
7
8
Setting

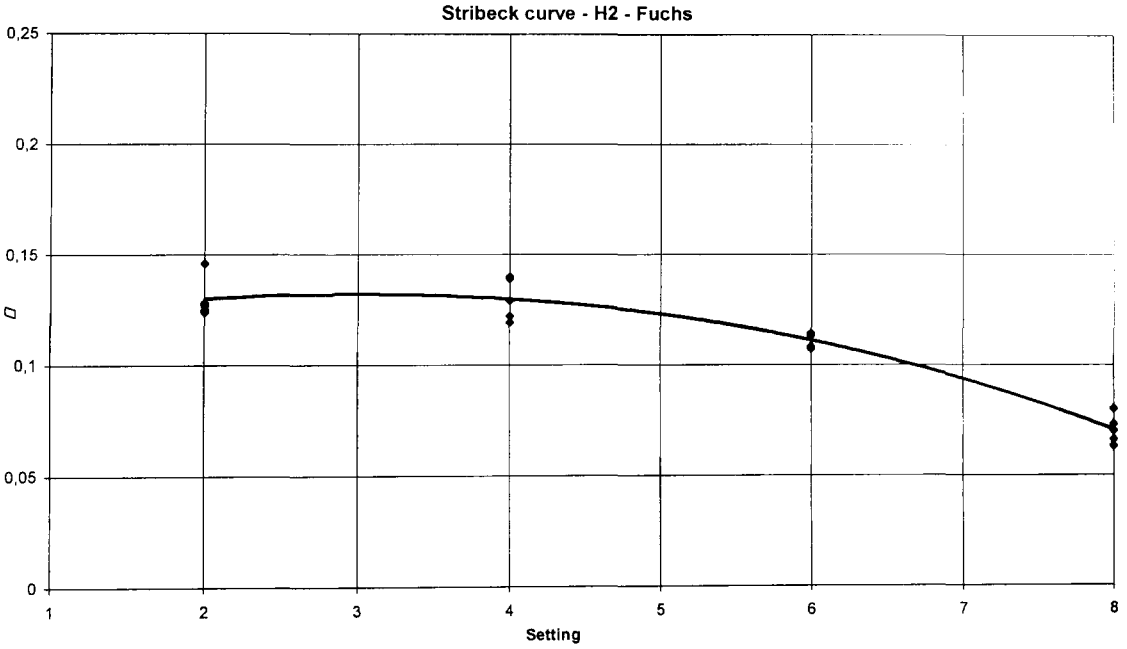
Stribeck curve - H2 - Fuchs
0,25
0,2
0,15
0,1
0,05
0
D
1
2
3
4
5
6
7
8
Setting

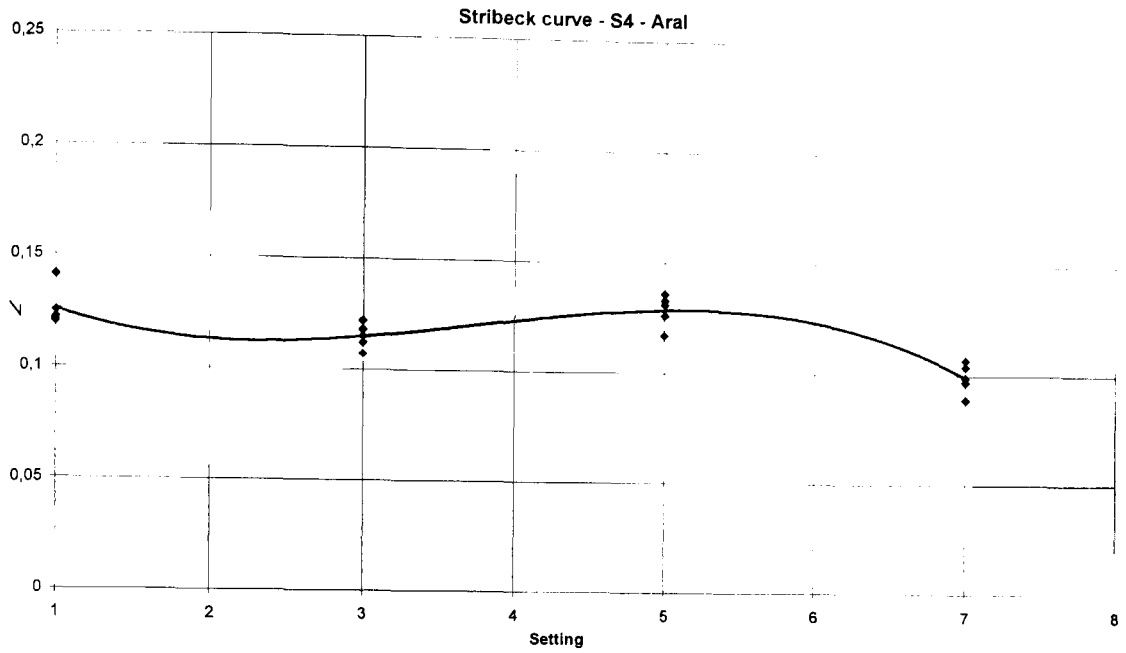
Stribeck curve - S4 - Aral
0,25
0,2
0,15
0,1
0,05
0
λ
1
2
3
4
5
6
7
8
Setting

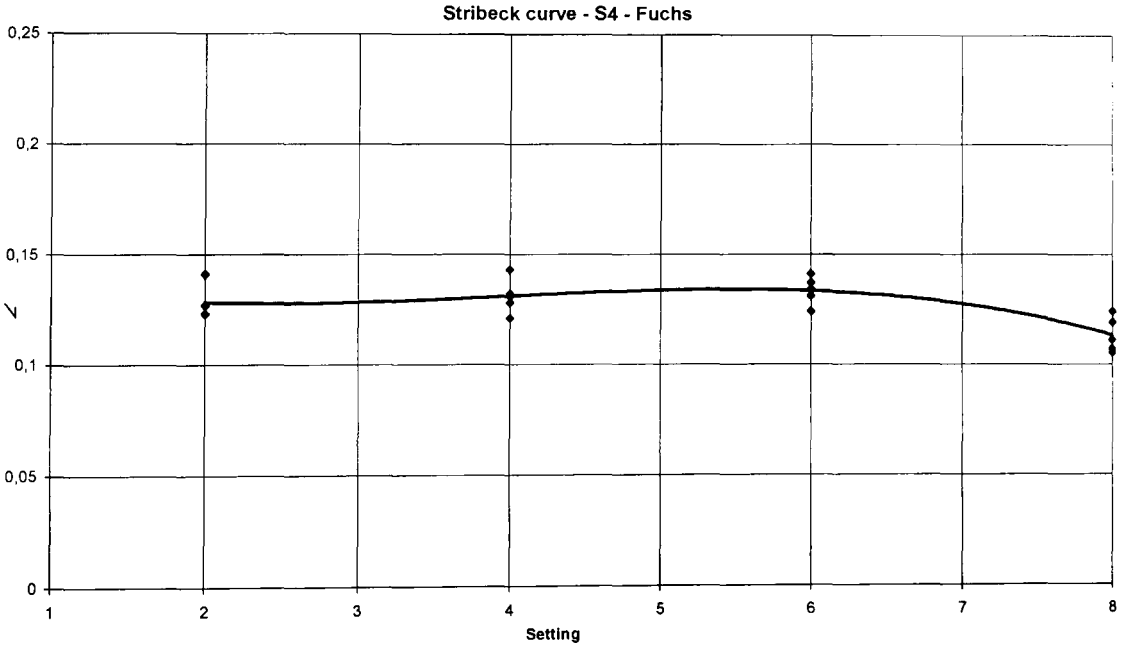
Stribeck curve - S4 - Fuchs
0,25
0,2
0,15
0,1
0,05
0
λ
1
2
3
4
5
6
7
8
Setting

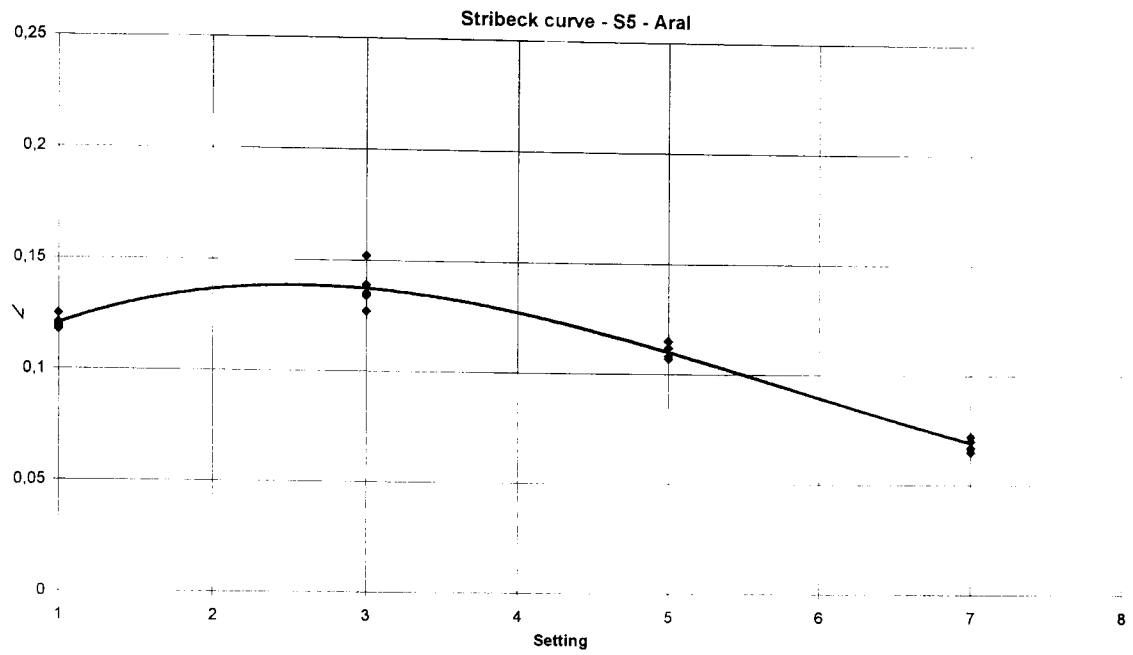
Stribeck curve - S5 - Aral
0,25
0,2
0,15
0,1
0,05
0
λ
1
2
3
4
5
6
7
8
Setting

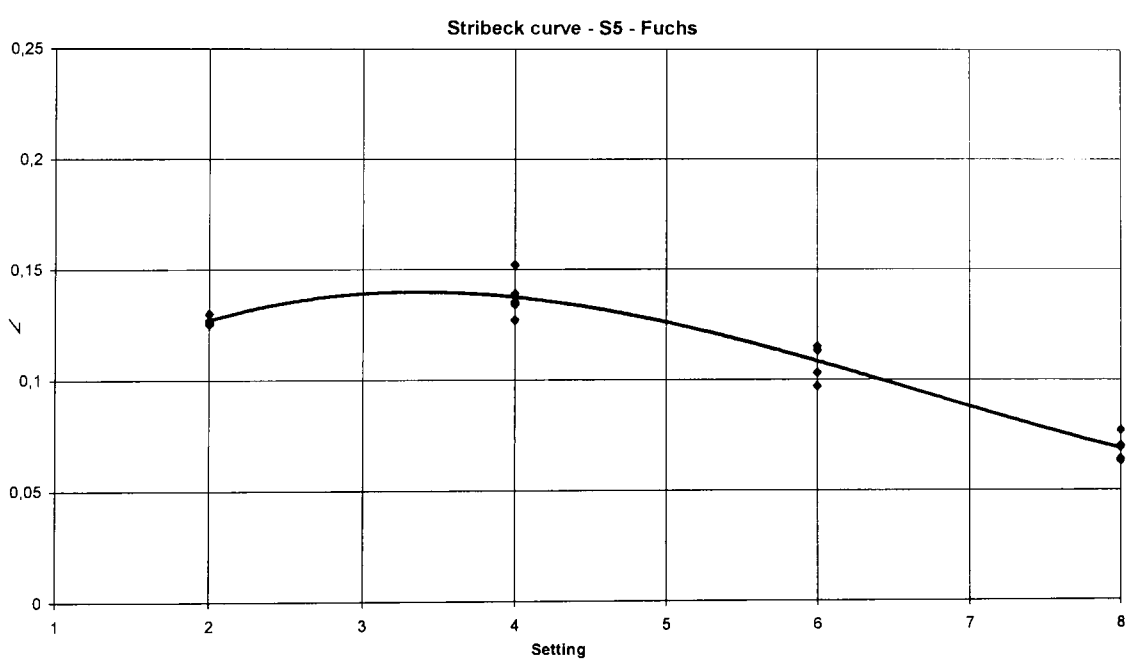
Stribeck curve - S5 - Fuchs
0,25
0,2
0,15
0,1
0,05
0
λ
1
2
3
4
5
6
7
8
Setting

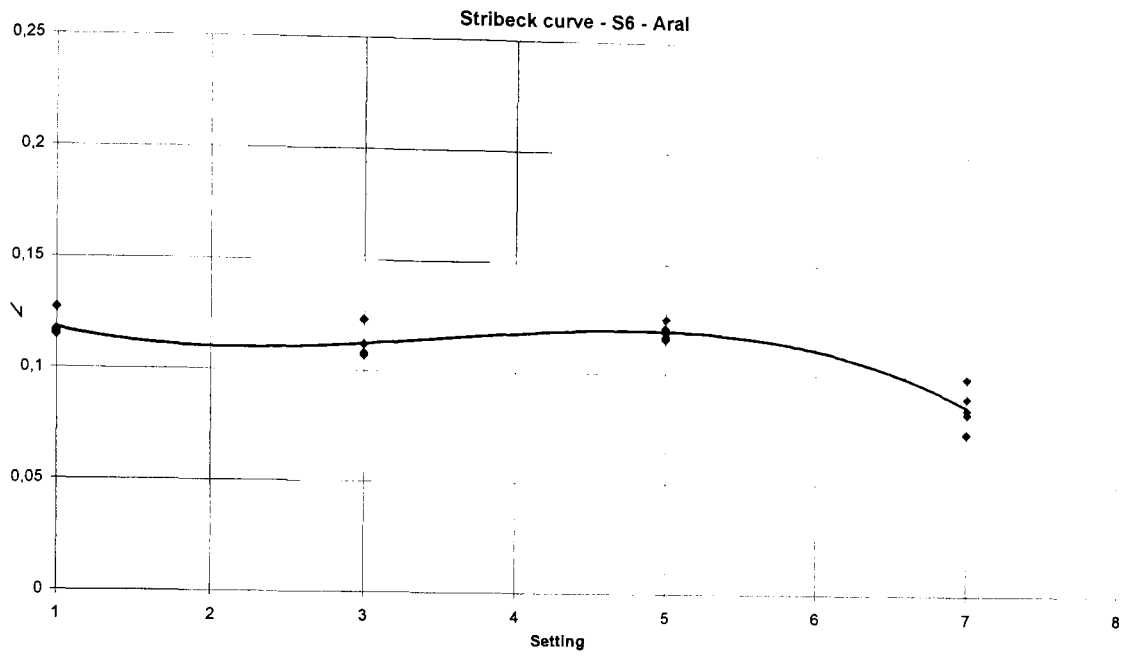
Stribeck curve - S6 - Aral
0,25
0,2
0,15
0,1
0,05
0
λ
1
2
3
4
5
6
7
8
Setting

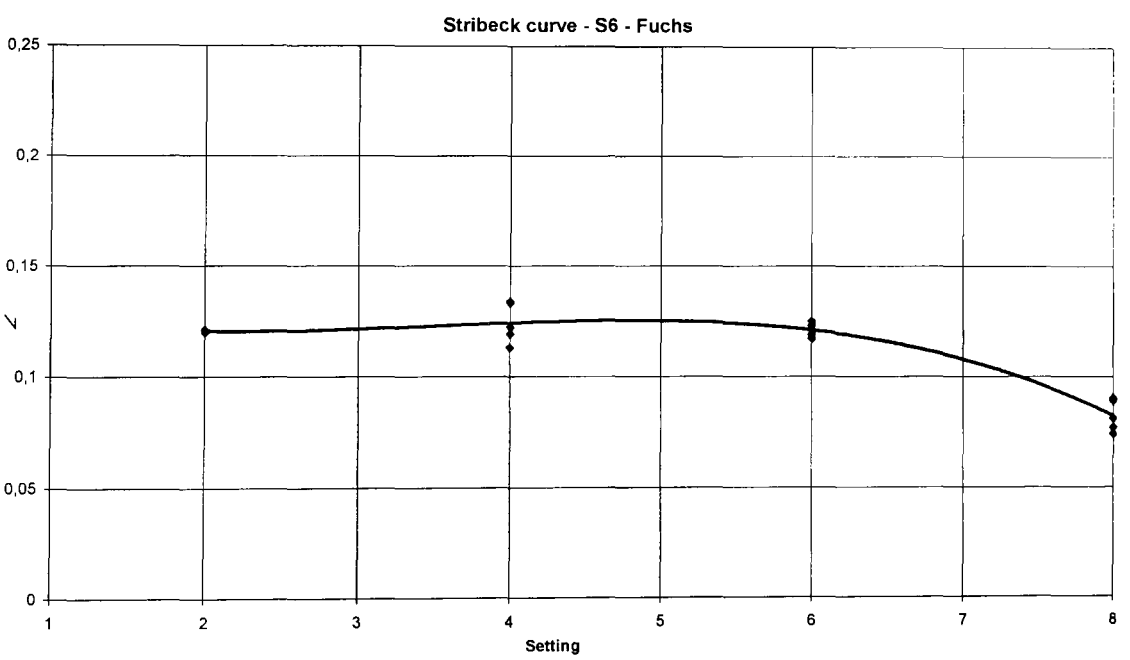
Stribeck curve - S6 - Fuchs
0,25
0,2
0,15
0,1
0,05
0
λ
1
2
3
4
5
6
7
8
Setting

A7.3 GA zinc coated materials

All these Stribeck curves can be clearly associated with the "Poor lubrication" behaviour presented in Chapter 5 section 5.5.1.

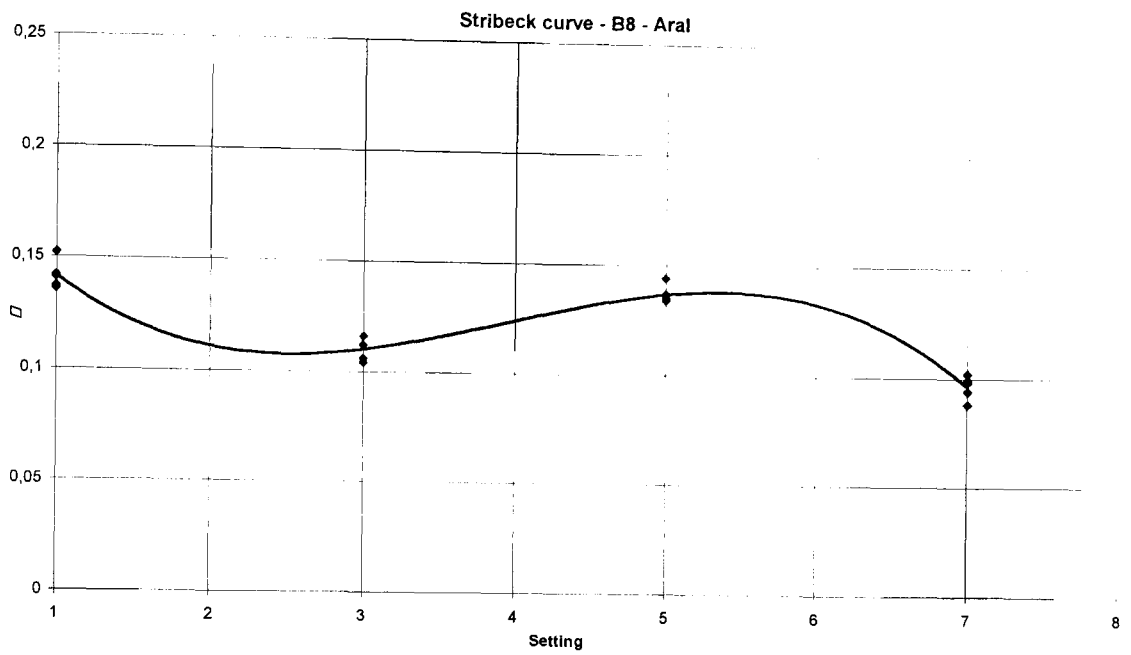

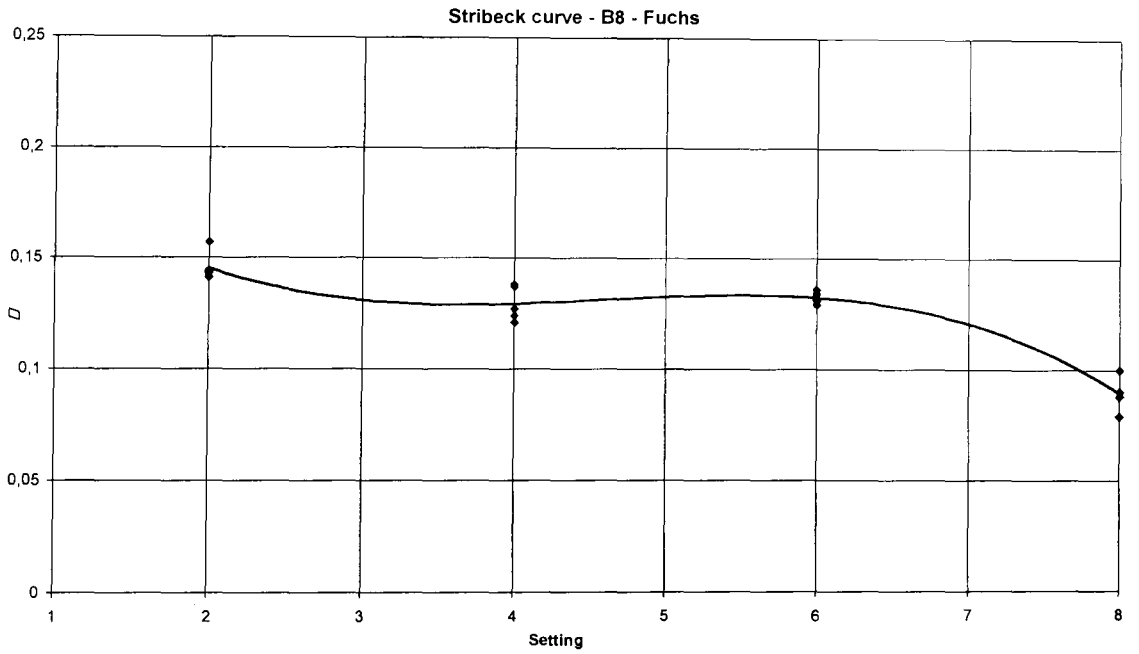

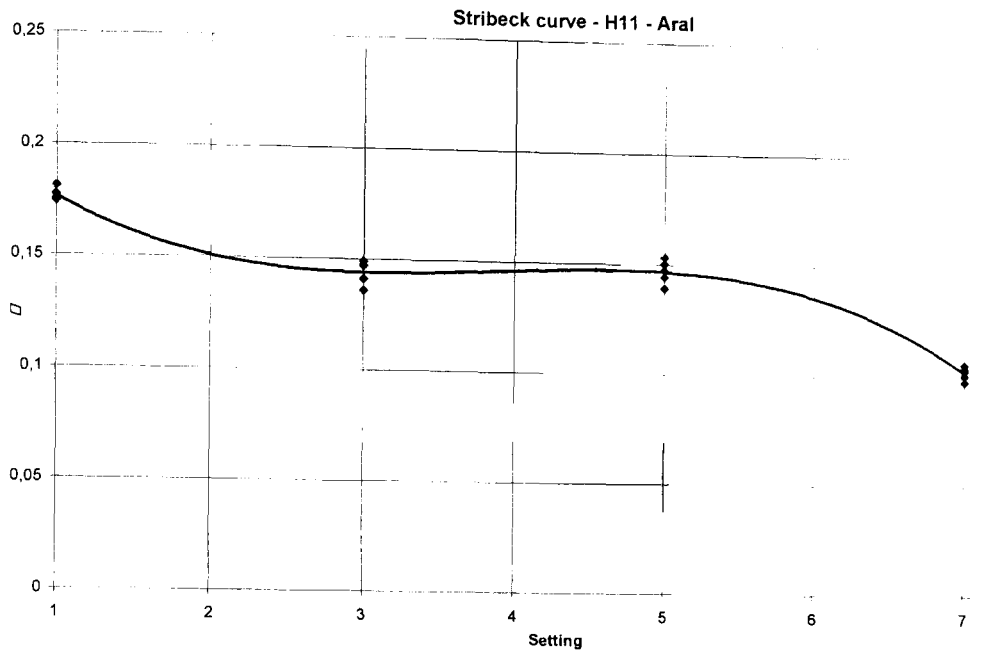
Stribeck curve - H11 - Aral
0,25
0,2
0,15
0,1
0,05
0
D
1
2
3
4
5
6
7
8
Setting

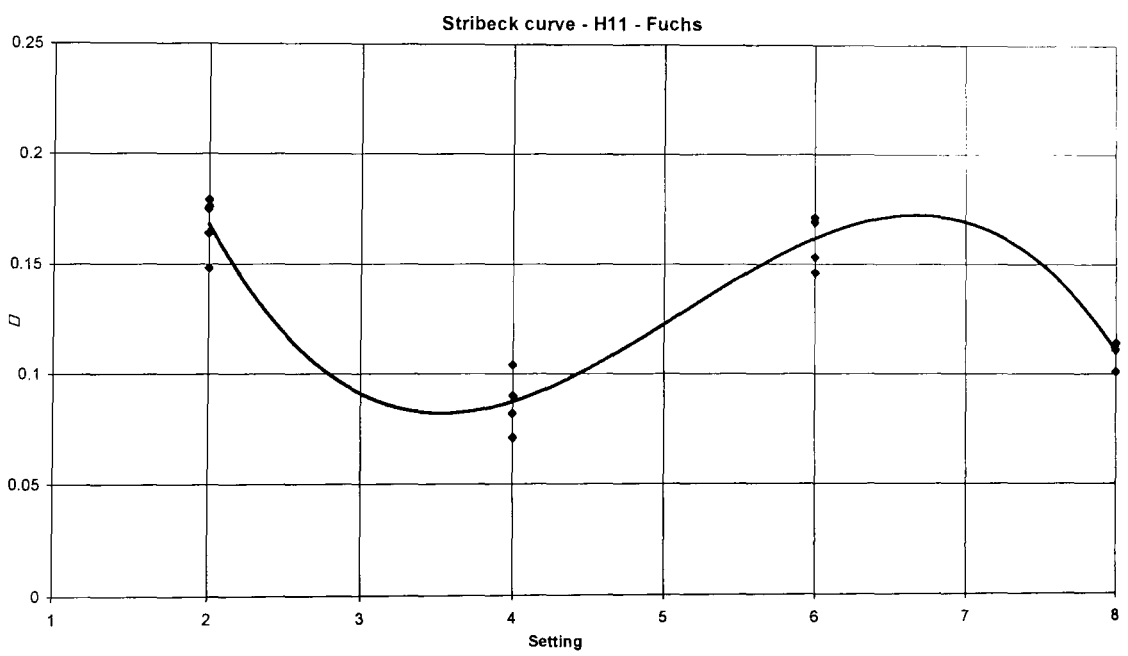
Stribeck curve - H11 - Fuchs
0.25
0.2
0.15
0.1
0.05
0
D
1
2
3
4
5
6
7
8
Setting

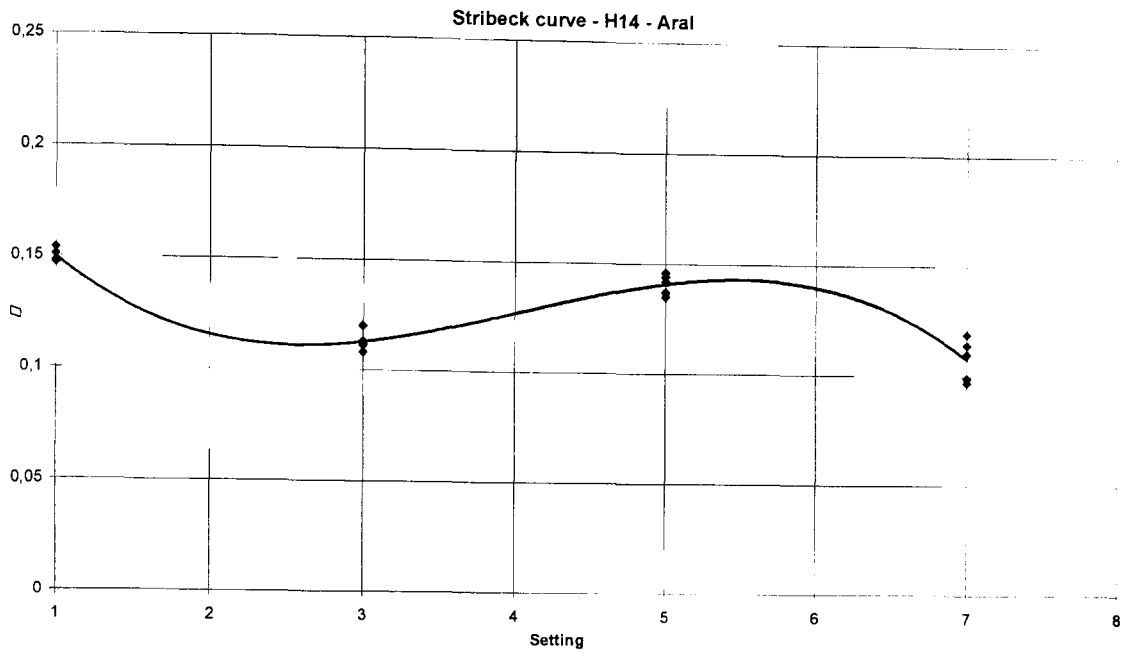
Stribeck curve - H14 - Aral
0,25
0,2
0,15
0,1
0,05
0
1
2
3
4
5
6
7
8
Setting

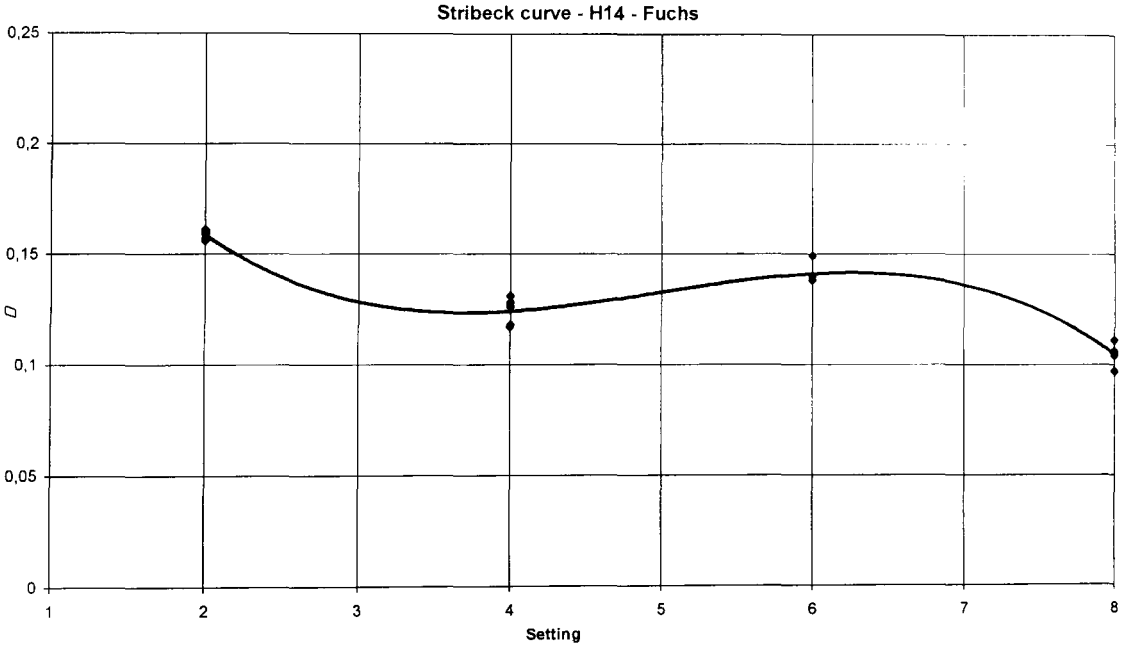
Stribeck curve - H14 - Fuchs
0,25
0,2
0,15
0,1
0,05
0
1
2
3
4
5
6
7
8
Setting

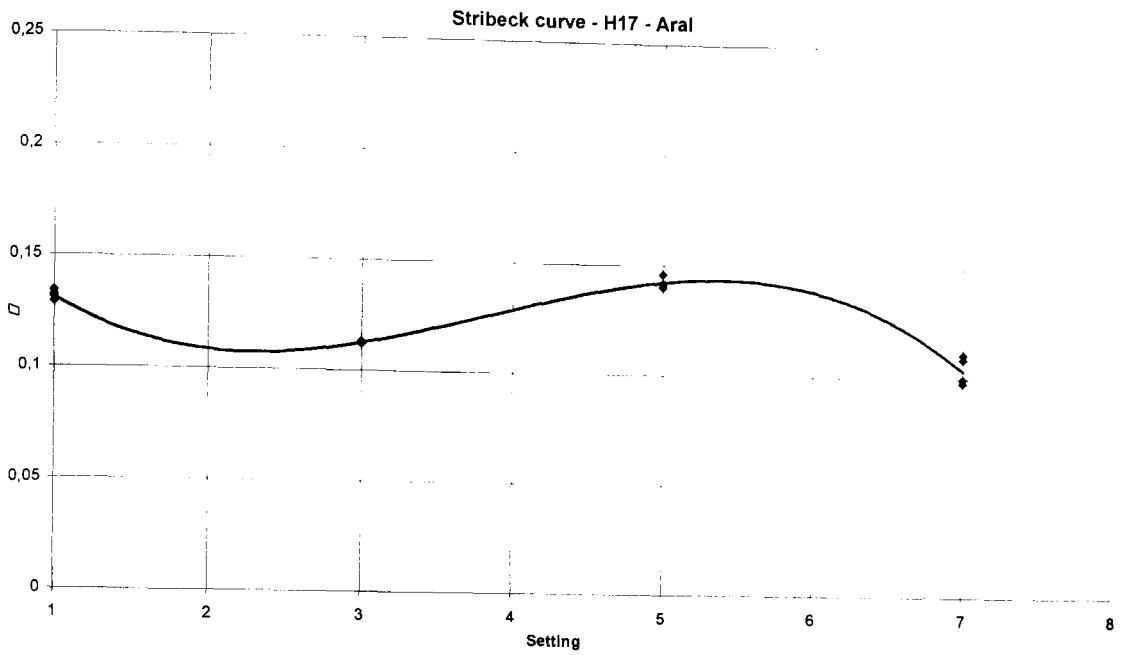
Stribeck curve - H17 - Aral
0,25
0,2
0,15
0,1
0,05
0
D
1
2
3
4
5
6
7
8
Setting

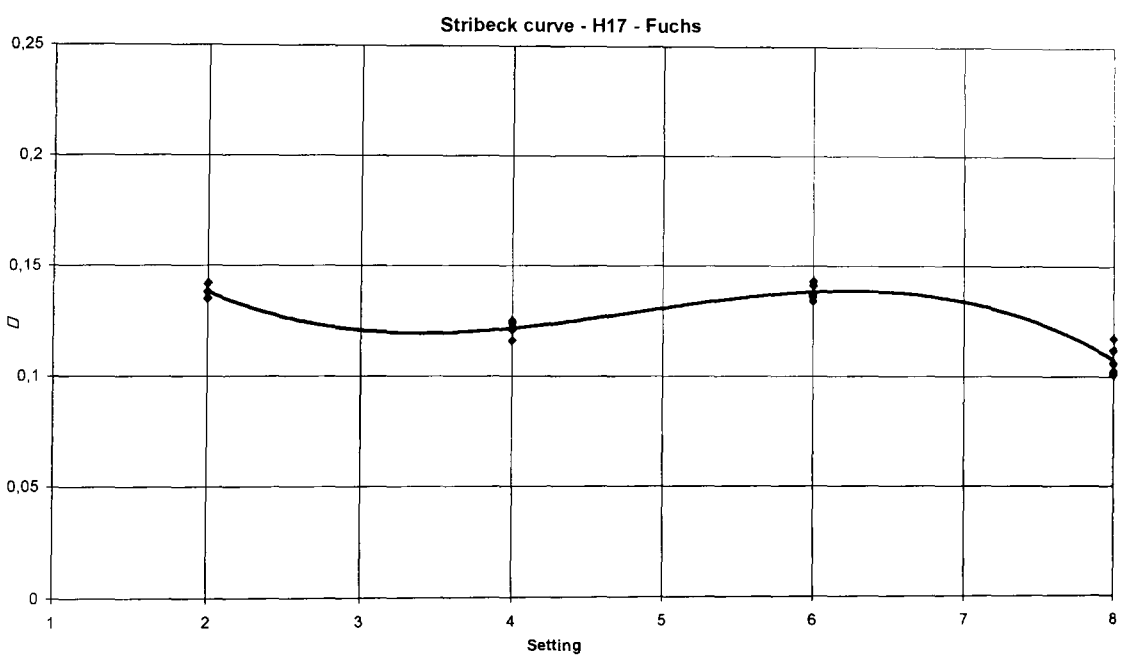
Stribeck curve - H17 - Fuchs
0,25
0,2
0,15
0,1
0,05
0
D
1
2
3
4
5
6
7
8
Setting

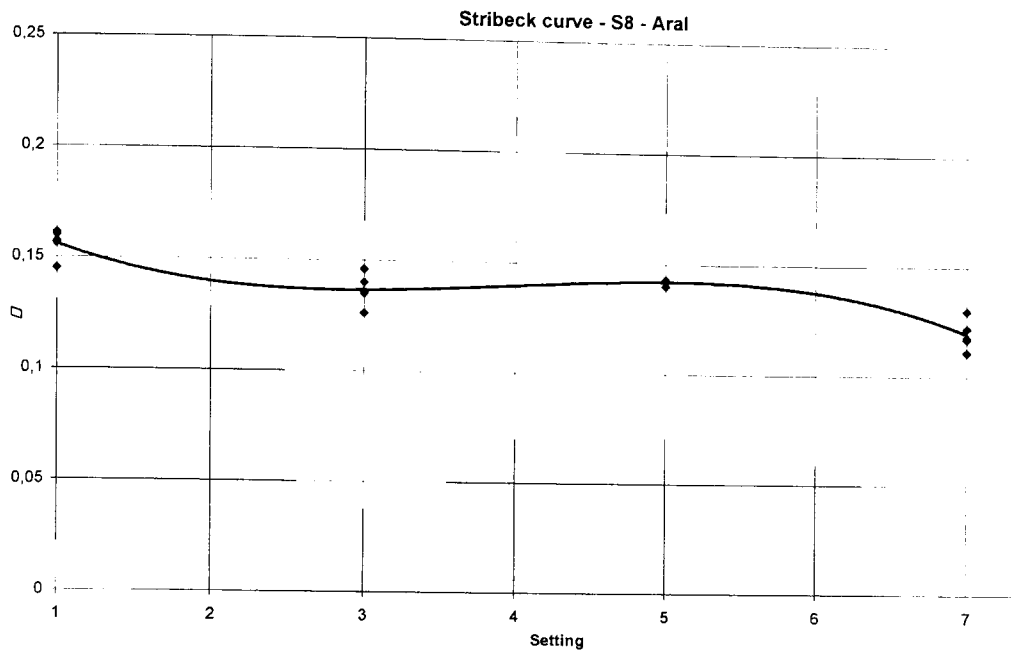
Stribeck curve - S8 - Aral
0,25
0,2
0,15
0,1
0,05
0
D
1
2
3
4
5
6
7
8
Setting

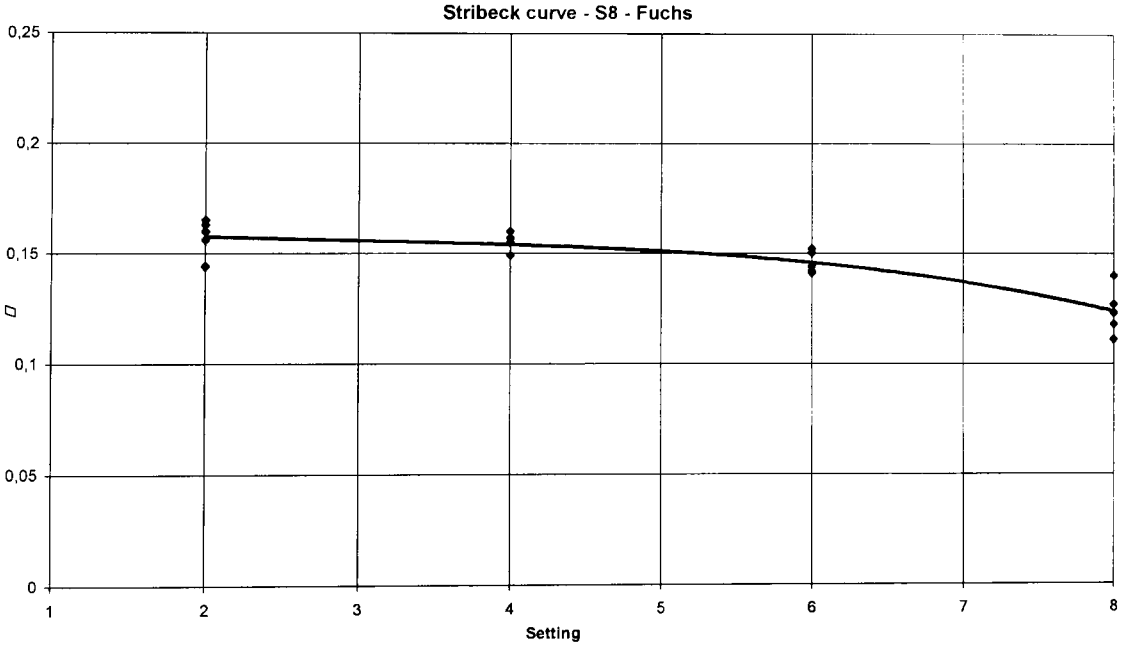
Stribeck curve - S8 - Fuchs
0,25
0,2
0,15
0,1
0,05
0
D
1
2
3
4
5
6
7
8
Setting

A7.4 Pretex - GI coated material (P2)

Due to a fire at the Salzgitter manufacturing plant, the experiments on P2 were performed several months later than all the other experiments and on a differently set testing device. This means that these results cannot be directly compared to any previous result due to a different testing device calibration.

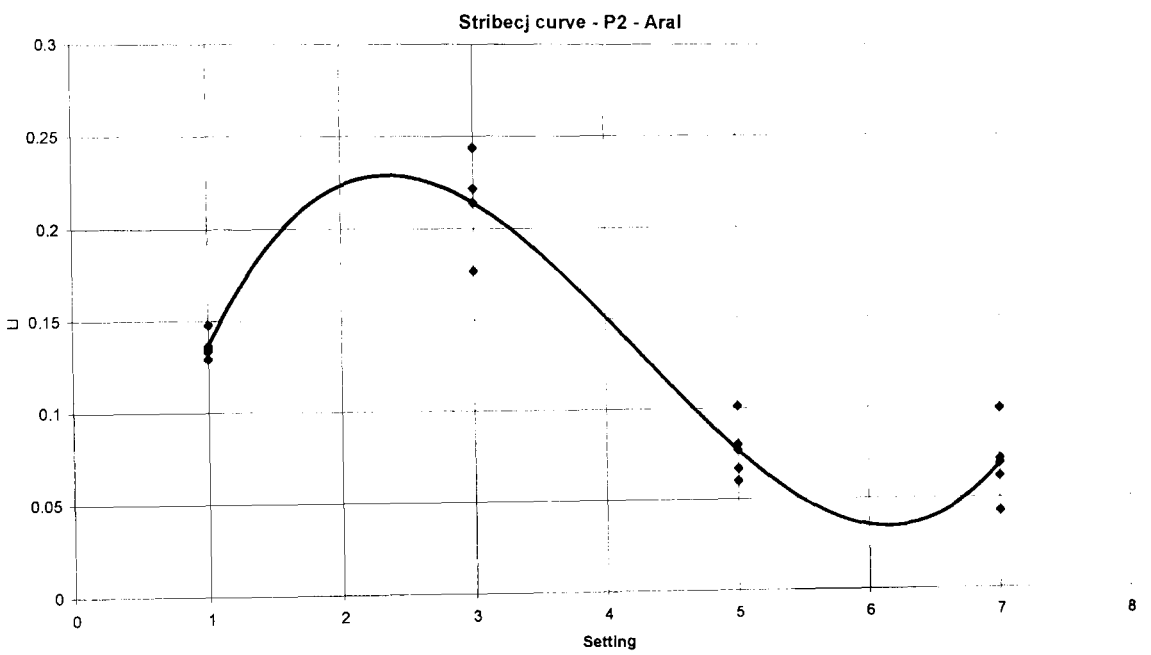

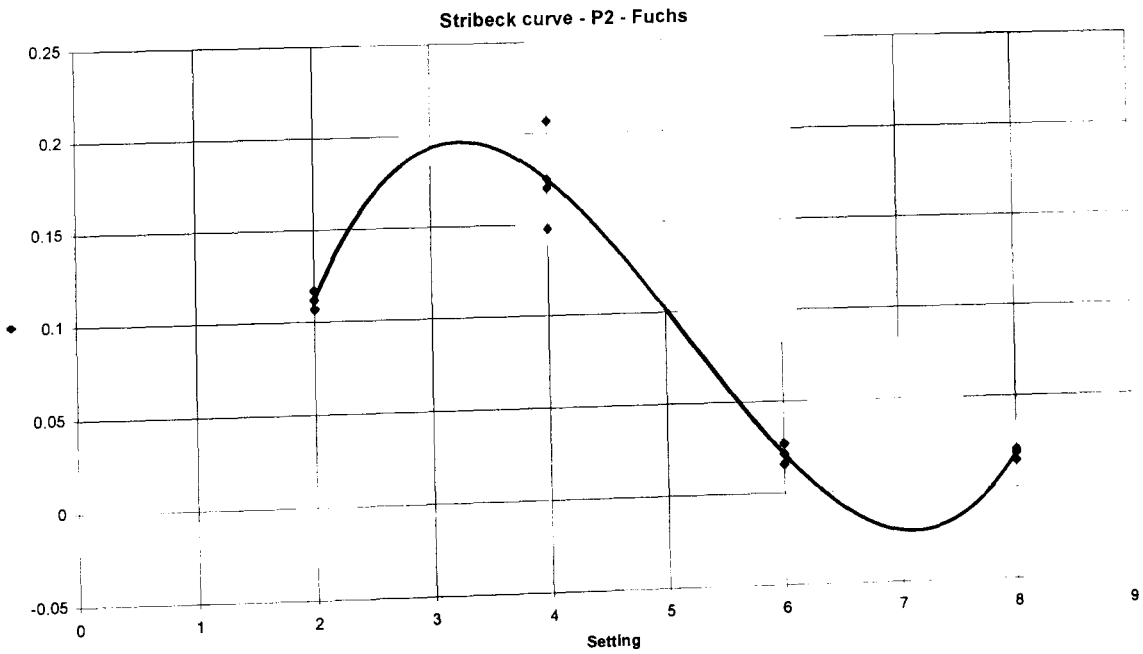

A8. Statistical analysis of friction experiments

In this appendix, the procedures and the statistical results are presented for the friction experiments. In all these tests, full factorial design was used.

The aim of this experimental set was to understand whether any of the following influence the friction coefficient:

- topography (not yet identified by a parameter, but through the "name" of the material)
- any interaction between topography and any other control factor

Further, it is expected also to understand which treatment combination produces the more stable coefficient of friction.

In order to analyse these results, the following tests were run for each coating type:

1. **Analysis of variance** (ANOVA) on all the control factors. During this stage the surface topography is identified through the "name" of the material described in Chapter 5 section 5.3.1
2. **Regression analysis** (correlation) between identified surface topography parameters and the measured coefficient of friction for every treatment combination of interest.

A8.1 Statistical analysis of GA coated materials

This statistical analysis was performed on the full range the GA coated materials. The list of control factors is presented in Table A8.1 below.

	Level				
Control Factor	**1**	**2**	**3**	**4**	**5**
A – Oil type	Low viscosity (Aral)	High viscosity (Fuchs)			
B – Sliding velocity	2 mm/s	200 mm/s			
C – Holding pressure	36 KN	107 KN			
D – Material type (topography)	B8	H11	H14	H17	S8

Table A8.1 – GA coated materials - DOE table

The output response was the coefficient of friction (μ). For convenience, in the ANOVA table below all the statistically important factors are highlighted , corresponding to a P value less than 0.01.

ANOVA table

Source	df	SeqSS	AdjSS	AdjMS	F	P
A	1	0.0001170	0.0001170	0.0001170	3.01	0.085
B	1	0.0085674	0.0085674	0.0085674	220	0.000
C	1	0.0532358	0.0532358	0.0532358	1369	0.000
D	4	0.0108909	0.0108909	0.0027227	70	0.000
A*B	1	0.0000006	0.0000006	0.0000006	0.02	0.901
A*C	1	0.0000378	0.0000378	0.0000378	0.97	0.325
A*D	4	0.0018706	0.0018706	0.0004677	12.03	0.000
B*C	1	0.0006516	0.0006516	0.0006516	16.76	0.000
B*D	4	0.0015283	0.0015283	0.0003821	9.83	0.000
C*D	4	0.0068321	0.0068321	0.0017080	43.94	0.000
A*B*C	1	0.0000092	0.0000092	0.0000092	0.24	0.626
A*B*D	4	0.0060904	0.0060904	0.0015226	39.17	0.000
A*C*D	4	0.0022478	0.0022478	0.0005620	14.46	0.000
B*C*D	4	0.0013875	0.0013875	0.0003469	8.92	0.000
A*B*C*D	4	0.0014517	0.0014517	0.0003629	9.34	0.000
Error	160	0.0062192	0.0062192	0.0000389		
Total	199	0.1011382				

Table A8.2 – GA coated materials - ANOVA table

Reading the ANOVA table above it is possible to state that a large number of factors and high order interactions are statistically significant. This means that friction is influenced by a large number of factors and this influence is extremely complex (interactions of order higher than 2 are difficult to interpret and will not explored further).

In order to try to understand all these complex influences, all the main effects were plotted and the results are presented below.

A8.1.1 Main effect plot for GA materials

These curves represent the influence of the control factors on the friction coefficient.

Reading the ANOVA table it is possible to notice that the oil type exhibit a P value of 8.5%. This means that no effect of lubricant type could be (statistically) found. Further, the effect plot shown in Figure A8.1 (left box in the plot) is an "almost" flat line showing that there is no relationship.

Conversely, all the other main factors (Pressure, Velocity and Material) exhibit P values lower than 1% in the ANOVA table shown in Table A8.1, hence they

are statistically significant. Similar information can be seen in the main effect plot shown in Figure A8.1 below, since:

- when the holding **pressure** changes from 1 to 10 MPa, the average coefficient of friction increases from 0.115 to 0.147 (increase of almost 50%). This could be interpreted as an increase of contact area between tool and sample due to the increase of holding pressure.
- In the same way, when the **sliding velocity** changes from 2 to 200 mm/s, the coefficient of friction decreases from 0.139 to 0.124. This is expected to be the effect of a larger oil amount dragged by the moving surface.

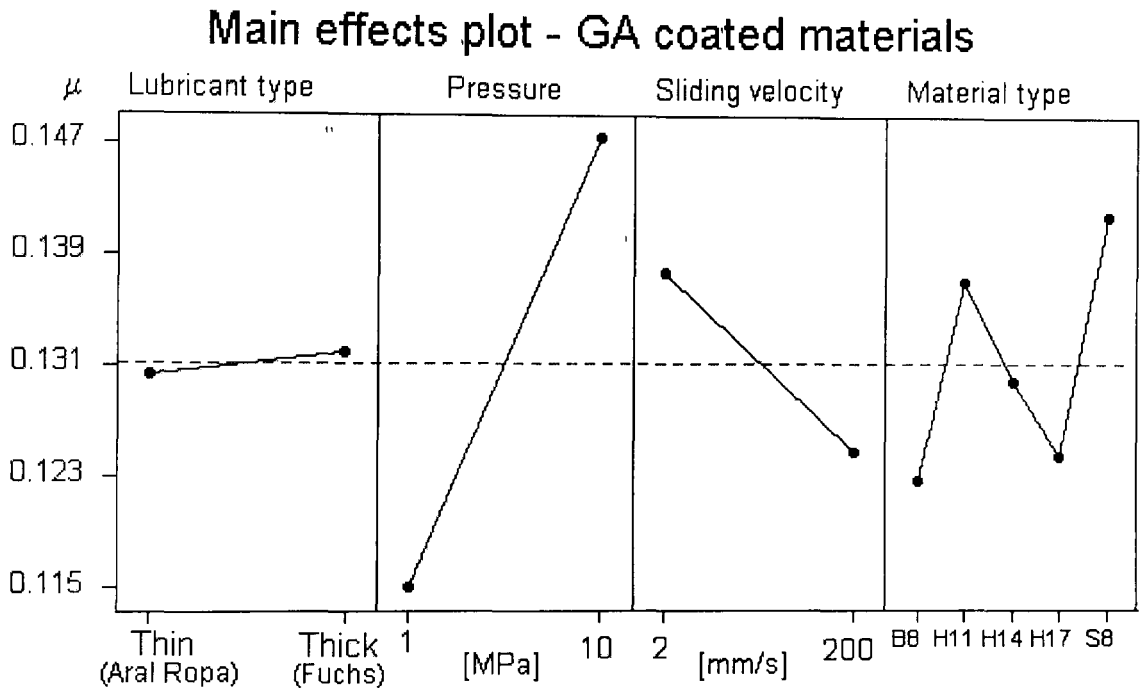

Figure A8.1 – GA coated materials - Main effect plot

Finally, to fully understand the effect of material type, a correlation analysis between surface topography parameters and coefficient of friction is now required. The description of the interactions between control factors is described below.

A8.1.2 First order interactions for GA materials

A8.1.2.1 Lubricant type and material type (A*D)

As one can read from the interaction plot shown in Figure A8.2, all the materials exhibit a higher coefficient of friction when lubricated with Fuchs 4107S (with the exception of H11 where it seems to be the opposite).

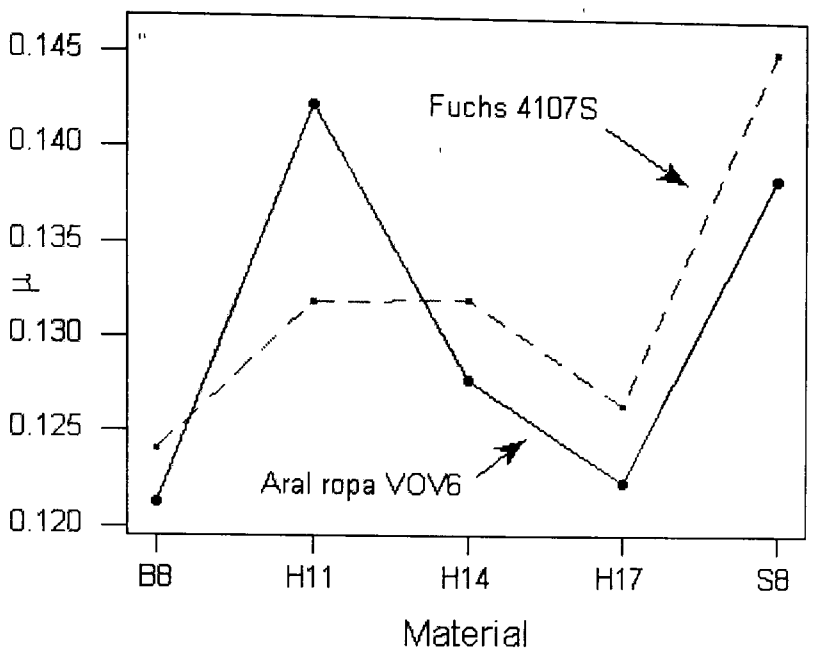

Figure A8.2 – GA coated materials - Interaction plot (lubricant and material)

Fuchs 4107S is the thicker lubricant of the two. This result appears to contrast with the expectation of thick lubricants being able to produce less friction. Unfortunately, further analysis of the reason of this behavior cannot be performed, since no details about the composition of any of the employed lubricants will be ever available.

A8.1.2.2 Sliding velocity and pressure (B*C)

As one can read from the interaction plot in Figure A8.3, at higher velocity (red dotted line) the coefficient of friction is more "pressure dependant" (the dotted line is slightly steeper than the black line).

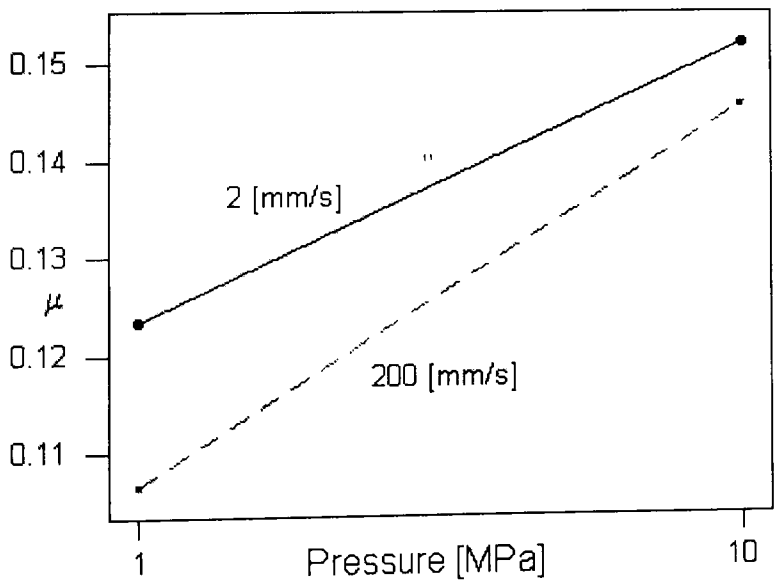

Figure A8.3 – GA coated materials - Interaction plot (pressure and velocity)

A8.1.2.3 Sliding velocity and material type (B*D)

As one can read from the interaction plot shown in Figure A8.4, this interaction is because the material H17 does not exhibit a markedly different coefficient of friction at the two velocities (see green circle inside the graph).

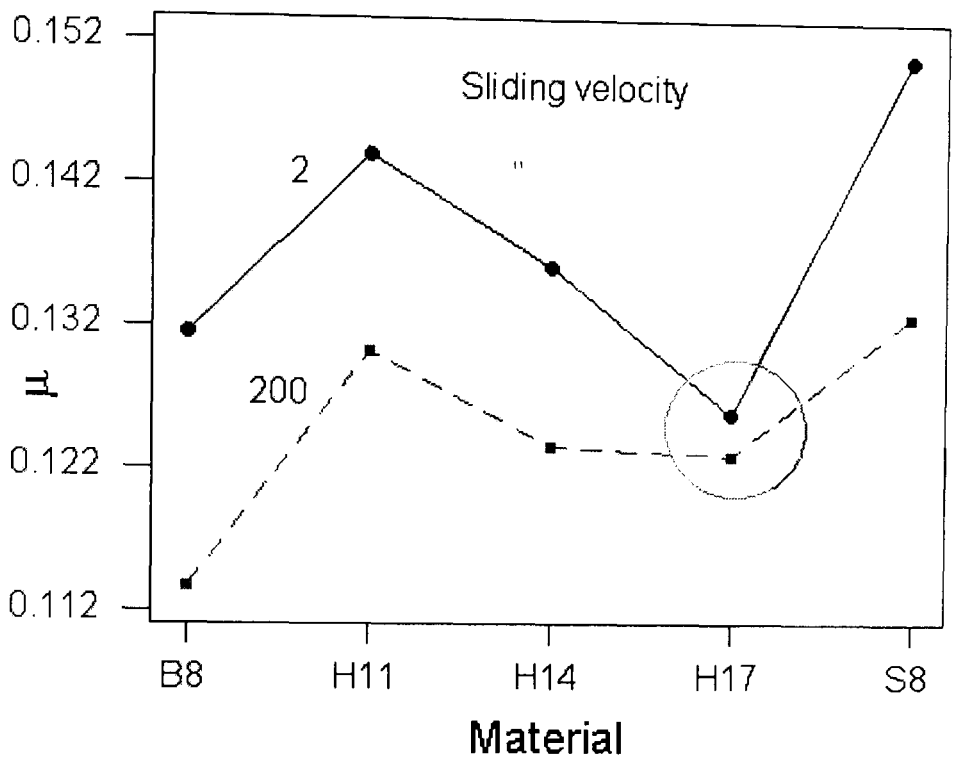

Figure A8.4 – GA coated materials - Interaction plot (velocity and material)

A8.1.2.4 Pressure and material (C*D)

Figure A8.5 shows the interaction plot between material and pressure. During this analysis, the yield strength of the materials was thought to be important, hence this was added to the graph.

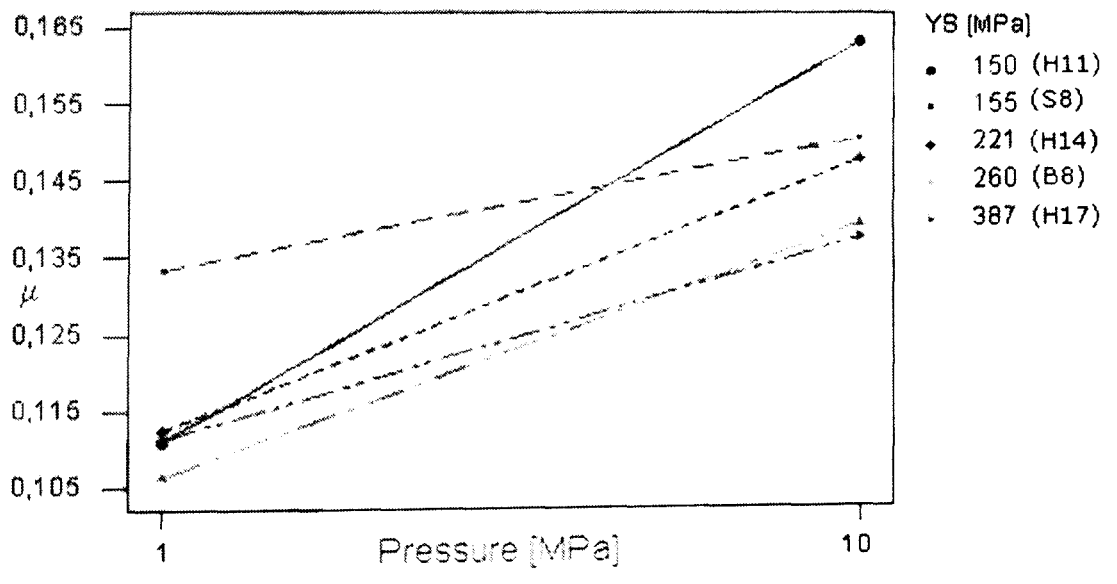

Figure A8.5 – GA coated materials - Interaction plot (pressure and material)

With the high yield strength materials (i.e. purple dotted line – 387MPa) the coefficient of friction is low and less pressure-dependant (i.e. less steep). The importance of a material yield strength will become clearer later during the presentation of the correlation analysis.

A8.1.3 Correlation analysis with surface parameters for GA coatings

All the experiments (even with different oils) will be tested together for correlation. During this set of experiments, the following parameters were found to influence the coefficient of friction:

- High pressure High velocity (see Table A8.3) - α calculated at h1g (definition in Chapter 5 section 5.4.1)
- High pressure Low velocity (see Table A8.4) – a linear combination (named generically "X" later) between α calculated at h1g and the material's yield strength
- Low pressure High velocity (see Table A8.5) – the extreme surface parameter S95p (definition in Chapter 2)
- Low pressure Low velocity – no correlations could be found

A8.1.3.1 Regression analysis - 10MPa and 200mm/s

Source	DF	SS	MS	F	P
Regression	2	0.00157395	0.00078698	16.37	0.000
Residual Error	47	0.00225917	0.00004807		
Total	49	0.00383312			

Regression equation found:
$\mu = 0.122 + 0.0545\ \alpha(h1g)$

Predictor	Coef	StDev	T	P
Constant	0.122224	0.007793	15.68	0.000
YS	-0.00001028	0.00001377	-0.75	0.459
α(h1g)	0.05448	0.01286	4.24	0.000

Table A8.3 – GA coated materials - Regression analysis (10MPa and 200mm/s)

Reading Table A8.3, it can be seen that there is statistical evidence of the influence of α(h1g) upon the friction coefficient (μ). Further, high area fraction of contacts lead to high coefficients of friction.

Looking at the "Predictor" table (Table A8.3) it can be also understood that – in this treatment combination (combination of velocity and pressure) – the yield strength does not influence to the coefficient of friction (P is 45.9%).

The regression plot is presented in Figure A8.6 below.

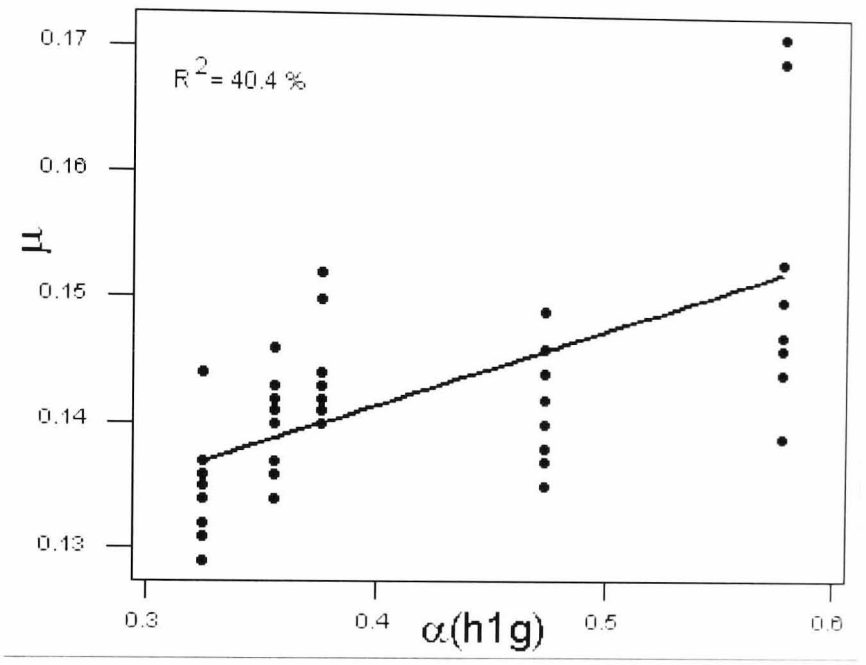

Figure A8.6 – GA coated materials - Regression plot (10MPa, 200mm/s)

A8.1.3.2 Regression analysis - 10MPa and 2mm/s

Source	DF	SS	MS	F	P
Regression	2	0.0080658	0.0040329	85.64	0.000
Residual Error	47	0.0022133	0.0000471		
Total	49	0.0102791			

Regression equation found:

$\mu = 0.144 - 0.000091\ YS + 0.0695\ \alpha(h1g)$

Predictor	Coef	StDev	T	P
Constant	0.144287	0.007714	18.71	0.000
YS	-0.00009077	0.00001363	-6.66	0.000
α(h1g)	0.06947	0.01273	5.46	0.000

Table A8.4 – GA coated materials - Regression analysis (10MPa and 2mm/s)

This regression equation in Table A8.4 shows that high yield strength materials exhibit low coefficients of friction. At the same time, materials with high α(h1g) exhibit high coefficients of friction.

The regression plot is presented in Figure A8.7 below.

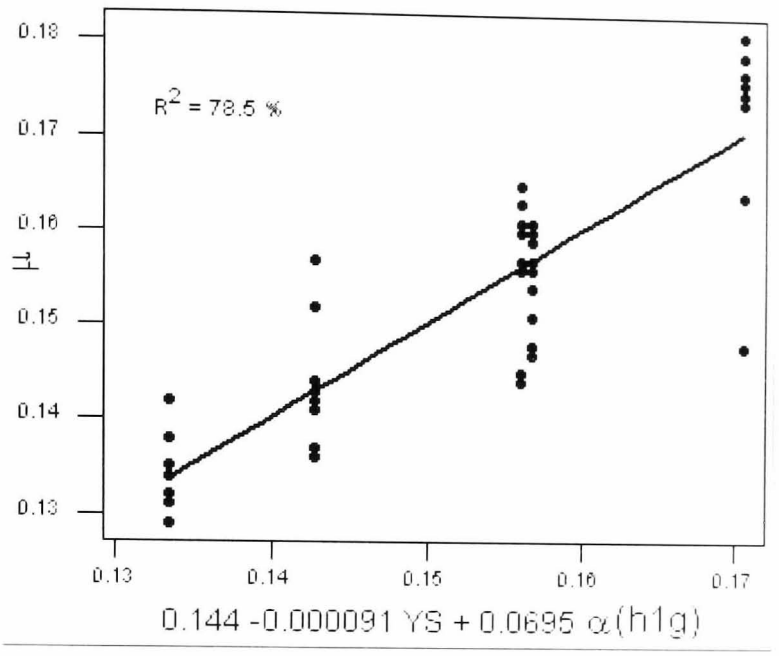

Figure A8.7 – GA coated materials - Regression plot (10MPa and 2mm/s)

A8.1.3.3 Regression analysis - 1MPa pressure and 200mm/s

Source	DF	SS	MS	F	P
Regression	1	0.0017954	0.0017954	18.22	0.000
Residual Error	48	0.0047291	0.0000985		
Total	49	0.0065245			

Regression equation found

$\mu = 0.0722 + 0.00989\ S95p$

Predictor	Coef	StDev	T	P
Constant	0.072237	0.008153	8.86	0.000
S95p	0.009890	0.002317	4.27	0.000

Table A8.5 – GA coated materials - Regression analysis (1MPa and 200mm/s)

Table A8.5 shows that there is statistical evidence of the influence of S95p (extreme parameter defined in Chapter 5 section 5.4.1) upon friction coefficient (μ). Further, a high peak height leads to a high coefficient of friction.

The regression plot is as shown in Figure A8.8 below.

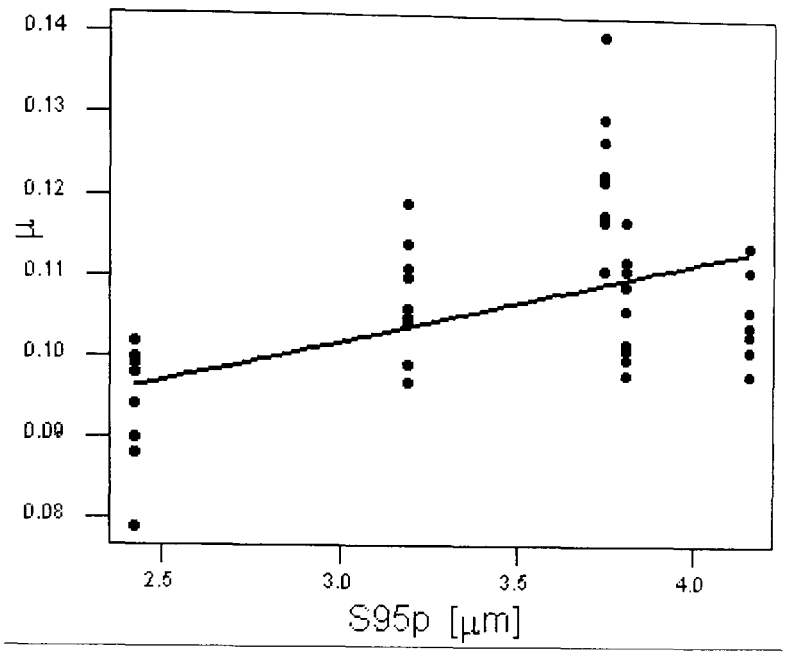

Figure A8.8 – GA coated materials – Regression plot (1MPa and 200mm/s)

A8.1.3.4 Regression analysis - 1MPa and 2mm/s

No correlation could be found for this test combination. All the materials exhibit similar coefficients of friction and the spread around the average is large (see Figure A8.9). This was interpreted to mean that this treatment combination leads to a mixed lubrication region (which is by definition impossible to predict).

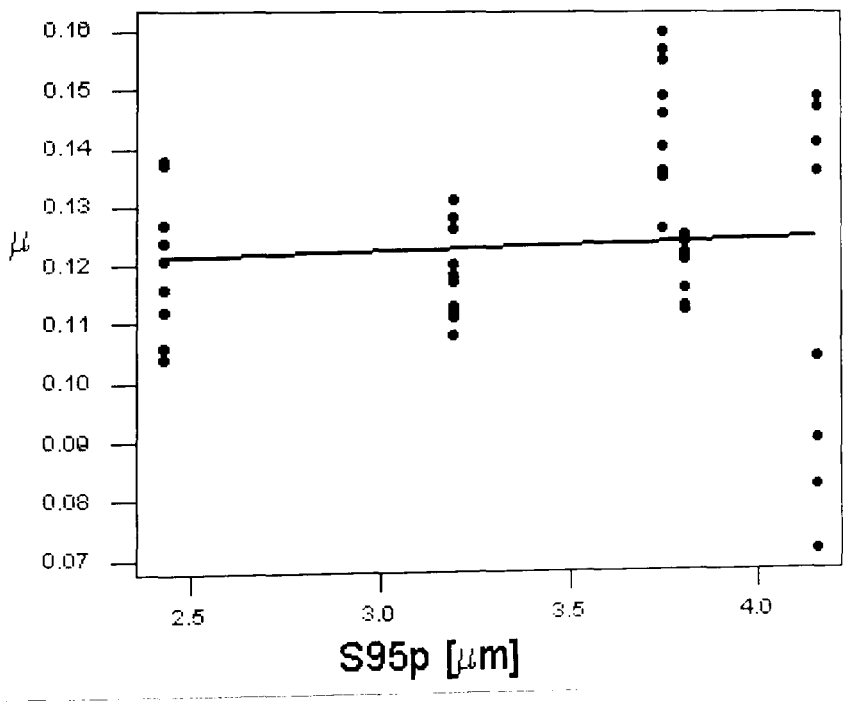

Figure A8.9 – GA coated materials - Regression plot (1MPa, 2mm/s)

A8.2 Statistical analysis of ELO coated materials

This statistical analysis was performed on the range of the ELO coated materials. The list of control factors is presented in Table A8.6 below.

	Level					
Control Factor	**1**	**2**	**3**	**4**	**5**	**6**
A – Oil type	Low viscosity (Aral)	High viscosity (Fuchs)				
B – Sliding velocity	2 mm/s	200 mm/s				
C – Holding pressure	36 KN	107 KN				
D – Material type (topography)	B1	B3	B3	S1	S2	S3

Table A8.6 – ELO coated materials - DOE table

The response was the coefficient of friction (μ). For convenience, in the ANOVA table below all the statistically important factors are highlighted (P value less than 1%).

Source	df	SeqSS	AdjSS	AdjMS	F	P
A	1	0.000630	0.000616	0.000616	5.38	0.021
B	1	0.349188	0.263444	0.263444	2302	0.000
C	1	0.029953	0.027173	0.027173	237.45	0.000
D	5	0.060665	0.060665	0.012133	106.02	0.000
A*B	1	0.000003	0.000032	0.000032	0.28	0.597
A*C	1	0.000003	0.000059	0.000059	0.52	0.473
A*D	5	0.004806	0.004806	0.000961	8.40	0.000
B*C	1	0.005724	0.004850	0.004850	42.39	0.000
B*D	5	0.085032	0.085032	0.017006	148.61	0.000
C*D	5	0.000808	0.000808	0.000162	1.41	0.221
A*B*C	1	0.000051	0.000016	0.000016	0.14	0.706
A*B*D	5	0.004693	0.004693	0.000939	8.20	0.000
A*C*D	5	0.003876	0.003876	0.000775	6.77	0.000
B*C*D	5	0.003781	0.003781	0.000756	6.61	0.000
A*B*C*D	5	0.005741	0.005741	0.001148	10.03	0.000
Error	232	0.026549	0.026549	0.000114		
Total	279	0.581504				

Table A8.7 – ELO coated materials - ANOVA table

Reading the ANOVA Table A8.7 it is possible to state that a large number of factors and high order interactions are statistically significant. This means that friction is influenced by a large number of factors and this influence is extremely complex (interactions of order higher than 2 are difficult to interpret and will not fully explored).

Further, looking at the Stribeck curves (shown in full in appendix 7), all ELO materials showed *"Rich Lubrication"* behaviour (see section 5.5.1 for a description). This means that they appear to have very little pressure dependence at 2mm/s velocity and strongly pressure dependence at

200mm/s velocity. Nevertheless, at 200mm/s velocity all the materials seem to exhibit similar (low) coefficients of friction as shown be the interaction plots below. In order to try to understand all these complex influences, all the main effects were plotted and the results are presented below in Figure A8.11, Figure A8.12 and Figure A8.13.

A8.2.1 Main effect plot for ELO materials

Similarly to the GA coated materials, looking at Table A8.7, one can see that the oil type exhibits a P value of 2.1%. This means that no effect of lubricant type could be (statistically) found. Further, the effect plot, shown in Figure A8.10 (left box in the plot), shows an "almost" flat line.

Conversely, all the other main factors (pressure, velocity and material type) exhibit P values lower than 1% in the ANOVA table shown in Table A8.7, hence they are statistically proven to influence the friction coefficient. Similar information can be obtained from the effect plot shown in Figure A8.10 below, since:

- when the holding **pressure** changes from 1 to 10 MPa, the average coefficient of friction increases by over 20%. Once more this can be interpreted as an increase of contact area between tool and sample due to the increase of the holding pressure.
- In the same way, when the **sliding velocity** changes from 2 to 200 mm/s, the coefficient of friction decreases even more: from 0.170 to 0.100 (41%). This is expected to be the effect of a larger lubricant amount dragged by the moving surface.

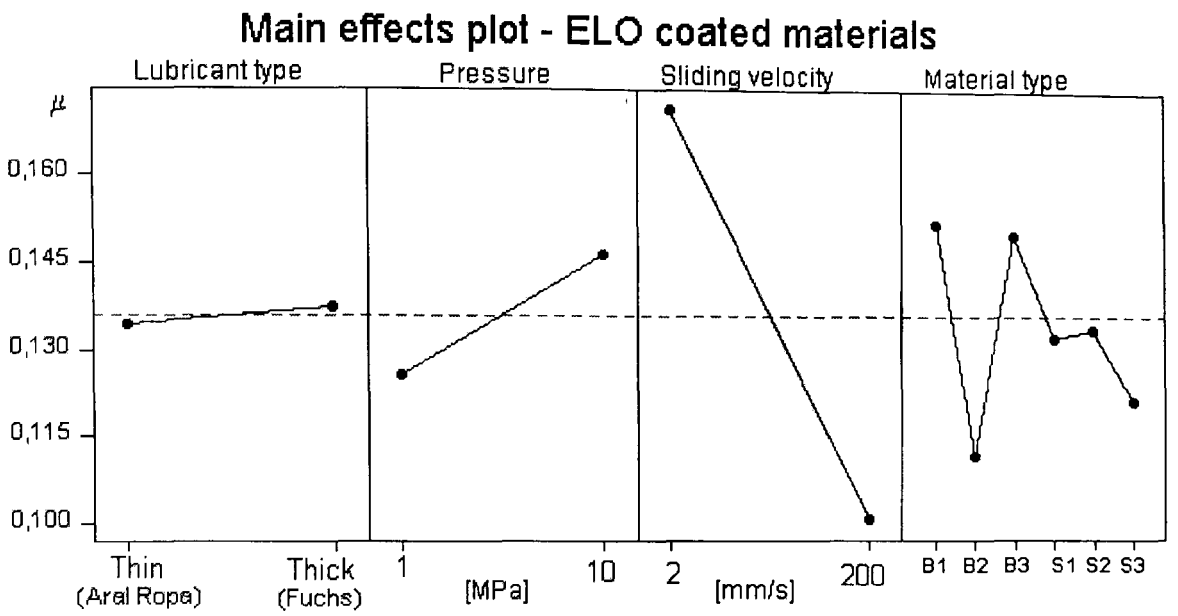

Figure A8.10 – ELO coated materials - Main effect plot

Finally, the effect of material type will be explored through the interaction plot and the Regression analysis given below.

A8.2.2 First order interactions for ELO materials

A8.2.2.1 Lubricant type and material type (A*D)

Similarly to GA coated materials, also during the ELO experiments, it was possible to observe an higher coefficient of friction when lubricating with Fuchs4107S (with the exception of B2).

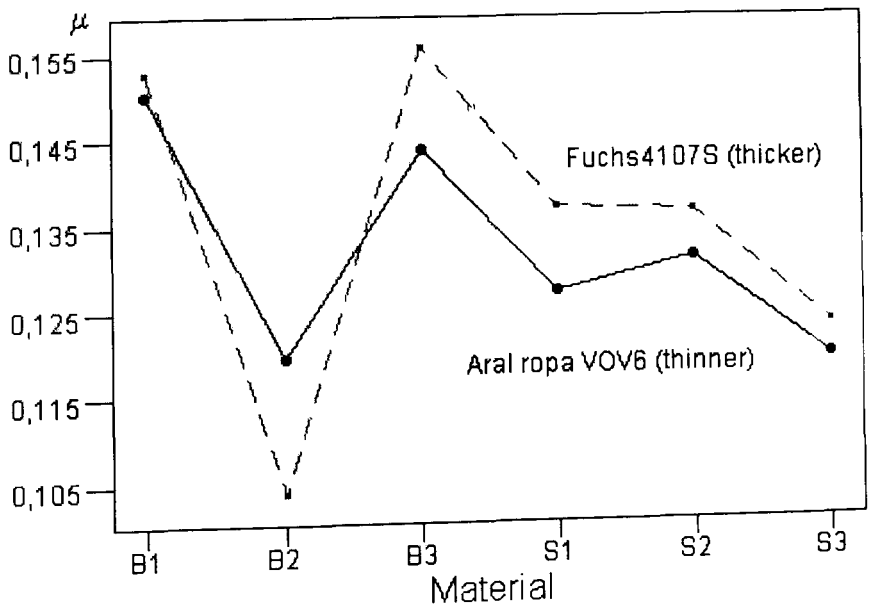

Figure A8.11 – ELO coated materials - Interaction plot (lubricant and material)

Fuchs4107S is the thicker lubricant of the two. This result appears to contrasts with the expectation that thick lubricants produce less friction. Unfortunately, a further analysis of the reason for this behavior is not possible because no details about the composition of any of the employed lubricants will be ever available.

A8.2.2.2 Sliding velocity and pressure (B*C)

As one can read from the interaction plot shown in Figure A8.12 that at high velocities (the red dotted line), the coefficient of friction is more "pressure dependant" (the dotted line is slightly steeper than the black line).

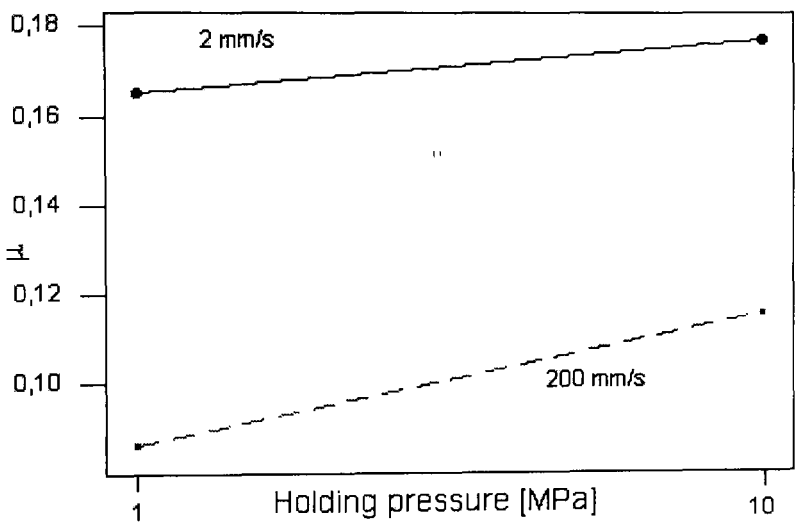

Figure A8.12 – ELO coated materials - Interaction plot (velocity and pressure)

A8.2.2.3 Sliding velocity and material type (B*D)

At 200mm/s sliding velocity all the materials seems to exhibit similar coefficients of friction (see red dotted line in Figure A8.13). Therefore at this sliding velocity, no interaction with any surface topography parameter will ever be possible, since all coefficients of friction are almost the same.

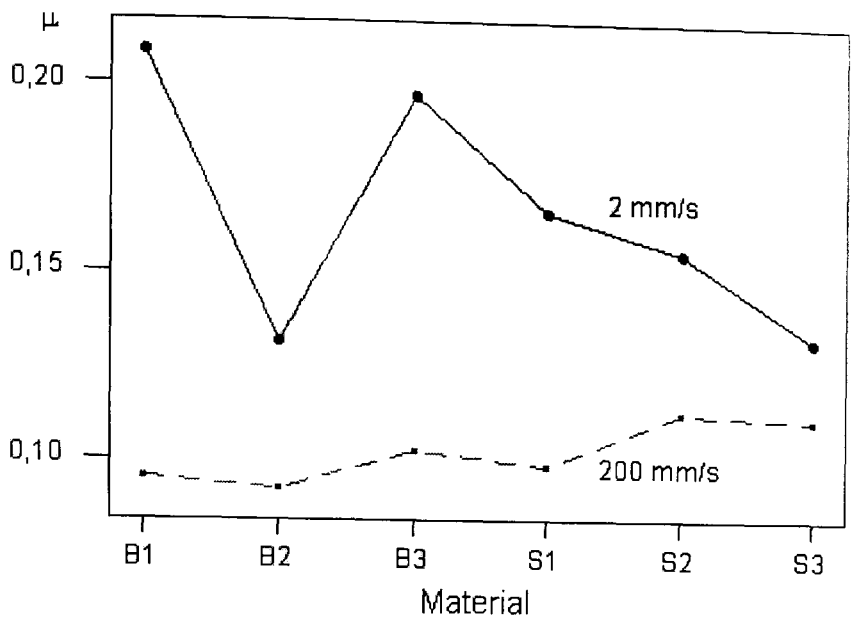

Figure A8.13 – ELO coated materials - Interaction plot (velocity and material)

On the other hand, at 2mm/s sliding velocity the different materials exhibit very different coefficients of friction. This can be considered the most interesting interaction of this experimental analysis since such measurement distribution is a good candidate to exhibit a good correlation with surface topography parameters (described below).

A8.2.3 Correlation analysis for surface parameters

During the ELO friction experiments, the parameter that appears to control the friction coefficient is ***Spa*** (average peak area) calculated at S95p/2 (see section 5.4.1) for all treatment combinations analysed.

This could be interpreted as the following: on larger peak area is more difficult to drag lubricant across than on smaller peak area (see Chapter 5 for details). Further, this observation allows one to estimate the tool penetration into the surface topography being (S95p/2). Because of the interaction between material type and sliding velocity (see Figure A8.13), was analysed for correlation only the 2mm/s experiments.

The ANOVA tables and regression plots for the treatment combinations of interest are presented in Table A8.8 and Figure A8.14.

A8.2.3.1 Regression analysis – 10MPa and thick oil (Fuchs)

Source	DF	SS	MS	F	P
Regression	1	0.030211	0.030211	84.79	0.000
Residual Error	33	0.011758	0.000356		
Total	34	0.041969			

Regression equation found:

$\mu = 0.136 + 4.39$ Spa(S95p/2)

Predictor	Coef	StDev	T	P
Constant	0.136457	0.005617	24.29	0.000
Spa(S95p/2)	4.3889	0.4766	9.21	0.000

Table A8.8 – ELO coated materials - Regression analysis (10MPa, thick oil)

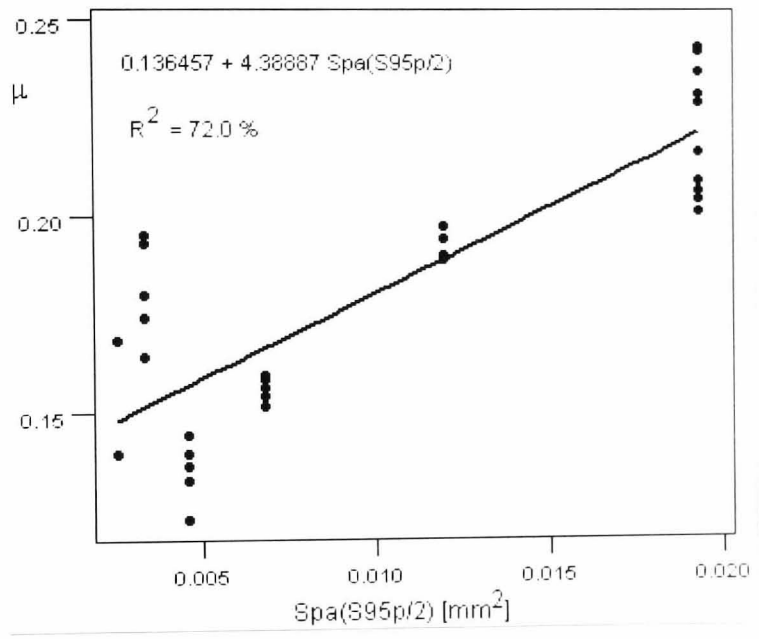

Figure A8.14 – ELO coated materials - Regression plot (10MPa thick oil)

A8.2.3.2 Regression analysis – 1MPa and thick oil (Fuchs)

Source	DF	SS	MS	F	P
Regression	1	0.042527	0.042527	43.77	0.00
Residual Error	33	0.032065	0.000972		
Total	34	0.074593			

Regression equation found:

$\mu = 0.116 + 5.21$ Spa(S95p/2)

Predictor	Coef	StDev	T	P
Constant	0.116233	0.009277	12.53	0.000
Spa(S95p/2)	5.2072	0.7871	6.62	0.000

Table A8.9 – ELO coated materials - Regression analysis (1MPa, thick oil)

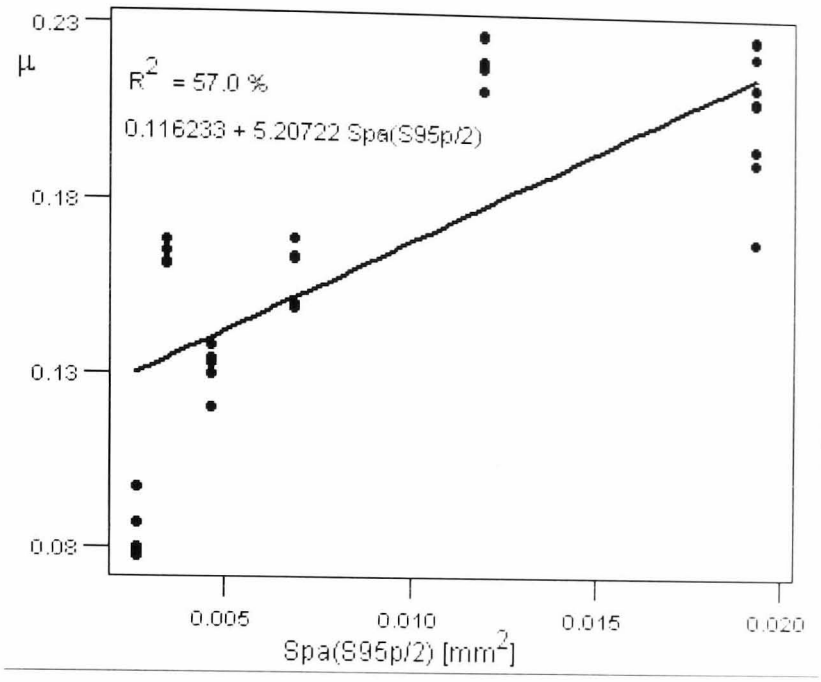

Figure A8.15 – ELO - Regression plot (1MPa thick oil)

A8.2.3.3 Regression analysis – 10 MPa and thinner oil (Aral)

Source	DF	SS	MS	F	P
Regression	1	0.019523	0.019523	74.26	0.000
Residual Error	33	0.008676	0.000263		
Total	34	0.028199			

Regression equation found:

$\mu = 0.141 + 3.53$ Spa(S95p/2)

Predictor	Coef	StDev	T	P
Constant	0.140949	0.004825	29.21	0.000
Spa(S95p/2)	3.5281	0.4094	8.62	0.000

Table A8.10 – ELO - Regression analysis (1MPa, thin oil)

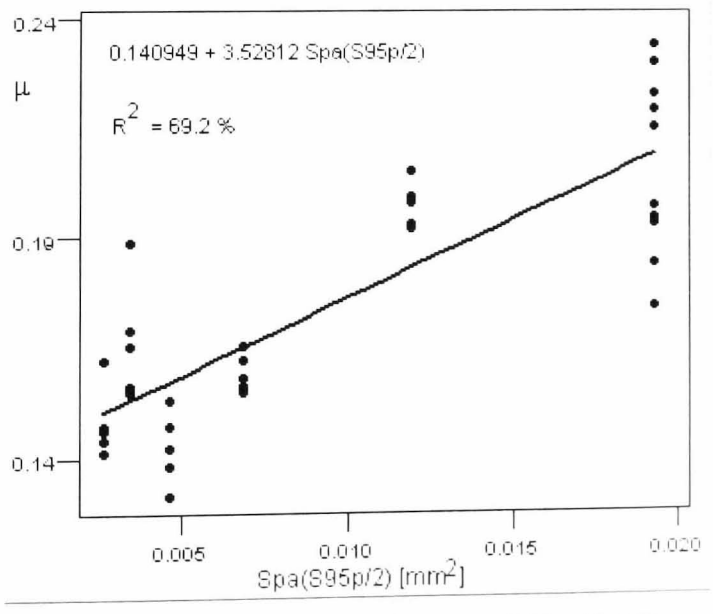

Figure A8.16 – ELO - Regression plot (10MPa thin oil)

A8.2.3.4 Regression analysis for - 1MPa and thinner oil (Aral)

Source	DF	SS	MS	F	P
Regression	1	0.024383	0.024383	64.10	0.000
Residual Error	33	0.012552	0.000380		
Total	34	0.036935			

Regression equation found:

$\mu = 0.126 + 3.94$ Spa(S95p/2)

Predictor	Coef	StDev	T	P
Constant	0.125926	0.005804	21.70	0.000
Spa(S95p/2)	3.9429	0.4925	8.01	0.000

Table A8.11 – ELO - Regression analysis (1MPa, thin oil)

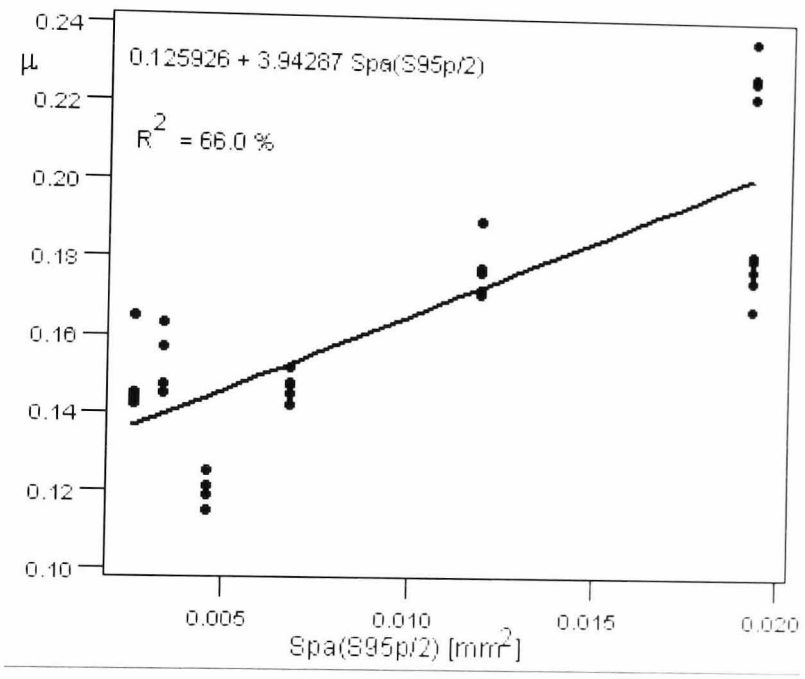

Figure A8.17 – regression plot at 1MPa, 2mm/s for ELO materials

A8.3 Statistical analysis of GI coated materials

This statistical analysis was performed on the range of GI coated materials. The list of control factors is presented in table A8.12 below.

	Level					
Control Factor	**1**	**2**	**3**	**4**	**5**	**6**
A – Oil type	Low viscosity (Aral)	High viscosity (Fuchs)				
B – Sliding velocity	2 mm/s	200 mm/s				
C – Holding pressure	36 KN	107 KN				
D – Material type	B5	H1	H2	S4	S5	S6

Table A8.12 – GI coated materials - DOE table

The response was the coefficient of friction (μ). In the ANOVA table A8.13 below, all the statistically important factors are highlighted (P value less than 1%).

Source	DF	Seq SS	Adj SS	Adj MS	F	P
A	1	0.0000580	0.0000580	0.0000580	1.39	0.240
B	1	0.0324337	0.0324338	0.0324338	777.63	0.000
C	1	0.0276920	0.0276920	0.0276920	663.94	0.000
D	5	0.0387910	0.0387910	0.0077582	186.01	0.000
A*B	1	0.0000353	0.0000353	0.0000353	0.85	0.359
A*C	1	0.0000216	0.0000216	0.0000216	0.52	0.473
A*D	5	0.0065030	0.0065030	0.0013006	31.18	0.000
B*C	1	0.0108273	0.0108273	0.0108273	259.59	0.000
B*D	5	0.0175896	0.0175896	0.0035179	84.35	0.000
C*D	5	0.0024965	0.0024965	0.0004993	11.97	0.000
A*B*C	1	0.0001093	0.0001093	0.0001093	2.62	0.107
A*B*D	5	0.0053167	0.0053167	0.0010633	25.49	0.000
A*C*D	5	0.0025940	0.0025940	0.0005188	12.44	0.000
B*C*D	5	0.0053824	0.0053824	0.0010765	25.81	0.000
A*B*C*D	5	0.0016495	0.0016495	0.0003299	7.91	0.000
Error	192	0.0080080	0.0080080	0.0000417		
Total	239	0.1595079				

Table A8.13 – GI coated materials - ANOVA table

With reference to this ANOVA Table A8.13 above, one can see that all the control factors (beside oil type) and all the interactions with factor "D" (material) are statistically significant. This can be interpreted as every material behave in its own peculiar way (no group comparisons are possible).

In fact, half the GI coated materials (see GI Stribeck curves in Appendix 7) showed a "*poor lubrication*" regime (H1, S4 and S6) whilst the others showed a "*rich lubrication*" regime (see section 5.5.1 for description).

A8.3.1 Main effect plot for GI materials

Note that in table A8.13, no lubricant effect could be observed since the P value for factor "A" is always above 1%. Nevertheless, because of the interaction between lubricant and material type, a correlation analysis was performed for the different lubricant types.

Both sliding velocity and holding pressure have a P value lower than 1% in the ANOVA table A8.13. Hence, there is statistical evidence to show that all factors except the type of oil influence the friction coefficient and their interpretation is similar to the one given for the other coated materials. Nevertheless, the main effect plot for all the control factors is presented in Figure A8.18.

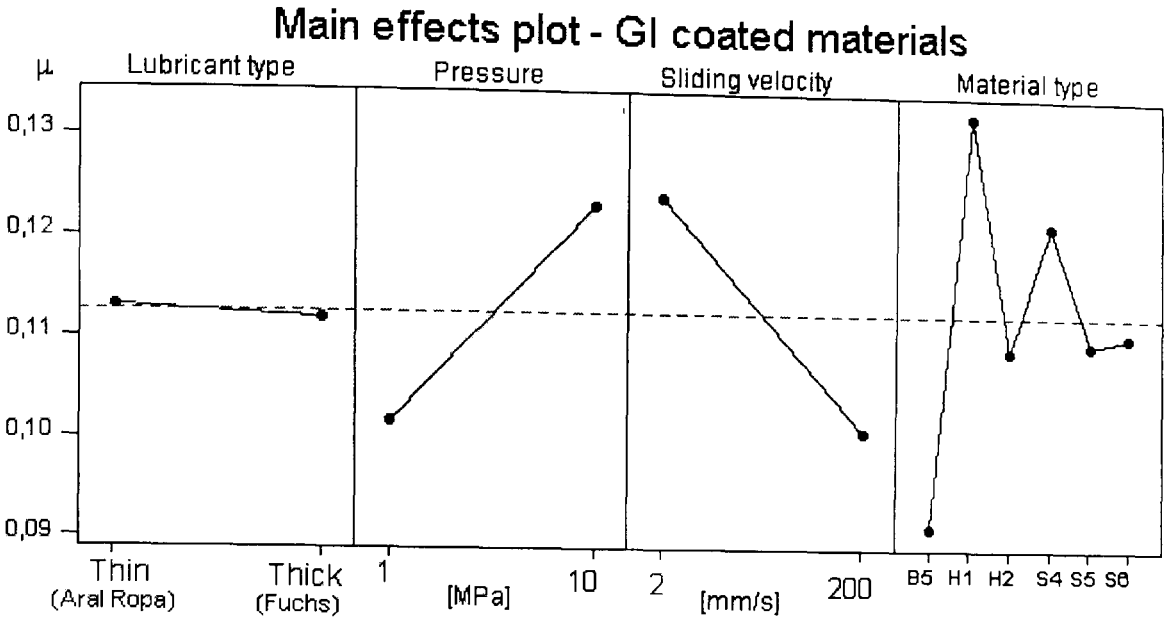

Figure A8.18 – GI coated materials - Main effect plot

Finally, the effect of material type will be explored through the interaction plot and the Regression analysis given below.

A8.3.2 First order interactions for GI materials

A8.3.2.1 Lubricant type and material type (A*D)

During the GI experiments, and as with both ELO and GA coated materials, a high coefficient of friction could be observed when lubricating with Fuchs4107S (with the exception of B5 where it seems to be the opposite), as shown in Figure A8.19 below.

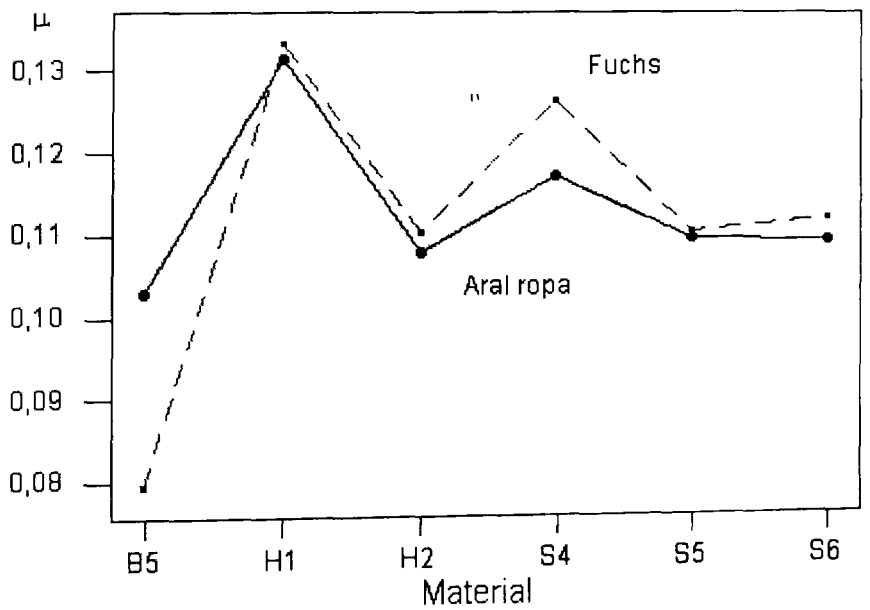

Figure A8.19 – GI - Interaction plot (oil and material)

A8.3.2.2 Sliding velocity and pressure (B*C)

As one can be read from the interaction plot of Figure A8.20 below, at high velocities (red dotted line), the coefficient of friction increases at high pressures (see dotted line slightly steeper than black line in Figure A8.20 below).

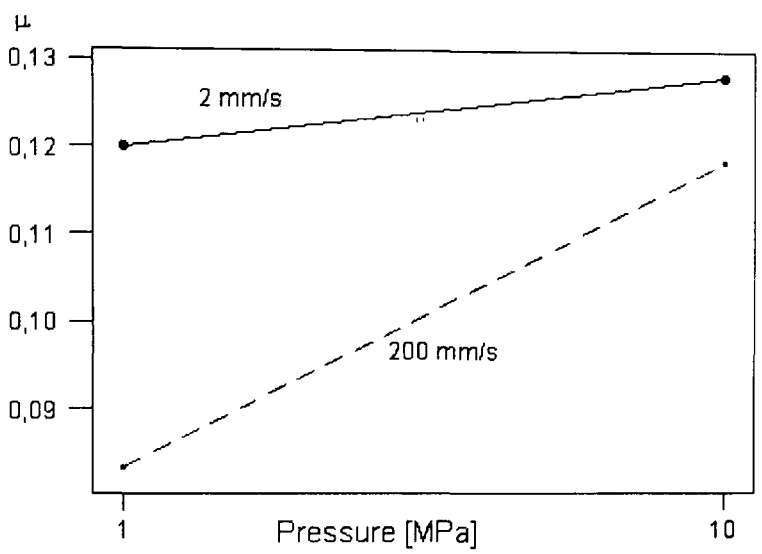

Figure A8.20 – GI - Interaction plot (velocity and pressure)

A8.3.2.3 Sliding velocity and material type (B*D)

Contrary to what was observed during the ELO experiments, at 200mm/s sliding velocity the GI experiments exhibit very different coefficients of friction, whereas at low velocity. The friction coefficient spread reduces dramatically at 2mm/s (see Figure A8.21 below).

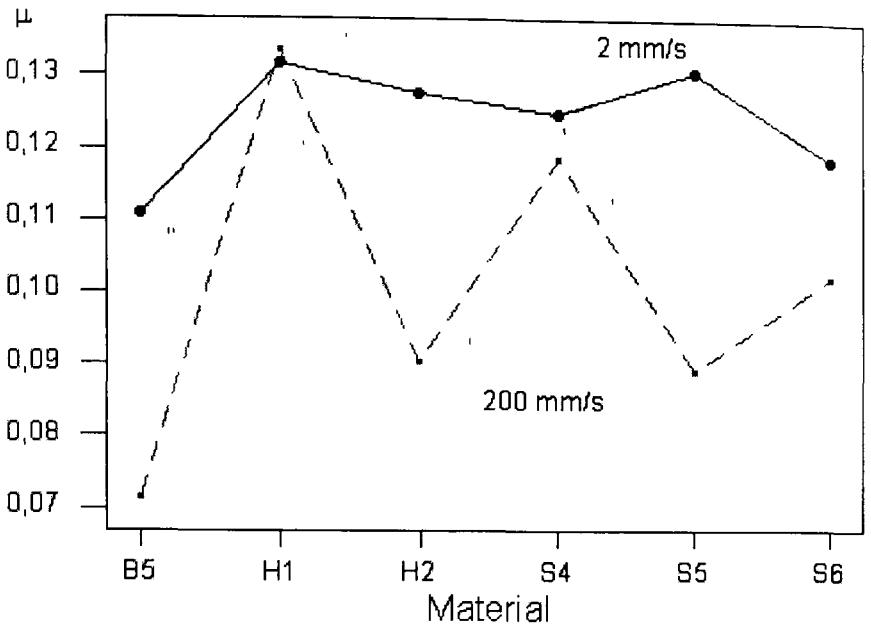

Figure A8.21 – GI - Interaction plot (velocity and material)

Further, some materials (H1 S4 and S6) exhibit very little or no velocity effect (see the points of the two lines almost overlapping) while all the other materials exhibit a lower coefficient of friction at higher velocities.

The behaviour of the H1, S4 and S6 group is typical of GA ("poorly lubricated" materials), while the behaviour of the remainder is typical of ELO ("richly lubricated" materials).

A8.3.2.4 Pressure and material (C*D)

Similarly to the previous interaction, the table A8.13 ANOVA P value for this interaction showed an interaction between these two factors (material and pressure). In this interaction "S4", "S5" and "S6" do not increase their friction coefficient because of pressure as much as is the case for the other materials (they are less pressure dependant). This is seen in the following Figure A8.22 where, although the two lines tend to follow each other, there is variability.

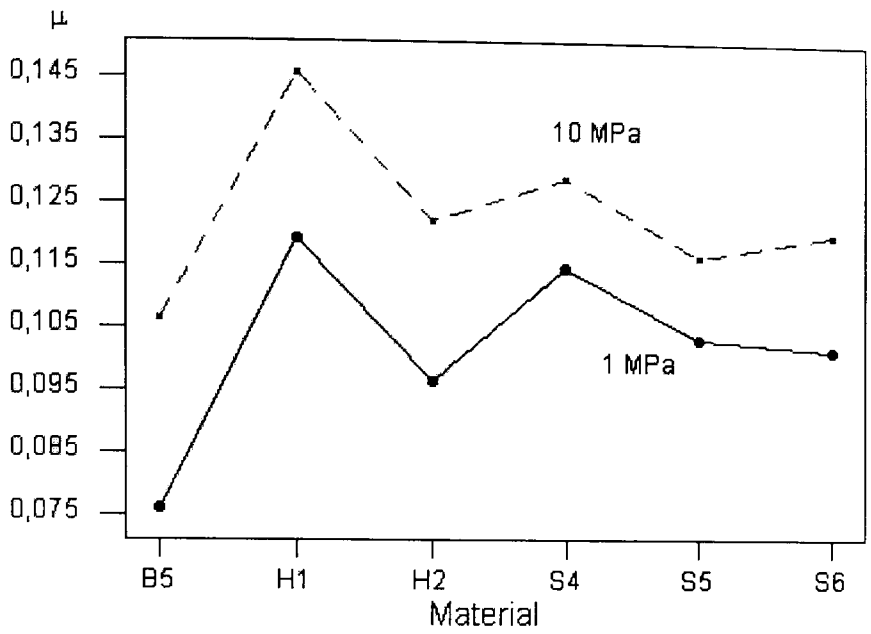

Figure A8.22 – GI - Interaction plot (pressure and material)

A8.3.3 Correlation analysis with surface parameters

The GI coated materials tend to exhibit two different kinds of behaviors, as follows:

- H1, S4 and S6 did behave similarly to GA coated material ("poor lubrication")
- B5, H2, S5 instead behaved similarly to ELO coated materials ("rich lubrication")

No correlation between friction and surface topography could found for these experiments. Nevertheless, when testing at 200mm/s velocity and 10Mpa pressure (both lubricant types), a correlation was found between friction coefficient and real tool pressure (measured on the samples).

The statistical analysis below (Table A8.14 and Figure A8.23) proves a good correlation between this measured pressure and the coefficient of friction.

A8.3.3.1 Regression analysis - 10MPa 200mm/s, thin oil (Aral)

Source	DF	SS	MS	F	P
Regression	1	0.010471	0.010471	70.45	0.000
Residual Error	38	0.005648	0.000149		
Total	39	0.016119			

The regression equation is
μ = - 1.05 + 0.118 MPress
(MPress is the measured pressure)

Predictor	Coef	StDev	T	P
Constant	-1.0531	0.1394	-7.55	0.000
MPress	0.11764	0.01402	8.39	0.000

Table A8.14 – GI – Regression analysis (10MPa, 200mm/s thin oil)

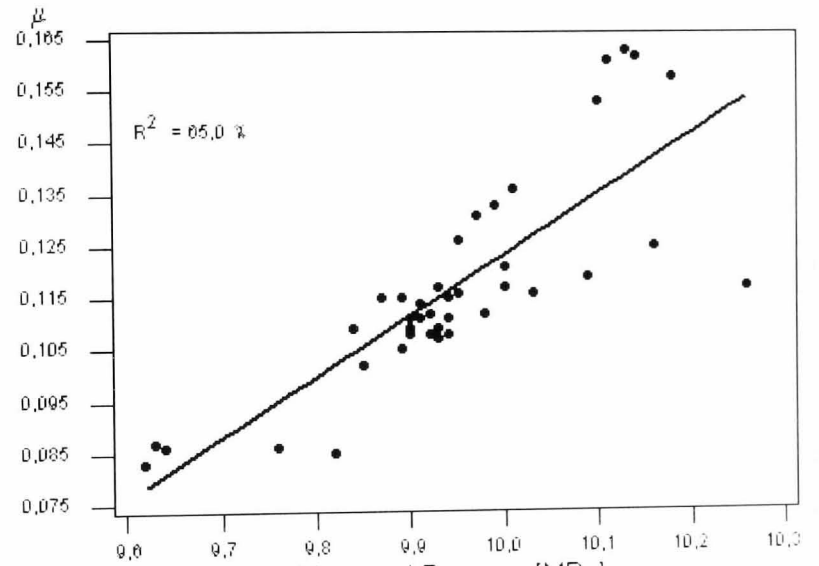

Figure A8.23 – GI - Regression plot (10MPa, 200mm/s thin oil)

Note that, for all the other testing conditions, no correlation with any control or measured parameter could be found (table A8.15 and Figure A8.24).

A8.3.3.2 Regression analysis - 10MPa, 200mm/s, thick oil (Fuchs)

Source	DF	SS	MS	F	P
Regression	1	0.0032820	0.0032820	13.03	0.001
Residual Error	38	0.0095738	0.0002519		
Total	39	0.0128558			

Regression equation found
μ = - 0.469 + 0.0590 MPress

Predictor	Coef	StDev	T	P
Constant	-0.4691	0.1620	-2.90	0.006
MPress	0.05903	0.01636	3.61	0.001

Table A8.15 – GI– Regression analysis (10MPa, 200mm/s thick oil)

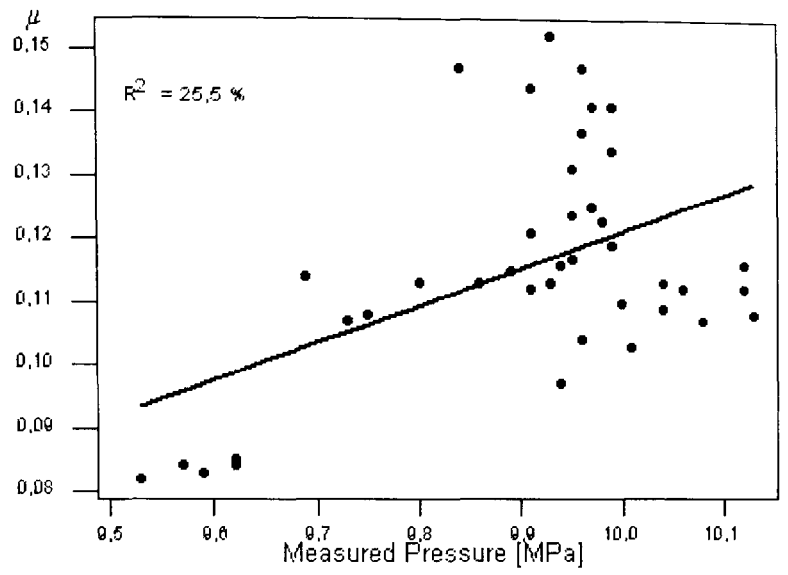

Figure A8.24 – GI - Regression plot (10MPa, 200mm/s thick oil)

A9. Deep drawing statistical analysis

A9.1 Correlation between NFH and %Draw

Two different measurements were taken during the MSD experiments, these were the %Draw and Fracture Height.

The aim of this initial investigation is to assess whether these two measurements provide the same information. In order to test this, a regression analysis was performed between the two. If the result is that the two measurements are correlated, then one of the two can be considered to be redundant. The statistical procedure is described in Appendix A4.5 and the results are shown in the Table A9.1. In this case, the p value limit is 5% since we are running only one test at any one time. Thus, if the p value of any factor is less than 0.05, there is statistical evidence that a correlation exists. In Table A9.1, the P value is less than 0.05, hence there is a correlation, as shown in the graph of Figure A9.1

Source	DF	SS	MS	F	P
Regression	1	1164.1	1164.1	397.44	0.000
Residual Error	34	99.6	2.9		
Total	35	1263.7			

Regression equation found:
NFH = 20.6 + 1.39 * %Draw

Predictor	Coef	StDev	T	P
Constant	20.5996	0.4994	41.25	0.000
%Draw	1.38846	0.06965	19.94	0.000

S = 1.711 R-Sq = 92.1% R-Sq(adj) = 91.9%

Table A9.1 – Initial investigation – regression analysis

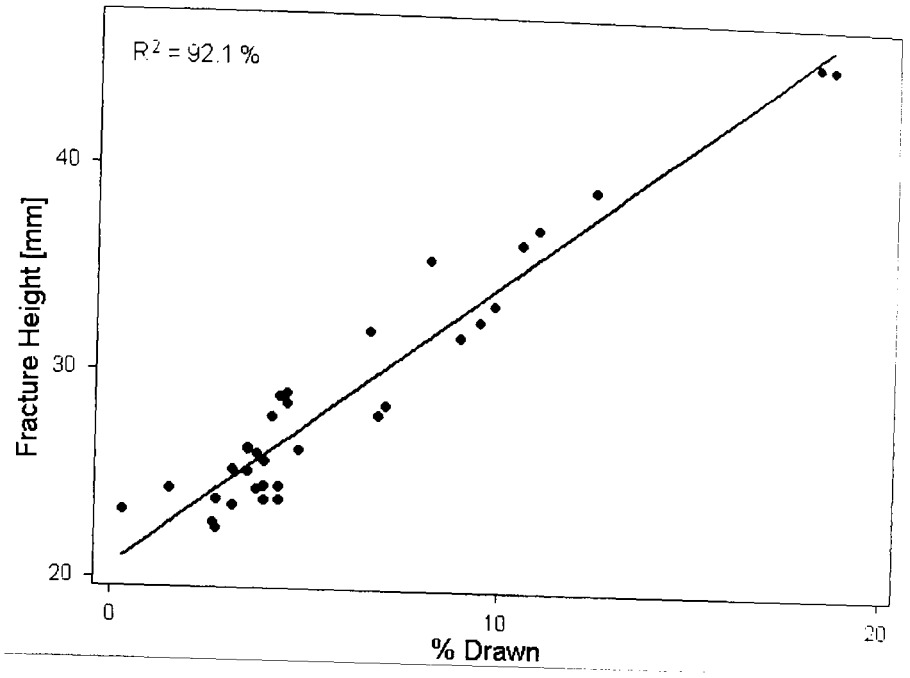

Figure A9.1 – Initial investigation – regression plot

The lack of fit test (see appendix 4 for details) proved that this correlation fits well. Thus, we can discard one of these and need only to use one for the remainder of this work. The one selected is the fracture height (FH) since this is the easiest to measure.

A9.2 Investigation of coating type

The aim of this set of experiments was to assess whether coating type or any interaction with other control factors affects the material drawability.

Unfortunately, there were insufficient materials available to run a full factorial because the companies were constrained by time and production requirements. Thus, we did not receive a full set of materials so could only run a fractional factorial set of tests. The list of control factors is presented in Table A9.2.

	Level 1	**Level 2**	**Level 3**
A – Material type (coating)	S2 (ELO)	B5 (GI)	B8 (GA)
B – Lubricant type	Aral Ropa	Fuchs	
C – Blankholder force	36 KN	107 KN	

Table A9.2 – Initial investigation – DOE table

The ANOVA table of these results is shown in Table A9.3 where the response is the normalised fracture height (NFH%), as is described in chapter 6 (Equation 6.2). Again, the significant factors having a P value less than 0.01 are highlighted.

Source	df	Seq SS	Adj SS	Adj MS	F	P
Coating	2	439.77	439.77	219.88	136.02	0.007
Lub	1	1.02	1.02	1.02	0.63	0.511
BHF	1	736.54	736.54	736.54	455.61	0.002
Coating*Lub	2	2.69	2.69	1.34	0.83	0.546
Coating*BHF	2	109.72	109.72	54.86	33.93	0.029
Lub*BHF	1	0.08	0.08	0.08	0.05	0.845
Error	2	3.23	3.23	1.62		
Total	11	1293.04				

Table A9.3 – Initial investigation – ANOVA table

From the ANOVA Table A9.3, it is possible to see that the coating type (factor "A") and blankholder force (factor "C") are the only two which are statistically significant.

In order to try to understand further the influence of these control factors have on drawability, the main effects were plotted and the result is presented in Figure A9.2. These curves represent the influence of the factors upon drawability. Here the higher the value of NFH%, the lower the coefficient of friction.

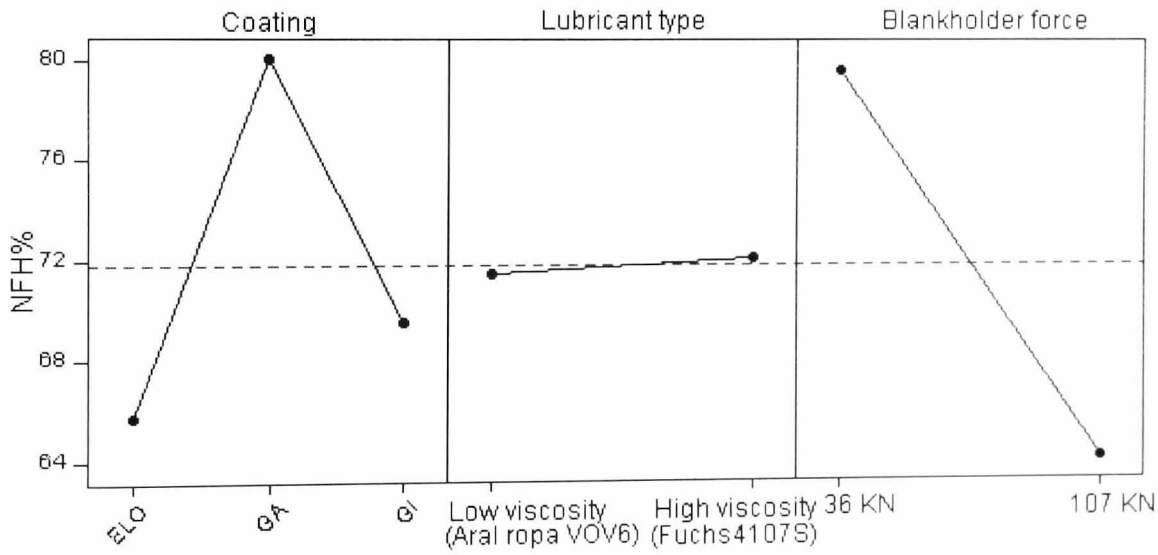

Figure A9.2 – Initial investigation – Main effect plot

Note that GA has the highest NFH% while ELO has the lowest.

A9.3 Statistical analysis of ELO coated materials

The aim of this experimental set was to assess the factor surface topography (or any interaction) with drawability. The list of control factors is presented in Table A9.4. For the reasons mentioned above in section A9.2, this design is based on a fraction factorial.

	Level 1	Level 2	Level 3	Level 4
A – Material type (topography)	B2	B3	S2	S3
B – Lubricant type	Aral Ropa	Fuchs		
C – Blankholder force	36 KN	107 KN		

Table A9.4 – ELO coated materials – DOE table

The response is the normalised fracture height (NFH%) described in chapter 6 (Equation 6.2). In the ANOVA Table A9.5, those factors which are significant and have a P value less than 0.01 are highlighted.

Source	DF	Seq SS	Adj SS	Adj MS	F	P
A	3	546.15	546.15	182.05	27.96	0.099
B	1	91.74	91.74	91.74	14.09	0.033
C	1	732.35	732.35	732.35	112.47	0.002
A*B	3	59.24	59.24	19.75	3.03	0.193
A*C	3	135.98	135.98	45.33	6.96	0.073
B*C	1	0.02	0.02	0.02	0.00	0.962
Error	3	19.54	19.54	6.51		
Total	15	1585.01				

Table A9.5 – ELO coated materials – ANOVA table

The ANOVA table shows that the significant factors are the material type (factor "A") and blankholder force (factor "C"). None of the interactions were found to be important.

In order to try to understand the kind of influence of these control factors, the main effects were plotted and the result is presented in Figure A9.3. These curves represent the influence of surface topography upon drawability. Here the higher the NFH%, the lower the coefficient of friction.

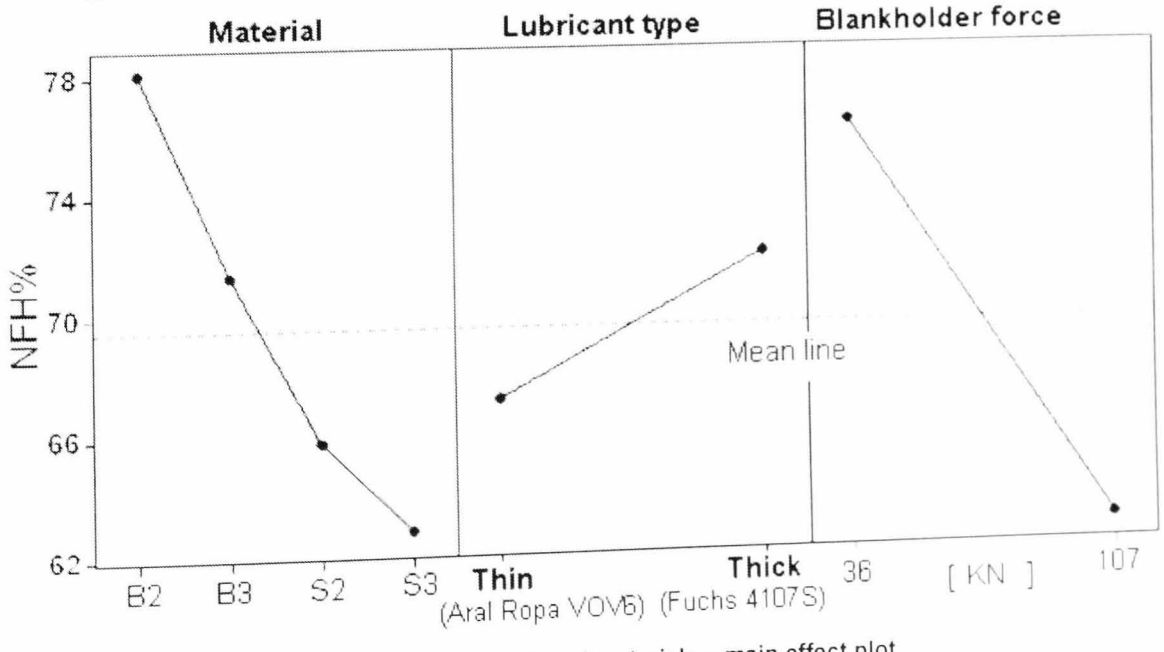

Figure A9.3 – ELO coated materials – main effect plot

Note that in the material plot, the materials are arranged in order of their hardness since B2 has the highest yield strength (181MPa) whilst B3 has the lowest (135MPa). Although the interaction between material and blankholder was statistically not significant, their interaction ("A*C") was since in the interaction plot of figure A9.4, the line for B2 is almost horizontal.

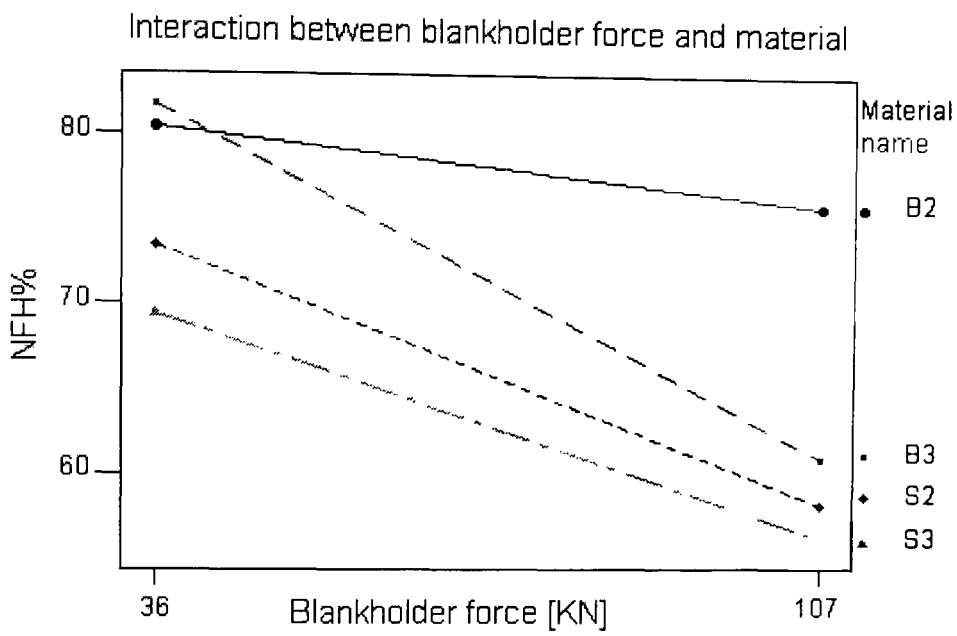

Figure A9.4 – ELO coated materials – interaction plot (blankholer force and material)

Unfortunately, the mechanical properties cannot be completely separated from the topography effect upon friction (as stated in chapter 5 and 6), therefore the materials effect could not be ordered by employing any surface parameter.

Nevertheless, a regression analysis was attempted and is presented below.

A9.4 Regression analysis for ELO - 107KN Aral

Unfortunately, no statistical evidence was found to correlate NFH% with the area fraction of contact since the P value in the ANOVA Table A9.6 is well over the 5% required for the regression analysis.

Source	DF	SS	MS	F	P
Regression	1	0,64	0,64	0,02	0,916
Residual Error	1	36,31	36,31		
Total	2	36,95			

Regression equation found:
NFH% = 74,5 + 103 Spa(S95p/2)

Predictor	Coef	StDev	T	P
Constant	74.477	6.554	11.36	0.056
Spa(S95p/2)	103.2	779.6	0.13	0.916

S = 6.026 R-Sq = 1.7% R-Sq(adj) = 0.0%

Table A9.6 – ELO coated materials – regression analysis with Spa

A further regression analysis was attempted between NFH% and the material "yield strength" (YS), as is shown in Table A9.7. Although the regression index is now improved (R^2 = 71,6%), the high P value shows that there is no correlation because of the small number of observations (only four materials).

Source	DF	SS	MS	F	P
Regression	1	173.98	173.98	5.04	0.154
Error	2	69.01	34.50		
Total	3	243,00			

Regression equation found:
NFH% = -2.63436 + 0.395967 YS

S = 5.87438 R-Sq = 71.6 % R-Sq(adj) = 57.4 %

Table A9.7 – ELO coated materials – regression analysis with YS

The regression plot is presented in Figure A9.5.

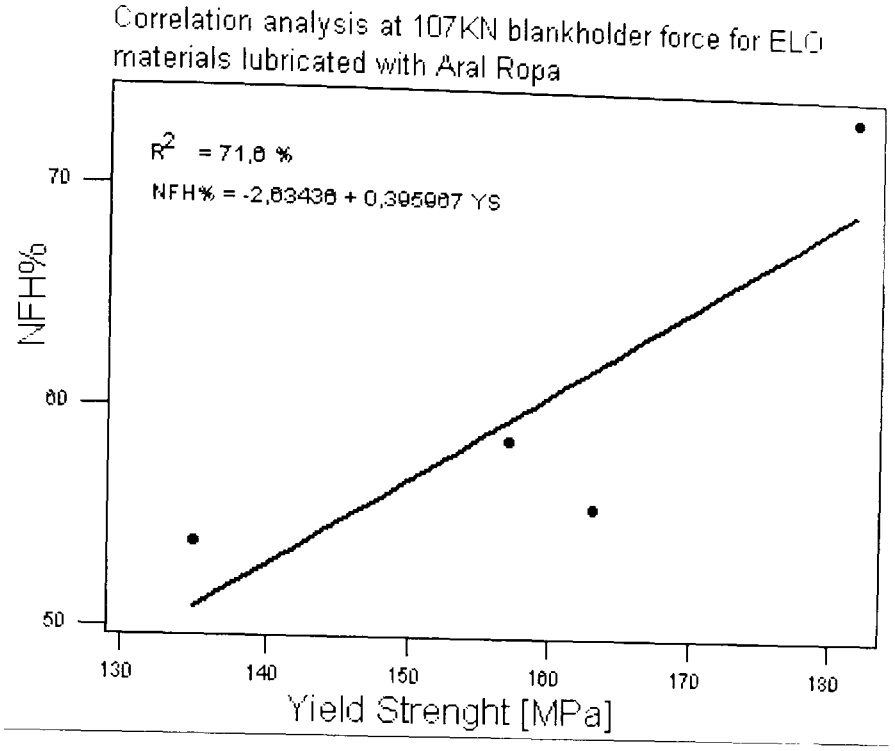

Figure A9.5– ELO coated materials – regression plot with YS

Note the small number (4) of points, which are highly scattered.

A9.5 Statistical analysis of GA coated materials

This statistical analysis was performed on the full range of the GA coated materials using a fractional factorial for the reasons mentioned above. The list of control factors is presented in Table A9.8.

Control Factor	Level 1	Level 2	Level 3
A – Material type (topography)	B8	H14	H17
B – Lubricant type	Aral Ropa	Fuchs	
C – Blankholder force	36 KN	107 KN	

Table A9.8 – GA coated materials – DOE table

The response was the Normalised fracture height (NFH%) described in chapter 6 (equation 6.2). For convenience, in the ANOVA table below all the statistically important factors are highlighted in green (P value less than 0.01).

Source	DF	Seq SS	Adj SS	Adj MS	F	P
A	2	41.477	41.477	20.738	244.30	0.004
B	1	10.940	10.940	10.940	128.87	0.008
C	1	160.778	160.778	160.778	1894.00	0.001
A*B	2	0.143	0.143	0.072	0.84	0.543
A*C	2	28.007	28.007	14.003	164.96	0.006
B*C	1	0.300	0.300	0.300	3.54	0.201
Error	2	0.170	0.170	0.085		
Total	11	241.814				

Table A9.9 – GA coated materials – ANOVA table

The ANOVA table shows three factors are significant and one interaction, these are A, B and C and A*C. In order to try to understand the kind of influence of these control factors, the main effects were plotted and the result is presented in Figure A9.6.

These curves represent the influence of surface topography upon drawability. The higher the NFH%, the lower is the coefficient of friction.

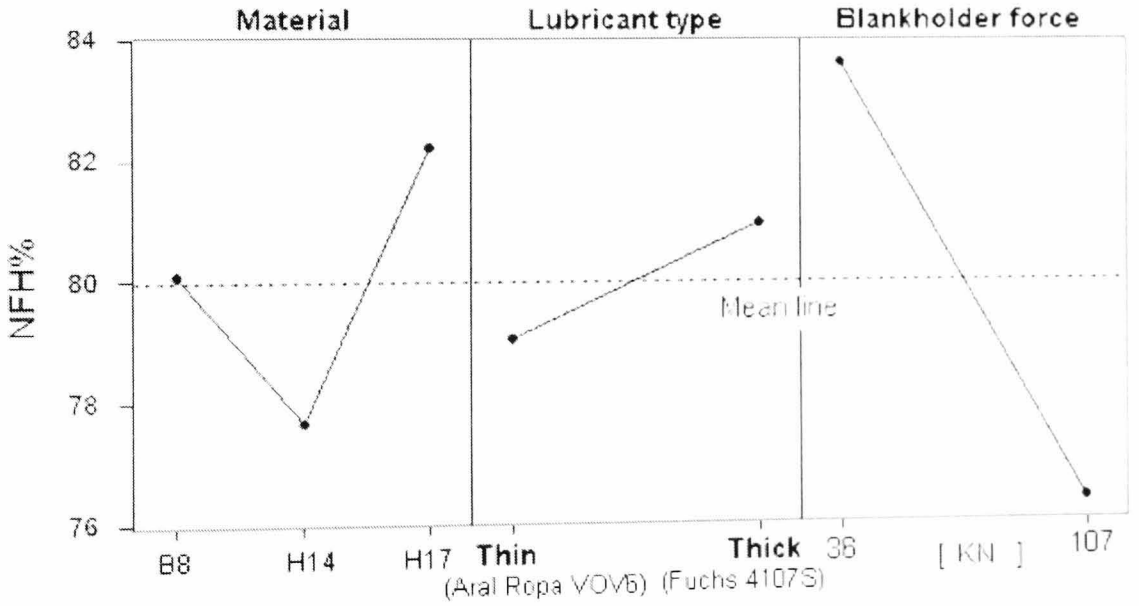

Figure A9.6 – GA coated materials – main effect plot

Note that H14 has the lowest yield strength (221MPa) while H17 has the highest (387MPa). This time the interaction between material and blankholder force was statistically significant and their interaction ("A*C") is shown in Figure A9.7.

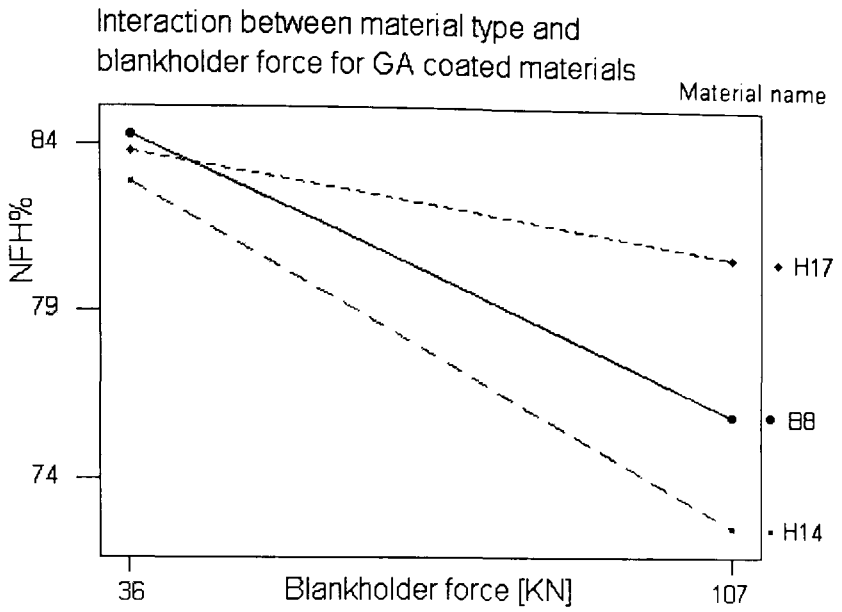

Figure A9.7 – GA coated materials – interaction plot (blankholder force and material)

The highest yield strength material (H17) is less dependant on the blankholder force since the line is fairly flat whereas the lowest strength material (H14) has the higher dependence (steepest line on the above graph). This further proves that mechanical properties cannot be totally separately from topography and friction in deep drawing. Nevertheless, a regression analysis was attempted and is presented below.

A9.6 Regression analysis for GA - 107KN Aral

Unfortunately, no significant statistical evidence was found to link NFH% can with the area fraction of contact since the P value of the ANOVA Table A9.10 is well over the required 5%.

Source	DF	SS	MS	F	P
Regression	1	18.70	18.70	1.02	0.496
Residual Error	1	18.25	18.25		
Total	2	36.95			

Regression equation found:
NFH% = 90,1 - 38,8 α(h1g)

Predictor	Coef	StDev	T	P
Constant	90.12	14.93	6.04	0.105
α(h1g)	-38.80	38.32	-1.01	0.496

S = 4.272 R-Sq = 50.6% R-Sq(adj) = 1.2%

Table A9.10 – GA coated materials – regression analysis with α

A further regression analysis was attempted between NFH% and the material "yield strength" (YS). The ANOVA Table A9.11 shows that, although the regression index is now improved (R^2 = 94,6%), there is still no statistical

evidence for a correlation due to the small number of observations (only three materials).

Source	DF	SS	MS	F	P
Regression	1	34.962	34.962	17.59	0.149
Residual Error	1	1.988	1.988		
Total	2	36.950			

Regression equation found:
NFH%= 61.2 + 0.0482 YS

S = 1.410 R-Sq = 94.6% R-Sq(adj) = 89.2%

Table A9.11 – GA coated materials – regression analysis with YS

The regression plot is presented in Figure A9.8.

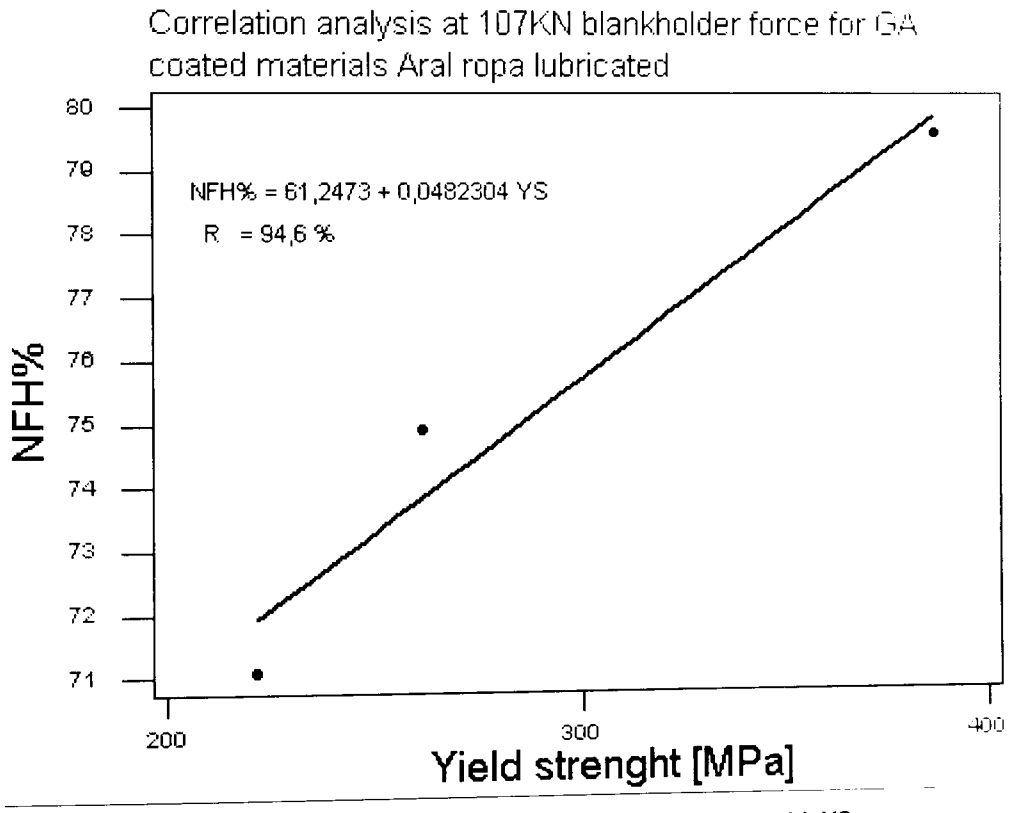

Figure A9.8 – GA coated materials – regression plot with YS

A9.7 Statistical analysis of GI coated materials

This statistical analysis was performed on the range of the GI coated materials using a fractional factorial due to the reasons mentioned above. The list of control factors is presented in Table A9.12.

	Level					
Control Factor	**1**	**2**	**3**	**4**	**5**	**6**
A – Material type	B5	B6	H5	H8	S5	S6
B – Lubricant type	Aral Ropa	Fuchs				
C – Blankholder force	36 KN	107 KN				

Table A9.12 – GI coated materials – DOE table

The response was the Normalised fracture height (NFH%) described in chapter 6 (equation 6.2). For convenience, in the ANOVA Table A9.13 all the statistically important factors are highlighted (P value less than 0.01).

Source	DF	Seq SS	Adj SS	Adj MS	F	P
A	5	1872.29	1872.29	374.46	886.22	0.000
B	1	2.75	2.75	2.75	6.50	0.051
C	1	949.79	949.79	949.79	2247.84	0.000
A*B	5	11.20	11.20	2.24	5.30	0.046
A*C	5	652.20	652.20	130.44	308.71	0.000
B*C	1	4.38	4.38	4.38	10.37	0.023
Error	5	2.11	2.11	0.42		
Total	23	3494.72				

Table A9.13 – GI coated materials – ANOVA table

The ANOVA Table A9.13 shows that the factors "A" and "C" and the interaction between material type and blankholder force ("A*C") were significant with respect to NFH%.

In order to try to understand the kind of influence of these control factors, the main effects were plotted and the result is presented in Figure A9.9. These curves represent the influence of surface topography upon drawability. The higher the NFH% value, the lower is the coefficient of friction.

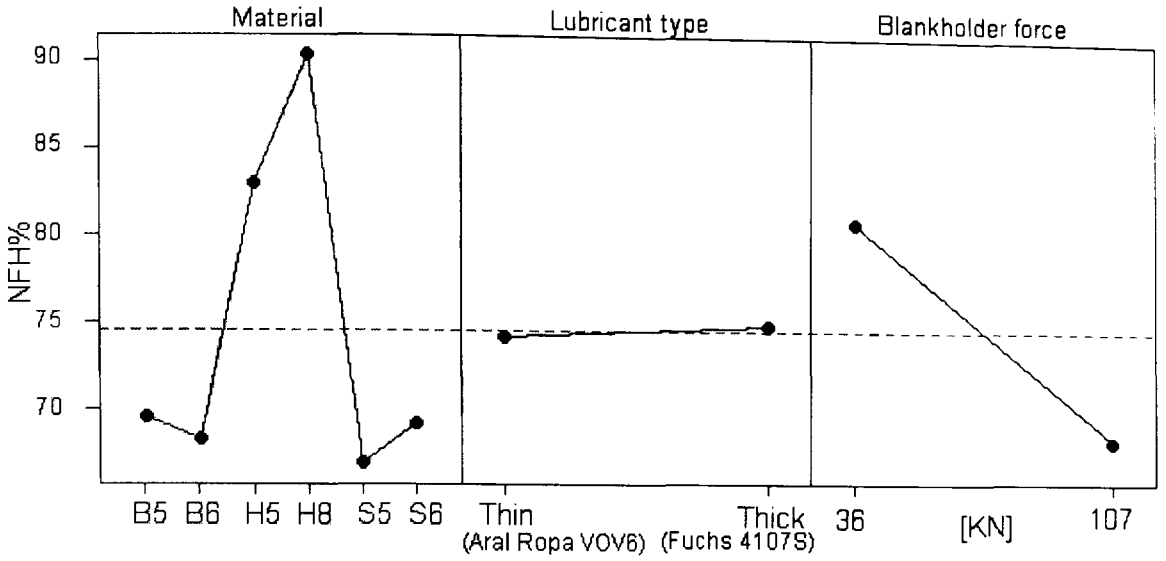

Figure A9.9 – GI coated materials – main effect plot

The results seem similarly to the GA results in that the B6 and S5 materials have the lowest yield strength (less than 160MPa) while H8 has the highest (256MPa). Once more the interaction between material and blankholder force was statistically significant and their interaction ("A*C") is shown in Figure A9.10.

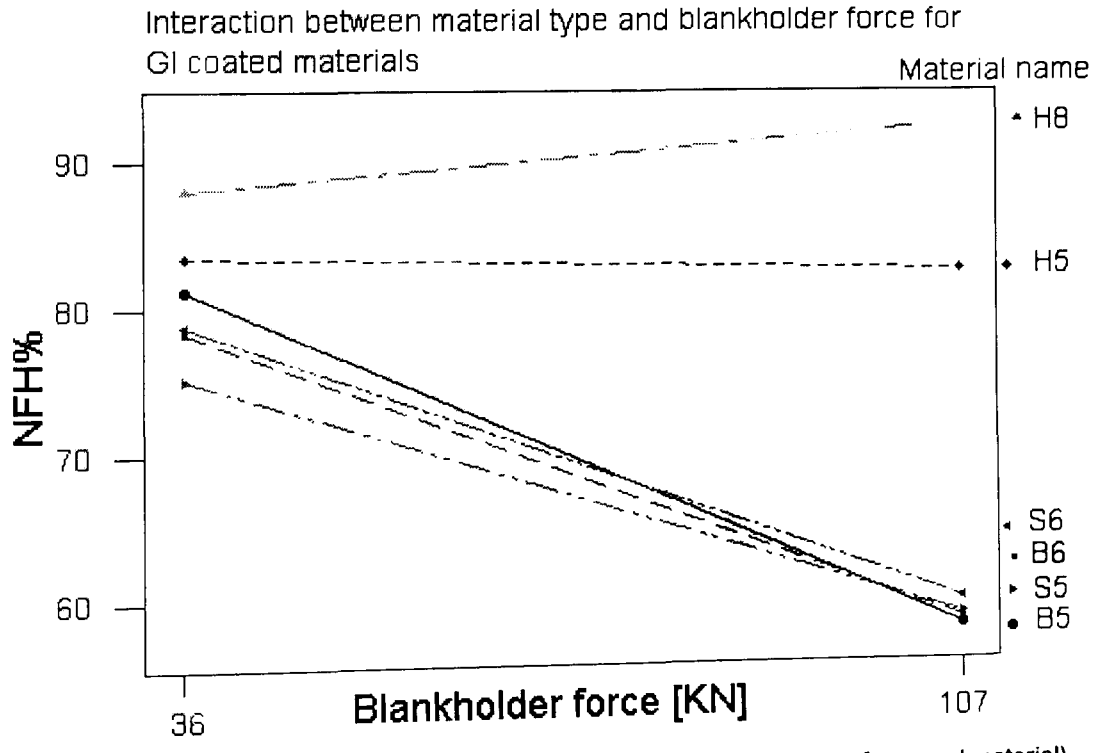

Figure A9.10 – GI coated materials – interaction plot (blankholder force and material)

The interaction between yield strength and blankholder force noticed during the previous drawability analyses are applicable to the GI coated materials. In fact, the highest yield strength material (H8) is less dependant on blankholder

force since the line is flatter, than the lowest one (B5) which, conversely has the higher dependence (the steepest line in Figure A9.10).

A regression analysis between material and drawability was undertaken and the resets are presented below.

A9.8 Regression analysis for GI - 107KN Aral

Because a higher number of test observations could be undertaken (six materials in total), strong statistical evidence was found to support the view that NFH% is influenced by the material yield strength since the P value of the ANOVA Table A9.14 is below the 0.05 limit.

Source	DF	SS	MS	F	P
Regression	1	994.71	994.71	44.07	0.003
Residual Error	4	90.29	22.57		
Total	5	1085.01			

Regression equation found:
NFH% = 36.2 + 0.139 YS

S = 4.751 R-Sq = 91.7% R-Sq(adj) = 89.6%

Table A9.14 – GI coated materials – regression analysis with YS

The regression plot is presented in Figure A9.11.

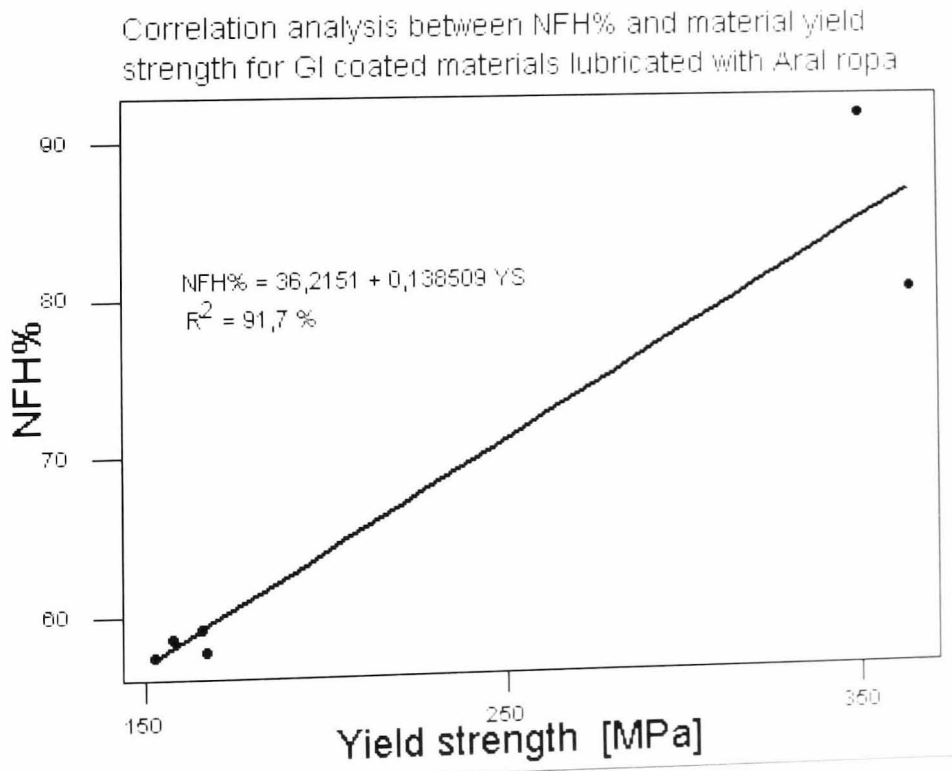

Figure A9.11 – GI coated materials – regression plot with YS

Although the graph shows that a high material yield strength leads to low friction drawing, there is still no evidence that surface topography effects drawability. Therefore, in order to test whether the chapter 5 friction experiments actually represent a real drawing operation, a correlation analysis was performed between. This last statistical analysis is presented below.

A9.9 Correlation between MSD and friction

The blankholder loads employed during this experiment were similar to those of the friction tests (see Table A9.15).

Blankholder Force	Contact Area	Blankholder Pressure	Friction experiment Pressure
36KN	$0.011m^2$	3.2MPa	1MPa
107KN	$0.011m^2$	9.8MPa	10MPa

Table A9.15 – Pressures comparison between MSD and friction experiments

In order to compare the results from the two experiments, two indexes (representing the two experiments) were devised. These are:

$$Diff_H = NFH(3MPa) - NFH(10MPa)$$

$$Diff_f = f(1MPa) - f(10MPa)$$

These two indices along with the yield strength were the three factors investigated. The results are shown in table A9.19:

Source	DF	SS	MS	F	P
Regression	2	43.596	21.798	41.14	0.000
Residual Error	7	3.708	0.530		
Total	9	47.304			

Regression equation found:

$Diff_H = 6.30 - 108\ Diff_f - 0.0181\ YS$

Predictor	Coef	StDev	T	P
Constant	6.303	1.291	4.88	0.002
Diff f	108.11	18.28	5.91	0.001
YS	-0.01	0.003	-4.71	0.002

S = 0.7279 R-Sq = 92.2% R-Sq(adj) = 89.9%

Table A9.16 – Correlation with friction – regression analysis

This table shows that there is statistical evidence to relate yield strength (YS) and frictional coefficient difference ($Diff_f$) to drawability difference ($Diff_H$).

The regression plot is presented in Figure A9.12.

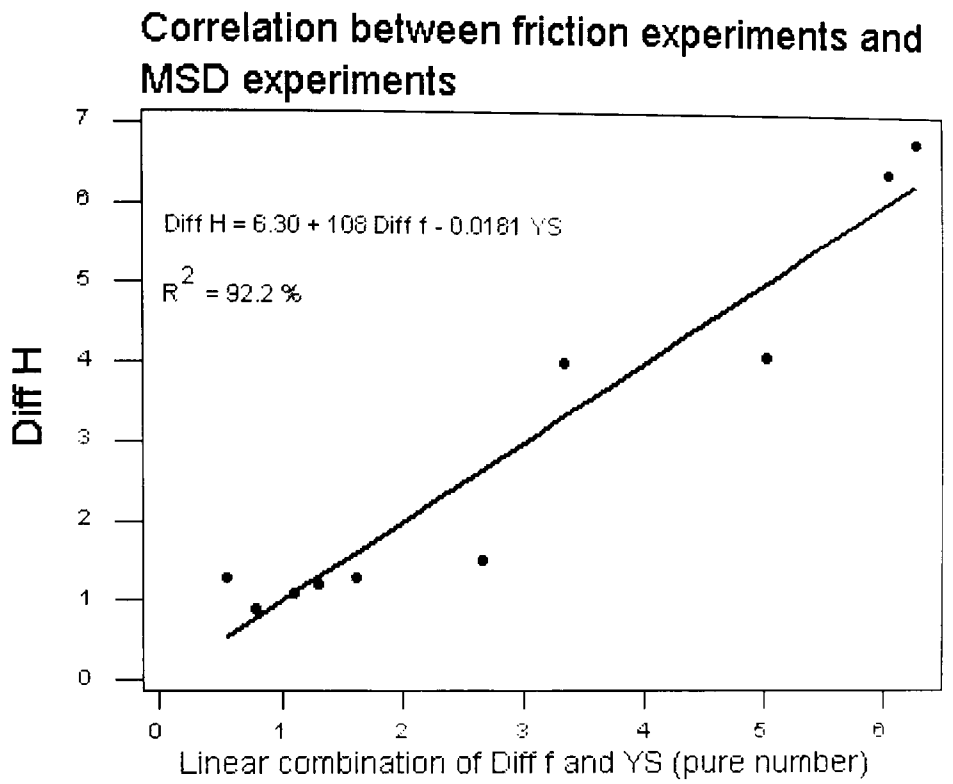

Figure A9.12 – Correlation with friction – Regression plot